

POLYMER NANOCOMPOSITE FILMS OF ZnO AND ZnO/MWNT FOR NONLINEAR OPTICAL APPLICATIONS

*A Thesis submitted
in partial fulfillment for the Degree of*

Doctor of Philosophy

by

HARIPADMAM P C



**DEPARTMENT OF PHYSICS
INDIAN INSTITUTE OF SPACE SCIENCE AND TECHNOLOGY
THIRUVANANTHAPURAM
JANUARY, 2015**

CERTIFICATE

This is to certify that the thesis entitled **Polymer Nanocomposite Films of ZnO and ZnO/MWNT for Nonlinear Optical Applications** submitted by **Haripadmam P C** to the Indian Institute of Space Science and Technology, Thiruvananthapuram, in partial fulfillment for the award of the degree of **Doctor of Philosophy** is a *bona fide* record of research work carried out by her under our supervision. The contents of this thesis, in full or in parts, have not been submitted to any other Institution or University for the award of any degree or diploma.

Dr. Pramod Gopinath

Supervisor

Department of Physics

Dr. Honey John

Co-Supervisor

Department of Chemistry

Thiruvananthapuram

January, 2015

Counter signature of the

Head of the Department (seal)

DECLARATION

I declare that this thesis entitled **Polymer Nanocomposite Films of ZnO and ZnO/MWNT for Nonlinear Optical Applications** submitted in partial fulfillment of the degree of **Doctor of Philosophy** is a record of original work carried out by me under the supervision of **Dr. Pramod Gopinath and Dr. Honey John**, and has not formed the basis for the award of any other degree or diploma, in this or any other Institution or University. In keeping with the ethical practice in reporting scientific information, due acknowledgements have been made wherever the findings of others have been cited.

Haripadmam P. C.
SC10D020

Thiruvananthapuram - 695 547

23.01.2015

ACKNOWLEDGMENTS

I am delighted to record my sincere love and gratitude to all those who have facilitated their valuable help for the successful completion of this study.

At the very outset, I am very much obliged to place on record my profound indebtedness to my thesis supervisor, Dr. Pramod Gopinath, Assistant Professor, Department of Physics, for his constant encouragement, diligence and invaluable guidance extended throughout this doctoral programme. I am delighted in this regard for his benevolent nature, patience, perfection and contextual support. He has taken a great amount of pain to go through each and every word of the manuscript and make it perfect.

It is my privilege to express my sincere gratitude and regards to my co-supervisor, Dr. Honey John, Associate professor, Department of Chemistry, for her inspiring guidance and scholarly assistance extended throughout the research work. Her motherly affection and valuable counselling helped me immensely to balance the time of academic and personal life. If I have succeeded in doing an interdisciplinary work, the credit goes to her.

I would like to thank my former guide and D C member, Dr. Bindu Krishnan, Assistant Professor, Sree Kerala Varma College, who encouraged me by giving wise suggestions and necessary criticisms. Her passion towards research has always inspired me. I express my sincere thanks to Dr. C. S. Narayanamurthy, HOD, Department of Physics, for his suggestions and invaluable helps.

I take this opportunity to thank the honourable Director, IIST for the IIST research fellowship. I would like to express my thanks to Dr. V. Adimurthy, former Dean R&D, and Dr. Thomas Kurian, Dean R&D for their support. My heartfelt thanks to Dr. Kuruvilla Joseph, HOD, Department of Chemistry, for the support and

help rendered to me by availing the facilities in the Department. I have no words to express my love and gratitude towards the lab and office staff in the Department of Physics and Chemistry for their assistance and love.

I am extremely thankful towards the members of my Doctoral Committee for their reviews and suggestions. Dr. Reji Philip, Associate Professor, RRI, Bangalore has been kind enough to provide experimental facilities and clarify my doubts without any hesitation. I have enjoyed the discussions with Dr. C. Vijayan, Professor, IIT, Madras whose approach towards science always fascinated me.

During the last four years I have cherished the love and friendship of research scholars of diversified areas, who kept me alive in the mid of frustrations of lab work. I thank my fellow researchers Kavitha, Remya, Sarah, Sarika and Jalaja for making the experimental sessions so vibrant. Kavitha has been a helping hand for me during the stages of synthesis of my samples and always been a supporting friend of mine. I appreciate Raneesh, Arun, Narasimman, Sujith, Srinivas, Rohith and Vinu for making me comfortable and safe to work with, during the late night lab sessions. Dhanya - the girl next door hold my hands tight whenever I needed and kept my presence of mind during the hard times. I remember Safakath, Anoop, Shafi, and Priya with regards for their assistance. With extreme pleasure I thank God for giving a wonderful and motivating friend like Smijesh who helped me in each and every step of my research, giving suggestions and criticizing at necessary situations. I would like to express my gratitude and respect to Mr. Suchand Sandeep for his selfless assistance. I appreciate Jijil, Sreekanth and Kavya for their altruistic nature.

I extend my sincere thanks to Library and Reprographic facility, IIST for the printing and binding facility. I would like to thank all the technicians of IITM, SAIF IITM, STIC CUSAT, NIIST, AIMS, IISU and LPSC who helped me for characterising the samples during the course.

I have no words to express the gratitude and love towards my parents and brother who always motivated, supported and stood with me in all my hardships. I am able to finish my thesis only because of the strength and courage they have offered me. The immense love, understanding, support and help provided by my husband Rajesh are beyond words to explain. He walked with me on the path of flowers and thorns without any complaint. I am indebted to my in laws for their understanding and constant support to finish this thesis successfully.

Last but not least, I express my love and sincere gratitude to my spiritual Guru and almighty God for showering their blessings and enabling me to stand where I am.

Haripadmam P C

ABSTRACT

The diverse applications utilizing nonlinear optical processes have imparted the requirement to invent materials possessing optical nonlinearity. However, the implementation of these materials can be accomplished only if films are fabricated by employing appropriate fabrication technique. Even though a large number of materials having nano meter size are nonlinear optical active in their colloidal form, the device fabrication of these materials is still not so popular. Polymer nanocomposite films are better candidates in this regard because apart from the desired properties, they can provide optical transparency.

The present investigation focuses on the fabrication of polymer nanocomposite films with the help of nanoparticles and transparent polymers and analyzes their nonlinear optical properties. Zinc oxide and multiwalled carbon nanotubes are two excellent materials to experiment with, in this regard. Both of these materials are known for their linear and nonlinear optical properties. A hybrid of these two materials is therefore expected to exhibit excellent nonlinear optical properties compared to their counterparts. Transparent polymers like polymethyl methacrylate and polystyrene are utilized as the matrices for preparing polymer nanocomposites. Films are fabricated with the help of spin and dip coating techniques.

Initially ZnO nanoparticles are synthesized from zinc acetate salt by solution precipitation method. Two types of ZnO nanoparticles are synthesized with the help of two different capping agents - polyethylene glycol and polyvinyl pyrrolidone. Detailed characterisation of these samples is performed to analyze their properties. The nanoparticles prepared with polyvinyl pyrrolidone is named as ZnO nanotops owing to their top like structure and these nanoparticles are proven to be good reverse saturable absorber, on investigating with open aperture Z-scan technique. Polymer nanocomposites of polymethyl methacrylate and the ZnO nanotops are synthesised and films are fabricated with the help of dip and spin coating technique. These films are found to be reverse saturable absorbers and posses larger nonlinear absorption coefficient compared to the nanotops in colloid form. The spin coated films exhibit improved nonlinear absorption compared to the dip coated films of same ZnO loading concentration. Based on the TGA analysis of the films, the reason for the same is explained. The nonlinear absorption coefficient of the spin coated films increased with the increase in loading concentration of the nanotops. An effective two photon absorption resulting from two photon absorption and excited state absorption is found to be the mechanism behind the exhibited optical nonlinear absorption (*Applied Physics Letters*, 2012).

Improved dispersion of the nanoparticles in the polymer matrix facilitates uniformity and optical transparency when films are fabricated. With the help of two kinds of dispersing agents (oleic acid and triton) polymer nanocomposite films of polymethyl methacrylate and ZnO nanotops are prepared so as to enhance their

uniformity and optical transparency. These films exhibit enhanced linear and nonlinear properties compared to the films prepared without the help of dispersing agent. Triton is found to be a better dispersing agent. The films exhibited a transition from reverse saturation to saturation of absorption with increase in loading concentration of ZnO nanoparticles incorporated in them. Dominance of two step absorption, two photon absorption and free carrier absorption is observed in these films. Apart from that, Pauli blocking is observed as the mechanism behind the saturation of absorption in films with higher loading of the nanotops. Films with tunable saturable and reverse saturable absorption nature could be thus fabricated enabling them for applications in optical limiting, optical bistable devices and laser mode locking (*Applied Physics Letters*, 2014).

Films with considerable nonlinear absorption coefficient and lower saturation intensity are required for applications involving protection from the hazards of high intensity lasers. Optical transparency is a desirable factor for transparent laser protection coatings. This lead to the fabrication of polymer nanocomposite films of ZnO nanotops with polystyrene employing spin and dip coating techniques. Another set of films with ZnO nanotops and a blend of polystyrene and polymethyl methacrylate are also fabricated with spin coating technique. The spin coated films prepared with ZnO nanotops and a blend of polystyrene and polymethyl methacrylate serve as better nonlinear absorbers and have better quality, uniformity and transparency (*Optics Letters*, 2014).

Multiwalled carbon nanotubes are fascinating materials with a wide range of applications in almost all fields. They have been identified to possess good nonlinear absorption property also. This motivated the synthesis of a hybrid material from ZnO nanotops and acid functionalised multiwalled carbon nanotubes. The hybrid is found to exhibit a fifth order nonlinear absorption behaviour due to cascaded one photon absorption. Films of the hybrid with polymethyl methacrylate are prepared with the help of spin coating technique. A comparative study has been carried out on the nonlinear absorption property of these films with another set of films prepared from the hybrid and a blend of polystyrene and polymethyl methacrylate. As expected, these films also exhibited a fifth order nonlinear optical property with considerable value of effective three photon absorption coefficient.

In total, the present investigation succeeded in fabricating good quality polymer nanocomposite films with considerable nonlinear absorption coefficient and low saturation intensity. The study highlights the synthesis, fabrication and characterisation techniques for efficient device fabrication of nonlinear optical materials like zinc oxide, multiwalled carbon nanotubes and their hybrid.

TABLE OF CONTENTS

DESCRIPTION	PAGE NUMBER
DEDICATIONS	iii
CERTIFICATE	v
DECLARATION	vii
ACKNOWLEDGEMENT	ix
ABSTRACT	xiii
LIST OF FIGURES	xxi
LIST OF TABLES	xxvii
ABBREVIATIONS	xxix
NOTATIONS	xxxiii
NOMENCLATURE	xxxix
1. INTRODUCTION	1
1.1. Optical nonlinearity	1
1.2. Nonlinear optical effects	3
1.2.1. Second order nonlinear optical effects	4
1.2.2. Third order nonlinear optical effects	6
1.2.3. Fifth order nonlinear optical effects	8
1.3. Origin of optical nonlinearity in various media	9
1.4. Techniques for evaluation of NLO parameters	12
1.4.1. Third harmonic generation	12
1.4.2. Degenerate four wave mixing	13
1.4.3. Optical Kerr gate	16
1.4.4. Self focusing and defocusing	17
1.5. Applications of nonlinear optics	20
1.6. Nonlinear optical materials	22

1.6.1.	Polymer nanocomposites	22
1.6.2.	ZnO nanoparticles	25
1.6.3.	Multiwalled carbon nanotubes	27
1.7.	Scope and objective of the thesis	30
1.8.	Organization of the thesis	31
2.	EXPERIMENTAL TECHNIQUES	33
2.1.	Synthesis methods	33
2.1.1.	ZnO	34
2.1.2.	ZnO/MWNT	34
2.2.	Preparation of polymer nanocomposites	35
2.3.	Fabrication techniques	35
2.3.1.	Solution casting	36
2.3.2.	Doctor blading	36
2.3.3.	Screen printing	37
2.3.4.	Dip coating technique	38
2.3.5.	Spin coating technique	38
2.4.	Characterization techniques	39
2.4.1.	Spectroscopic techniques	40
2.4.1.1.	X-ray Diffraction (XRD)	40
2.4.1.2.	UV-visible absorption spectroscopy	41
2.4.1.3.	Photoluminescence spectroscopy	42
2.4.1.4.	Fourier transform infrared spectroscopy	43
2.4.1.5.	Raman spectroscopy	44
2.4.2.	Microscopic techniques	45
2.4.2.1.	Transmission Electron Microscope (TEM)	45
2.4.2.2.	Scanning Electron Microscope (SEM)	45
2.4.3.	Thermogravimetric analysis	46
2.4.4.	White light interferometry	46

2.5.	Nonlinear absorption : phenomena, mechanism and measurement techniques	47
2.5.1.	Nonlinear absorption	47
2.5.2.	Mechanisms	47
2.5.3.	Measurement techniques	56
3.	SYNTHESIS AND FABRICATION OF PMMA-ZnO NANOCOMPOSITE FILMS FOR LINEAR AND NONLINEAR OPTICAL APPLICATIONS	65
3.1.	Introduction	65
3.2.	ZnO nanoparticles	67
3.2.1.	Synthesis	67
3.2.2.	Characterization	69
3.2.3.	Nonlinear absorption studies	74
3.3.	PMMA-ZnO nanocomposite films	79
3.3.1.	Dip coated films	79
3.3.1.1.	Fabrication	79
3.3.1.2.	Characterization	80
3.3.1.3.	Nonlinear absorption studies	82
3.3.2.	Spin coated films	83
3.3.2.1.	Fabrication	83
3.3.2.2.	Characterization	84
3.3.2.3.	Nonlinear absorption studies	86
3.4.	Conclusion	89
4.	SATURATION AND REVERSE SATURATION OF ABSORPTION IN PMMA-ZnO NANOCOMPOSITE FILMS	91
4.1.	Introduction	91
4.2.	PMMA-ZnO nanocomposite films by using dispersing agent	94
4.2.1.	Oleic acid dispersed film	94
4.2.1.1.	Fabrication	94

4.2.1.2.	Characterization	95
4.2.1.3.	Nonlinear absorption studies	100
4.2.2.	Triton dispersed films	105
4.2.2.1.	Fabrication	105
4.2.2.2.	Characterization	105
4.2.2.3.	Nonlinear absorption studies	109
4.2.3.	Fluence dependent studies	111
4.3.	Conclusion	113
5.	FABRICATION OF PS-ZnO AND PS/PMMA-ZnO FILMS WITH EXCELLENT NONLINEAR ABSORPTION	115
5.1.	Introduction	115
5.2.	PS-ZnO nanocomposite films	117
5.2.1.	Fabrication	117
5.2.2.	Characterization	117
5.2.3.	Nonlinear absorption studies	121
5.3.	PS/PMMA-ZnO nanocomposite films	124
5.3.1.	Fabrication	124
5.3.2.	Characterization	125
5.3.3.	Nonlinear absorption studies	128
5.4.	Conclusion	133
6.	SYNTHESIS AND FABRICATION OF POLYMER- ZnO/MWNT COMPOSITE FILMS WITH ENHANCED NONLINEAR ABSORPTION	135
6.1.	Introduction	135
6.2.	Functionalized MWNTs	138
6.2.1.	Functionalisation	138
6.2.2.	Characterization	139
6.2.3.	Nonlinear absorption studies	141

6.3.	Polymer-fMWNTs composite films	143
6.3.1.	Fabrication	143
6.3.2.	Characterization	143
6.3.3.	Nonlinear absorption studies	145
6.4.	ZnO-fMWNT hybrids	146
6.4.1.	ZnO/acetic acid dispersed fMWNT	146
6.4.1.1.	Synthesis	146
6.4.1.2.	Characterization	146
6.4.1.3.	Nonlinear absorption studies	147
6.4.2.	Polymer-hybrid composite films	148
6.4.2.1.	Fabrication	148
6.4.2.2.	Characterization	148
6.4.2.3.	Nonlinear absorption studies	149
6.4.3.	ZnO/PVP dispersed MWNT	149
6.4.3.1.	Synthesis	149
6.4.3.2.	Nonlinear absorption studies	150
6.4.3.3.	Characterization	151
6.4.3.4.	Fluence dependent transition from SA to RSA in hybrid colloid	155
6.4.4.	Polymer-ZnO/MWNT composite films	156
6.4.4.1.	Fabrication	156
6.4.4.2.	Characterization	157
6.4.4.3.	Nonlinear absorption studies	160
6.5.	Conclusion	166
7.	CONCLUSION	167
	REFERENCES	173
	PUBLICATIONS BASED ON THE THESIS	201

LIST OF FIGURES

FIGURE	TITLE	PAGE NUMBER
1.1	Second harmonic generation	5
1.2	Sum and difference frequency generation	5
1.3	Third harmonic generation	6
1.4	Stimulated Raman scattering	7
1.5	Stimulated Brillouin scattering	8
1.6	(a) Backward geometry and (b) Forward geometry of DFWM	14
1.7	Self focusing	17
1.8	Wurtzite structure of ZnO	26
1.9	SWNTs and MWNTs	28
2.1	Method of solution casting	36
2.2	Method of doctor blading	37
2.3	Method of screen printing	37
2.4	(a) Dip coating unit (b) Schematic of dip coating process	38
2.5	(a) Spin coating unit (b) Schematic of spin coating process	39
2.6	Process of two photon absorption	50
2.7	Process of three photon absorption	52
2.8	Excited state absorption	53
2.9	Free carrier absorption	54
2.10	Z-scan set up	60

2.11	Rayleigh length of a Gaussian beam	62
3.1	XRD patterns of ZnO nanoparticles	69
3.2	TEM images of ZnO nanoparticles	70
3.3	UV-vis absorption spectra of ZnO nanoparticles	71
3.4	Tauc plot of ZnO nanoparticles	72
3.5	Photoluminescence spectra of ZnO nanoparticles excited at 325 nm	72
3.6	Open aperture Z-scan plots of ZnO nanoparticles	74
3.7	Fluence dependent transmittance of ZnO nanoparticle colloid	77
3.8	UV-vis absorption spectra of F2D3	81
3.9	Photoluminescence spectra of F2D3	81
3.10	Step thickness of F2D3	82
3.11	Normalized Z-scan transmittance of (a) PMMA film (b) F2D1 and (c) F2D3	83
3.12	UV-vis absorption spectrum of F2S3	84
3.13	Photoluminescence spectra of F2S3	85
3.14	SEM image of F2S3	85
3.15	Step thickness of selected film	86
3.16	Open aperture Z-scan plots of spin coated films	86
3.17	TGA plot of dip and spin coated films with 2 weight % ZnO	89
4.1	Structure of oleic acid	93
4.2	Structure of Triton-X 100	93
4.3	UV-vis absorption spectra of selected (a) dip coated and (b) spin coated films	96

4.4	Tauc plots of selected (a) dip coated and (b) spin coated films	97
4.5	Photoluminescence spectra of selected dip coated films (a and b) and spin coated films (c and d)	98
4.6	SEM image of dip coated and spin coated films with 2 weight % ZnO	99
4.7	Surface profile of (a) dip coated and (b) spin coated films	99
4.8	Step thickness of (a) dip coated and (b) spin coated films	100
4.9	Normalized transmittance curves of (a) FD3O and (b) FS3O	100
4.10	Normalized Z-scan transmittance of selected dip coated films for varying loading concentration of ZnO	101
4.11	Normalized Z-scan transmittance of selected spin coated films for varying loading concentration of ZnO	102
4.12	UV-vis absorption spectra of selected spin coated films	106
4.13	Tauc plot for the selected spin coated films	106
4.14	Photoluminescence spectra of selected spin coated films	107
4.15	SEM image of F2S3T	108
4.16	Surface profile of selected film	108
4.17	Step thickness of selected film	108
4.18	Open aperture Z-scan plot for triton dispersed spin coated films of varying concentration	109
4.19	Open aperture Z-scan plot for PMMA-triton film	110
4.20	Open aperture Z-scan plot for F2S3O and F2S3T at various fluences	111
5.1	UV-vis absorption spectra of (a) dip coated and (b) spin	118

	coated films for various loading concentration of ZnO	
5.2	Tauc plot of (a) PF2D3 (b) PF2S3	118
5.3	Photoluminescence spectra of (a) PF2D3 (b) PF2S3 for an excitation wavelength of 325 nm	119
5.4	SEM image of (a) PF0.5D3 (b) PF0.5S3	120
5.5	Surface profile of (a) dip coated and (b) spin coated films	120
5.6	Step thickness profiles of selected films	121
5.7	Open aperture Z-scan plots for (a) dip coated and (b) spin coated films with varying loading concentration of ZnO in the film	122
5.8	Variation of β_{eff} with loading concentration of ZnO in the monomer for a) spin coated and b) dip coated films	122
5.9	TGA plot of dip coated and spin coated films	123
5.10	Photograph of PS/PMMA films	124
5.11	UV-vis absorption spectra of PS/PMMA-ZnO nanotop composite films with varying concentration of ZnO	126
5.12	Tauc plot for selected PS/PMMA-ZnO nanotop composite films	126
5.13	Photoluminescence spectra of selected PS/PMMA-ZnO nanotop composite films at excitation wavelength of 325 nm	127
5.14	SEM image of PPF2S3T	127
5.15	(a) Surface profile and (b) 3D surface image of selected film	128
5.16	Step thickness profile of the selected film	128
5.17	Open aperture Z-scan result of PS/PMMA-ZnO nanotop composite films	129
5.18	Input fluence Vs normalized transmittance plot of	130

	PPF6S3T	
5.19	Fluence dependent response of nonlinear absorption of PPF2S3T	131
6.1	Scheme of the functionalisation reaction of MWNT	138
6.2	UV-vis absorption spectra of pristine and functionalized MWNTs	139
6.3	Photoluminescence spectra of functionalized MWNTs	140
6.4	TGA plot of MWNTs	141
6.5	Open aperture Z-scan result of MWNTs	142
6.6	UV-vis absorption spectra of FCS3T and PPCS3	143
6.7	SEM image of FCS3T	144
6.8	(a) Surface profile and (b) 3D surface image of selected film	144
6.9	Step thickness profile of the selected film	145
6.10	Nonlinear optical response of (a) polymer-fMWNT and (b) polymer-ZnO nanotop composite films	145
6.11	UV-vis absorption spectra of the hybrids	147
6.12	Nonlinear optical response of the hybrids	147
6.13	UV-vis absorption spectra of hybrid composite films	149
6.14	Nonlinear optical response of hybrid composite films	149
6.15	Open aperture Z-scan of hybrid dispersed in water at a fluence 3.3 J/cm^2	150
6.16	FTIR spectra of (a) fMWNTs (b) Hybrid	151
6.17	UV-vis absorption spectra of the hybrid	152
6.18	XRD pattern of the hybrid	152
6.19	SEM image of the hybrid	153

6.20	TGA plot of fMWNTs, ZnO and the hybrid	153
6.21	Raman spectra of pMWNTs, fMWNTs and the hybrid	154
6.22	Photoluminescent spectrum of the hybrid at an excitation wavelength 325 nm.	155
6.23	Open aperture Z-scan plot for the hybrid dispersion at various incident fluences	155
6.24	UV- vis absorption spectra of the composite films of the hybrid with (a) PMMA and (b) PS/PMMA for varying loading of the hybrid	157
6.25	Photoluminescent spectra of the composite films of the hybrid with (a)&(b) PMMA and (c)&(d) PS/PMMA for varying loading of the hybrid	158
6.26	SEM image of the composite films (a) FH0.5S3T and (b) PPH0.5S3T	158
6.27	Surface profile of the selected composite films of hybrid with (a) PMMA and (b) PS/PMMA	159
6.28	Step thickness profile of the selected composite films of hybrid with (a) PMMA and (b) PS/PMMA	160
6.29	Nonlinear optical response of the composite films of hybrid with PMMA for varying loading of the hybrid	161
6.30	Fluence dependent nonlinear optical response of FH0.5S3T	162
6.31	Nonlinear optical response of the composite films of hybrid with PS/PMMA for varying loading of the hybrid	163
6.32	Fluence dependent nonlinear optical response of PPH0.5S3T	164

LIST OF TABLES

TABLE	TITLE	PAGE NUMBER
3.1	Calculated nonlinear optical parameters of ZnO nanoparticles	77
3.2	Effective nonlinear absorption coefficients (β_{eff}) and saturation intensities (I_{sat}) calculated for ZnO nanotops, by varying the input fluence.	78
3.3	Calculated values of viscosities for the polymer nanocomposites by varying the polymerization time	80
3.4	Optimized parameters of dip coating	80
3.5	Effective two photon absorption coefficients (β_{eff}) and saturation intensities (I_{sat}) calculated for the films	87
4.1	Optimized parameters of dip coating technique	95
4.2	Optical bandgap calculated for selected films	97
4.3	Effective two photon absorption coefficients (β_{eff}) and saturation intensities (I_{sat}) calculated for the dip coated films	101
4.4	Effective two photon absorption coefficients (β_{eff}) and saturation intensities (I_{sat}) calculated for the spin coated films prepared with oleic acid by varying ZnO loading concentration	103
4.5	Effective two photon absorption coefficients (β_{eff}) and saturation intensities (I_{sat}) calculated for the spin coated films prepared with triton by varying ZnO loading concentration	110
4.6	Effective two photon absorption coefficients (β_{eff}) and saturation intensities (I_{sat}) calculated for F2S3T and F2S3O by varying the input fluence	112
5.1	Effective two photon absorption coefficients (β_{eff}) and saturation intensities (I_{sat}) calculated for the spin coated films prepared with triton by varying ZnO loading	129

	concentration	
5.2	Effective two photon absorption coefficients (β_{eff}) and saturation intensities (I_{sat}) calculated for PPF2S3T by varying the input fluence	131
6.1	Effective three photon absorption coefficients (γ_{eff}) and saturation intensities (I_{sat}) calculated for the hybrid dispersions	148
6.2	Effective three photon absorption coefficients (γ_{eff}) and saturation intensities (I_{sat}) calculated for the hybrid colloid by varying input fluence	156
6.3	Effective three photon absorption coefficients (γ_{eff}) and saturation intensities (I_{sat}) calculated for PMMA-hybrid composite films	161
6.4	Effective three photon absorption coefficients (γ_{eff}) and saturation intensities (I_{sat}) calculated for FH0.5S3T by varying the input fluence	162
6.5	Effective three photon absorption coefficients (γ_{eff}) and saturation intensities (I_{sat}) calculated for PS/PMMA-hybrid composite films	164
6.6	Effective three photon absorption coefficients (γ_{eff}) and saturation intensities (I_{sat}) calculated for PPH0.5S3T by varying the input fluence	165

ABBREVIATIONS

Å	Angstrom
°C	Degree Celsius
μJ	Microjoule
μm	Micrometre
1PA	One photon absorption
3D	Three Dimensional
3PA	Three photon absorption
BPO	Benzoyl peroxide
CARS	Coherent anti-Stokes Raman scattering
CCD	Charge coupled device
CCI	Coherence correlation interferometer
CD	Compact disc
cm	Centimeter
CNTs	Carbon nanotubes
CTAB	Cetyl trimethylammonium bromide
CVD	Chemical Vapour Deposition
cw	Continuous wave
DC	Direct current
DEG	Diethylene glycol
DFWM	Degenerate four-wave mixing
DVD	Digital versatile disc
ESA	Excited state absorption

esu	Electrostatic units
eV	Electron volt
FCA	Free carrier absorption
fs	Femto second
FTIR	Fourier Transform Infrared
gm	gram
hrs	hours
HRTEM	High resolution transmission electron microscopy
IR	Infrared
J	Joule
LED	Light emitting diode
LT	Linear transmittance
m	Meter
min	Minute
MBE	Molecular beam epitaxy
mg	Milli gram
ml	Milli litre
mm	Milli meter
MMA	Methyl methacrylate
MWNTs	Multiwalled carbon nanotubes
NaOH	Sodium hydroxide
Nd:YAG	Neodymium-doped Yttrium Aluminium Garnet
NIR	Near infrared
NLA	Nonlinear absorption

NLO	Nonlinear optical
NLS	Nonlinear scattering
nm	Nano meter
NR	Nonlinear refraction
ns	Nano second
OKG	Optical Kerr gate
OLED	Organic light emitting diode
PANI	Polyaniline
PE	polyethylene
PEG	Polyethylene glycol
pH	Potential of Hydrogen
PL	Photoluminescence
PLD	Pulsed Laser Deposition
PMMA	Polymethyl methacrylate
PNC	Polymer nanocomposite
PP	Polypropylene
PPA	Poly phenylacetylene
ps	Pico second
PS	Polystyrene
PVA	Polyvinyl alcohol
PVC	Polyvinyl chloride
PVP	Polyvinyl pyrrolidone
RF	Radio frequency
RSA	Reverse saturable absorption

s	Second
SA	Saturable absorption
SBS	Stimulated Brillouin scattering
SEM	Scanning electron microscopy
SFG	Sum frequency generation
SHG	Second harmonic generation
SLM	Spatial light modulator
SPR	Surface plasmon resonance
SRS	Stimulated Raman scattering
SWNTs	Singlewall carbon nanotubes
TEM	Transmission electron microscopy
TGA	Thermogravimetric analysis
THG	Third harmonic generation
TPA	Two photon absorption
TWM	Three-wave mixing
UV-vis	Ultra violet- visible
W	Watts
XRD	X-ray diffraction

NOTATIONS

α	Nonlinear absorption coefficient
μ	Permeability of the medium
μ_0	Permeability of free space
c	Velocity of light
C	Concentration in mole/cm ³
c_m	Concentration of the absorbing species
d	Inter planar spacing
d_c	Mean dimension of the crystal size
E_g	Band gap
E_p	Kane energy parameter
F_0	Fluence of the laser at the focus
H	Planck's constant
I	Intensity of incident radiation
I_0	Intensity of incident radiation in linear absorption
I_D	Intensity of D band in Raman spectrum
I_G	Intensity of G band in Raman spectrum
I_p	Peak intensity of the beam at the focus
I_{probe}	Probe intensity
I_{pump}	Pump intensity
$I_{reference}$	Peak intensity obtained for reference
I_{sample}	Peak intensity obtained for sample
I_{sat}	Saturation intensity

I_t	Intensity of transmitted radiation
\vec{J}	Current charge density
k	Wave vector
K	Kerr constant
$K_{2\theta}$	FWHM on the 2θ scale in radian
l	Length/thickness of sample
l_c	Coherence length
L_{eff}	Effective thickness of the sample for Z scan experiment
l_i	Interaction length
\ln	Natural logarithm
$l_{reference}$	Path length of the reference
l_{sample}	Path length of the sample
n	Total refractive index of the medium
N	Number density of the molecules in a system
n_{\perp}	Refractive index for light polarized perpendicular to the DC field
n_{\parallel}	Refractive index for light polarized parallel to the DC field
n_0	Linear refractive index
n_2	Third order nonlinear refractive index
n_4	Fifth order nonlinear refractive index
N_a	Avogadro's number
$N_c(I)$	Intensity dependent carrier density
O_i	Oxygen interstitial

P	Effective polarization of the medium
P_c	Critical input power
P_i	i^{th} component of effective polarization
R	Surface reflectivity of the sample
S	Instantaneous input power
T	Transmittance of the sample
T_g	Glass transition temperature
V_O	Oxygen vacancy
V_{Zn}	Zinc vacancy
Z	Position
Z_0	Rayleigh length
Zn_i	Zinc interstitial
z_{sf}	Self focusing distance
α_0	Linear absorption coefficient
β	Two photon absorption coefficient
β_{eff}	Effective third order nonlinear absorption coefficient
γ	Three photon absorption coefficient
γ_{eff}	Effective fifth order nonlinear absorption coefficient
ΔE	Energy difference between the ground state and the excited state
ε	Permittivity of the medium
ε_0	Permittivity of free space
ε_m	Molar extinction coefficient
θ	Bragg diffraction angle

θ_{sf}	Self focusing angle
λ	X-ray wavelength
λ_0	Vacuum wavelength
λ_{max}	Wavelength of maximum absorption
ρ	electric charge density
σ_c	Free carrier cross section
σ_{ex}	Excited state absorption cross section
σ_g	Ground state absorption cross section
τ	Lifetime of the excited state
ν	Frequency of photon
χ	Linear susceptibility of the medium
$\chi^{(n)}$	n th order nonlinear susceptibility
Ω	Frequency of acoustic wave
ω	Frequency of incident radiation
ω_0	Beam waist
ω_s	Stokes shifted frequency
$\Delta\Phi_0(t)$	On axis phase shift
$\chi^{(3)}$	Third order nonlinear optical susceptibility
$\chi_{sample}^{(3)}$	Third order nonlinear optical susceptibility of the sample
$\chi_{reference}^{(3)}$	Third order nonlinear optical susceptibility of the reference
$\chi_I^{(3)}$	Imaginary part of third order nonlinear optical susceptibility

$\chi_R^{(3)}$	Real part of third order nonlinear optical susceptibility
\vec{B}	Magnetic field
\vec{D}	Electric displacement
\vec{E}	Electric field
\vec{H}	Magnetic field strength
\vec{P}_L	Linear polarization of the medium
\vec{P}_{NL}	Nonlinear polarization of the medium

NOMENCLATURE

Ag	Silver
C ₆₀	Fullerene
Au	Gold
Bi	Bismuth
C	Carbon
C ₁₄ H ₂₂ O(C ₂ H ₄ O) _n	Triton-X 100 (octyl phenol ethoxylate)
C ₁₈ H ₃₄ O ₂	Oleic acid
C ₂ H ₅ OH	Ethanol
C ₄ H ₁₀	Butane
CaCO ₃	Calcium carbonate
CdS	Cadmium sulfide
CdSe	Cadmium selenide
CdTe	Cadmium telluride
Co	Cobalt
-COOH	Carboxylic acid group
CS ₂	Carbon disulfide
Cu	Copper
Fe	Iron
Ge	Germanium
H ₂	Hydrogen
H ₂ SO ₄	Sulfuric acid
HCl	Hydrochloric acid

HNO ₃	Nitric acid
KBr	Potassium bromide
NaOH	Sodium hydroxide
O	Oxygen
PbS	Lead sulfide
PbSe	Lead selenide
Pt	Platinum
SF ₆	Sulphur hexa fluoride
Si	Silicon
SiO ₂	Silicon dioxide
TiO ₂	Titanium dioxide
Zn	Zinc
ZnO	Zinc oxide
ZnS	Zinc sulfide

CHAPTER 1

INTRODUCTION

This chapter throws light on the basics of optical nonlinearity, discussing the different nonlinear optical processes, their measurement techniques and applications. A review is conducted on various nonlinear optical materials and the origin of their optical nonlinearity. The properties and applications of ZnO nanoparticles and multiwalled carbon nanotubes are also discussed. The last session of the chapter briefs the scope and objectives of the thesis.

1.1. Optical nonlinearity

The demonstration of second harmonic generation (SHG) by Franken et al. has given a new direction to the investigations on light matter interaction (Franken et al., 1961). This attempt came to reality with the help of lasers which can provide sufficiently high intense light. Electric polarization and magnetization is induced to a medium when an electromagnetic wave propagates through it. This induced electric polarization and magnetization in the medium is a result of the motion of the electrons and nuclei on interaction with the electromagnetic wave. The fields radiated by the induced polarizations or magnetizations then interact with the incident electromagnetic field. When the incident optical intensity is low, the induced fields are proportional to the incident fields and the response of the medium is linear. However, the increase in incident radiation causes the behaviour of the medium, nonlinear.

Optical nonlinearity is a consequence of intense light matter interaction and it is manifested by changes in the optical properties of a medium as the intensity of the incident light is increased. There are two categories of optical nonlinearity: intrinsic and extrinsic. When the absorption or emission of light changes the composition of

the medium and thereby changes its properties, then the optical nonlinearity is termed as extrinsic nonlinearity. Such change can occur in (a) relative populations of ground and excited states (b) the numbers of optically effective electrons. The optical nonlinearity arising from the nonlinear response of the individual molecule or unit cell to the fields of two or more light waves is termed as intrinsic nonlinearity. The optical properties of the medium depend on the intensity of the light both in extrinsic and intrinsic nonlinearities (Baldwin, 1969; Butcher and Cotter, 1991).

During the propagation and interaction of an electromagnetic wave in a medium, the changes in the properties of the medium are represented macroscopically by the electric polarization and the magnetization. Considering the propagation of an electromagnetic wave through a dielectric medium, which is homogeneous (ϵ and μ have the same value at all points), isotropic (ϵ and μ are independent of the direction of propagation), non conducting (no net charge and net current) and non magnetic ($\mu=\mu_0$), the Maxwell's equations for the electric and magnetic fields in the material can be represented as,

$$\vec{\nabla} \cdot \vec{D} = 0 \quad (1.1)$$

$$\vec{\nabla} \cdot \vec{B} = 0 \quad (1.2)$$

$$\vec{\nabla} \times \vec{E} = -\frac{\partial \vec{B}}{\partial t} \quad (1.3)$$

$$\vec{\nabla} \times \vec{H} = \frac{\partial \vec{D}}{\partial t} \quad (1.4)$$

In the above equations, $\vec{D} = \epsilon \vec{E}$ and $\vec{B} = \mu \vec{H}$, since linear medium is considered. Here ϵ and μ are the permittivity and permeability of the medium respectively. \vec{E} is the electric field and \vec{B} represents the magnetic field. \vec{D} and \vec{H} represent the electric displacement and the magnetic field strength.

Considering the relation between the electric displacement and the electric field,

$$\vec{D} = \epsilon \vec{E} = \epsilon_0 \vec{E} + \vec{P}_L = \epsilon_0 (1 + \chi) \vec{E} \quad (1.5)$$

where
$$\vec{P}_L = \epsilon_0 \chi \vec{E} \quad (1.6)$$

represents the linear polarization of the medium (dipole moment per unit volume) by the influence of the electromagnetic wave, χ represents the linear susceptibility of the medium and ϵ_0 represents the permittivity of free space.

In a nonlinear medium, the effective polarization (\vec{P}) is a sum of the linear part (\vec{P}_L) and higher order nonlinear contributions (\vec{P}_{NL}),

$$\vec{P} = \vec{P}_L + \vec{P}_{NL} \quad (1.7)$$

\vec{P}_L corresponds to the regime where the optical properties of a medium are independent of the field intensity. In other words, \vec{P}_L corresponds to linear optical effects, whereas \vec{P}_{NL} arises when the incident intensity is sufficiently high.

1.2. Nonlinear optical effects

The i^{th} component of effective polarization (where $i = x, y$ or z) of a medium can be represented as a power series expansion in the field strength, incorporating the higher order nonlinear susceptibilities ($\chi^{(n)}$) as,

$$P_i(r, t) = \epsilon_0 \left[\sum_j \chi_{ij}^{(1)} E_j(r, t) + \sum_{jk} \chi_{ijk}^{(2)} E_j(r, t) E_k(r, t) + \sum_{jkl} \chi_{ijkl}^{(3)} E_j(r, t) E_k(r, t) E_l(r, t) + \dots \right] \quad (1.8)$$

Here $\chi^{(n)}$ represents the n^{th} order nonlinear susceptibility. It is a tensor of rank $n+1$. The presence of n^{th} order nonlinearity in a medium depends upon the

microscopic structure of the material also. In a centrosymmetric medium, all even order nonlinear susceptibilities vanish and the third order nonlinearity becomes the lowest order nonlinearity. A non centrosymmetric medium exhibits odd and even order nonlinearities (Pradeep, 2012). The n^{th} order susceptibility of the medium, $\chi^{(n)}$ gives rise to a large variety of nonlinear optical phenomena. Depending upon the nature of the medium and the intensity of incident radiation, the medium exhibits different order of susceptibility.

Consider the linear interaction of electromagnetic radiation with a medium (lower intensity). The linear polarization induced in the medium is,

$$P_i = \varepsilon_0 \sum_j \chi_{ij}^{(1)} E_j(r, t) \quad (1.9)$$

where $\chi_{ij}^{(1)}$ represents the linear susceptibility of the medium. The linear susceptibility is related to linear optical effects including absorption, refraction, diffraction, birefringence, elastic and inelastic scattering. In a linear medium all these parameters are independent of the incident intensity.

1.2.1. Second order nonlinear optical effects

In a non centrosymmetric medium, the polarization induced due to the interaction with a high intensity incident electromagnetic radiation gives rise to different second order nonlinear optical (NLO) effects. The second order polarization is represented as,

$$P_i = \varepsilon_0 \sum_{jk} \chi_{ijk}^{(2)} E_j(r, t) E_k(r, t) \quad (1.10)$$

where $\chi_{ijk}^{(2)}$ represents the second order nonlinear optical susceptibility. The second order nonlinear optical susceptibility gives rise to nonlinear optical phenomena like second harmonic generation (SHG), sum frequency generation, difference frequency generation, etc. (Boyd, 2003).

Second harmonic generation is a frequency mixing process in which two independent incident waves of frequency ω interact and result in a wave with frequency 2ω as shown in Figure 1.1. SHG is also known as frequency doubling.

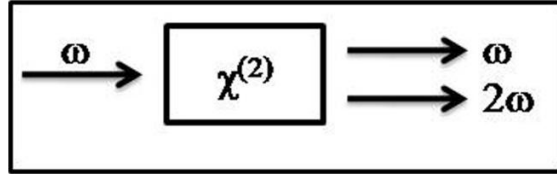


Figure 1.1 Second harmonic generation

The induced polarization in the medium on interacting with a laser beam of electric field strength,

$$\tilde{E}(t) = Ee^{-i\omega t} + c.c. \quad (1.11)$$

can be represented as,

$$\tilde{P}^{(2)}(t) = 2\chi^{(2)}EE^* + (\chi^{(2)}E^2e^{-2i\omega t} + c.c.) \quad (1.12)$$

In sum and difference frequency generation, two waves of different frequency ω_1 and ω_2 interact nonlinearly to produce the third wave having either a sum frequency $\omega_3 = \omega_1 + \omega_2$ or a difference frequency $\omega_3 = \omega_1 - \omega_2$ as shown in Figure 1. 2.

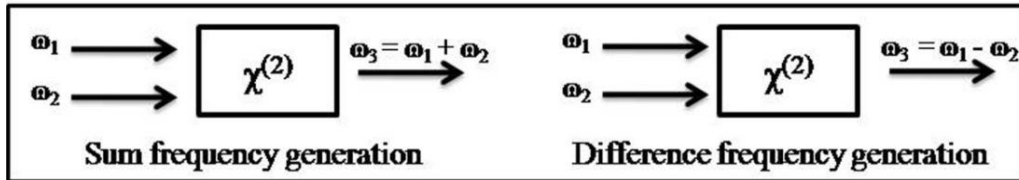


Figure 1.2 Sum and difference frequency generation

Consider the incident waves having two different frequencies

$$\tilde{E}(t) = E_1e^{-i\omega_1 t} + E_2e^{-i\omega_2 t} + c.c. \quad (1.13)$$

The total nonlinear polarization of the medium in this case is,

$$\tilde{P}^{(2)}(t) = \sum_n P(\omega_n) e^{-i\omega_n t} \quad (1.14)$$

So that this gives rise to a sum frequency term,

$$P(\omega_1 + \omega_2) = 2\chi^{(2)}E_1E_2 \quad (1.15)$$

and a difference frequency term,

$$P(\omega_1 - \omega_2) = 2\chi^{(2)}E_1E_2^* \quad (1.16)$$

1.2.2. Third order nonlinear optical effects

Third order susceptibility gives rise to nonlinear optical phenomena like third harmonic generation (THG), intensity dependent refractive index and absorption coefficient, stimulated Raman scattering, DC Kerr effect, Brillouin scattering, etc. (Boyd, 2003; Sutherland, 2003; Murti and Vijayan, 2014).

Corresponding polarization term is given by,

$$P_i = \epsilon_0 \sum_{jkl} \chi_{ijkl}^{(3)} E_j(r,t) E_k(r,t) E_l(r,t) \quad (1.17)$$

where $\chi_{ijkl}^{(3)}$ represents the third order nonlinear optical susceptibility.

Since the analysis of higher order nonlinear processes are complicated, consider the applied field as,

$$\tilde{E}(t) = E \cos \omega t \quad (1.18)$$

for simplicity of the expressions. Then the resultant polarisation can be represented as,

$$\tilde{P}^{(3)}(t) = \frac{1}{4} \chi^{(3)} E^3 \cos 3\omega t + \frac{3}{4} \chi^{(3)} E^3 \cos \omega t \quad (1.19)$$

The first term in equation (1.19) describes the third harmonic generation.

In third harmonic generation, the interaction of three independent incident waves of frequency ω results in the generation of a wave with frequency 3ω as shown in Figure 1.3.

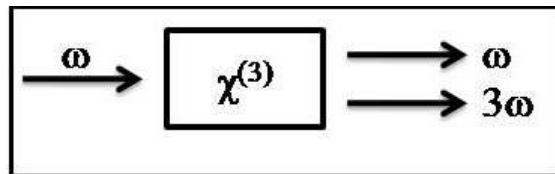


Figure 1.3 Third harmonic generation

The second term in equation (1.19) containing ‘ ω ’ represents the nonlinear optical processes at the frequency of the incident wave. These processes include nonlinear refraction (NR) and nonlinear absorption (NLA). In this regime, the total refractive index of the medium becomes intensity dependent and can be represented as,

$$n(I) = n_0 + n_2 I \quad (1.20)$$

where n_0 and n_2 are the linear and third order nonlinear refractive index respectively, and I represents the intensity of the incident radiation. The intensity dependent refractive index cause self focusing or defocusing of laser beam inside a medium.

The absorption coefficient of the material also becomes intensity dependent in third order nonlinear regime. The total absorption coefficient then becomes,

$$\alpha(I) = \alpha_0 + \beta I \quad (1.21)$$

where α_0 is the linear absorption coefficient and β is the two photon absorption coefficient. The third order nonlinear absorption processes like two photon absorption (TPA), saturable absorption (SA) and reverse saturable absorption (RSA) are particularized in Chapter 2.

The process of stimulated Raman scattering is as shown in Figure 1.4 is another important third order optical nonlinearity. Here, a photon of frequency ω is annihilated and another photon of frequency $\omega_s = \omega - \omega_v$ is created. The creation of ω_s named as Stokes shifted frequency, leaves the molecule in an excited state with energy $\hbar\omega_v$.

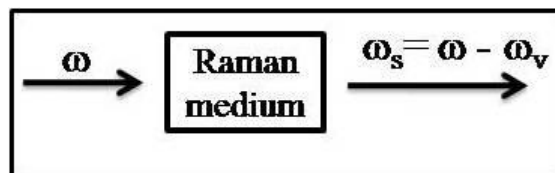


Figure 1.4 Stimulated Raman Scattering

Consider an incident wave of frequency ω_1 which scatters from a periodic acoustic wave of frequency Ω , the scattered light then has a frequency $\omega_2 = \omega_1 - \Omega$, and it is referred to as the Stokes wave. The resulting phenomenon named stimulated Brillouin scattering (SBS) corresponds to a stimulated phonon emission and is shown in Figure 1.5. Materials have a tendency to become optically dense in regions of high optical intensity and this is the basis of SBS. SBS can be used for self phase conjugation.

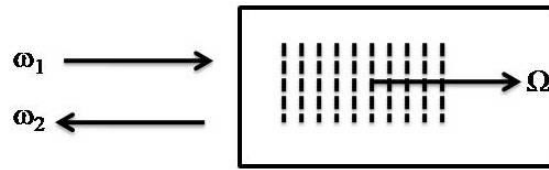


Figure 1.5 Stimulated Brillouin scattering

The DC Kerr effect is also a third order nonlinear optical process which includes the changes in the refractive index of a medium due to the interaction with a strong DC field. The DC field creates a refractive index difference between the two polarizations given by,

$$n_{\parallel} - n_{\perp} = \frac{3\chi_2^K E_y^2(0)}{n} \quad (1.22)$$

where n_{\parallel} and n_{\perp} are the respective indices of light polarised parallel and perpendicular to the DC field, and n is the zero field index. K is the Kerr constant of the medium which is defined as,

$$\Delta n = n_{\parallel} - n_{\perp} = \lambda_0 K E^2(0) \quad (1.23)$$

where λ_0 is the vacuum wavelength.

1.2.3. Fifth order nonlinear optical effects

Fifth order susceptibility is also associated with intensity dependent nonlinear absorption and nonlinear refraction. Three photon absorption is a fifth order nonlinear

absorption process. Here three photons of the incident radiation are absorbed by the medium at a time and the nonlinear absorption coefficient can be represented as,

$$\alpha(I) = \alpha_0 + \beta I + \gamma I^2 \quad (1.24)$$

where α_0 , β and γ are linear, two photon and three photon absorption coefficient respectively. I is the intensity of incident radiation.

The intensity dependent refractive index of the medium becomes,

$$n(I) = n_0 + n_2 I + n_4 I^2 \quad (1.25)$$

where n_0 , n_2 and n_4 are the linear, third order and fifth order nonlinear refractive indices.

At sufficiently high intensities, a few lower order linear/nonlinear effects in a medium successively produce an effective higher order nonlinear process, known as cascaded nonlinearity. A stepwise linear absorption of two photons can cause two photon absorption, which is a third order nonlinear process. A two photon absorption followed by a linear absorption or linear absorption of three photons gives rise to an effective fifth order nonlinear absorption. Photorefractive effect is another example for cascaded nonlinear effect where a linear absorption is followed by the occurrence of quadratic electro-optic effect (Sutherland, 2003).

1.3. Origin of optical nonlinearity in various media

The mechanism behind the nonlinear optical behaviour differs from material to material. At higher incident laser intensities, a change in the refractive index changes the polarization which in effect influences the nonlinear optical properties of materials. Nonlinear optical phenomena can be due to electronic, thermal or anisotropic orientation processes. The electronic nonlinearity arises from electronic structural change due to distortion of electronic clouds or distribution of electrons to different levels. The thermal nonlinearity occurs as a result of generation of phonons

on absorption of light. The orientational nonlinearity is due to birefringence when off resonance and dichroism on resonance (Pradeep et al., 2013). In precise, molecular orientation, electrostriction, atomic alignment, change in population equilibrium, nonlinear absorption, excitonic absorption, free carrier absorption, nonlinear scattering, etc. are reported to be the driving force for nonlinear optical behaviour (Bredas et al., 1994; Sutherland, 2003). A brief review of the nonlinear optical mechanisms of crystals, metal nanoparticles, semiconductor nanoparticles and organic materials are given below.

Optical nonlinearity arises in crystals mainly due to electronic nonlinearities. Review on the nonlinear optical studies carried out on crystals reveals SHG and optical birefringence are exhibited by them (Lin et al., 2003a; Lin et al., 2003b; Luo et al., 2011).

Metal particles support the collective oscillation of conduction electrons, known as surface plasmon resonance (SPR). The optical and nonlinear optical response of metal nanostructures is strongly influenced by this collective oscillation. A large number of researchers report surface plasmon resonance as the mechanism of the exhibited optical and nonlinear optical properties of metal nanoparticles (Kelly et al., 2003; Maier and Atwater, 2005; Sato et al., 2014). In nanocomposites of metals, SPR leads to an increase in the electric field inside the metal, yielding to the enhancement of their optical nonlinearities (Wang et al., 2005; Liu et al., 2010). At nonresonant wavelengths, the optical nonlinearity is reported to be due to nonlinear absorption (Karthikeyan et al., 2006; Papadopoulos et al., 2006).

The mechanism behind optical nonlinearity of semiconductors is basically assigned to the refractive index change caused to the medium by high intensity light. The free carriers present in the semiconductors also have an equivalent role in inducing the optical nonlinearity. The factors which induce optical nonlinearity in semiconductors can be generally categorized as anharmonic response of bound

electrons, presence of free carriers and their transitions, valence to conduction band transitions, impurity transitions and excitonic transitions (Fainman et al., 1993). Nonlinear absorption in semiconductors and their oxides is reported to be due to two photon absorption, three photon absorption and two photon induced excited state nonlinearities (Kurian et al., 2007; Xing et al., 2008; Dehghani et al., 2011).

Organic materials like dyes, polymers and carbon nanotubes are reported to exhibit optical nonlinearity. Nonlinear optical properties of organic materials arise from nonlinear absorption, thermal variation of local refractive index of the medium, presence of conjugated electron system, self defocusing or strong donor-acceptor intermolecular interaction (Sendhil et al., 2005; Ali and Palanisamy, 2006; Rao et al., 2011; Pradeep et al., 2013; Pramodini and Poornesh, 2014a).

Carbon nanotubes (CNTs) are a category of carbon family and exhibits good nonlinear absorption properties. The basic mechanism behind the nonlinear optical behaviour of these nanoparticles have been studied and reported by many groups. Nonlinear scattering (NLS) and nonlinear absorption (NLA) are the two different mechanisms attributed to the optical nonlinearity of these samples. At high incident intensities, CNTs absorb the strong laser radiation and this induces heating to the carbon particles. As a result, microplasma is formed which rapidly expand to the surrounding liquid. This microplasma strongly scatters the incident laser light. In addition, at incident energies well above a threshold, the strong heating leads to bubble formation and further enhances the scattering process (Sun et al., 1998; Vivien et al., 2002). In nonlinear absorption, two photon absorption and three photon absorption are reported to be the mechanism behind the nonlinear absorption property (Anand et al., 2013). Other than NLS and NLA, self focusing and thermal lensing are also reported to have role in the nonlinear optical behaviour of CNTs (Vivien et al., 1999; Vivien et al., 2001).

1.4. Techniques for evaluation of NLO parameters

The experimental techniques which are commonly used to characterize the third order nonlinear optical processes are detailed in this section. Most of the methods applied for the characterization of third order optical nonlinearities are also used for the evaluation of fifth order optical nonlinearities. The different techniques include third harmonic generation, degenerate four wave mixing, optical Kerr gate and self focusing and defocusing (Bredas et al., 1994).

1.4.1. Third harmonic generation

The pure electronic third order susceptibility in centrosymmetric materials can be characterized by employing third harmonic generation (THG) technique. This is based on the fact that pure non resonant electron cloud distortion can respond rapidly to produce a nonlinear polarization oscillating at the third harmonic of the incident wave. Several researchers have developed techniques based on THG to evaluate the third order nonlinear optical parameters (Buchalter and Meredith, 1982; Thalhammer and Penzkofer, 1983; Kajzar and Messier, 1987).

In the experimental arrangement for THG, a laser source of appropriate wavelength is selected and the beam is split into two components. One beam is used to generate the third harmonic signal in the sample. The other beam is taken as the reference. The path length of the sample and the reference is varied. The third harmonic signal is monitored as a function of the interaction length l_i to obtain the fringes. The coherence length (l_c) of sample and reference can be calculated from these fringes. The coherence length is given by

$$l_c = \frac{\pi}{\Delta k} \quad (1.26)$$

where the wave vector mismatch, $\Delta k = k_{3\omega} - 3k_\omega = 3\omega \frac{(n_{3\omega} - n_\omega)}{c}$ (1.27)

Here n_ω and $n_{3\omega}$ are the refractive indices at frequency ω and 3ω respectively. The third order susceptibility can be calculated by,

$$\chi_{\text{sample}}^{(3)} = \chi_{\text{reference}}^{(3)} \sqrt{\frac{\left(\frac{I_{3\omega,\text{sample}}}{I_{3\omega,\text{reference}}}\right)}{\left(\frac{l_{c,\text{reference}}}{l_{c,\text{sample}}}\right)^2}} \quad (1.28)$$

The advantage of this technique is that even nanosecond laser pulses can be used as source without any difficulty in the measurement. The poor accuracy of the experimental value of $\chi^{(3)}$ is the disadvantage of this technique. Since all media (including the air surrounding the medium) generate the third harmonic signal, these additional contributions interfere coherently with the third harmonic generated in the sample and complicate the data analysis.

THG has been reported to measure the third order nonlinear susceptibility of liquids, solids and gases (Bloembergen et al., 1969; Burns and Bloembergen, 1971; Kanbara et al., 1997; Thalhammer and Penzkofer, 1983). Recent reports involve the studies conducted in bulk gold (Boyd et al., 2014).

1.4.2. Degenerate four wave mixing (DFWM)

Degenerate four wave mixing is a popular method for directly measuring the third order nonlinear susceptibility of materials. The process allows an interaction between three beams to generate a fourth beam of the same frequency.

There are two types of geometries that are used to implement DFWM: backward geometry and forward geometry. In backward geometry (Figure 1.6 (a)), the beam from the laser source is split into two: a forward pump beam and a probe beam. The backward pump beam is created by reflection of the forward pump beam. The probe beam is directed on the sample at a small angle with these pump beams. The probe beam experiences an index grating created in the medium due to the

interaction of the pump beams. The pump beams thus get scattered in the direction of the conjugate beam, counter propagating to the direction of the probe beam. The output signal is measured placing the detector opposite to the direction of the probe beam.

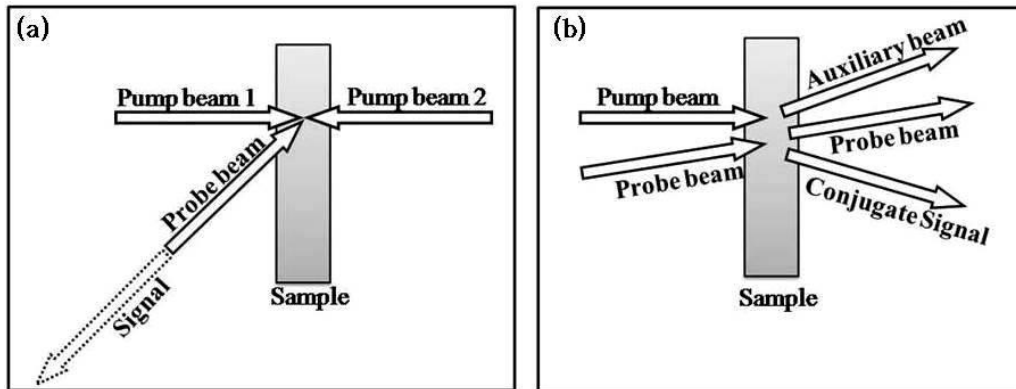


Figure 1.6 (a) Backward geometry and (b) Forward geometry of DFWM

In the forward geometry all the beam travels in the same direction as shown in Figure 1.6 (b). There is a single pump beam and the probe beam is incident on the sample from the same side of the pump beam. Within the medium these beams interact and the output waves produced include the transmitted pump and probe beams, a conjugate wave and a fourth wave called the auxiliary wave. In an optically thin medium, there can be a large number of output waves. This is because, the pump and probe waves create an index grating in the nonlinear medium and self-diffracts the incident waves and hence generate a multitude of diffracted waves. Any method can be selected according to the experimental conditions, to measure all the independent components of $\chi^{(3)}$ of isotropic materials.

The objective of this technique is to measure the intensity of the phase conjugate beam or equivalently the phase conjugate reflectance and yield the $\chi^{(3)}$ tensor components of the medium. The probe intensity (I_{probe}) is related to the pump intensity (I_{pump}) as

$$I_{probe} = \eta I_{pump} \quad (1.29)$$

where

$$\eta = \frac{I_c}{|kL|^2 I_{pump}} \quad (1.30)$$

and the data obtained is then fitted to the form,

$$I_c = b' I_{pump}^3 \quad (1.31)$$

and the effective value of third order nonlinear optical susceptibility is,

$$\chi_{eff}^{(3)} = \frac{\epsilon_0 n_0^2 c \lambda}{3\pi L} \sqrt{\frac{b'}{\eta}} \quad (1.32)$$

Usually in DFWM experiments, the measurements are taken with respect to a standard material because of the difficulty in characterizing the laser parameters precisely. The peak intensity is proportional to the average power or pulse energy and this makes the measurement easier because of easiness in the measurement of power or energy. From the peak intensity obtained for both the sample and the reference, the value of susceptibility is obtained by using the following equation,

$$\chi_{sample}^{(3)} = \chi_{reference}^{(3)} \left(\frac{n_{sample}}{n_{reference}} \right)^2 \left(\frac{l_{reference}}{l_{sample}} \right) \left(\frac{I_{sample}}{I_{reference}} \right)^{1/2} \quad (1.33)$$

where n_i is the refractive index and l_i is the path length in medium i .

The advantage of this technique is that it is possible to measure all of the independent tensor components of $\chi^{(3)}$ of an isotropic material with a single experiment. An important disadvantage is that other techniques should be employed to measure the real and imaginary part of the susceptibility. Also the nonlinear absorption coefficient and nonlinear refractive index cannot be measured directly by employing this technique.

Reports are available on the investigation of third and fifth order nonlinear susceptibility employing DFWM (Botti et al., 2003; Dharmadhikari et al., 2004; Naranjo et al., 2007).

1.4.3. Optical Kerr gate (OKG)

The basic mechanism of the optical Kerr gate technique is optically induced birefringence caused by a nonlinear phase shift. The nonlinearly induced birefringence affects the polarization properties of optical waves propagating through the medium. The objective of these methods is to transmit light of a known polarization state through the nonlinear material and then measure the resultant intensity of the light that passes through a final polarizer. The nonlinear susceptibility is obtained by inversion of the formulas.

The nonlinear polarization in this case can be represented as,

$$P_i(\omega) = \chi_{iikk}^{(3)}(-\omega; \omega, \omega, -\omega) E_j(\omega) E_k(\omega) E_l(\omega) \quad (1.34)$$

This technique probes the evolution of the birefringence and hence the response time of $\chi^{(3)}$ can be probed. For this, a laser source is used and the beam is split in a strong orienting pump pulse and a weak probe pulse. Both beams are linearly polarized. To retrieve the optical birefringence information, the probe beam passes through an analyzer (cross polarizer). The intensity of the probe beam transmitted through the Kerr cell is measured as a function of the delay between pump and probe.

The advantages of this technique are the simplicity in experimental set up and data analysis. The real and imaginary part of $\chi^{(3)}$ can be measured using this technique. The disadvantage of optical Kerr gate measurement is that all the tensor components of $\chi^{(3)}$ cannot be measured by this technique. The technique has been utilized to measure the nonlinear refractive index of materials (Aber et al., 2000; Slepko et al., 2002).

1.4.4. Self focusing and defocusing

In the nonlinear optical regime the absorption coefficient and refractive index of the medium can be intensity dependent. This may lead to various nonlinear optical phenomena. The technique to calculate the nonlinear refractive index and nonlinear absorption coefficient employing self focusing and defocusing of the medium is discussed here.

Nonlinear refraction

The nonlinear refractive index of the medium can lead to self focusing/defocusing of the incident Gaussian beam. Self focusing is a self action in which a beam itself distorts its wavefront on travelling through a nonlinear medium. Consider the equation (1.20) representing nonlinear refractive index, $n(I) = n_0 + n_2 I$. Here n_2 is a function of the incident intensity. The value of n_2 can be positive or negative depending upon the nature of the material. When the beam traverse through a material having positive value of n_2 , the central part of the beam where it has the maximum intensity experiences a larger refractive index compared to the edge. This larger refractive index slows down the beam velocity at the center compared to its edges. As the beam travels further through the medium, the induced distortion increases progressively and results in the focusing of the beam.

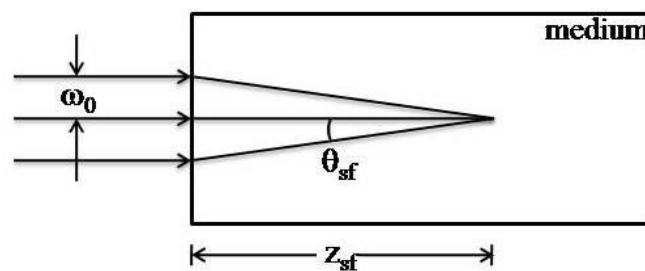


Figure 1.7 Self focusing

Consider a collimated beam of radius ω_0 travelling through a nonlinear optical material having positive value of n_2 , as shown in Figure 1.7. The linear refractive index n_0 . The total refractive index of the medium is given by equation (1.20). The self focusing angle (θ_{sf}) is,

$$\theta_{sf} = \sqrt{2n_2 I / n_0} \quad (1.35)$$

and the self focusing distance (z_{sf}) is,

$$z_{sf} = \omega_0 \sqrt{\frac{n_0}{2n_2 I}} \quad (1.36)$$

Self defocusing is a reverse process of self focusing which happens in materials with negative value of n_2 . Here the refractive index of the medium decreases with increasing optical intensity and the laser beam experiences much lower refractive index at the centre of the beam compared to its edges. This leads to the defocusing of the beam by itself (Boyd, 2003; Sutherland, 2003).

Nonlinear absorption

Materials manifest nonlinear absorption of the incident radiation in two ways namely: saturable absorption (SA) and reverse saturable absorption (RSA). Saturable absorption is exhibited by materials having lowered excited state absorption cross section compared to the ground level absorption cross section. Whereas the materials having greater excited state absorption cross section compared to the ground level absorption cross section, exhibits reverse saturable absorption. The transmitted intensity of SA (RSA) materials increases (decreases) with increase in intensity. A detailed discussion on the nonlinear absorption process and the various mechanisms associated with it is carried out in chapter 2.

The self focusing and defocusing action are utilized to measure parameters associated with the third and fifth order nonlinear optical processes. There are two methods for measuring the nonlinearity using these self actions: optical power limiter and Z-scan.

The technique of optical power limiter is based on self focusing and intensity dependent absorption mechanism. The technique focuses a beam from the laser source to a sample with high nonlinear refractive index. The transmitted light is focused through a pinhole on a detector. At low intensities output will be considerable. At higher intensities the transmittance decreases due to self focusing.

The critical input power (P_c),

$$P_c = \frac{3.72c\lambda^2}{32\pi^2 n_2} \quad (1.37)$$

determines the limit of the transmitted power. In the above equation, c is the velocity of light and λ is the wavelength of the incident laser.

Z-scan is a highly sensitive single beam technique for the measurement of nonlinear optical parameters. The technique developed by Bahae et al., helps to evaluate both nonlinear refractive index and absorption coefficient (Sheik-Bahae et al., 1989; Sheik-Bahae et al., 1990). In their first report Bahae et al. has proposed the method of calculation of sign and magnitude of nonlinear refractive index (Sheik-Bahae et al., 1989). The subsequent publication in 1990 explains the method to calculate the nonlinear absorption coefficient, refractive index and hence the third order nonlinear optical susceptibility. Z-scan focuses a Gaussian beam to the sample and measures the output transmittance as a function of sample position. It can be used in two ways; with and without using an aperture before the output detector. If the aperture is placed before the detector, the technique is named closed aperture Z-scan and it measures the nonlinear refractive index of the material. When the aperture is not used, the open aperture Z-scan measures the nonlinear absorption coefficient. The technique is explained in detail with supporting theory in Chapter 2.

Since the invention of Z-scan technique, substantial investigations have been carried out on numerous materials to calculate their third and fifth order nonlinear optical parameters (Zhang et al., 2007; Kong et al., 2009; Pramodini et al., 2014b; Kole et al., 2014). The tremendous interest created by Z-scan technique lies in its

convenience in terms of experimentation and data analysis. Moreover the data analysis provide an appropriate way to calculate the nonlinear absorption coefficient and refractive index independently. These values can be used to calculate the real and imaginary part of third and fifth order nonlinear optical susceptibility, which are complex quantities.

1.5. Applications of nonlinear optics

Nonlinear optics is a broad field of research and technology that contribute to diverse fields like physics, chemistry, biology and engineering. Depending on the different order of nonlinear optical processes, their applications also differ. Second harmonic generation (SHG) is a second order nonlinear optical effect having large number of applications. Second harmonic generation can be fulfilled in nanoparticles since they break their inversion symmetry whereas the bulk material is centrosymmetric. SHG effect is utilized mainly in optical computing and communication. Applications of SHG in waveguides include the efficient generation of UV light for read/write processes in high memory optical storage devices as well as optical modulators for far infrared optical sources. Frequency doubling of semiconductor lasers for optical data storage application can be done through SHG. SHG experiments are also utilized in getting information of the molecular orientation of smaller non centrosymmetric units. SHG and sum frequency generation (SFG) from isotropic or centrosymmetric media can be developed into powerful and versatile probes of surfaces and interfaces, to understand molecular arrangement, orientation, and reactivity at buried interfaces, without any difficulty (Miragliotta, 1995; Garmire, 2012).

Sum and difference frequency generation are also second order optical nonlinearities. The technological significance of these processes is in generating coherent radiation at new frequencies that are not usually available with lasers. The generation of such new frequencies is necessary for spectroscopy, remote sensing,

optical radar, and various other applications. Optical parametric generation is a key element in studying some fundamental properties of quantum mechanics, such as the observation of correlated quantum states. Parametric devices have been used to generate a non classical form of radiation called squeezed light (Sutherland, 2003).

Third harmonic generation is a third order nonlinear optical process and has been utilized in diverse fields from image processing to microscopy (Yelin and Silberberg, 1999; Fuentes-Hernandez et al., 2009).

Nonlinear absorption is a nonlinear optical process by which the transmittance of a material increases/decreases with increase in incident laser intensity. Materials exhibiting NLA have applications depending upon the nature of their nonlinear absorption. Materials exhibiting saturable absorption (SA) are widely used for optical switching applications (optical bistable devices). Such materials are used for optical data storage applications. Reverse saturable absorption (RSA) is a nonlinear optical mechanism by which materials exhibit a decrease in transmittance as the intensity/fluence of incident laser pulses increases above a certain threshold. Materials exhibiting RSA have applications in the area of laser protection coatings, optical pulse processing and computing (Tutt and Boggess, 1993; Beecroft and Ober, 1997; Mathews et al., 2007; Wang et al., 2009; Naseema et al., 2010; Tuhl et al., 2012;). The combination of SA and RSA materials can be used for laser pulse compression and mode locking (Reddy, 1991). This combination is also proven to be acting as optical diodes (Philip et al., 2007; Anand et al., 2013).

Materials exhibit intensity dependent refractive index, which is also a third order nonlinear optical effect named as nonlinear refraction. This effect occurs through a modulation of the phase or amplitude of an intense optical wave propagating through a nonlinear medium. Materials of nonlinear refractive index have great scientific and technological interest because of their significant applications in the fields of nonlinear spectroscopy, optical logic gates, optical data

processing, passive laser mode locking, and waveguide switches and modulators. Another third order nonlinear optical effect is stimulated Raman scattering (SRS), which is utilized in the development of tunable lasers. Materials exhibiting SRS are also useful in high energy pulse compression (Garmire, 2012).

1.6. Nonlinear optical materials

Nonlinear optical materials have great importance because of their applications in optoelectronics, communication and industry. Several organic crystals, nanoparticles of metals and semiconductors, organic compounds, materials of carbon family like carbon nanotubes, fullerene, graphene are reported as NLO materials (Munn and Ironside, 1993; Bredas et al., 1994; Nalwa, 1999). Even hybrids of metal-metal, semiconductor-semiconductor, organic-inorganic materials and several other compounds are being experimented over the years and are proven to be having nonlinear optical behaviour. Other than these materials in colloidal or powder form, fabricating films of these materials maintaining their NLO behaviour, is also attempted by many research groups (You et al., 2006; Irimpan et al., 2008a; Wang et al., 2009).

Among these, zinc oxide (ZnO) and multiwalled carbon nanotubes (MWNTs) are two important NLO materials which exhibit considerable nonlinear absorption. So fabrication of nonlinear absorbers using ZnO and MWNTs, maintaining optical transparency is advantageous with regard to photonic applications. In this regard, polymer nanocomposite films are appreciable because the films fabricated from composites of suitable polymers and nanofillers itself act as photonic devices.

1.6.1. Polymer nanocomposites

The word “nanocomposite” is defined as composite in which at least one of the phases shows dimensions in the nanometer range (Roy et al., 1986). Polymer nanocomposites (PNCs) comprise of nanosized filler domains finely dispersed in a

polymer matrix. Molecular interaction between the polymer and the nanoparticles help the nanoparticles to exhibit enhanced properties in terms of their dispersion, optical, electrical, thermal and mechanical properties. Depending upon the application of the polymer nanocomposites, the polymer matrix and the nanoparticle inclusions can be selected. The main advantage of using polymer nanocomposites is that these composites can be prepared by varying, the matrix and inclusion parameters in different ways. Varying the inclusion parameters like size, shape and fraction and the matrix parameters like their molecular weight, viscosity, conductivity and transparency dramatic changes can be introduced in the properties of the resultant composites. The combination of organic and inorganic materials results in composites having advantages of both organic polymers (flexibility, transparency, ductility, dielectric) and inorganic components (rigidity, high thermal stability, strength, hardness, high refractive index, high optical properties).

There are various methods for the preparation of polymer nanocomposites which include solution mixing, melt processing, emulsion polymerization and *in situ* polymerization. In solution mixing, the polymer and the nano inclusions are dissolved in the same solvent and are mixed together to form the PNC. Melt processing includes melting of the polymer and adding inclusions to the melt polymer. In the case of *in situ* polymerization, the composite is obtained by polymerizing the monomer containing nanofillers in it whereas in the case of emulsion polymerization, the monomer enters the micelles and undergoes polymerization inside them.

Polymers like polyethylene (PE), polyamides, polyimides, polyvinyl alcohol (PVA), polyvinyl chloride (PVC), etc. are commonly utilized as matrices for polymer nanocomposite preparation. Based on the applications, the matrices used for the preparation of PNCs can be categorized as industrial plastics (nylon 6, nylon MXD6, polyimide, polypropylene (PP)), conducting polymers (polypyrrole, polyaniline (PANI)), and transparent polymers (polymethyl methacrylate (PMMA), polystyrene (PS), polyvinyl pyrrolidone (PVP)) (Li et al., 2010).

The various inclusions reported in the preparation of polymer nanocomposites are nanoparticles of metals (Ag, Au, Pt, Cu, Co, Ge, Pt and Fe), semiconductors (ZnO, TiO₂, SiO₂, Ge, Si, ZnS, PbSe, PbS, CdS, CdSe and CdTe), clay minerals (montmorillonite, vermiculite, hectorite and CaCO₃) and carbon based materials (SWNT, MWNT, graphite, etc.). Polymer nanocomposites for optical applications have been prepared with various nanofillers and transparent polymers. In most of the investigations, the nanofillers and polymers are selected in such a way that the nanofillers provide the desired property, whereas the matrix helps to enhance these properties by proper dispersion, in addition to maintaining optical transparency.

Polymer nanocomposites of metal nanoparticles have been reported to be useful as sensors (Atmeh et al., 2011) and for sub wavelength imaging (Wu et al., 2014). Polymer-semiconductor nanocomposites are also enormously reported for applications like UV absorption (Nussbaumer et al., 2003), light emitting diodes (Willander et al., 2011) and photocatalysis (Mukherjee et al., 2013).

Optical transparency is a requirement for polymers to be useful for optical applications. Usually amorphous polymers are transparent in nature whereas crystalline polymers are not. Polymer nanocomposites prepared from transparent polymers and inorganic fillers have applications in optical coatings for UV protection, laser protection and many more photonic applications (Srivastava et al., 2008; Tu et al., 2010; Zhang et al., 2013).

Transparent polymers

Polymethyl methacrylate (PMMA) is an amorphous thermoplastic with considerable optical transparency even after fabricating into film. PMMA can be prepared from its monomer methyl methacrylate, via free radical, suspension and bulk polymerization techniques. The glass transition temperature of PMMA is approximately 105 °C. Polymer nanocomposites of PMMA with organic and

inorganic nanoparticles are reported to be useful for applications like UV shielding (Anžlovar et al., 2008) biomedical (Lopes et al., 2009), THz applications (Macutkevic et al., 2012) and nonlinear optical applications (Sun et al., 2014).

Polystyrene (PS) is an amorphous polymer. It is one of the few polymers that can be prepared from its monomer styrene by radical, ionic, and bulk polymerization. Polystyrene is extensively used as disposable plastic materials, CD and DVD cases, smoke-detector housings, etc. The glass transition temperature for polystyrene is 100 °C. Below T_g, amorphous polystyrene is brittle, rigid, and hard whereas above T_g, it behaves like rubber or viscous liquid. Polymer nanocomposite of polystyrene with inorganic/organic materials has been reported for applications involving photocatalysis (Zan et al., 2004), UV shielding (Tu et al., 2010), photonics applications (Jeeju et al., 2012), antibacterial materials (Palomba et al., 2012) and in photoconductivity (Chaudhuri et al., 2013). PS is selected as another matrix for the preparation of polymer nanocomposite films in the present study.

1.6.2. ZnO nanoparticles

ZnO is a captivating material for the scientific community owing to its viability in tuning the properties which facilitates its utilization in a wide range of applications from UV protection to optoelectronic device fabrication (Schmidt-Mende and MacManus-Driscoll, 2007; Willander et al., 2008). ZnO is widely used in many fields including paints, cosmetics, pharmaceuticals, plastics, batteries, electrical equipment and textiles. Early literatures say that ZnO have been known from 1912 and W. L. Bragg has elucidated the crystal structure of wurtzite ZnO shortly after the invention of X-ray diffraction (Ellmer et al., 2008).

ZnO crystallizes in the wurtzite structure, cubic zinc blend and rocksalt structures. Wurtzite structure (Figure 1.8) is a hexagonal lattice characterized by two interconnecting sublattices of Zn²⁺ and O²⁻, such that each zinc (Zn) ion is surrounded

by tetrahedra of oxygen (O) ions, and vice versa. ZnO has an inherent polar symmetry along the hexagonal axis due to its tetrahedral coordination and this enables it to possess spontaneous polarization and various kinds of defects (Coleman and Jagadish, 2006). The bandgap of bulk ZnO has been calculated by many and is reported to be 3.3 - 3.4 eV (Mang et al., 1995; Wang, 2004).

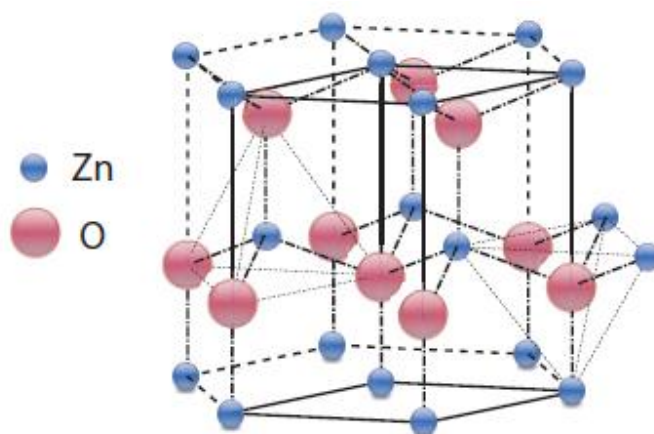


Figure 1.8 Wurtzite structure of ZnO (Lafrentz et al., 2013)

The different synthesis techniques for the growth of ZnO nanostructures with different morphology, growth mechanisms, properties and potential applications are discussed in several reviews (Wang, 2004; Özgür et al., 2005). The growth and morphology of ZnO nanostructures depend on several factors like reaction solvents, pH, concentration, reaction time, etc. (Cheng and Samulski, 2004; Amin et al., 2011). Wide variety of studies on electrical and optical properties of ZnO is available (Seitz and Turnbull, 1959). The investigation on ZnO has been recharged by the reports proving ZnO as a photonic material (Coleman and Jagadish, 2006). With the evolution of nanotechnology, ZnO has become an optical material whose properties are tunable by different synthesis routes (Fan and Lu, 2005; Kołodziejczak-Radzimska and Teofil Jesionowski, 2014).

A large number of studies have been carried out on the optical properties of ZnO nanostructures, which are based on synthesizing ZnO nanostructures especially

for optical applications (Guo et al., 2000; Sekiguchi et al., 2000; Yang et al., 2002; Xu et al., 2004; Makino, 2005; Maensiri et al., 2006; Sridevi and Rajendran, 2009; Peić et al., 2012;). ZnO nanoparticles of different morphologies are also reported to exhibit good optical properties (Pan et al., 2005; Tong et al., 2006; Peng et al., 2010). One of the important application for which ZnO is widely accepted and used is as a UV protection material. Technological applications involve the effort to fabricate UV protection coatings. Lima et al., reports the fabrication of transparent dip coated films which act as a UV protective coating (Lima et al., 2012). An interesting work by El-Hady et al. state that coating with ZnO improved the UV protection property of cotton/polyester fabrics (El-Hady et al., 2013).

The emissive nature of ZnO has been explored by many researchers. Yang et al., reports the enhanced UV emission from surface modified ZnO nanostructures whereas green emission is quenched (Yang et al., 2001). This is due to the surface passivation of defects states by the polymer, coated on the surface of ZnO nanoparticles by surface modification. Other reports reveal that the geometry and size of the ZnO nanoparticles also affect their emissive nature (Enculescu et al., 2007; Ábrahám and Dékány, 2010). There are several efforts carried out to study the defect related emission of ZnO in order to use it as an emissive material for light emitting diode fabrication (Saito et al., 2002; Leiter et al., 2003; Li et al., 2004; Antony et al., 2005; Zubiaga et al., 2006; Han et al., 2012). ZnO nanoparticles are very good nonlinear optical material, exhibiting considerable nonlinear absorption and refraction (Irimpan et al., 2008b; Kumari et al., 2011) and hence are useful for applications like optical limiting, bistable devices and Q-switching.

1.6.3. Multiwalled carbon nanotubes

Carbon nanotubes (CNTs), discovered by Iijima has attained considerable attention for the past few years due to their unique electronic, thermal, optical and mechanical properties (Iijima, 1991; Treacy et al., 1996; Tans et al., 1997; Scarselli et

al., 2012). Carbon nanotubes have been recognized as the stiffest and strongest man-made material and since their discovery; CNTs have been used mostly as a reinforcing material by preparing polymer composites for mechanical applications.

Carbon nanotubes form in two categories: single walled nanotubes (SWNTs) and multiwalled carbon nanotubes (MWNTs) as shown in Figure 1.9. The single walled nanotubes has single layer graphite cylinder extending from end to end and possess good uniformity in diameter. The multiwalled carbon nanotubes are made of concentric cylinders placed around a common central hollow, with spacing between the layers close to that of the interlayer distance in graphite (Ajayan, 1999).

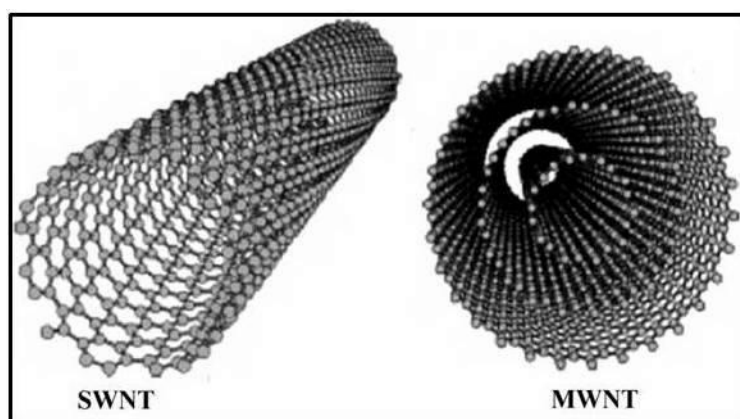


Figure 1.9 SWNTs and MWNTs

Different from other carbon materials, like graphite, fullerene, diamond etc., CNTs have an aspect ratio greater than 1000 which enable them for applications in a wide range of areas. However this high aspect ratio makes them prone to entanglement and bundling also. CNTs are bundled with strong van der Waals interaction energy of tube–tube contact (Girifalco et al., 2000). Dispersion and processing of CNTs is made challenging by such high interaction energy. In order to achieve dispersed nanotubes, mechanical and chemical treatments can be carried out. The mechanical treatments include ultrasonication of nanotubes in suitable solvent. This method have some advantages like, the vigorous sonication causes shortening on

nanotubes and decrease their aspect ratio. In some cases it is reported that the nanotubes dispersed during sonication, settle down after sometime. The chemical modification of nanotubes involves noncovalent and covalent functionalisation methods. Noncovalent functionalisation uses polymers, aromatic molecules and bio molecules to modify the surface of the nanotubes. Covalent functionalisation mainly includes the carboxylation of nanotubes by treating with acids. The covalently attached moieties change the chemical, optical and electrical properties of the CNTs (Chen et al., 2011). The different types of functionalisation techniques adopted over the years and the resultant properties of nanotubes are discussed in quite a lot of reports (Kuzmany et al., 2004; Liu, 2005; Panchakarla and Govindaraj, 2008; Ma et al., 2010).

The nonlinear optical properties of MWNTs are influenced by several factors like, the aggregation of nanotubes, bundle size, solvent used to disperse them, the wavelength of the laser source and so on. Investigations on the nonlinear optical properties of MWNTs are available in literature, trying to increase their NLO activity by modifying the nanotube surface by different methods (Chen et al., 2007; Vivien et al., 2002).

Since ZnO nanoparticles and carbon nanotubes are excellent nonlinear optical materials, combining these two materials is expected to bring forth properties of both the materials, in fact enhance them. A hybrid of ZnO and MWNT synthesized *in situ* is expected to exhibit enhanced nonlinear absorption compared to mixing the two materials together. In view of this, reports on the synthesis of ZnO/CNT for diverse applications are available (Skandani et al., 2012; Ahmad et al., 2013; Chen et al., 2013) but few works are done in synthesizing this hybrid for nonlinear optical applications (Zhu et al., 2006). In addition to that since films can serve as a unique entity, transparent polymer nanocomposite films of the ZnO/MWNT and their individual components is expected to exhibit considerable nonlinear optical properties.

1.7. Scope and Objectives of the Thesis

The above mentioned detailed review leads to a conclusion that fabrication of nonlinear optical materials in the form of films is as important as its synthesis due to the enormous requirement and applications of these materials. The aim of the present study is to fabricate polymer nanocomposite films for nonlinear optical applications, especially for applications involving nonlinear absorption.

The main objective of this study can be summarized as follows.

1. Synthesis of ZnO nanoparticles by solution precipitation technique and characterization of the material by spectroscopic and microscopic techniques.
2. Study the linear and nonlinear optical properties of the ZnO nanoparticles.
3. Synthesize polymer nanocomposites of ZnO nanoparticles with PMMA and fabricate films using spin and dip coating techniques.
4. Optimize the film fabrication parameters to get transparent polymer nanocomposite films with nonlinear absorption property.
5. Fabrication of polymer nanocomposite films to study the influence of dispersing agent, polymer matrix, nanoparticle loading concentration and the incident fluence of the films on their optical nonlinearity.
6. Synthesis of hybrids of ZnO nanoparticles with functionalized multiwalled carbon nanotubes and characterization of the materials by spectroscopic and microscopic techniques.
7. Study the linear and nonlinear optical properties of the hybrid materials.
8. Synthesize polymer nanocomposites of hybrid materials with optimized polymer matrices and fabricate films.
9. Study the linear and nonlinear optical properties of the polymer nanocomposite films of hybrids.

1.8. Organization of the Thesis

The thesis is categorized into seven chapters as follows.

The first chapter gives a general idea on the concept of nonlinear optics and its basics. The chapter details the various NLO processes and their mechanism in different materials. The techniques used for measuring the parameters associated with each nonlinear process are explained. The applications of various nonlinear optical processes in science and technology are reviewed. A note on ZnO nanoparticles and carbon nanotubes and their applications are also given. An idea on polymer nanocomposites and their applications in optical and other fields are discussed. The scope and objective of the thesis is also mentioned in the last section.

Experimental technique used for the present study is detailed in Chapter 2. The synthesis technique for ZnO nanoparticles and ZnO/MWNTs is described. The preparation of polymer nanocomposites and the fabrication technique for preparing films is also explained. The characterization techniques used in the present investigation are discussed with the support of necessary theory. The last part of the chapter describes the process of nonlinear absorption in detail. Various mechanisms and measurement techniques reported for nonlinear absorption are narrated with adequate theoretical support. The open aperture Z-scan technique is explained with the procedure used for giving the experimental data, a theoretical fit.

Chapter 3 narrates the detailed procedure used for the synthesis ZnO nanotops. The nature of nonlinear response of the synthesized nanoparticles is studied in detail. This chapter also gives an outline of the optimization of film fabrication using polymer nanocomposite. Effect of fabrication parameters on optical nonlinearity of the films is also studied in particular.

Chapter 4 describes the fabrication of polymer nanocomposite films of PMMA and ZnO nanotops prepared with the help of a dispersing agent. It deals with

the studies on the role of dispersing agents to maintain a dispersed uniform composite medium and fabrication of films thereafter for applications involving nonlinear absorption.

Chapter 5 explores the role of matrix used in the preparation of polymer nanocomposite films in absorptive nonlinearity of the polymer-ZnO nanotop composite films. Transparent matrices like PMMA and a blend of PS and PMMA are used as polymer matrices. Nonlinear absorption nature of the films is studied experimentally and the results are analyzed.

Chapter 6 brings forth the details of functionalisation of MWNTs, PNC film fabrication and their nonlinear optical studies. Synthesis of hybrids of ZnO nanoparticles with functionalized MWNTs is specified. Film fabrication of polymer nanocomposites of the hybrid and their characterization is discussed in detail. The tuning of nonlinearity of the synthesized hybrid by fabricating films with different polymers is also dealt with. The analysis of the mechanism behind the exhibited nonlinearity is also carried out.

The final chapter concludes with all the results obtained from the present study along with the directions for further explorations on the present investigation.

CHAPTER 2

EXPERIMENTAL TECHNIQUES

Experimental techniques used for the present study are explained explicitly in this chapter. Techniques regarding synthesis, composite preparation, spectroscopic and microscopic techniques for characterizing the samples in the present investigation are explained in detail. The last section of the chapter brings forth the various techniques to measure optical nonlinearity of the sample, with a special note on Z-scan technique. Various mechanisms reported for exhibiting nonlinear absorption is also explained with necessary theory.

2.1. Synthesis methods

The synthesis routes adopted for preparing nanoparticles play a critical role in determining their properties and applications. Depending on the synthesis routes, nanoparticles of different size and shape can be prepared, which in effect influence their linear and nonlinear optical properties. Because of the tremendous interest in ZnO nanoparticles owing to their diverse applications, a large number of literatures are available on the synthesis of these nanoparticles. Most of the reports in this regard focus on hydrothermal, solvothermal and microwave assisted synthesis methods (Cho et al., 2008; Sridevi and Rajendran, 2009). Other reports involve preparation by spray pyrolysis, vapour deposition techniques, epitaxial techniques, and laser deposition techniques (Özgür et al., 2005). Solution based synthesis methods are also available in the literature (Kołodziejczak-Radzimska and Jesionowski, 2014). Whereas MWNTs is another awesome material suitable for optical applications though most of the researches focus on their mechanical properties. A combination of ZnO nanoparticles and MWNTs has been utilized for applications like photocatalysis and dye sensitized solar cells (Chang et al., 2012; Chen et al., 2013). ZnO nanoparticles and MWNTs exhibit good nonlinear optical properties in colloidal form

and film form (Chan et al., 2008; Chattopadhyay et al., 2009; Lin et al., 2005; Wang et al., 2009). The combination of these two materials synthesized as a hybrid, is therefore expected to exhibit enhanced properties compared to their individual components. A general view of the methods adopted for the synthesis of ZnO nanoparticles and the hybrid of ZnO nanoparticles with MWNTs is given in the section below. The detailed synthesis procedure for ZnO nanoparticles and the hybrid are explained in chapter 3 and 6 respectively.

2.1.1. ZnO

In the present study, Zinc Oxide (ZnO) nanoparticles are synthesized using solution precipitation technique. The precursor used is zinc acetate salt. The salt along with a capping agent, polyvinyl pyrrolidone (PVP), is dissolved in acidic medium (acetic acid) with continuous stirring. The precursor complex formed with the capping agent is precipitated to ZnO nanostructures using NaOH in millimolar concentration. The synthesis is repeated by using another capping agent, polyethylene glycol (PEG). The precipitate is filtered, washed and dried in vacuum oven.

2.1.2. ZnO/MWNT

In the present investigation, pristine MWNTs are acid treated using nitric acid for the incorporation of carboxy groups on nanotubes. The acid treated nanotubes are used for hybrid synthesis. Two types of hybrids are synthesized. In both cases PVP is used as the capping agent. In the first method, nanotubes dispersed in acetic acid is mixed with zinc acetate - PVP complex and ultrasonicated well. Several sets of such precursors are prepared by varying the loading concentration of MWNTs in the reaction mixture, in order to find the maximum loadable amount of MWNTs without aggregation. The precursors are then precipitated using millimolar NaOH. The precipitates are washed and dried to get the hybrid powders. In the second method, a hybrid of ZnO nanoparticles is synthesized with the nanotubes dispersed in PVP, instead of acetic acid.

2.2. Preparation of polymer nanocomposites

Polymer nanocomposites are prepared using *in situ* bulk polymerisation technique. Two types of nanocomposites are prepared; with and without using a dispersing agent. In the first method, the nanoparticles are dispersed in monomer by ultrasonication. The monomer-nanoparticle dispersion is then polymerized using benzoyl peroxide (BPO) as initiator. The reaction is kept in oil bath to control the temperature and the reaction time is monitored at time intervals. In the second case, the nanoparticles are first dispersed in two types of dispersing agents (oleic acid and triton) and then mixed with the monomer. Using BPO, the dispersion is polymerized to get the polymer nanocomposite.

2.3. Fabrication techniques

The limitations in incorporating solution/dispersion of nanoparticles with excellent properties into devices enhance the demand for films of these nanostructures. Optical transparency of these films is an important factor with regard to linear and nonlinear optical applications. The fabrication of semiconductor nanoparticles especially ZnO, has been carried out by several techniques for making them technological materials. The techniques reported for the fabrication of thin film of ZnO for optical applications include Chemical Vapour Deposition technique (CVD), R F sputtering, spray pyrolysis, Molecular beam epitaxy (MBE), Pulsed Laser Deposition (PLD) etc. There are techniques like, screen printing (Ismail et al., 2001), drop casting (Irimpan et al., 2008a) and doctor blading (Dumbrava et al., 2013) which are used for fabricating films from solution/sol/dispersion of ZnO.

Polymer nanocomposite films fabricated from polymer matrix and nanoparticle inclusion are also reported for optical and nonlinear optical applications. The usual techniques used for the fabrication of such films are solution casting, spin coating and dip coating technique, doctor blading etc. (Krishnakumar et al., 2012;

Kulyk et al., 2009; Pasquarelli et al., 2011; Ribeiro et al., 2014; Srivastava et al., 2008).

2.3.1. Solution casting

Solution casting is one of the simplest techniques to fabricate films of polymer nanocomposites. In this technique, the composite is dropped on a cleaned substrate and is allowed to dry as shown in Figure 2.1. It is possible to prepare thick films using this technique but the control over the thickness is a difficult issue. Sometimes on drying there are chances of precipitation of the solution at the edges of the substrate. The advantage is that no equipment is needed apart from a horizontal work surface.

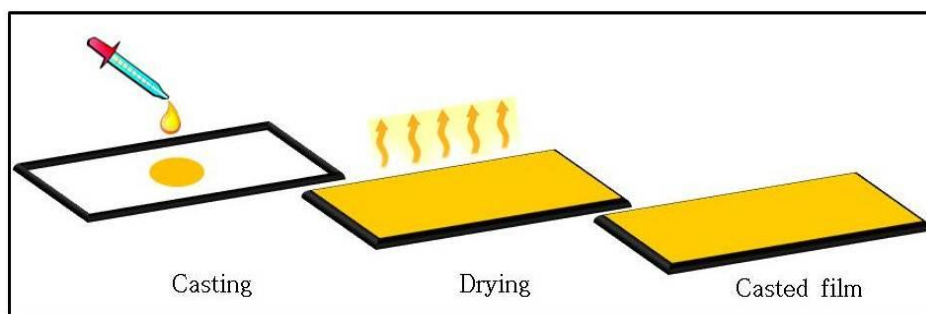


Figure 2.1 Method of solution casting

2.3.2. Doctor blading

In this technique, a sharp blade is placed at a fixed distance from the substrate surface that is to be coated. The coating solution is then placed in front of the blade that moved linearly across the substrate as shown in Figure 2.2. The motion leaves a thin wet film after the blade. The film is then dried. The doctor blading technique is relatively slow and the chances of the dissolved material to aggregate at high concentration are more in this technique.

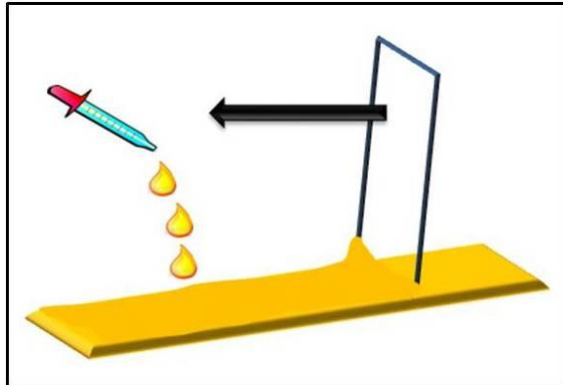


Figure 2.2 Method of doctor blading

2.3.3. Screen printing

In this technique, first a screen of woven material is glued to a frame under tension. The pattern is obtained by filling the screen with the desired solution in the areas where no print should appear. The area of the printed pattern is kept open. The screen is then filled with coating solution and brought into proximity of the substrate. A so called squeegee is forced into the screen bringing it in contact with the substrate and then drawn linearly across the screen. This motion forces the coating solution to go through the open areas onto the surface of the substrate. The process of screen printing is shown in Figure 2.3 (Pasquarelli et al., 2011).

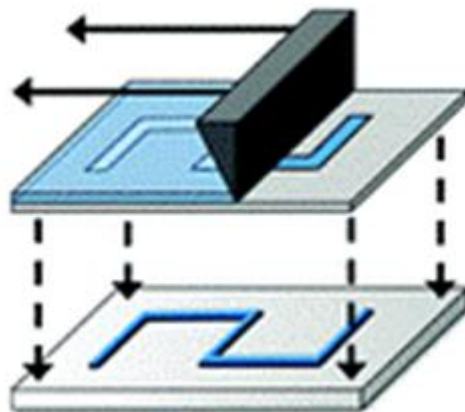


Figure 2.3 Method of screen printing

2.3.4. Dip coating technique

Dip coating technique (Brinker et al., 1994) is a well known technique for coating sol on to a substrate. Figure 2.4a shows a dip coating unit used for the present study along with a schematic (2.4b) of the process of dip coating technique.

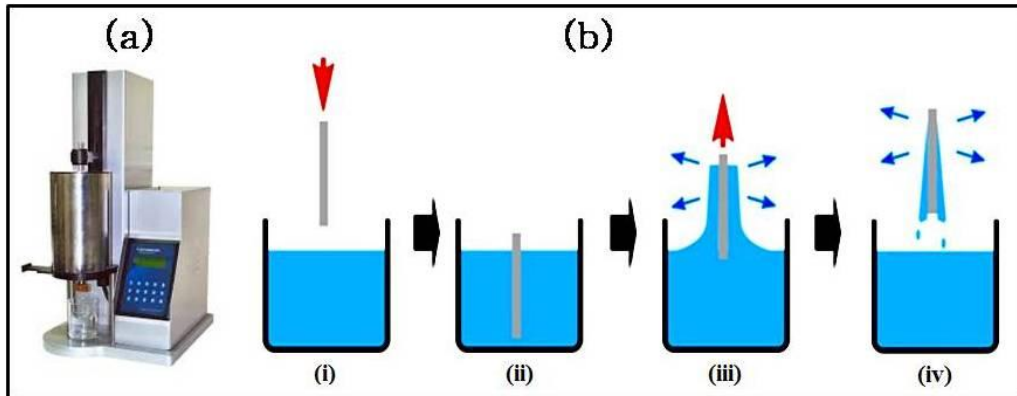


Figure 2.4 (a) Dip coating unit (b) Schematic of dip coating process

As shown in Figure 2.4, the sol to be coated is taken in suitable glassware. The substrate is fixed on a groove and is dipped into the sol at a constant speed. Keeping the substrate for an appropriate time in the sol, helps to adhere the sol on the surface of the substrate. The substrate is then withdrawn from the sol at a constant rate. Some amount of the sol drips back into the container and the rest of the sol is adhered on the substrate, depending upon the viscosity and the retrieval speed of the dip coating unit. The dipping and retrieval speed and the dipping duration are controlled with the help of software. The film is then dried and multilayer coating can be done by repeating the above process. The microstructure and properties of the film depend on the size and structure of the sol species, the magnitude of the capillary pressure exerted during drying and the relative rates of condensation and drying.

2.3.5. Spin coating technique

The spin coating unit used for fabrication in the present investigation is shown in Figure 2.5(a).

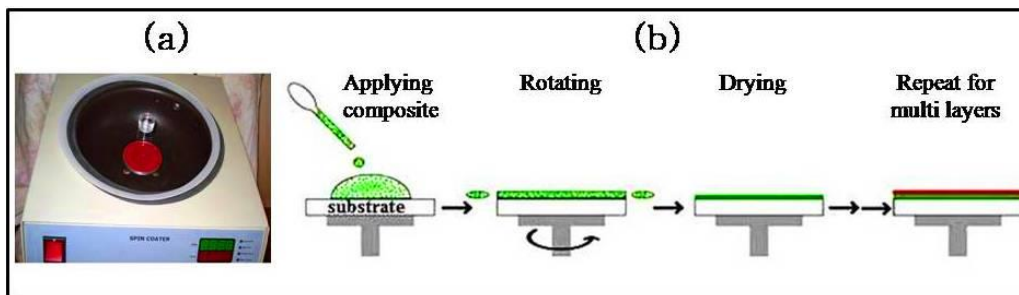


Figure 2.5 (a) Spin coating unit (b) Schematic of spin coating process

The process of spin coating involves depositing a small puddle of a sol on the centre of a substrate and then spinning the substrate at high speed (Figure 2.5b). Centripetal acceleration causes the sol to spread to, and eventually off, the edge of the substrate leaving a thin film on the surface. Final film thickness and other properties will depend on the nature of the sol (viscosity, drying rate, percentage of solids, surface tension, etc.) and the parameters chosen for the spin process. Factors such as final rotational speed and acceleration contribute to the properties of the coated films. One of the most important factors in spin coating is ease in repeatability. Subtle variations in the parameters that define the spin process can result in drastic variations in the coated film (Hall et al., 1998).

Among these techniques spin coating and dip coating techniques provide an efficient way for the fabrication of thin films.

2.4. Characterization techniques

A complete analysis of the nanoparticles and the polymer nanocomposite films are performed to analyze their structural, morphological, thermal and optical properties. There are several tools by which the study can be carried out. In the present study, spectroscopical, microscopical and thermal analyses have been carried out on all the samples.

X-ray diffraction (XRD) pattern of the nanoparticles are used to analyze the crystallinity of the synthesized particles and also for calculating their size. UV-visible absorption spectroscopy and fluorescence spectroscopy are used to characterize the nature of light absorption and emission of the samples. Fourier transform infrared spectroscopy (FTIR) and Raman spectroscopy are performed to study the chemical structure and the nature of defects present in the nanotubes and hybrid samples. Microscopic techniques like Scanning Electron Microscopy (SEM) and Transmission Electron Microscopy (TEM) are used to analyse the morphology of the samples. The thermal stability of the samples are carried out by using Thermogravimetric Analysis (TGA). Thickness and surface analysis of the film samples are measured by White Light Interferometric technique.

2.4.1. Spectroscopic techniques

2.4.1.1. X-ray Diffraction (XRD)

X-ray diffraction is a widely applied tool for material characterization. Usually crystalline materials (solid or powder) are analyzed using this technique to understand their crystallographic structure, crystallite size and preferred orientation of the crystal planes. This is because, crystalline materials act as three dimensional diffraction gratings for X-rays. X-ray diffraction studies are carried out by illuminating the sample with monochromatic X-rays. The interaction of X-rays with the crystal lattices of the sample produces diffraction pattern (Cullity et al., 1978). The constructive interference of X-rays from the different atomic planes of the crystals has been formulated by W. L. Bragg and the Bragg's law of diffraction is represented as (Bragg, 1912),

$$n\lambda = 2d \sin \theta \quad (2.1)$$

where n is an integer describing the order of reflection

λ is wavelength of X-ray

d is the interplanar spacing

θ is the Bragg angle at which diffraction maximum occurs

Each material gives well defined peaks characteristic of its crystal structure. The size of the crystallites can be calculated from the broadening of the peaks using Debey-Scherrer formula (Cullity et al., 1978),

$$d_c = \frac{0.9\lambda}{K_{2\theta} \cos \theta_B} \quad (2.2)$$

θ_B is the Bragg angle

d_c is the mean dimension of the crystal size

$K_{2\theta}$ is the FWHM on the 2θ scale in radian

The powder method of X-ray diffraction is devised independently in 1916 by Debye and Scherrer in Germany and in 1917 by Hull in the United States. X-ray diffraction pattern is recorded using X-ray diffractometer in which monochromatic X-ray beam is used to examine polycrystalline specimens. The beam gets diffracted from the sample and the equipment records a spectrum of diffraction intensity versus the angle between incident and diffraction beam. This is done by continuously changing the incident angle of the X-ray beam. The resultant data is analyzed by comparing with a database of known crystalline substances (Cullity et al., 1978).

In the present work, X-ray Diffraction (XRD) analysis of the synthesized ZnO nanotops and ZnO/MWNT samples in powder form, are performed with a Bruker AXS D8 Advance X-ray diffractometer using Cu K_α ($\lambda=1.54 \text{ \AA}$).

2.4.1.2. UV-vis absorption spectroscopy

Molecules undergo electronic transitions on irradiating with electromagnetic radiation in the ultraviolet (UV) and visible range to near infrared (NIR). In other words, electrons of the molecules in the ground state absorb energy from the radiation and jumps to an excited state. These electronic transitions can be studied by using UV-vis absorption spectroscopy. UV-vis absorption spectrometer is equipped with sources for producing UV and visible light which will be used to excite the sample molecules. The wavelength at which the sample absorbs the maximum is recorded as

peaks represented as λ_{\max} . Deuterium discharge lamp is generally used as source for UV radiation whereas tungsten lamp is used for visible and NIR radiation.

The data is analysed using Beer-Lambert Law. Beer's law states that absorption is proportional to the number of absorbing molecule. For dilute solutions, the number of absorbing molecules indicates the concentration of absorbing molecules. According to Lambert's law, the fraction of radiation absorbed is independent of the intensity of the radiation. Combining these two laws, the absorbance of the solution is given by,

$$\log_{10} \frac{I_0}{I_t} = \epsilon_m l c_m \quad (2.3)$$

where I_0 is the intensity of incident radiation

I_t is the intensity of transmitted radiation

ϵ_m is molar extinction coefficient

l is the path length of the absorbing solution

c_m is the concentration of the absorbing species

In the present work, the UV-vis absorption spectra of ZnO nanoparticles, MWNTs and hybrid nanoparticles are taken by dispersing these nanoparticles in methanol and taking pure methanol as reference. The absorption of the composite films is measured by using pure polymer films as reference. The spectra are recorded on a Varian Cary Bio 100 UV Spectrophotometer at room temperature in the wavelength ranging from 210 nm to 600 nm.

2.4.1.3. Photoluminescence spectroscopy

Luminescence is the emission of light from any material, and occurs from electronically excited states. When the material is excited with radiation of suitable wavelength, electrons in the lowest vibrational energy absorb photons to undergo transition to higher vibrational levels. Return of the excited electrons to the ground state is associated with the emission of photons which can be recorded by a

fluorescence spectrometer. Most of the spectrofluorimeters record both excitation and emission spectra. An excitation spectrum is recorded by exciting the material over a range of excitation wavelength and measuring the emission intensity at a single wavelength. The fluorescence emission spectrum is recorded as a plot of fluorescence intensity versus wavelength or wavenumber, exciting at a single wavelength. Xenon lamp is generally used as source in a fluorescence spectrometer and photomultiplier tubes as detectors (Lakowicz et al., 1991).

Photoluminescence spectra of the synthesized nanoparticles in the present investigation are taken, using Jobin Yvon Fluorolog 3-11 spectrofluorimeter. All the samples are prepared as dilute solutions by dispersing them in methanol. The emission of films is measured with the help of a film holder, keeping at 60° to avoid the detection of the incident radiation.

2.4.1.4. Fourier transform infrared spectroscopy

Fourier transform infrared (FTIR) spectroscopy is used to analyze the structural properties of materials. In this technique, the source radiates IR energy which is directed to the sample. The absorption of infrared radiation occurs when the frequency of incident radiation matches with the frequency of vibration of molecules in the material under investigation. These vibrations cause the excitation of the molecule from a lower to higher vibrational level. The spectrometer records loss in the frequency of output radiation occurred due to absorption. Materials in solid, liquid or gas form can be analyzed using FTIR.

The instrument used for the present study is Perkin Elmer 100 FTIR spectrometer with diffuse reflectance accessory. The sample is analyzed over a spectral range of $4000 - 400 \text{ cm}^{-1}$ having scans repeated 32 times. The powder samples are made pellets using KBr for the measurement.

2.4.1.5. Raman spectroscopy

The phenomenon of inelastic scattering of light, first observed experimentally by Raman and Krishnan (Raman and Krishnan, 1928) is the basic mechanism of Raman spectroscopy. In this technique, sample is irradiated with a single frequency. Light interacts with the molecule and distorts the cloud of electrons and the nuclei. The energy will be then transferred either from the incident photon to the molecule or from the molecule to the scattered photon. Since this process is inelastic, energy of the incident and scattered photon will be different. These scattered radiations from the sample are detected. Usually a visible or NIR laser is used as source and CCD for detection of signal (Smith and Dent, 2005).

Raman spectroscopy is a valuable probe to analyze the sp^2 and sp^3 hybridizations of carbon atoms in carbon nanotubes and other carbon based materials. The technique helps to understand the electronic structure in carbon nanotubes and presence of defects. The first order Raman spectra corresponds to two bands - *D* band and *G* band, induced by double resonance process. The *D* band is usually attributed to the presence of amorphous or disordered carbon in the CNT samples whereas the *G* band originates from in-plane tangential stretching of the carbon- carbon bonds in graphene sheets. The increase in intensity of the *D* band is related to sp^3 hybridization of carbon and the increase in intensity of the *G* band is related to sp^2 hybridization. Usually the I_G/I_D ratio is taken as a measure of defect concentration (Datsyuk et al., 2008).

WiTech alpha 300 Raman system with 488 nm excitation is used in the study to record the spectra for the powder samples of MWNTs and hybrid.

2.4.2. Microscopic techniques

2.4.2.1. Transmission Electron Microscope (TEM)

Transmission electron microscopy is a tool for material imaging at submicrometer to atomic level. The technique uses electrons as probe. Electrons are first directed to the sample from an electron gun, with controlled intensity and angular convergence. Usually very thin samples are analyzed using TEM because transmission of the sample is an important factor here. The collision of the electron beam with the specimen results in directly transmitted electrons, backscattered electrons, secondary electrons, Auger electrons, etc. The transmitted electrons and the scattered electrons from selected areas of the specimen produce a diffraction pattern. The image formation is done by focusing of the electrons with magnetic lenses. The image formed is magnified and projected into a fluorescent screen (De Graef, 2003). The technique helps to study the structure and morphology of the specimen.

The morphology of the nanoparticles is characterized by FEI Quanta High Resolution 105 Transmission Electron Microscope (HRTEM). The samples are dispersed in methanol and placed on a grid of copper. After drying the sample in vacuum, images are taken.

2.4.2.2. Scanning Electron Microscope (SEM)

Scanning electron microscope also uses electrons for probing the specimen. The secondary electrons and backscattered electrons from the specimen are detected. The backscattered electron image gives an idea about the specimen composition and topography. The normal emission of secondary electrons is sometimes hindered by charging of the specimen, especially when nonconductive specimen is used. To prevent this, the nonconductive specimen is coated with conductive metal before scanning. For higher magnification and resolution, sample should be free of contamination. Reducing the electron probe diameter also helps to get high resolution images (Newbury et al., 1987).

The dispersions of the sample in methanol are prepared for SEM analysis. The dispersion is taken on a piece of carbon tape and after drying, gold sputtering is applied. The specimen is analyzed by using FEI Quanta FEG 200 high resolution scanning electron microscope.

2.4.3. Thermogravimetric analysis

The thermal stability of a material and hence the presence and fraction of volatile components in a specimen is analyzed, using thermogravimetric analysis. This is done by heating/cooling the specimen over a temperature range and monitoring the weight loss as a function of temperature. The measurement is normally carried out in air or in an inert atmosphere. The weight loss of the sample is monitored upto a maximum temperature at which the sample weight loss becomes stable. The thermogram obtained after scanning the entire range of temperature can be analyzed to get the percentage of weight loss at different temperatures.

The Thermogravimetric analysis in the present study is carried out in nitrogen atmosphere at a heating rate of 10 °C/min. The range of scan is from room temperature to 800 °C.

2.4.4. White light interferometry

White light interferometer is a measurement technique with high accuracy and long measurement range. The surface profile and thickness of thin films can be measured using white light interferometric technique. The interferometer usually consists of white-light source and the associated optics. The surface of the sample is illuminated with the source and multiple reflections are recorded by the instrument. The reflected light from the sample and the reference create interference fringes which are monitored.

Taylor Hobson Talysurf CCI profiler is used in the present study for analyzing the surface of the polymer nanocomposite films and measuring their

thickness. The CCI (Coherence Correlation Interferometer) is a type of scanning white light interferometer. Here, the incoming light from the source (LED) is split into two beams inside the CCI. One beam is directed to an internal reference surface and the other to the sample. After reflection the two light beams recombine inside the CCI, undergoing constructive and destructive interference and producing light and dark fringe pattern. The CCI algorithm is used to calculate surface topography from this fringe pattern. Films upto four layers and thickness upto 20 μm can be measured by using the equipment.

2.5. Nonlinear absorption : phenomena, mechanism and measurement techniques

2.5.1. Nonlinear absorption

The intense monochromatic radiation from a laser can induce profound changes in the optical properties of a material and can lead to processes like absorption, reflection, transmission or scattering of incident radiation. Nonlinear absorption refers to an intensity/fluence dependent change in transmittance of a material on exposure to intense radiation. The probability of a material to absorb more than one photon before it relaxes to the ground state, can be greatly enhanced by the presence of an intense radiation. Such high intense radiations are provided by lasers. Intense laser fields can induce materials to undergo population redistribution resulting in stimulated absorption, stimulated emission and generation of free carriers in the case of solids. Reduced or increased optical transmittance of materials give information about these kinds of phenomena occurring in them.

2.5.2. Mechanisms

Saturable and reverse saturable absorption

When matter absorbs radiation, the energy of the incident photon is absorbed by electrons of the atom. In most of the absorbing materials, the rate of absorption linearly increases with increase in input irradiance, giving rise to a constant output transmittance. This phenomenon is referred to as linear absorption and here the

absorption coefficient of the material is independent of the incident intensity. For linearly absorbing materials, the process is explained based on Beer-Lambert law,

$$I = I_0 e^{-\alpha_0 l} \quad (2.4)$$

where I and I_0 are the transmitted and incident intensity respectively. α_0 is the linear absorption coefficient of the material with a length or thickness l .

When a material deviates from this behaviour, the absorption of the material is said to be nonlinear. This nonlinearity is intensity/fluence dependent. In this scenario, the absorption coefficient of a material can be expressed as,

$$\alpha(I) = \alpha_0 + \beta I \quad (2.5)$$

where the effective absorption coefficient, $\alpha(I)$ becomes a sum of linear absorption coefficient, α_0 and an intensity dependent nonlinear absorption coefficient, β . This kind of behaviour of the material is due to the modification of its optical parameters with the interaction of incident light.

Depending primarily on the ground state and excited state absorption cross sections, materials behave either as saturable absorbers or reverse saturable absorbers. Saturable absorbers exhibit an enhanced transmittance at higher incident light intensities whereas reverse saturable absorbers exhibit a decrease in transmittance with intensity. In material systems saturable absorption becomes prominent when the incident intensity is high enough so that the ground state population is depleted and the population of the upper and lower states tends to equalize. On the other hand, effects like two-photon absorption, multiphoton absorption, excited state absorption, and free carrier absorption, or a combination of these, can cause reverse saturable absorption.

The intensity required to reduce the absorption of a material to one half of the linear absorption is called saturation intensity (I_{sat}). The intensity dependent absorption coefficient $\alpha(I)$ can be represented in terms of saturation intensity as,

$$\alpha(I) = \frac{\alpha_0}{1 + (I / I_{sat})} \quad (2.6)$$

$$\text{where } I_{sat} = \frac{\Delta E}{\sigma_g \tau} \quad (2.7)$$

In the above equation, τ represents the lifetime for the return of the population to the ground state or lifetime of the excited state. $\Delta E = \hbar\omega$, the energy difference between the ground state and the excited state. σ_g is the absorption cross section of the ground state.

Saturable absorbers are widely utilized in Q-switching and mode-locking to produce short and ultrashort laser pulses. They are also used for building bistable devices similar to a toggle switch or flip flop (Nie, 1993). Reverse saturable absorbers can be used as optical power limiters, laser protection coatings and molecular spatial light modulators (SLM) (Reddy, 1991).

Depending on the electronic structure of the system, nonlinear absorption can be mediated through many processes like, two photon absorption (TPA), three photon absorption, multi photon absorption, excited state absorption, free carrier absorption or a combination of these processes (Sutherland, 2003).

Two photon absorption

Two photon absorption (TPA) involves a transition from the ground state of a system (level G) to a higher-lying state (level E) by the simultaneous absorption of two photons from an incident radiation field. As seen in the schematic representation (Figure 2.6), two photons from the same optical field oscillating at frequency ω are absorbed by the material to make the transition. The intermediate state is not real; rather it is a virtual level (level V). Hence the system absorbs two photons simultaneously and makes the process sensitive to the instantaneous optical intensity. Two photon absorption is a third order nonlinear process. The impurities or defects

present in the system have a major role in this process. These impurities can help linear absorption and serves as an additional loss mechanism.

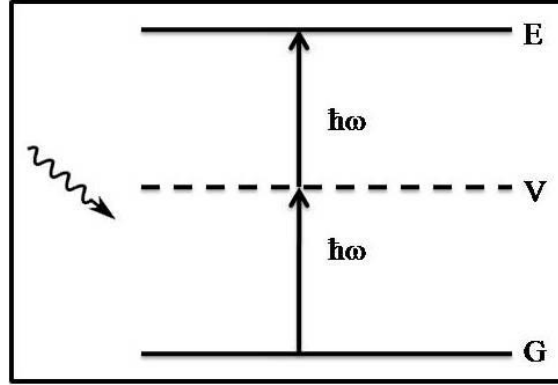


Figure 2.6 Process of two photon absorption

The optical loss on the propagation of a linearly polarized Gaussian beam of laser through the material can be represented as,

$$\frac{dI}{dz} = -\alpha_0 I - \beta I^2 \quad (2.8)$$

Here, α_0 is the linear absorption coefficient and β is the genuine two photon absorption coefficient. β depends on the number density of the molecules in the system, N . The two photon absorption cross section is given by,

$$\sigma_{TPA} = \frac{\hbar\omega\beta}{N} \quad (2.9)$$

where ω is the frequency of incident radiation.

The experimental measurement of nonlinear absorption mostly prefers the measurement of the output transmittance of the material. So the equation of propagation (2.8) is solved to get the transmittance of the material and is represented as,

$$T(z, S=1) = \left(\frac{(1-R)^2 \exp(-\alpha_0 L)}{\sqrt{\pi} q_0(z, 0)} \right) \int_{-\infty}^{\infty} \ln \left[1 + q_0(z, 0) e^{-\tau^2} \right] d\tau \quad (2.10)$$

where R is the Fresnel reflection coefficient at the interface of the material with air, α_0 is the linear absorption coefficient and L is the length of the medium (sample thickness), q_0 is given by

$$q_0 = \beta I_p L_{eff} \quad (2.11)$$

where I_p is the on-axis peak incident intensity ($z = 0$), β is the two photon absorption coefficient and L_{eff} is the effective length of the medium and is represented as,

$$L_{eff} = \frac{(1 - e^{(-\alpha_0 L)})}{\alpha_0} \quad (2.12)$$

The third order nonlinear susceptibility is a complex quantity and has a real and imaginary part represented as

$$\chi^{(3)} = \chi_R^{(3)} + i\chi_I^{(3)} \quad (2.13)$$

The real part is related to the nonlinear refractive index. The imaginary part $\chi_I^{(3)}$ determines the strength of the nonlinear absorption of a material and is related to the two photon absorption coefficient by the relation,

$$\chi_I^{(3)} = \frac{\epsilon_0 n_0^2 c \lambda}{3\pi} \beta \quad (2.14)$$

where n_0 is the linear refractive index of the medium.

Three photon absorption

Three photon absorption is a fifth order nonlinear optical process in which three photons of frequency ω , are absorbed simultaneously by a material from the incident radiation to undergo a transition from the ground state G, to the excited state, E. A schematic representation of three photon absorption is given in Figure 2.7.

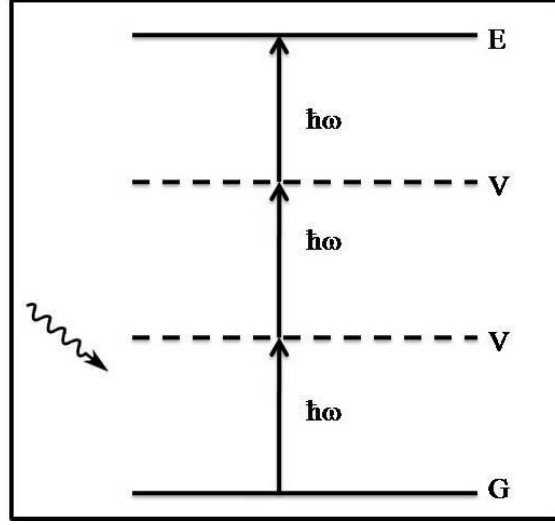


Figure 2.7 Process of three photon absorption

The optical loss of the medium due to the propagation of laser pulse in the case of a fifth order nonlinear process is represented as,

$$\frac{dI}{dz} = -\alpha_0 I - \gamma I^3 \quad (2.15)$$

where α_0 is the linear absorption coefficient of the material and γ is the three photon absorption coefficient. Here the beam is assumed to be Gaussian and linearly polarized. In a system with three photon absorption, the transmittance can be represented as,

$$T = \frac{\left((1-R)^2 \exp(-\alpha_0 L) \right)}{\sqrt{\pi p_0}} \times \int_{-\infty}^{+\infty} \ln \left[\sqrt{1 + p_0^2 \exp(-2t^2)} + p_0 \exp(-t^2) \right] dt \quad (2.16)$$

$$\text{where } p_0 = \sqrt{2\gamma(1-R)^2 I_p^2 L_{eff}} \quad (2.17)$$

I_p is the on-axis peak incident intensity, R is the surface reflectivity and L_{eff} is the effective thickness of the sample given by,

$$L_{eff} = \frac{(1 - \exp(-2\alpha_0 L))}{2\alpha_0} \quad (2.18)$$

The fifth order susceptibility also has two components – nonlinear absorption and nonlinear refraction. Accordingly, nonlinear refraction corresponds to the real part of $\chi^{(5)}$ whereas the nonlinear absorption corresponds to the imaginary part. So the three photon absorption coefficient, γ is related to the imaginary part of fifth order nonlinear optical susceptibility by the relation,

$$\chi_1^{(5)} = \frac{n_0^3 \epsilon_0^2 c^2 \lambda}{5\pi} \gamma \quad (2.19)$$

Excited state absorption

Excited state absorption (ESA) is the absorption of light from a lower excited state to a higher excited state by an atom, ion or a molecule. ESA can happen when an electron is already excited to the lower excited state, mostly by the absorption of photons. The lower excited state will be a higher energy level than the ground state while the higher excited state will be still higher energy level compared to lower excited state. This happens in a molecular system when the incident intensity is well above saturation intensity so that the excited states become significantly populated and the ground state gets depleted. The excitation to the higher lying states occurs before the electrons could relax to the ground state. The process here is well depicted in Figure 2.8.

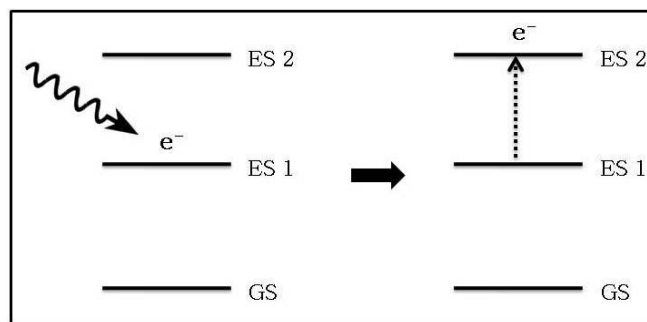


Figure 2.8 Excited state absorption

Depending on the absorption cross section of the excited state and ground state, the material exhibits SA or RSA. When the excited state absorption cross

section is smaller than that of the ground state, the material exhibits saturable absorption because the transmittance increases due to high density of excited states. Whereas the transmittance of the material considerably decreases when excited, if the absorption cross section of the excited state is larger than that of the ground state.

Free carrier absorption

When a semiconductor is excited with a radiation of energy greater than its bandgap, an electron is promoted from the valence band to the conduction band. This electron acts as a free carrier. The excited electron will rapidly thermalize and relax to the bottom of the conduction band. A recombination of this electron with an excited hole in the valence band occurs after a characteristic recombination time. However, there is a chance that this electron in the conduction band absorbs another photon, at higher intensities. This process is called free carrier absorption (Figure 2.9) and this act as the main reason for optical nonlinearity of semiconductor samples. In the weak absorption regime the optical attenuation induced to the material can be represented as,

$$\frac{\partial I}{\partial z} = -\alpha_0 I - \sigma_c N_c(I) I \tag{2.20}$$

where $N_c(I)$ is the intensity dependent carrier density, and σ_c is the free carrier cross section.

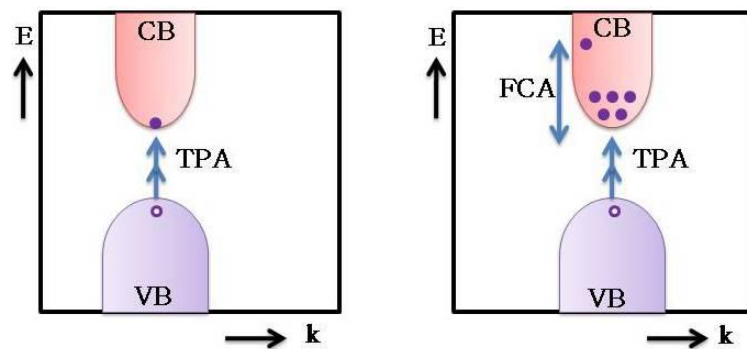


Figure 2.9 Free carrier absorption

Two photon induced excited state absorption

Two photon induced excited state absorption occurs in a material with strong two photon absorption. Excited state absorption occurs from the two photon pumped states. Polyatomic molecules and semiconductors mainly exhibit this kind of phenomenon. The transmittance of the system is found by solving the attenuation equation and excited state population equation given by,

$$\frac{\partial I}{\partial z} = -\alpha_0 I - \beta I^2 - \sigma N I \quad (2.21)$$

$$\text{and } \frac{\partial N}{\partial t} = \frac{\beta I^2}{2\hbar\omega} - \frac{N}{\tau} \quad (2.22)$$

where τ is the lifetime of two photon excited states.

Optical Limiting

Optical limiting is the increased absorption or reduced transmittance of materials when irradiated with high intense lasers. Materials exhibiting this phenomenon have linear transmittance at lower fluences which gradually change to decreased transmittance with increase in fluence. In other words, the output transmittance is clamped at some value which is always less than the amount required to damage the system which is to be protected from the hazards of intense radiation. This critical point is called the threshold of the optical limiter. The value of the clamped output is referred to as the limiting value of intensity or fluence.

Many processes can result in optical limiting of pulses namely, nonlinear absorption, nonlinear refraction, non linear scattering, photo refraction and optically induced phase transitions. Two-photon absorption, excited state absorption, or free carrier absorption can lead to nonlinear absorption. Nonlinear refraction is caused by molecular reorientation, excitation of free carriers, photorefractive, electronic Kerr effect, or thermal processes taking place in the material. Thermal energy produced in the material in the presence of highly intense radiation causes plasma generation in

the sample and lead to scattering. An optical limiter ideally should have good linear transmittance along with high nonlinear absorption. A low limiting threshold is desirable in a broad band and should be devoid of scattering. Optical limiters find applications in optical pulse shaping and smoothing, pulse compression and laser protection coatings.

2.5.3. Measurement techniques

The general methods which are used to measure the nonlinear absorption of materials yield the parameters like effective two photon absorption (β_{eff}), effective three photon absorption (γ_{eff}), imaginary part of third order or fifth order nonlinearity, etc. Important parameters of optical nonlinearity like ground state and excited state absorption cross section of the material of known concentration can be calculated, once the nonlinear absorption coefficient is known.

The nonlinear absorption of a material can be studied using any of the following techniques.

- (a) Three-wave mixing
- (b) Two-photon fluorescence
- (c) Photothermal techniques
- (d) Degenerate four-wave mixing
- (e) Heterodyned Kerr effect measurements
- (f) Chirped-pulse pump-probe technique
- (g) Transmission measurements
- (h) Pump-probe technique
- (i) Z-scan technique

Three-wave mixing (TWM)

Three-wave mixing (TWM) is also known as coherent anti-Stokes Raman scattering (CARS). Here the interference between Raman and other two-photon

resonant processes is utilized to measure the absorptive nonlinearities. The technique uses two beams of frequencies ω and $\omega - \Delta\omega$ which are made to overlap in the sample to produce a new beam having frequency $\omega + \Delta\omega$. The intensity of the beam with frequency $\omega + \Delta\omega$ is measured. This measured intensity is proportional to the absolute square of the third order susceptibility and hence the TPA coefficient is calculated.

The advantage of this technique compared to transmission measurement is the generation of a signal with a low noise. Even continuous wave (cw) lasers may be employed if photon counting is used. This technique has some disadvantages like, the frequency of the generated and incident pulse will be close to each other. Also it is difficult to resolve the probe pulse from a much higher intense pump pulse.

Two-photon fluorescence

In two-photon fluorescence, the two-photon fluorescence intensity is measured as a function of the energy of the incident photons. The fluorescence intensity is then compared to a reference material and the TPA cross-section is calculated. This technique also shares the advantage of obtaining the signal with low noise. The disadvantage is the low quantum fluorescence yields of some materials which affect the resultant signal.

Photothermal methods

The photothermal methods measure nonlinear absorption by relating the temperature changes in the material during linear or nonlinear absorption. This is because, during the measurement process when the material is irradiated with laser, some energy is absorbed by the material which is converted to heat. This internal change in energy of the material is measured as a direct change in temperature. Otherwise it can be measured as an optical property that depends on temperature. Photothermal methods consider either changes in the refractive index of the material or measure the temperature changes directly.

Degenerate four-wave mixing (DFWM)

DFWM technique is used to measure third order optical susceptibility of materials. The technique measures the modulus of $\chi_I^{(3)}$. Experimentally during the DFWM process, the presence of a double peak in the resultant phase conjugate signal indicates TPA. Also if the minimum between the two peaks of the pulse does not go to zero then the imaginary part of the susceptibility is nonzero. If the minimum goes to zero then, the phase conjugate signal is due to scattering of the pump beams from a pure two-photon absorption grating. So the technique monitors the signal at the minimum between the two peaks of the phase conjugate pulse as a function of pump energy. The value of β is calculated from the value of $\chi_I^{(3)}$. The advantage of this technique is that the signal is strong. The disadvantage is the difficulty in pulse detection and monitoring.

Heterodyned Kerr effect measurements

The optical Kerr effect measurement incorporated with a local oscillator beam that mixes with the Kerr effect signal is employed in Heterodyned Kerr effect measurement technique. The contribution from real or the imaginary part of the third order susceptibility can be enhanced by optical phase adjustments between the local oscillator and the nonlinear response of the medium. The advantage in this technique is that real and imaginary parts can be separated and measured through the experiment. Disadvantage to be noted is the complication in the technique. Also the technique instead of giving the value β directly, gives the two-photon equivalent of a dichroic absorption coefficient.

Chirped-pulse pump-probe technique

The pump-probe technique is modified by the use of chirped pulse here. The sample is pumped by a strong pump pulse and the probe pulse is measured as done in pump-probe technique. The transmittance is measured as a function of the delay time

between pump and probe and the resultant curve is processed to get third order susceptibility. The advantage of this technique is that real and imaginary components of $\chi_I^{(3)}$, can be measured. The characterization of the laser chirp or calibration against a reference with known response time is an important disadvantage of this technique.

Transmission measurements

The main feature of nonlinear absorption is the change in the output transmittance of the material with respect to incident fluence. So the measurement of transmittance gives an effective measure of nonlinear absorption. This also helps to calculate parameters like nonlinear absorption and ground and excited absorption cross sections along with the imaginary part of nonlinear susceptibility. The simplicity of the experimental technique is the main advantage of transmission measurements. The disadvantage is the measurement of the small signal in a large background.

In this regard there are two techniques that fulfil the requirement

Pump-probe technique

Pump-probe experiment uses a laser source as pump and probe pulse. The probe pulse is given an appropriate delay and made to overlap with the pump pulse within the sample. The reference beam and the beam transmitted through the sample are collected and coupled to a grating spectrometer and then directed to a dual photodiode array for processing the signal.

Z-scan technique

Z-scan is an easy and convenient technique to measure the optical nonlinearity of a thin material. This technique developed by Sheik-Bahae et al. is used to calculate the nonlinear absorption coefficient and nonlinear refractive index (Sheik-Bahae et al., 1989). The advantage of this method is that both the magnitude

and the sign of the absorption coefficient and refractive index can be determined. The nature of the Z-scan trace gives an idea about the sign of the calculated parameter. Z-scan involves focusing a laser beam through a thin sample and detecting the transmitted light in the far field. Transmittance is measured for a constant laser input as the sample is scanned along the z-direction through the focus of the lens. Hence the measurement method has come to be known as the Z-scan. It can be used in two ways – open aperture Z-scan and closed aperture Z-scan. Transmittance detected by placing an aperture in front of the detector helps to measure the magnitude and sign of nonlinear refractive index and is known as closed aperture Z-scan whereas removing the aperture helps to measure the magnitude and sign of nonlinear absorption coefficient, known as open aperture Z-scan. Z-scan analysis explicitly assumes Gaussian beam propagation, and it is important to assure that the incident beam follows this behaviour.

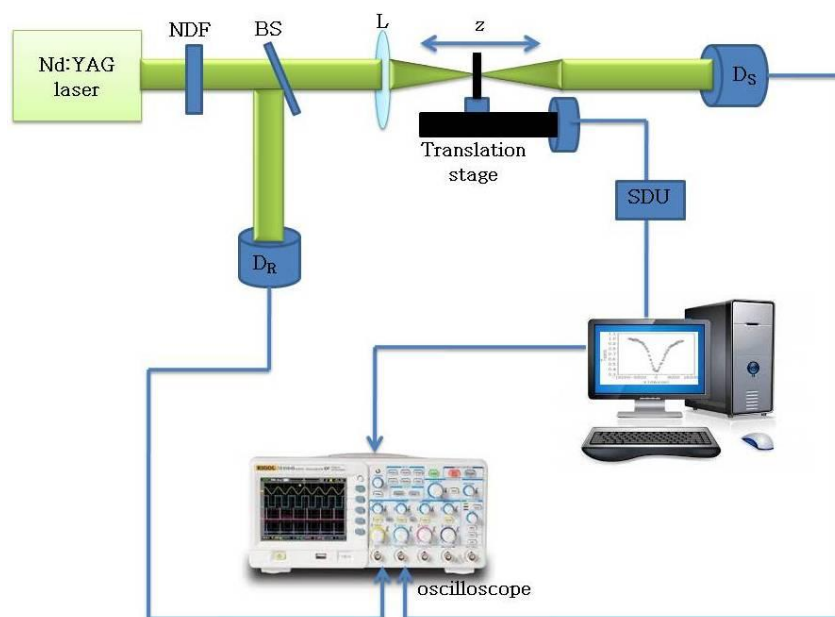


Figure 2.10 Z-scan set up

In the present investigation, we prefer open aperture Z-scan technique to measure the absorptive nonlinearity of the samples in colloidal and film form. As shown in Figure 2.10, a frequency-doubled Nd:YAG laser (Spectra Physics,

GCR-150, 7 ns, 532 nm, single shot) is used as the light source. The laser pulses were plane polarized with a Gaussian spatial profile. The laser beam is focused using a lens of focal length 10.5 cm and the sample is moved along the beam axis (z axis). The sample experiences varying intensity as it moves with respect to the focal point, having maximum intensity at the focus. A reference beam is taken using a beam splitter along the path of the incident beam. The energy of the reference beam and the transmitted beam are measured by an energy ratio meter (Rj7600, Laser Probe Corp.) having two identical pyroelectric detector heads (RjP735). Thus the experimental data gives position dependent, hence intensity dependent transmission through the sample. The Z-scan system is calibrated using carbon disulfide (CS₂) as a standard. The effect of fluctuations of laser power is eliminated by dividing the transmitted power by the power obtained at the reference detector.

The data obtained from the open aperture experiment was analyzed using the procedure described by Bahae et al. (Sheik-Bahae, 1989; Sheik-Bahae et al., 1990). The nonlinear absorption coefficient and the saturation intensity of the sample can be calculated from a theoretical fit given to the experimental data according to the equations discussed in the sections of two photon absorption and three photon absorption.

Theory of open aperture Z-scan

In open aperture Z-scan technique, the input beam is assumed to be Gaussian, propagating in the 'z' direction as shown in Figure 2.11. The magnitude of electric field (E) can be represented as,

$$|E(r, z, t)| = |E(t)| \frac{\omega_0}{\omega(z)} \exp\left[-\frac{r^2}{\omega^2(z)}\right] \quad (2.23)$$

where E_0 denotes the radiation electric field at the focus and contains the temporal envelope of the laser pulse. The beam spot size, $\omega(z)$ is,

$$\omega(z) = \omega_0 \sqrt{1 + \left(\frac{z}{z_0}\right)^2} \quad (2.23)$$

ω_0 is the beam waist and Z_0 is referred to as the Rayleigh length (Rayleigh range).

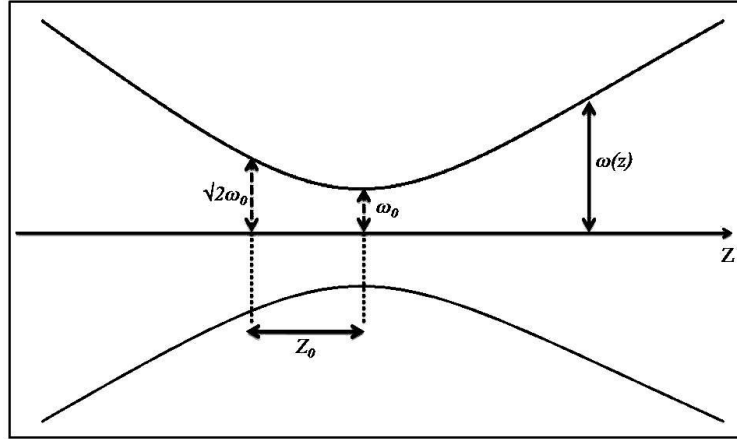


Figure 2.11 Rayleigh length of a Gaussian beam

Rayleigh length of a beam is the distance from the beam waist (ω_0) where the beam radius is increased by a factor of $\sqrt{2}$. The Rayleigh length is related to the beam waist and the wavelength of the incident beam (λ) as,

$$Z_0 = \frac{\pi\omega_0^2}{\lambda} \quad (2.24)$$

When the beam traverse through a nonlinear medium, the amplitude of the beam is unchanged by diffraction or nonlinear focusing within the medium if the thickness of the sample is less than the Rayleigh length. However the amplitude may get changed by linear or nonlinear absorption whereas the phase of the incident wave is distorted. So an essential requirement for performing Z-scan measurement is that the sample length should be less than Z_0 .

With this assumption, the amplitude and nonlinear phase change, $\Delta\phi$ of the electric field within the sample can be represented as,

$$\frac{d\Delta\phi}{dz} = \frac{2\pi}{\lambda} \quad (2.25)$$

$$\text{and} \quad \frac{d|E|}{dz} = -\frac{\alpha_0}{2}|E| \quad (2.26)$$

where α_0 is the linear absorption coefficient. Equations (2.25) and (2.26) can be solved to get the phase shift, $\Delta\phi$ at the exit surface of the sample,

$$\Delta\phi(r, z, t) = \frac{kn_2}{\beta} \ln[1 + q(r, z, t)] \quad (2.27)$$

where $k = \frac{2\pi}{\lambda}$ is the wave vector, n_2 is the nonlinear refractive index, β is the TPA coefficient and $q(r, z, t)$ is given by equation 2.1. The irradiance distribution of the beam is represented in terms of irradiance of the laser beam within the sample (I),

$$I_e(z, r, t) = \frac{I(z, r, t)}{1 + q(z, r, t)} e^{-\alpha_0 l} \quad (2.28)$$

Solving equations (2.25) and (2.26) the complex field at the exit surface of the sample becomes,

$$E_e = E(z, r, t) e^{-\alpha_0 l/2} (1 + q)^{ikr/\beta - 1/2} \quad (2.29)$$

Integrating equation (2.26) at z over r we get the transmitted power $P(z, t)$ as follows:

$$P(z, t) = P_i(t) e^{-\alpha_0 l} \frac{\ln[1 + q_0(z, t)]}{q_0(z, t)} \quad (2.30)$$

$$\text{where} \quad P_i(t) = \frac{\pi\omega_0^2 I_0(t)}{2} \quad (2.31)$$

is the instantaneous input power within the sample.

For temporally Gaussian pulse, equation (2.30) can be time integrated to get the normalized energy transmittance,

$$T(z, S=1) = \left(\frac{1}{\sqrt{\pi} q_0(z, 0)} \right) \int_{-\infty}^{\infty} \ln[1 + q_0(z, 0) e^{-\tau^2}] d\tau \quad (2.32)$$

The experimental data from the Z-scan measurement is given a theoretical fit based on equations (2.11), (2.12) and (2.32) assuming that the sample reflectance, $S=1$. From the theoretical fit, the TPA coefficient can be calculated. For evaluating three photon absorption coefficients also the same procedure is followed using equations (2.16), (2.17) and (2.18). Once the value of β and γ are known, the imaginary part of third order and fifth order nonlinear optical susceptibility can be calculated from equations (2.14) and (2.19) respectively.

CHAPTER 3

SYNTHESIS AND FABRICATION OF PMMA-ZnO NANOCOMPOSITE FILMS FOR LINEAR AND NONLINEAR OPTICAL APPLICATIONS

This chapter presents the synthesis and fabrication of PMMA-ZnO composite films. ZnO nanoparticles are synthesized using solution precipitation technique and are characterized using spectroscopic and microscopic analysis techniques. Open aperture Z-scan reveals that these nanoparticles in colloidal form excel in reverse saturation of absorption. PMMA-ZnO nanocomposite films are fabricated using dip and spin coating technique. These films are found to have increased nonlinear absorption compared to colloid of ZnO, indicating that these films are useful as reverse saturable absorbers.

3.1. Introduction

Nanotechnology has opened a new path towards many technological oriented materials through the ability to tune their optical, electrical and mechanical properties. This has been achieved through novel synthesis techniques which helped to prepare nanoparticles of desired size and shape. Synthesis of ZnO nanoparticles having desired properties is one of its kinds. Over the years, ZnO nanoparticles of different size and morphology have been synthesized and reported, including nanorods, nanowires, nanobelts, nanorings, nanocombs, nanospirals, nanosponges (Wang, 2004), etc. Films of ZnO nanoparticles are also prepared by various fabrication techniques like pulsed laser deposition (Ohtomo and Tsukazaki, 2005), R F sputtering (Lim et al., 2006a), spin and dip coating (Znaidi, 2010), spray pyrolysis (Lehraki et al., 2012) and atomic layer deposition (Tynell and Karppinen, 2014). The synthesized nanoparticles and their films are widely utilized as luminescent materials (Pyshkin and Ballato, 2013), sensors (Özgür et al., 2010) and as optoelectronic materials (Djurišić et al., 2010). However the main challenges in

preparing good quality ZnO films for optoelectronic applications is the durability of the films and maintaining visible light transmittance. This is mainly because of the tendency of the nanoparticles to agglomerate with size reduction. For optical applications, transparent films of nanostructures are preferred. Use of a polymer provides long term stability for the nanoparticles dispersed in it. Polymers consist of large molecules linked together in repeated fashion to form long chains. The nanoparticles trapped inside long polymer chains get arrested on fabrication of film. Apart from this, polymers provide transparent medium and ease of fabrication due to their flexibility.

A thorough review of literature reveals a handful of reports on applicability of polymer nanocomposites and their films in various fields like UV protection coatings (Ge et al., 2010), textile fabrication (Farouk et al., 2014; Farouk et al., 2010), dielectrics (Roy et al., 2013), nonlinear optical application especially as saturable absorbers (Karthikeyan et al., 2006) and reverse saturable absorbers (Deng et al., 2008; Lee et al., 2006; Shen et al., 2006; Sreeja et al., 2010; Yuwono et al., 2003). Recent reports state that polymer nanocomposites are used as energy storage systems (Siddabattuni and Schuman, 2014; Sambasivarao, 2014) and sensors (Du et al., 2007).

Composites and composite films of polymer-ZnO are also widely utilized in variety of fields, especially in optics. Vutha et al., (2006) reports the fabrication of composite films by dissolving ZnO and PMMA powders in chloroform and depositing the composite on a substrate. These films exhibit random lasing at temperature ranging from 6 to 250 K. They attribute the exhibited lasing action to the ZnO nanoparticles and argue that the polymer matrix offers ease of fabrication. In 2009, Son et al. have reported the fabrication of polymer-ZnO quantum dot composite films which can act as an optical bistable device. PMMA-ZnO composite films can act as UV- shielding material (Li et al., 2007; Tang et al., 2006a; Tang et al., 2007), luminescent material (Jiang et al., 2008; Sun et al., 2009; Zhang et al.,

2013) and solar cell (Plank et al., 2008) as well. Very few reports are available on polymer-ZnO nanocomposite films as optical limiters (Jeeju et al., 2014; Kulyk et al., 2009; Sreeja et al., 2010; Thankappan et al., 2013).

Being organized in two sections, this chapter details the synthesis of ZnO nanostructures and fabrication of their polymer nanocomposite films for nonlinear optical applications. The first section describes the synthesis of novel ZnO nanostructures by solution precipitation technique and explores their nonlinear absorption property. The nanoparticles are characterized using spectroscopic and microscopic techniques to understand their properties. Fabrication of PMMA-ZnO nanocomposite films using spin and dip coating technique and studies on their absorptive nonlinearity comprise of the second section. In short, this chapter emphasize on the fabrication of good quality PMMA-ZnO composite films with increased nonlinearity compared to the nanoparticles in colloidal form.

3.2. ZnO nanoparticles

3.2.1. Synthesis

Solution precipitation technique is a general technique for the synthesis of nanoparticles. The technique involves the precipitation of a solid from a solution. The reaction can be in the aqueous or non-aqueous solutions containing the soluble or suspended salts. Once the solution becomes supersaturated with the product, the precipitate is formed by either homogeneous or heterogeneous nucleation. The formation of a stable material with (without) the presence of a foreign species is referred to as heterogeneous (homogeneous) nucleation. The growth of the nuclei after formation usually proceeds by diffusion, in which case, concentration gradients and reaction temperatures are very important in determining the growth rate of particles, to form the mono dispersed particles. For the formation of unagglomerated particles with a very narrow size distribution, all the nuclei must be formed at nearly the same time and the subsequent growth must occur without further nucleation or

agglomeration of particles (Rahman, 2011). It has been reported that polymers like polyvinyl pyrrolidone (PVP) and polyethylene glycol (PEG) play an important role in modifying the surface morphology and controlling the size of the nanocrystallites formed (Thirugnanam, 2013). Rate of particle aggregation is a major factor that controls the morphology and crystallinity of the nanoparticles. If the nanoparticles get isolated on nucleation itself, agglomeration along with their further growth can be blocked to some extent. Use of suitable capping agent in right amount can solve this issue and nanoparticles of desired morphology can be synthesized without agglomeration (Shong et al., 2010).

In the present investigation, Zinc Oxide (ZnO) nanoparticles are synthesized at room temperature using solution precipitation technique. Zinc acetate salt dissolved in aqueous solution of acetic acid is used as the precursor. Polyvinyl pyrrolidone (PVP) and polyethylene glycol (PEG) are used as capping agents. 0.219 g zinc acetate dihydrate (Merck) is stirred well with 0.05 % solution of PVP (in 1 % acetic acid) at room temperature for 24 hours to form zinc acetate-PVP complex. In this reaction PVP can influence the growth of ZnO in three ways. (1) The water adsorption property of PVP helps to accelerate dehydration reaction of zinc hydroxide by consuming water formed during the reaction. (2) PVP promotes ZnO nucleation at low temperature. (3) Ordered chain structure of PVP helps them to get adsorbed on the surface of nanoparticles on nucleation through electrostatic adsorption process and reduce aggregation (Kavitha et al., 2014; Thirugnanam, 2013). Nanoparticles of ZnO are precipitated from zinc acetate-PVP complex using sodium hydroxide (NaOH) solution. The molar ratio of zinc acetate and NaOH solution is maintained at 1:6. Stirring is continued for 12 hrs to complete the precipitation. The precipitate is filtered, washed and dried at 100 °C for 12 hrs in vacuum oven. The synthesis is repeated using polyethylene glycol (PEG) as capping agent. ZnO nanoparticles synthesized using PVP is named PVP-capped ZnO nanoparticles and the latter one is named as PEG-capped ZnO nanoparticles.

3.2.2. Characterization

X-ray Diffraction (XRD) analysis of both the samples is performed on their powder, and the patterns obtained are shown in Figure 3.1. The sharp intense peaks obtained indicate the crystalline nature of the samples, oriented along the (1 0 1) plane unlike along the commonly dominant (0 0 2) plane with lowest surface energy. This preferential growth exposing the high energy surface is due to the influence of the capping agent (Kavitha et al., 2014). The growth rate of the crystals in certain facet will be confined in the presence of capping agents, improving the crystallinity of samples. The peaks in the XRD pattern originated from (1 0 0), (0 0 2), (1 0 1), (1 0 2), (1 1 0), (1 0 3), (2 0 0), (1 1 2) and (2 0 1) are reflections of hexagonal wurtzite structure. The pattern matches well with the earlier reports (Singh et al., 2008; Yang et al., 2005).

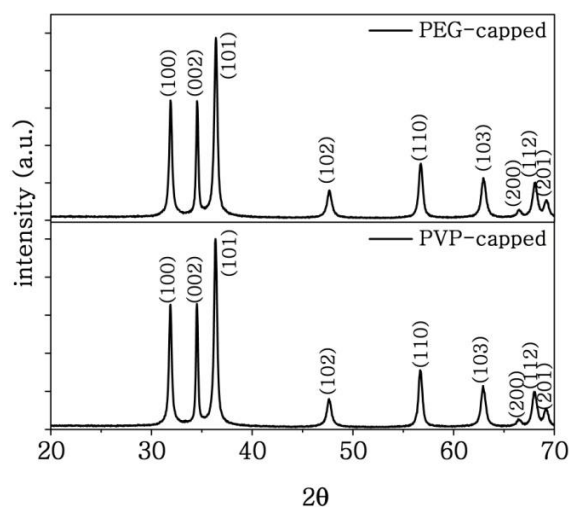


Figure 3.1 XRD patterns of ZnO nanoparticles

The XRD pattern is used to calculate the crystallite size of the nanoparticles applying Scherrer equation (2.2). The calculated average crystallite size of PEG-capped and PVP-capped ZnO nanoparticles are found to be 23 nm and 24 nm respectively.

The morphology of the nanoparticles is characterized by High Resolution Transmission Electron Microscope (HRTEM). Figure 3.2 shows the TEM image of ZnO nanoparticles.

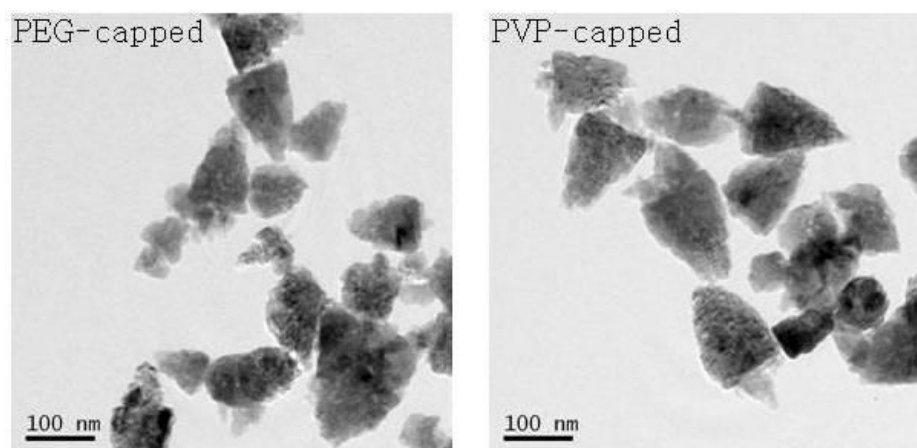


Figure 3.2 TEM images of ZnO nanoparticles

The TEM image shows that PVP-capped nanoparticles are uniform and have a “top” like structure, whereas PEG-capped nanoparticles are of non-uniform size and shape. The difference in the uniformity and shape is due to the influence of capping agent. The strong adhesion nature of PVP make it stronger capping agent compared to PEG and enhances the formation of nanoparticles of uniform morphology (Thirugnanam, 2013).

Linear absorption property of the nanoparticles is studied using UV-vis absorption spectra of ZnO nanoparticles dispersed in methanol. The spectra are taken at room temperature in the wavelength range from 210 nm to 600 nm, and are shown in Figure 3.3. The nanoparticles have absorption maximum in the UV region of electromagnetic spectrum. ZnO absorbs UV radiation via a process of electron excitation called band-gap absorption. The absorption mainly depends upon the optical bandgap of the nanoparticles. Any radiation matching with the optical bandgap is absorbed through electron excitation.

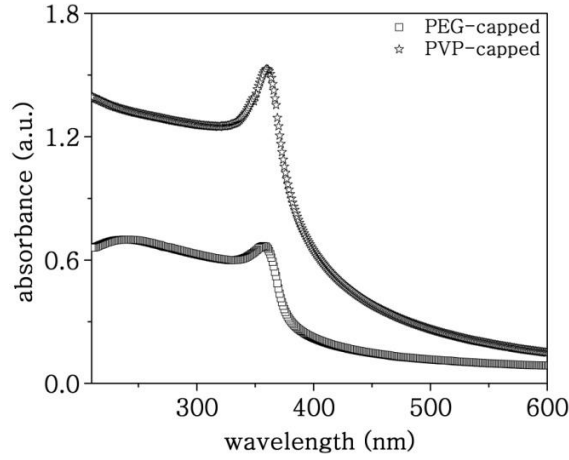


Figure 3.3 UV-vis absorption spectra of ZnO nanoparticles

Figure 3.3 shows that the nanoparticles exhibit a blue shift in the absorption maximum compared to that of bulk ZnO reported at 380 nm (Liu et al., 2006a). PEG-capped ZnO shows an absorption peak at 357 nm and PVP-capped ZnO shows the peak maximum at 359 nm. The observed blue shift in the absorption edge of PEG-capped nanoparticles is attributed to the reduced particle size which is in accordance with the results of XRD analysis.

Optical bandgap of the nanoparticles play an important role in their linear and nonlinear optical properties. For direct bandgap semiconductors, optical band gap can be calculated using Tauc equation

$$\alpha h\nu = k(h\nu - E_g)^{1/2} \quad (3.1)$$

where $h\nu$ is the photon energy, E_g is the band gap of the material and k is a constant. Extrapolation of the linear part until it intersects the $h\nu$ axis gives the bandgap of the material (Tauc, 1966). Tauc plot of $h\nu$ Vs $(\alpha h\nu)^2$ for PEG-capped and PVP-capped nanoparticles is shown in Figure 3.4. Bandgap values calculated are 3.23 eV and 3.28 eV for PVP-capped and PEG-capped nanoparticles respectively. The result justifies the difference in crystallite size calculated for the nanoparticles from XRD pattern. It should be noted that the bandgap calculated for the nanoparticles is lower than the bandgap of bulk ZnO (3.3 eV) (Mang et al., 1995).

This difference is resulted from the existence of valence band donor transitions due to defects present in the nanoparticles (Srikant and Clarke, 1998).

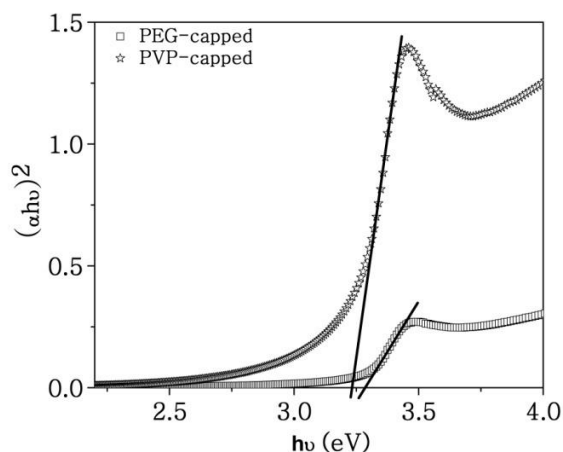


Figure 3.4 Tauc plot of ZnO nanoparticles

Photoluminescence spectra of the synthesized nanoparticles are taken in order to get an idea of the emissive nature of the nanoparticles and to identify the defects introduced during the synthesis. The nanoparticles dispersed in methanol are excited at 325 nm and the spectra recorded are shown in Figure 3.5.

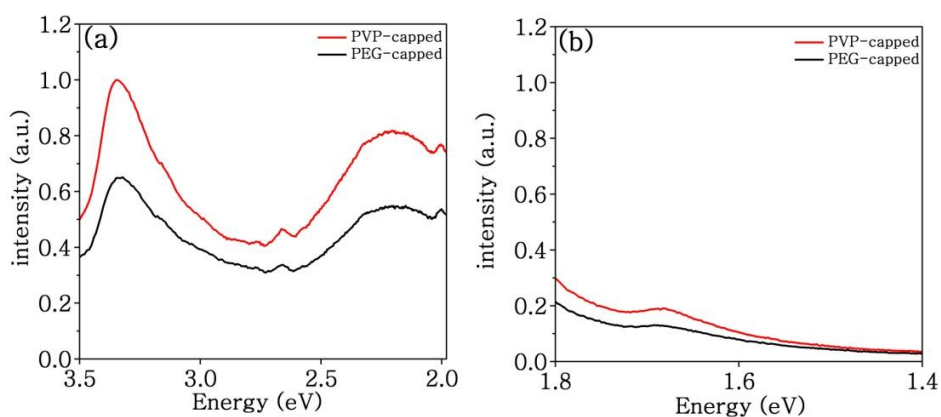


Figure 3.5 Photoluminescence spectra of ZnO nanoparticles excited at 325 nm

The nanoparticles exhibit a characteristic band edge emission in the ultraviolet region due to the photo-generated electron recombination with holes in the valence

band or in traps near the valence band (Xiong, 2010). PEG-capped ZnO nanoparticles exhibit the characteristic band edge emission at 374 nm (3.32 eV) while the emission is at 371 nm (3.34 eV) for PVP-capped ZnO nanoparticles.

The sharp ultraviolet emission is followed by blue, green, red and red-NIR emissions indicating that the synthesized nanoparticles are rich in defects. The defects responsible for visible emission (defect level emissions) in ZnO are attributed to native defects, which are zinc vacancy (V_{Zn}) (Li et al., 2013), oxygen vacancy (V_O) (Van Dijken et al., 2000), Zn interstitial (Zn_i) (Knutsen et al., 2012), and oxygen interstitial (O_i) (Djurišić et al., 2006).

The nanoparticles in the present study exhibited prominent broad emission from 480 nm to 600 nm centered at ~ 563 nm (2.2 eV) corresponding to green emission and an emission at 620 nm (2 eV) corresponding to the orange-red emission which are reported to be due to the presence of oxygen vacancies (V_O) and oxygen interstitials (O_i) (Kumar et al., 2013; Studenikin et al., 1998; Zhang et al., 2001). Oxygen vacancy is a stable deep donor and will not get ionized even at temperatures well above room temperature (Janotti et al., 2012). Emission in blue region, at 467 nm (2.65 eV) indicates the presence of Zn vacancies. The blue emission is ascribed to the electronic transition from the donor energy level of Zn interstitials to acceptor energy level of Zn vacancies (Wei et al., 2007; Zhaoyuan and Huoquan, 2005).

A red-NIR emission ranging from 710 nm to 800 nm, centered at 739 nm (1.68 eV) is observed in the samples which results from oxygen related defects. Defects due to oxygen in the sample either appear as oxygen vacancies (V_O) (Liu et al., 2004) or promote V_{Zn} and O_i defects (Erhart et al., 2006; Janotti and de Walle, 2007) in ZnO. In the present study, the green emission dominates all defect emissions so that V_O will be dominating compared to O_i . However the presence of blue emission centered at 2.65 eV gives evidence for V_{Zn} also. These V_{Zn} can promote red

and red-NIR emissions in the present samples. Thus the synthesized nanoparticles have defects such as V_O and V_{Zn} which will enhance their nonlinear absorption properties. A close observation of the samples reveals that the PVP-capped nanoparticles have intense emission compared to PEG-capped nanoparticles with same concentration. Thus it can be concluded that the nanoparticles prepared in the presence of PVP are defect rich with V_O and V_{Zn} which will enhance their nonlinear absorption.

3.2.3. Nonlinear absorption studies

Nonlinear absorption properties of the synthesized nanoparticles are evaluated by using open aperture Z-scan technique. The nanoparticles are dispersed in water and the linear transmittance of the samples is kept as 65 %. The input fluence in the present investigation is 16.5 J/cm^2 . The far field normalized transmittance as a function of the distance for the ZnO nanoparticle (PEG-capped and PVP-capped) dispersions are shown in Figure 3.6.

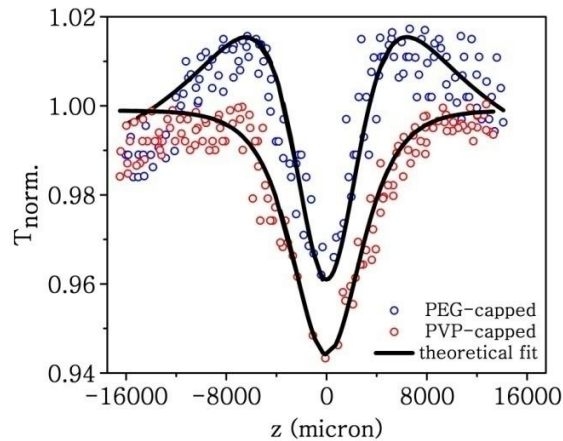


Figure 3.6 Open aperture Z-scan plots of ZnO nanoparticles

Both dispersions exhibit a normalized transmittance valley, indicating the presence of reverse saturable absorption. This point merits special attention because it renders practical applicability to the nanoparticles as optical limiters. The experimental data is given a theoretical fit according to third order nonlinear

absorption process, using equation for normalized transmittance (2.10), where we take the assumption that the sample reflectance $R=1$.

$$T(z, S = 1) = \left(\frac{\exp(-\alpha_0 L)}{\sqrt{\pi} q_0(z, 0)} \right) \int_{-\infty}^{\infty} \ln \left[1 + q_0(z, 0) e^{-\tau^2} \right] d\tau \quad (3.2)$$

where $q_0(z, 0)$ and L_{eff} are calculated using Equations (2.11) and (2.12) respectively. This equation fits well in the valley region of the experimental data where limiting prevails and in the wings where the saturable absorption occurs. The Rayleigh length, Z_0 is evaluated by using the Equation (2.19) and it is found to be 2.1 mm, greater than the thickness of the sample, which is an essential requirement for Z-scan experiments.

The analysis of the experimental data revealed the fact that considerable two photon absorption is taking place in the nanoparticle dispersions. However the semiconductor nanoparticles in the present study have large particle size and there is an obvious chance of free carrier absorption (FCA). The FCA lifetime of ZnO is reported to be 2.8 ns and in the present work 7 ns laser pulse is used. So there is a strong possibility of the excitation of the free carriers generated by two photon absorption. Therefore two photon absorption assisted free carrier absorption is the main mechanism behind the exhibited nonlinearity (Haripadmam et al., 2012). Saturable absorption also has a key role in the exhibited nonlinearity. It is evident from Figure 3.6 that in PEG-capped sample saturation of absorption dominates RSA whereas RSA dominates SA in PVP-capped one.

The nonlinear absorption coefficient measured for the samples, from the theoretical fit is an effective nonlinear absorption coefficient. It is represented as β_{eff} rather than the usual notation for TPA coefficient β . For PEG-capped ZnO nanoparticles β_{eff} is found to be 0.16×10^{-10} m/W whereas for PVP-capped nanoparticles the value is slightly increased to 0.21×10^{-10} m/W. The saturation intensity (I_{sat}) of PEG and PVP capped ZnO are 13×10^{12} W/m² and

$12.6 \times 10^{12} \text{ W/m}^2$, respectively. The superiority of saturable absorption in PEG-capped nanoparticles as seen from Figure 3.6 is reflected in its effective NLA coefficient also. The increase in β_{eff} observed for the PVP-capped nanoparticles can be attributed to their increased size and hence the reduced bandgap. The fact that the rate of TPA increases with decrease in bandgap has been theoretically proposed by van Stryland et al. (van Stryland et al., 1985) and experimentally proven by several groups (Irimpan et al., 2008b; Sreeja et al., 2010). According to van Stryland et al., optical bandgap is related to TPA by the relation,

$$\beta(\omega) = C' \frac{\sqrt{E_p}}{n_0^2 E_g^3} F\left(\frac{2\hbar\omega}{E_g}\right) \quad (3.3)$$

where C' is a material-independent constant, n_0 is the linear refractive index, E_g is the bandgap of the material and E_p is the Kane energy parameter with a value of $\sim 21 \text{ eV}$, which is a material independent parameter for direct bandgap materials. The function F , whose exact form depends on the assumed band structure, is a function only of the ratio of the photon energy $h\nu$ to E_g , which determines the states that are optically coupled.

The value of β_{eff} , obtained from the theoretical fit is used to calculate the imaginary part of third order susceptibility, $\chi_I^{(3)}$. The effectiveness of optical limiting is determined by the ratio of cross sections ($\sigma_{\text{ex}}/\sigma_g$) called the figure of merit (FOM) where the excited state absorption cross section is given by,

$$\sigma_{\text{ex}} = \frac{2h\nu q_0}{F_0 L_{\text{eff}}} \quad (3.4)$$

and ground state absorption cross section is, $\sigma_g = \frac{\alpha}{N_a C}$, (3.3)

F_0 is the fluence of the laser at the focus, N_a is Avogadro's number, and C is the concentration in mole/cm^3 . The calculated parameters are given in Table 3.1.

Table 3.1 Calculated nonlinear optical parameters of ZnO nanoparticles

Sample	$\chi_I^{(3)}$ ($\times 10^{-22}$) (esu)	σ_g ($\times 10^{-19}$) (cm^2/mol)	σ_{ex} ($\times 10^{-19}$) (cm^2/mol)	FOM ($\times 10^2$)
PEG-capped	1.18	0.25	355.00	14.2
PVP-capped	1.51	0.25	363.94	14.6

The results show that the excited state absorption cross section is always greater than ground state absorption cross section for PVP and PEG-capped nanoparticles and hence it is confirmed that these sample undergoes RSA (Sutherland, 2003). An increase of 28 % is observed in the value of nonlinear susceptibility for the PVP-capped nanoparticles compared to PEG-capped one, indicating that PVP-capped nanoparticles are better reverse saturable absorbers.

PVP-capped ZnO nanoparticles are selected for further studies and are named ZnO nanotops due to its “top” like shape. The fluence dependent nonlinear absorption studies of the ZnO nanotop dispersion in water is shown in Figure 3.7. The linear transmittance is kept as 65 % and the incident fluence is varied from 0.5 to 16.5 J/cm².

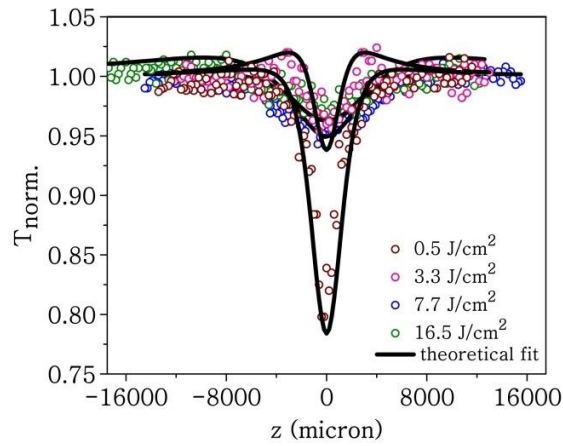


Figure 3.7 Fluence dependent transmittance of ZnO nanotop colloid

Effective nonlinear absorption coefficient and the saturation intensity calculated for all trials are tabularized in Table 3.2. It is very clear from the table that the nonlinear absorption coefficient is dependent on the incident fluence.

Table 3.2 Effective nonlinear absorption coefficients (β_{eff}) and saturation intensities (I_{sat}) calculated for ZnO nanotops, by varying the input fluence.

Fluence (J/cm^2)	$\beta_{\text{eff}} \times 10^{-10}$ (m/W)	$I_{\text{sat}} \times 10^{12}$ (W/m^2)
0.5	1.72	2.40
1.1	1.28	2.40
1.6	0.77	4.80
2.2	0.67	4.80
3.3	0.67	4.80
7.7	0.27	14.00
11.0	0.24	13.00
16.5	0.21	12.60

A detailed analysis of the fluence dependent study carried out also confirms that the mechanism behind the exhibited nonlinearity is not genuine two photon absorption. The effective NLA coefficient measured is found to decrease with increase in fluence. Since the NLA coefficient is linearly related to the population difference between ground state (valence band) and the excited state (conduction band), it is not affected by light of low fluence. At high fluence, the number of incident photons will be so high that it excites most of the electrons from the valence band to the conduction band. The emission rate will be slow due to defect level absorption. The presence of rich defect level states are evident from the PL spectrum of ZnO nanotops (Figure 3.5). Also, electrons which transit to the valence band again get excited to the conduction band. Altogether the ground state faces a partial depletion of electrons which in effect reduces the nonlinear absorption and thereby the effective NLA coefficient, with increase in fluence.

3.3. PMMA-ZnO nanocomposite films

In the present work, polymer nanocomposites are prepared using ZnO nanotops and the transparent matrix, polymethyl methacrylate (PMMA). ZnO nanotops are dispersed in the monomer methyl methacrylate and polymerized it to get PMMA-ZnO nanotop composite. Apart from transparency and ease in fabrication of films, the compatibility of the monomer with the ZnO nanoparticles is the main reason for selecting PMMA as the matrix. Desired weight % of ZnO nanotops are dispersed in methyl methacrylate by ultrasonication. Nanotop dispersed monomer is polymerized by bulk polymerization technique using benzoyl peroxide (BPO) as initiator. Polymerization is done in an oil bath for controlling the temperature. The polymer nanocomposite formed is fabricated into films by dip and spin coating techniques.

3.3.1. Dip coated films

3.3.1.1. Fabrication

Dip coating technique provide a convenient way to coat polymer nanocomposites. For optimizing the viscosity of the composite, PMMA-ZnO nanocomposites of varying viscosities are prepared by adjusting the polymerisation time. 2 weight % ZnO nanoparticles are dispersed in the monomer (methyl methacrylate) through ultrasonication for 3 hours. The dispersion is then polymerized at 70-80 °C using bulk polymerisation technique with benzoyl peroxide (BPO) as initiator. The polymerisation time is varied from 20 minutes to 50 minutes to get nanocomposites of different viscosities. The polymerization time varied and the resultant viscosity measured are shown in Table 3.3.

After cooling for 5 minutes, the polymer nanocomposites are coated on a glass substrate using dip coating technique. A uniform transparent film is obtained for the composite with a viscosity 10 m Pa s, which is prepared by polymerizing ZnO dispersed monomer for about 30 minutes, at 70-80 °C. Composite with viscosity less

than 10 m Pa s did not adhere properly on the substrate whereas when viscosity is larger than 10 m Pa s, the film formed is not uniform. The large viscosity of the composite hinders the easy movement of the glass plate on dipping and retrieval.

Table 3.3 Calculated values of viscosities for the polymer nanocomposites by varying the polymerization time

Polymerisation time (min)	Viscosity (m P s)
20	07.0
30	10.0
40	17.5
50	20.0

Other than single coat film, films with three and five numbers of coats are fabricated by multilayer coating using dip coating technique. They are named as F2Dx where x is the number of coats and 2 indicate composite with 2 weight % ZnO in it. ‘D’ denotes the dip coating technique. The parameters associated with dip coating are optimized to get good quality uniform films and the optimized parameters are given in Table 3.4. Film with 5 numbers of coats is found to be non-uniform and is not used for further studies.

Table 3.4 Optimized parameters of dip coating

Dipping speed	5000 $\mu\text{m/s}$
Retrieval speed	5000 $\mu\text{m/s}$
Dipping duration	12 s
Dry duration	1 min
Drying temperature	65 $^{\circ}\text{C}$

3.3.1.2. Characterization

The UV-vis absorption spectrum of F2D3 is shown in Figure 3.8. The film shows maximum absorption in the UV region, as observed in the case of ZnO

nanotop dispersion, confirming that the nanoparticles maintain their property even after fabrication to films.

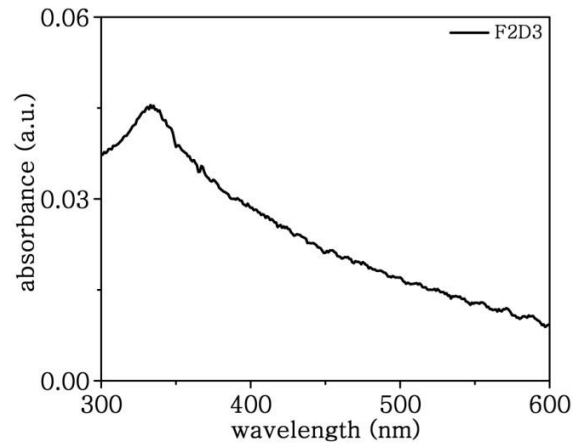


Figure 3.8 UV-vis absorption spectra of F2D3

It can also be concluded that polymer is not affecting any optical properties of ZnO but just act as a transparent matrix for the dispersions of ZnO. The presence of the absorption peak (excitonic peak at 333 nm) indicates the high crystallinity of the ZnO nanotops since they are dispersed well in the matrix (Kulyk et al., 2009).

Figure 3.9 shows the photoluminescence spectrum of F2D3, excited at 325 nm. The characteristic band edge emission of the film is shifted to 3.16 eV (393 nm).

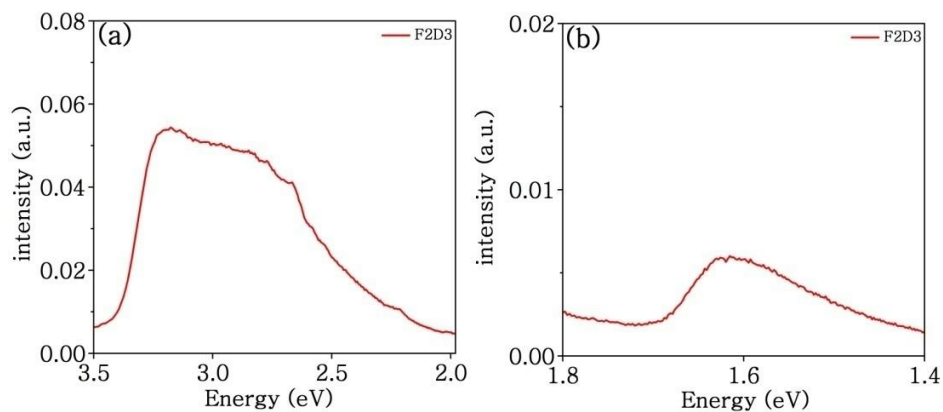


Figure 3.9 Photoluminescence spectra of F2D3

The films also emit in the red-NIR region as exhibited by the nanoparticle dispersion. However other defect related emission peaks such as blue, green and red region appear as a broad emission. Since visible emission is weak, there is a chance of reduction in defect states of the nanoparticles. The defect states in ZnO nanoparticles can be modified by (i) the polymer matrix acting as a surface passivator to fill the defects in the nanoparticles or (ii) the fabrication technique modifying the defect states on the surface, thereby quenching the visible emission (Xiong, 2010).

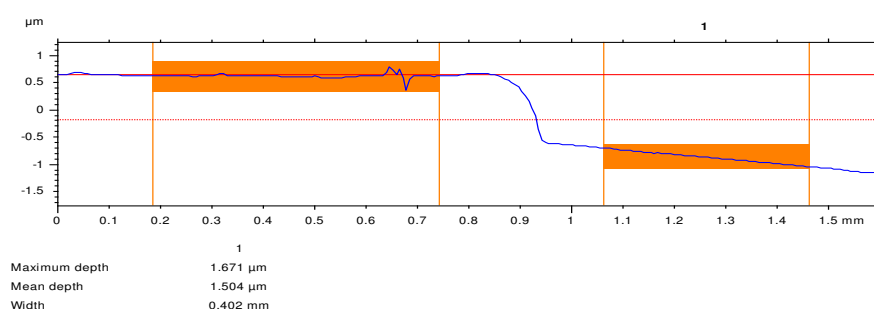


Figure 3.10 Step thickness of F2D3

The thickness of the films is measured using white light interferometer technique. Figure 3.10 shows the step thickness profile of F2D3 from which the thickness of the film is calculated to be 1.5 μm.

3.3.1.3. Nonlinear absorption studies

Nonlinear optical response of the fabricated films is studied using open aperture Z-scan technique at 532 nm. Normalized transmittance with respect to the position of films for a single coat and 3 numbers of coats at an input fluence, 26.7 J/cm² is shown in Figure 3.11 along with the result of pure PMMA film.

Film with a single coat (Figure 3.11b) did not show any nonlinearity. This may be due to the fact that there are insufficient numbers of nanoparticles which can induce nonlinearity. Whereas film fabricated with three coats exhibit a decreased transmittance, indicating RSA nature. Since the matrix, PMMA is not exhibiting

nonlinearity (Figure 3.11a), the nanoparticles will be solely responsible for inducing nonlinearity in the film.

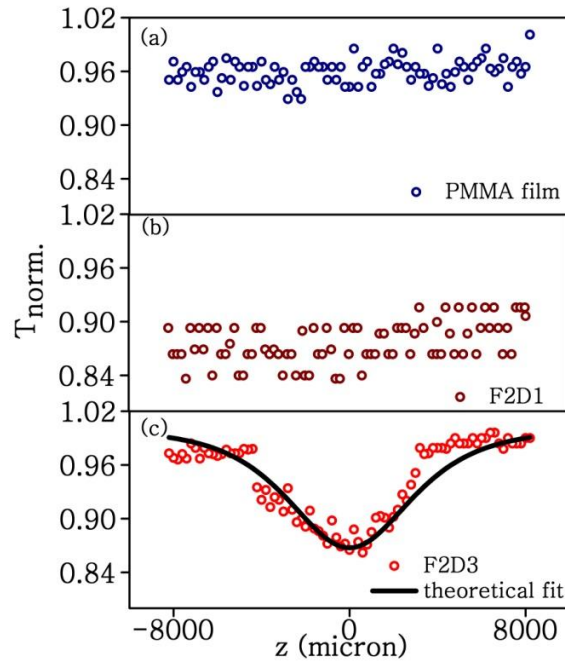


Figure 3.11 Normalized Z-scan transmittance of (a) PMMA film (b) F2D1 and (c) F2D3

From the theoretical fit given to the data, the nonlinear absorption coefficient and the saturation intensity are calculated and are found to be 1.2×10^{-10} m/W and 12.6×10^{12} W/m², respectively. Hence films with three coats are found to be having RSA nature and the effective NLA coefficient is greater than that of the colloid. Thus dip coated films are found to be applicable for laser safety devices and can be used as energy limiters also.

3.3.2. Spin coated films

3.3.2.1. Fabrication

Composites of ZnO nanotops with PMMA is prepared with varying ZnO nanotops loading in the monomer as 0.5 to 10 weight % in steps of 0.5 weight %. The number of coats is kept as three and films are fabricated using spin coating technique.

Uniform films are obtained with a spin speed of 5000 rpm for the spin coating unit. A glass substrate is used to fabricate films and the films are named as FxS3, where 'x' indicates the loading concentration of ZnO nanotops and 'S' indicates the spin coating technique.

3.3.2.2. Characterization

UV absorption property of the films is tested by taking UV-vis absorption spectra of the films. Figure 3.12 shows the UV absorption spectrum of F2S3 and it is clear that the absorption property of the spin coated films is improved compared to dip coated film, for the same loading concentration of ZnO. The absorption maximum has shifted to 321 nm indicating that the nanotops are more dispersed and maintain their crystallinity (Kulyk et al., 2009).

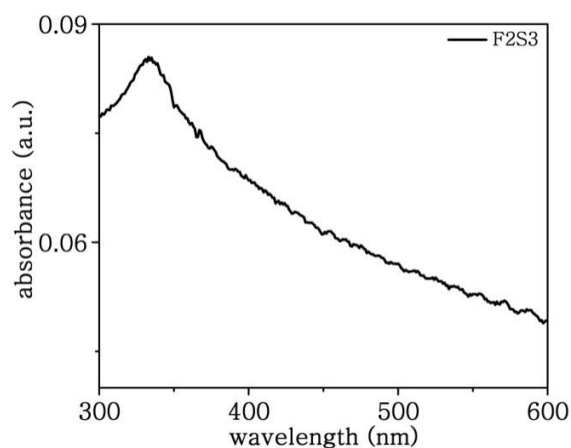


Figure 3.12 UV-vis absorption spectrum of F2S3

Figure 3.13 shows the photoluminescence spectrum of F2D3, taken by exciting at 325 nm. The characteristic band edge emission of the film is shifted to 3.19 eV (389 nm) which is a lower wavelength emission compared to that of dip coated film. The films emit in the red-NIR region also. Other defect related emission peaks appear as a broad emission.

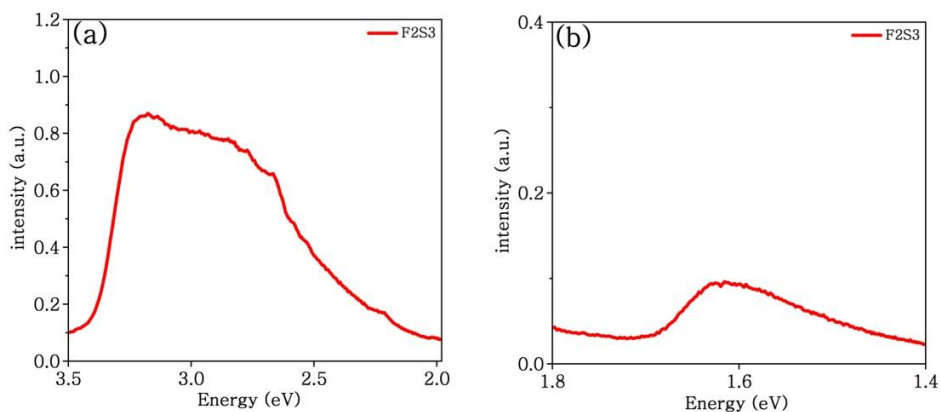


Figure 3.13 Photoluminescence spectra of F2S3

It can be assumed that the number of defects have been reduced in the film. This is evident from the emission curve itself, because the spin coated film shows a smoother emission curve compared to that of dip coated film. The intensity of emission for the spin coated film is found to be greater compared the dip coated film of the same loading concentration. This can be attributed to the large number of nanoparticles incorporated into the spin coated. The polymer matrix and the fabrication technique have a prominent role in influencing the emission of the coated film.

The surface morphology of the film F2S3 is evaluated using SEM image as shown in Figure 3.14. The film is uniform and the polymer is well blended with the nanotops.

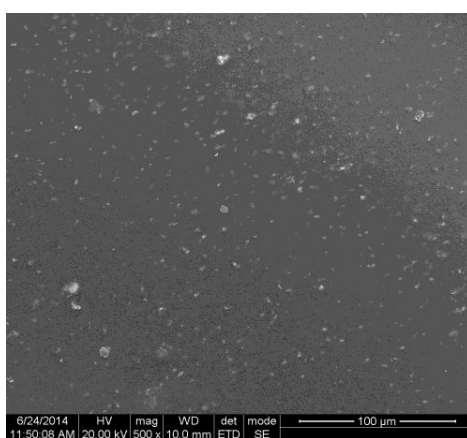


Figure 3.14 SEM image of F2S3

The step thickness profile of the film F2S3 measured using white light interferometer is shown in Figure 3.15. The thickness of the film is measured to be 1.3 μm .

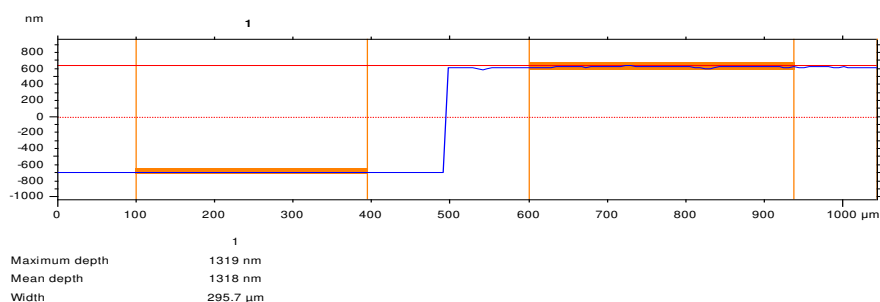


Figure 3.15 Step thickness of selected film.

3.3.2.3. Nonlinear absorption studies

The open aperture Z-scan of films fabricated from composites with varying ZnO concentration and having three numbers of coats are carried out at an input fluence 26.7 J/cm^2 . Among all, only two films exhibit nonlinear absorption. The response obtained for the films, F0.5S3, F2S3, F4.5S3 and F8S3 is shown in Figure 3.16.

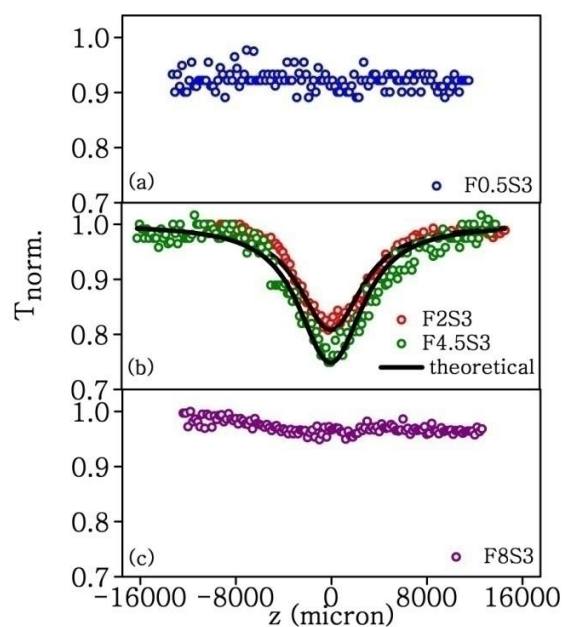


Figure 3.16 Open aperture Z-scan plots of spin coated films

The calculated values of effective TPA coefficient and saturation intensity for the films are given in Table 3.5.

Table 3.5 Effective two photon absorption coefficients (β_{eff}) and saturation intensities (I_{sat}) calculated for the films

Sample	$\beta_{\text{eff}} (10^{-10}) (m/W)$	$I_{\text{sat}} (x 10^{12}) (W/m^2)$
F2S3	1.4	7.4
F4.5S3	1.7	7.8

Films with lowest concentrations of ZnO (0.5 weight % to 1.5 weight %) did not show any trace of nonlinearity due to poor loading concentration of the ZnO particles. From 2 weight %, the films start exhibiting nonlinear absorption. The effective NLA coefficient is calculated to be $1.4 \times 10^{-10} m/W$ with saturation intensity of $7.4 \times 10^{12} W/m^2$. Films with higher loading concentration, F4.5S3 also exhibits RSA, with an increased value of NLA coefficient $1.7 \times 10^{-10} m/W$ and saturation intensity of $7.8 \times 10^{12} W/m^2$. But on further increase of loading concentration, the films did not respond well due to their poor quality. The reduced quality of the films with higher loading concentration may be attributed to the fact that with the increase of loading, the monomer may not be able to disperse all nanoparticles. This leads to agglomeration of nanoparticles and non-uniformity in the film which ultimately lead to poor quality of the films.

In the present section it has been observed that the films fabricated from PMMA-ZnO nanotop composite exhibited absorptive nonlinearity in response to a laser of wavelength 532 nm. The parameters associated with film fabrication are also optimized here. The spin coated film exhibited nearly 33 % increase in the measured value of effective TPA coefficient compared to dip coated film, for the same weight % of ZnO. The UV-vis absorption spectra of dip and spin coated films show that UV absorption has increased for the spin coated film compared to dip coated film of the same ZnO loading. The absorption maximum has blue shifted for spin coated film, compared to dip coated film indicating that the coating technique has helped to

fabricate uniformly dispersed film. Another observation is that the increase of loading concentration in spin coated films increases the nonlinear absorption. But this is limited by the agglomeration of nanoparticles at higher loading concentrations.

In order to find out the reason for the variation in the properties of the films with respect to fabrication technique, a better understanding of the basic mechanism of spin and dip coating techniques is required. In spin coating process, solution is first deposited on the substrate, and the substrate is then accelerated rapidly to the desired rotation rate. Liquid flows radially, owing to the action of centrifugal force, and the excess is ejected off the edge of the substrate. The film continues to thin slowly until disjoining pressure effects cause the film to reach an equilibrium thickness or until it turns solid-like due to a dramatic rise in viscosity through solvent evaporation. The final thinning of the film is usually due to solvent evaporation, if volatile solvents are used (Hall et al., 1998; Sahu et al., 2009). In our case the polymer matrix is not getting evaporated instead it gets solidified due to the rise in viscosity caused by the completion of polymerization of MMA to PMMA and thereby form a well dispersed polymer nanocomposite film. On the other hand in dip coating, the substrate is normally withdrawn vertically from the liquid bath at a particular speed. The moving substrate entrains the liquid in a fluid mechanical boundary layer that splits into two, above the liquid bath surface, the outer layer returning to the bath (Brinker et al., 1994; Kaneva and Dushkin, 2011). In the case of composite films, dip coating does not help to complete the polymerization and hence there is no increase in viscosity during the dipping process, leading to excess draining of the composite solution back to the liquid bath. Thus for the same number of coating layers, more amount of composite may get coated on the substrate during spin coating compared to dip coating. To confirm this fact, we have conducted thermogravimetric analysis (TGA) of the composite films, F2D3 and F2S3 and the result is shown in Figure 3.17.

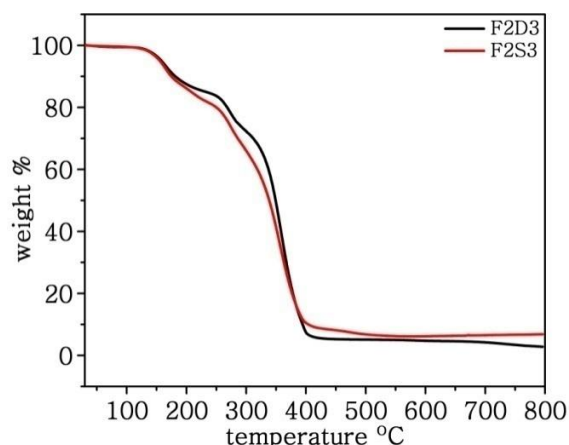


Figure 3.17 TGA plot of dip and spin coated films with 2 weight % ZnO

Equal weight of the spin and dip coated films F2D3 and F2S3 are taken. The samples are then heated from 30 °C to 800 °C. A weight over the temperature range 130 °C to 550°C is observed due to the decomposition of the capping agent and the polymer matrix. After 550 °C, there is no considerable weight loss indicating the presence of pure ZnO. The dip coated film has a residue of 2.8 % whereas the spin coated film has 6.82 %. Since the residue of dip coated film is smaller than the spin coated film, it can be concluded that the number of ZnO particles present in the dip coated film is less compared to that of the spin coated film. This may be due to the fact that the heavy ZnO nanoparticles move towards the bottom of the film and may drop out along with the outer layer of the composite solution due to gravity, whereas gravity has little role in spin coated films. Thus the TGA results confirm that on fabricating films with composites of same loading concentration of ZnO, the dip coated film could not accommodate desired amount of ZnO nanoparticles. This factor adversely affects its linear and nonlinear optical properties as seen in our study.

3.4. Conclusion

ZnO nanoparticles have been synthesized using solution precipitation technique, using two types of capping agents. Morphological and spectroscopic characterizations are carried out to study the properties of the nanoparticles. PVP-capped nanoparticles having a novel ‘top’ like structure are found to have good

nonlinear optical response and they are called ZnO nanotops. PMMA-ZnO nanotop composites are prepared and fabricated into films using spin and dip coating technique. Film fabrication parameters are optimized to get good quality films with nonlinear optical response. The open aperture Z-scan results show that films fabricated by dip and spin coating techniques exhibit increased nonlinear absorption with decreased saturation intensity, compared to the colloid of ZnO nanotops. These films are found to be applicable as reverse saturable absorbers.

CHAPTER 4

SATURATION AND REVERSE SATURATION OF ABSORPTION IN PMMA-ZnO NANOCOMPOSITE FILMS

This chapter describes the fabrication of PMMA-ZnO nanotop composite films in which the nanotops are dispersed in the matrix with the help of dispersing agents. Oleic acid and triton are used as dispersing agents and the composite films are fabricated by dip and spin coating technique. Nonlinear absorptive nature of the films is analyzed by using open aperture Z-scan technique. Tuning of the loading concentration of ZnO nanotops in the films enabled them to act as either saturable or reverse saturable absorbers. Two photon absorption, two-step absorption, and free carrier absorption are found to have distinct roles in the observed nonlinear absorption of the samples.

4.1. Introduction

The most challenging part of fabricating a good quality polymer nanocomposite film is the dispersion of nanoparticles in the polymer matrix. The adverse factor limiting the quality of the composite is the tendency of nano inclusions to agglomerate due to their high surface energy with reduced size. The physical and optical properties of nanoparticles can change with the aggregation ratio, even though the system contains nanoparticles of identical size (Horikoshi and Serpone, 2013). In order to have a better nonlinear optical response, the strategy adopted can be modified in three ways as follows: (1) adopting physical blending method (2) modifying the surface of the nanoparticles with stabilized ligands (Khrenov et al., 2005) (3) using a dispersing agent to prevent agglomeration. Among these, using a dispersing agent to prevent agglomeration is very suitable for preparing good polymer nanocomposite films.

Morino and Ferrari reports that there are several category of materials which act as dispersing agents which include electrolytes, surfactants, adsorbed polymers, adsorbed charged polymers, coupling agents, non-adsorbing polymers, potential-determining ions, etc. (Moreno and Ferrari, 2012). Various mechanisms through which dispersion is maintained are electrostatic repulsion, combination of adsorption and electrostatic repulsion, steric hindrance, combination of steric hindrance and electrostatic repulsion and depletion stabilisation. Polyethylene glycol (PEG), polyvinyl pyrrolidone (PVP), polyvinyl alcohol (PVA), etc. are polymeric surfactants whereas cetyl trimethylammonium bromide (CTAB), sodium dodecyl sulphate (SDS), triton-X 100, diethyleneglycol (DEG), tween 20, oleic acid, etc. are nonionic surfactants.

Dispersing agents can be used in the synthesis stage of nanoparticles to stabilize them where they are more accurately called as capping agents or surfactants. According to Heijman and Stein, poly acrylic acid can stabilize titanium dioxide (TiO_2) dispersions by electrostatic and steric stabilization acting simultaneously (Heijman and Stein, 1995). There are reports in which surface modification of TiO_2 nanoparticles by polyethylenimine has been found to improve the dispersion of nanoparticles (Sakka et al., 2005). The adsorption of polyacrylamide is reported to increase the dispersion of TiO_2 nanoparticles by steric stabilisation (Deiss et al., 1996). Among the various dispersing agents available, oleic acid and triton are two important dispersing agents and hence they are used in the present investigation. Oleic acid ($\text{C}_{18}\text{H}_{34}\text{O}_2$) is an organic dispersing agent, having molecular formula $\text{CH}_3(\text{CH}_2)_7\text{CH}=\text{CH}(\text{CH}_2)_7\text{COOH}$. It is a fatty acid that occurs naturally in various animal and vegetable fats and oils. In chemical terms, oleic acid is classified as a monounsaturated omega-9 fatty acid. It is odourless and colourless oil and the structure is as shown in Figure 4.1.

Oleic acid is mostly used for the surface modification of nanoparticles during the synthesis itself so as to make them dispersible in solvents (Tao et al., 2011). Many

studies report the synthesis of ZnO nanoparticles with the help of oleic acid as both capping agent and surfactant (Fakhroueian et al., 2013; Hong et al., 2006). Liu and Su report that the surface modification of ZnO nanoparticles by oleic acid has improved their dispersion in organic solvents (Liu and Su, 2006). A composite of these ZnO nanoparticles with PMMA showed good UV absorption also.

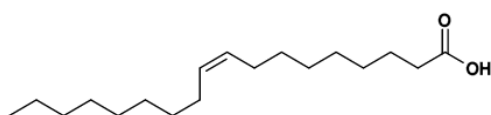


Figure 4.1 Structure of oleic acid

Triton-X 100 (octyl phenol ethoxylate) $C_{14}H_{22}O(C_2H_4O)_n$ ($n=9-10$) is a non ionic surfactant that has a hydrophilic polyethylene oxide chain and an aromatic hydrocarbon lipophylic or hydrophobic group as shown in Figure 4.2.

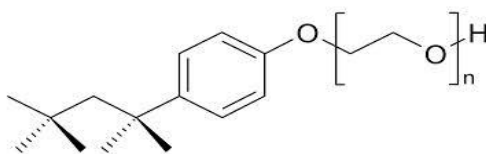


Figure 4.2 Structure of Triton-X 100

Use of dispersing agents for stabilization of nanoparticles after their synthesis is very rare and lack of published reports. Dispersing agents like Dolapix CA, Dalais PC21, Reotan LA, PEI, Dolapix A88, KV9021, Dolapix ET85, Dolapix PC80, Dolapix CE64 and Tiron are tried to get TiO_2 -water dispersion by Sentein et al. Their aim is to recover the nanopowders directly in water at the exit of the reaction zone, mainly for safety reasons (Sentein et al., 2009).

In the present study, hydrophilic ZnO and hydrophobic PMMA do not blend easily and thus produce aggregation and clustering of the nanoparticles on increasing the loading of ZnO. ZnO nanotops and the fabricated films discussed in chapter 3 have exhibited considerable optical nonlinearity but lack of proper dispersion is the

only adverse factor here. So use of a dispersing agent during the stage of preparation of polymer nanocomposite can solve this issue.

4.2. PMMA-ZnO nanocomposite films by using dispersing agent

In the present study we use oleic acid and triton-X 100 as dispersing agents. These dispersing agents are used during the preparation of polymer nanocomposite so as to get the ZnO nanotops well dispersed. PMMA is used as the matrix for the preparation of polymer nanocomposite films of ZnO nanotops. As discussed in the previous chapters, in addition to optical transparency, the amorphous nature of PMMA enables ease of fabrication of films due to its flexibility compared to other transparent polymers like PS and poly imides. PMMA helps the nanoparticles to be dispersed and stable (Sreeja et al., 2010) and diminishes the thermal effects (Kulyk et al., 2009). Even though PVA is a flexible transparent polymer matrix and PVA-ZnO films with NLO properties are reported (Jeeju et al., 2014), its hydrophilic nature promotes moisture absorption and hence adversely affect the fabrication of optoelectronic devices. The ZnO nanotops are first dispersed in desired amount of dispersing agent and then mixed with methyl methacrylate. This helps the hydrophilic part of the dispersing agent to link with ZnO and the hydrophobic part with the monomer.

4.2.1. Oleic acid dispersed films

4.2.1.1. Fabrication

The compatibility of the dispersing agent with the monomer is to be checked first before using it for the composite preparation. For this, the dispersing agent is mixed with the monomer, and the mixture is polymerized and coated on a glass plate. Spin coated and dip coated films are prepared keeping the number of coats as three. Spin and dip coated films of oleic acid-PMMA are named FS3O and FD3O respectively.

Since the films fabricated are found to be uniform and does not affect their transparency, ZnO nanoparticles dispersed in oleic acid is used to prepare composite films with polymer. Preweighed ZnO nanoparticles (1 weight % to 10 weight %) are dispersed in oleic acid through ultra sonication for 30 minutes. Methyl methacrylate (7 ml) is added slowly to this and again ultrasonicated for 2 hrs. Well dispersed ZnO-monomer dispersion is then polymerized by bulk polymerization technique using benzoyl peroxide as initiator. The polymer nanocomposite is then allowed to cool before fabrication. Films are fabricated on a clean glass plate by using spin and dip coating techniques, keeping the number of coats as three. The optimized parameters of dip coating are shown in Table 4.1. The optimized rotational speed for the spin coating technique is 1000 rpm. Dip coated films are named as FxD3O and spin coated films are named FxS3O where ‘x’ refers to the loading concentration.

Table 4.1 Optimized parameters of dip coating technique

Dipping speed	5000 $\mu\text{m/s}$
Retrieval speed	500 $\mu\text{m/s}$
Dipping duration	8 sec
Dry duration	1 m
Drying temperature	65 $^{\circ}\text{C}$

4.2.1.2. Characterization

Polymer nanocomposite films fabricated using spin and dip coating techniques are characterized to study their surface morphology, thickness, linear and nonlinear optical properties. Figure 4.3 (a) and (b) shows the UV-vis absorption spectra of dip coated and spin coated films, respectively.

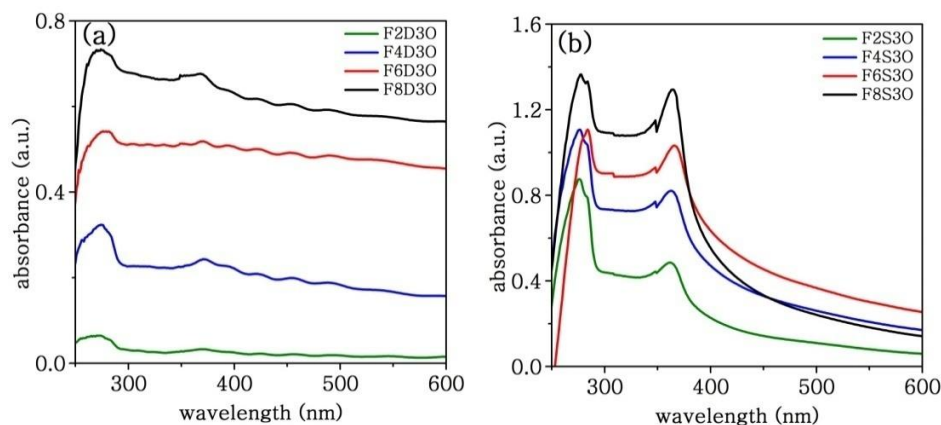


Figure 4.3 UV-vis absorption spectra of selected (a) dip coated and (b) spin coated films

The UV absorption intensity increases with increase in loading concentration for both set of films as expected. The spin coated films are found to be good UV absorbers compared to dip coated films. This may be due to the fact that, during dip coating process some amount of the nanocomposite drips back to the container from the glass substrate due to gravity. So the films may have reduced amount of the nanoparticles compared to spin coated films. The presence of excitonic peak in spin coated films (363 nm) indicates that the nanoparticles are well dispersed in these films. The spin coated films show peaks indicating the enhanced crystallinity of the nanoparticles in the matrix (Kulyk et al., 2009). However the dip coated films show excitonic peak at 367 nm. The absorption maximum has blue shifted for the spin coated films which again support the fact that the dispersing agent and the fabrication technique have helped to prepare uniformly dispersed films.

Tauc plot for selected spin and dip coated films are shown in Figure 4.4. The bandgap of films with 8 weight % of ZnO is found to be lower than that of films with 2 weight % ZnO.

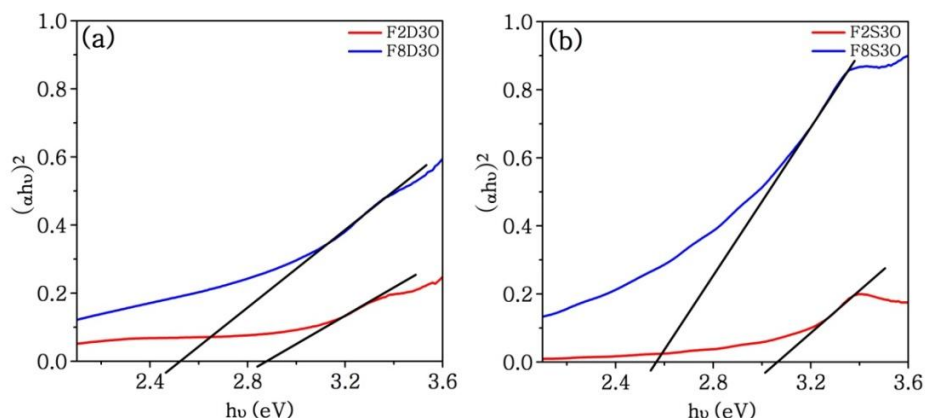


Figure 4.4 Tauc plots of selected (a) dip coated and (b) spin coated films

Bandgap values evaluated from the plot are given in Table 4.2. In the case of ZnO nanoparticles it has been observed that, the bandgap decreases with the increase in the size of the nanoparticles. Film prepared here also showed a decrease in the bandgap with increase in loading concentration. This may be attributed to a small scale aggregation of nanoparticles in the films with higher loading concentration.

Table 4.2 Optical bandgap calculated for selected films

Film	Bandgap (eV)
F2D3O	2.87
F8D3O	2.51
F2S3O	3.06
F8S3O	2.56

The photoluminescence spectra of the selected spin and dip coated films are shown in Figure 4.5. At an excitation wavelength of 325 nm, the films exhibit emission in the UV region followed by a broad emission from blue-green to red-NIR region, as observed for the synthesized nanoparticles. Emission in UV region is the characteristic band edge emission, due to the photo-generated electron recombination with holes in the valence band or in traps near the valence band. Whereas the emission in the visible region can be attributed to the surface defects present.

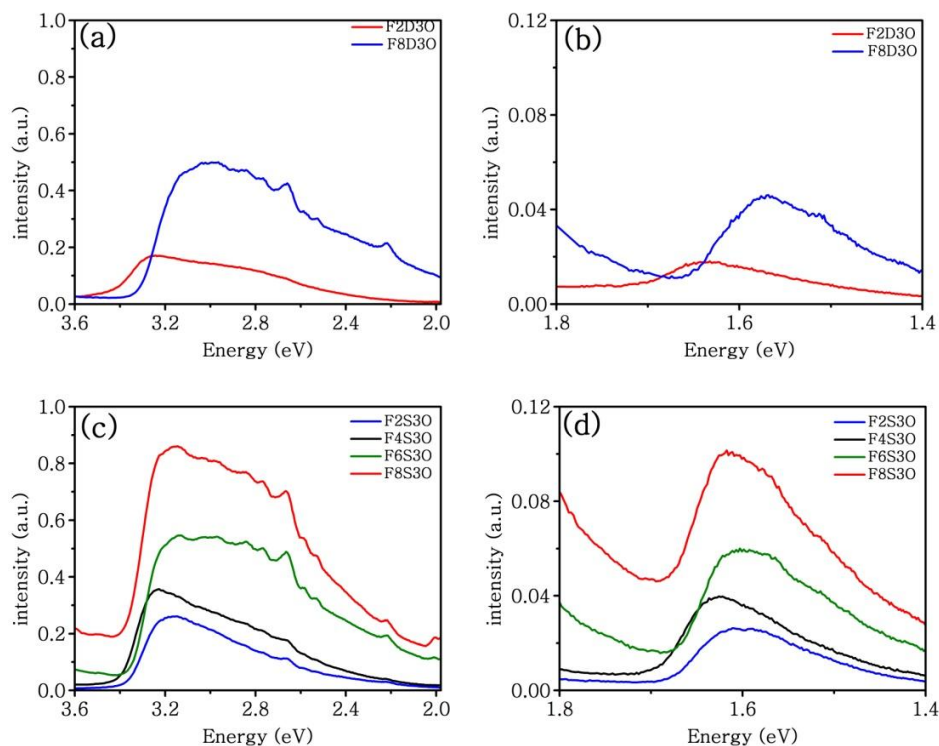


Figure 4.5 Photoluminescence spectra of selected dip coated films (a and b) and spin coated films (c and d)

The intensity of emission is increased with respect to increase in loading concentration due to the presence of more number of light emitters. The spin coated films are found to have more intense emission compared to the dip coated films which can be attributed to the quality of the films. There are reports where surface defects, which cause visible emission in nanoparticles, get passivated by the use of polymers (Liu and Su, 2006). But in the present study the nanoparticles are very good visible light emitters even in the presence of PMMA. This can be due to the presence of the dispersing agent, which hinders the formation of polymer coating on the surface of nanoparticles and thereby reduces the surface passivation to some extent. The amount of polymer in the nanocomposites may not be sufficient enough to surface passivate the defects of all nanoparticles since the amount of monomer is kept constant and the loading concentration of ZnO is increased.

Figure 4.6 shows the scanning electron micrograph of films with 2 weight % ZnO fabricated by dip and spin coated films. The SEM images clearly show that oleic acid dispersed the nanoparticles well and helped to get uniform films.

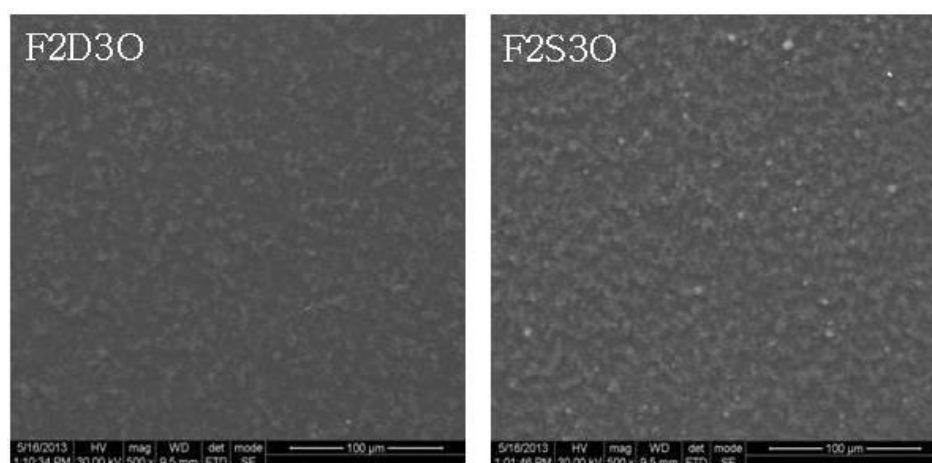


Figure 4.6 SEM image of dip coated and spin coated films with 2 weight % ZnO

The thickness of the films is measured by using white light interferometer technique. The surface profile of the selected dip and spin coated films is shown in Figure 4.7. The images show uniform surface of dip and spin coated films and it is in agreement with the SEM images.

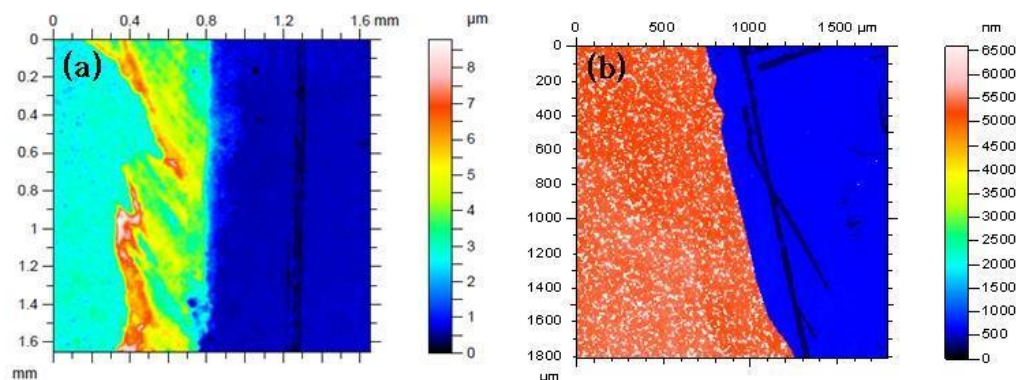


Figure 4.7 Surface profile of (a) dip coated and (b) spin coated films

Average thickness of the films is obtained from the step thickness profile (Figure 4.8.) and is $6.8 \mu\text{m}$ for the dip coated films and $5.3 \mu\text{m}$ for the spin coated films.

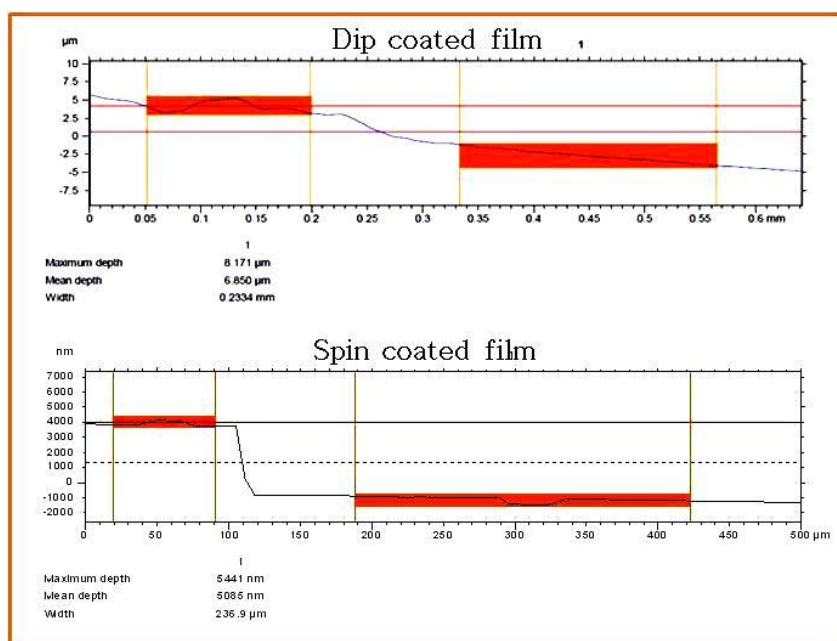


Figure 4.8 Step thickness of (a) dip coated and (b) spin coated films

4.2.1.3. Nonlinear absorption studies

Spin and dip coated films of oleic acid-PMMA are scanned with open aperture Z-scan at fluence 2.2 J/cm^2 and the plot is given in Figure 4.9.

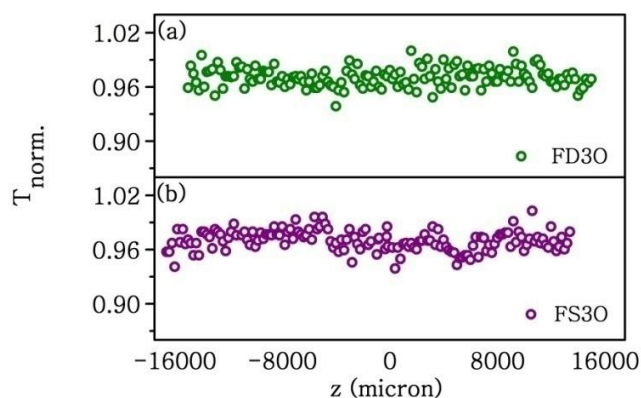


Figure 4.9 Normalized transmittance curves of (a) FD30 and (b) FS30.

The films did not show any nonlinear response indicating that oleic acid will not alter nonlinear absorption properties of polymer nanocomposites.

Open aperture Z-scan measurement of dip coated polymer composite films are carried out at a fluence 3.3 J/cm^2 and at 532 nm wavelength. Figure 4.10 shows the results of the selected dip coated composite films.

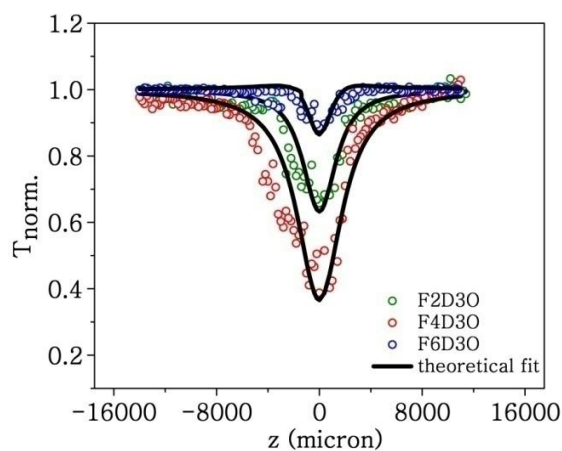


Figure 4.10 Normalized Z-scan transmittance of selected dip coated films for varying loading concentration of ZnO

All the dip coated films exhibit decreased transmittance with increase in loading concentration of ZnO nanotops indicating RSA nature.

Table 4.3 Effective two photon absorption coefficients (β_{eff}) and saturation intensities (I_{sat}) calculated for the dip coated films

Film	$\beta_{\text{eff}} (\times 10^{-10}) (\text{m/W})$	$I_{\text{sat}} (\times 10^{12}) (\text{W/m}^2)$
F2D30	69	8.00
F4D30	220	8.00
F6D30	235	8.00
F8D30	258	8.00

The experimental data is given theoretical fit and the effective nonlinear absorption coefficient and saturation intensity have been calculated. All the calculated parameters for the dip coated films are shown in Table 4.3.

Open aperture Z-scan results of spin coated polymer composite films at a fluence 3.3 J/cm^2 is shown in Figure 4.11. The spin coated films exhibit a slow shift from a reduced transmission to a substantially increased transmission with increase in loading concentration.

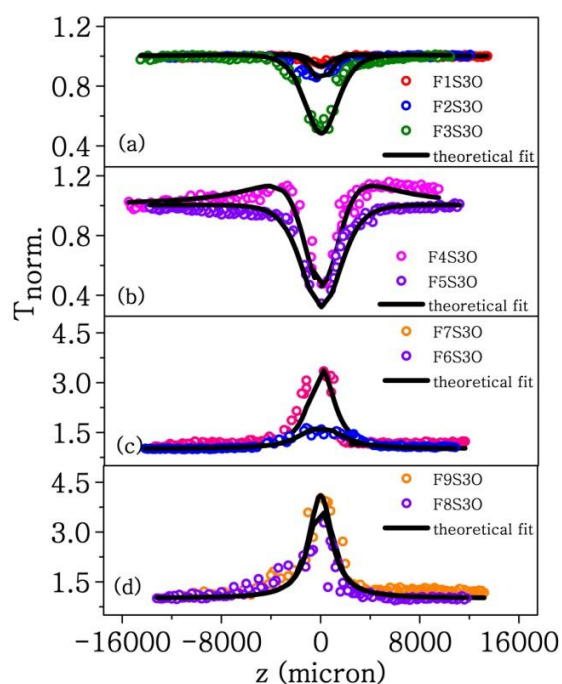


Figure 4.11 Normalized Z-scan transmittance of selected spin coated films for varying loading concentration of ZnO

The effective nonlinear absorption coefficient and saturation intensity have been calculated and are shown in Table 4.4.

Table 4.4 Effective two photon absorption coefficients (β_{eff}) and saturation intensities (I_{sat}) calculated for the spin coated films prepared with oleic acid by varying ZnO loading concentration

Film	β_{eff} ($\times 10^{-10}$) (m/W)	I_{sat} ($\times 10^{12}$) (W/m²)
F1S3O	26	10.0
F2S3O	62	9.5
F3S3O	240	9.5
F4S3O	640	2.2
F5S3O	1200	2.2
F6S3O	170	6.2
F7S3O	31	6.2
F8S3O	26	6.2
F9S3O	18	6.2

The absorptive nonlinearity exhibited by the films can be explained as follows. During the preparation and fabrication of polymer-ZnO nanotop composite films, the ZnO nanotops are well dispersed in the polymer matrix with the help of oleic acid and a good interaction between polymer chains and nanoparticles arises. Thus in addition to the dispersing agent, the matrix also helps to get a well dispersed nanocomposite. As a result the nanoparticles in the film are not much hindered from exhibiting their inherent properties. When these films are exposed to laser pulses, a dielectric dipole layer is generated on the nanoparticle surface due to electric charge interaction between the polymer and the nanoparticle. This dielectric confinement effect, is a surface polarization effect depending on the permittivity ratio of the particles and the surrounding medium (Takagahara, 1993). Thus the separation of excited charges increases and the electric field inside the nanoparticles also increases (Ai et al., 1994; Wu et al., 1997). Also the change in charge density distribution of the nanoparticle surface strengthens an harmonic vibrations of surface electrons (Wang et al., 2001). Thus the nanocomposites will be able to exhibit stronger nonlinear response.

From the linear absorption spectra of the films (Figure 4.3) it is obvious that the films have absorption at the excitation wavelength (532 nm). The films have more absorption at the two-photon wavelength of 266 nm, indicating the existence of excited states suitable for two-step as well as genuine two-photon absorption processes (Khatei et al., 2012; Mary et al., 2011). As the measured NLA coefficients are found to vary with incident intensity in our samples, the observed NLA should have less contribution from genuine TPA and more contribution from a two-step absorption process (He et al., 2008; Rumi and Perry, 2010). Since the laser pulsewidth used for the present study (7 ns) is greater than the free carrier lifetime of ZnO nanoparticles (Zhang et al., 1997), there is a chance for strong FCA by the photogenerated carriers. The variation of NLA coefficient with intensity also confirms this fact (Kurian et al., 2007). Thus in general; TPA, two-step absorption, and FCA have distinct roles in the observed nonlinear absorption of our samples.

In the present study, the Z-scan data fits well to a theoretical model where both saturable absorption and two-photon absorption take place in the system, as shown in Figure 4.11. The Z-scan plots show that films with higher ZnO concentration exhibit saturable absorption. SA is related to the process of electron excitation from the valence band to the conduction band by photon absorption. Once the electrons accumulate in the conduction band and some of them undergo FCA, the initial states of the absorbing transition will be depleted and the final states will get occupied. As a result, further absorption is reduced. This effect is known as Pauli blocking (Bao et al., 2009). Pauli blocking is a consequence of the exclusion principle according to which electron transitions are inhibited if the final state is occupied by another electron. According to Zitter (1969) who has given a theoretical framework for this phenomenon, a semiconductor absorbing a monochromatic light beam will generate enough number of carriers to fill band states up to and including those of the optical transition. Optical absorption will be then saturated and a condition of transparency shall be resulted (Zitter, 1969). The study shows that in this regime the absorption coefficient varies inversely with light intensity.

This fact agrees well with the experimental results obtained from the photoluminescence spectra (Figure 4.5) and the bandgap values (Table 4.2). The photoluminescence spectra clearly show that films with higher loading of ZnO nanotops, exhibiting saturation of absorption, are having more number of defects. The bandgap values calculated for the films F8D3O and F8S3O are having lower values compared to F2D3O and F2S3O. This also indicates the increased number of defects for the films. As the density of defects increases the rate of two photon absorption also increases as per equation 3.6. Thus there may arise a situation in which most of the two photon excited carriers get trapped in these defects, reducing the population of ground state and enhancing the chance of saturation of absorption (Haripadmam et al., 2014a).

4.2.2. Triton dispersed films

4.2.2.1. Fabrication

The polymer nanocomposites are prepared using triton as dispersing agent following the same procedure as explained above. The polymer nanocomposite films with varying concentration of ZnO nanotops (1 weight % to 10 weight %) are fabricated by using spin coating technique, keeping the number of coats 3. The rpm is optimized to be 1000, to get uniform films. Films are named as F1S3T through F10S3T. Here we have not fabricated films using dip coating technique, because the previous section showed that the NLA of dip coated films is less compared to spin coated films.

4.2.2.2. Characterization

Figure 4.12 shows the UV-vis absorption spectra of all the spin coated films fabricated on glass. It is clear from the figure that the increase in loading concentration increases the UV absorption as expected. Also these films exhibited enhanced UV absorption and sharp excitonic peaks compared to oleic acid dispersed films (Figure 4.3). The enhanced UV absorption and the improved crystallinity of the nanoparticles can be attributed to two factors: (1) triton is acting as a very good

dispersing agent by dispersing the nanotops through steric hindrance (2) spin coating technique has helped to fabricate uniform films and improved the dispersion of the nanotops in the film.

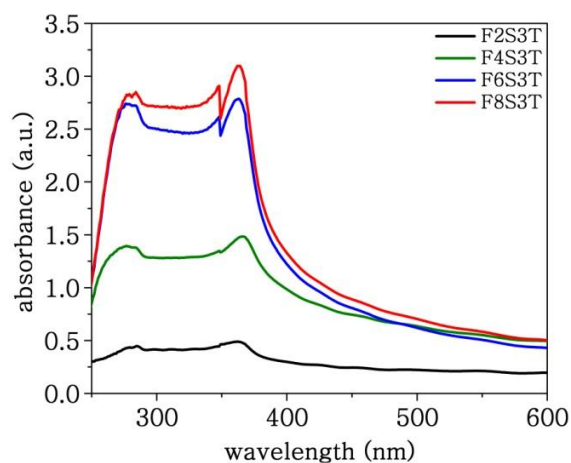


Figure 4.12 UV-vis absorption spectra of selected spin coated films

The optical bandgap of the films are obtained from Tauc plot as shown in Figure 4.13. The bandgap of the films found to decrease with increase in loading concentration.

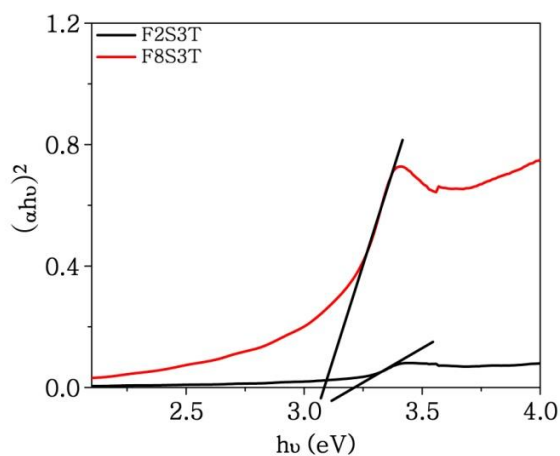


Figure 4.13 Tauc plot for the selected spin coated films

For F2S3T the bandgap calculated is 3.2 eV whereas for F8S3T, it is 3.09 eV. These films exhibited larger optical bandgap compared to oleic acid dispersed films,

indicating the more uniform dispersion while using triton. In triton, the bulky benzene groups, which will impart steric hindrance, help in better dispersion of ZnO nanotops.

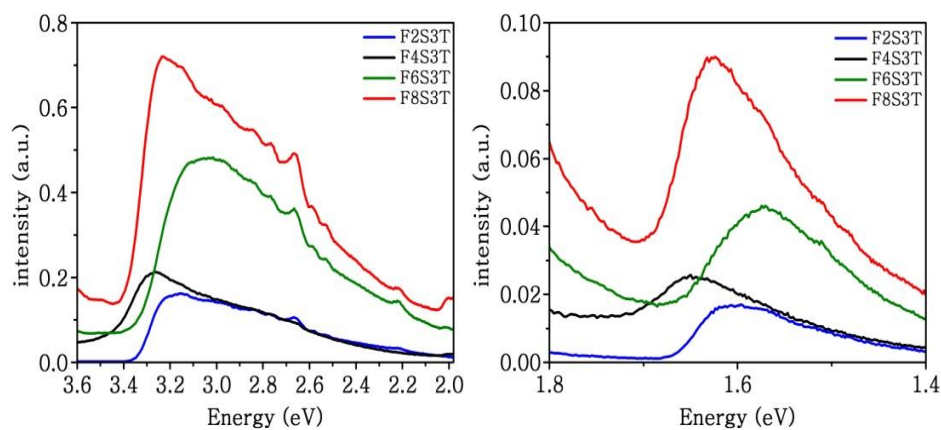


Figure 4.14 Photoluminescence spectra of selected spin coated films

The films exhibit characteristic band edge emission and red-NIR emission as shown in Figure 4.14. Band edge emission is more intense compared to red-NIR emission and the intensity of emission is increased with respect to increase in loading concentration.

Compared to oleic acid dispersed films, these films exhibit reduced emission. The reason can be that in a well dispersed medium of nanoparticles, there is a chance that the nanoparticles are trapped inside the polymer chains and both the polymer and the dispersing agent cap the nanoparticles. Thus there is a possibility of the polymer to act as a surface passivator and reduce the defect states, leading to reduced emission.

The SEM image of F2S3T (Figure 4.15) as a representative film of spin coated PMMA-ZnO nanotop film prepared by using triton as dispersing agent shows the uniform dispersion of nanotops.

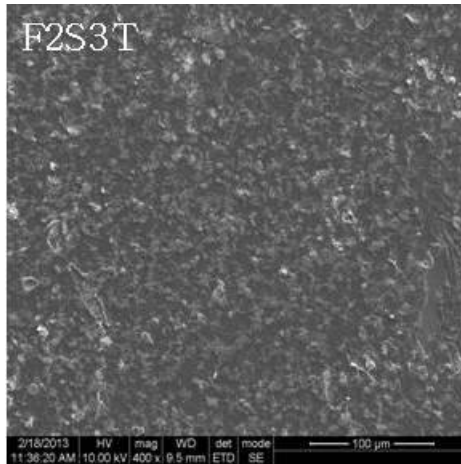


Figure 4.15 SEM image of F2S3T

The surface profile and step thickness of the selected film is shown in Figure 4.16 and 4.17 respectively. The average thickness of the films is measured to be 5.5 µm.

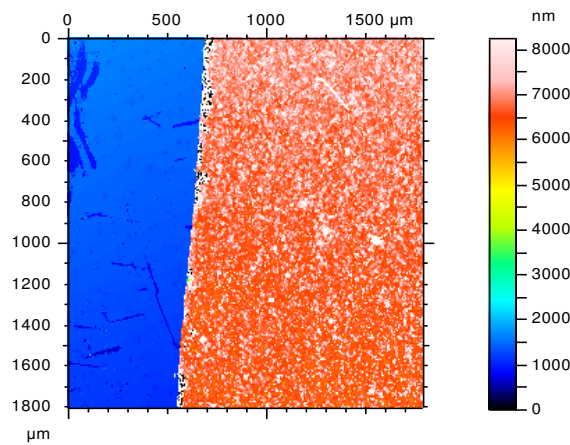


Figure 4.16 Surface profile of selected film

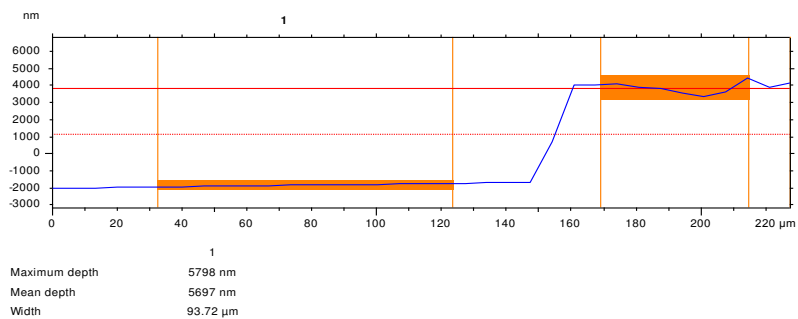


Figure 4.17 Step thickness of selected film

4.2.2.3. Nonlinear absorption studies

Figure 4.18 shows the open aperture Z-scan result of the selected spin coated composite films scanned at 3.3 J/cm^2 . The NLA coefficient and the saturation intensity calculated are shown in Table 4.5.

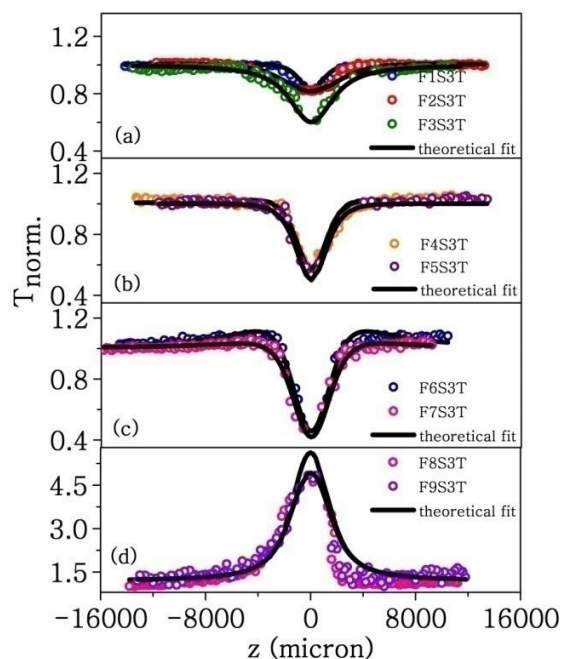


Figure 4.18 Open aperture Z-scan plot for triton dispersed spin coated films of varying concentration

Triton dispersed films also exhibited a switch over from RSA to SA as observed for oleic acid dispersed films. The theoretical fit given to the experimental data revealed the fact that TPA, two-step absorption, and FCA have distinct roles in the observed nonlinear absorption of the films. The effective NLA coefficient and saturation intensity calculated for all the films shows that the RSA-SA transition appeared only above 7 weight % of ZnO loading. However for the films prepared using oleic acid, RSA nature sustained only up to 5 weight % loading of ZnO in the matrix. So triton is proved to be a better dispersing agent, maintaining the RSA nature of the nanoparticles. However the value of effective NLA coefficient is less for triton

dispersed films, compared to oleic acid dispersed films. This is in agreement with the calculated value of the bandgap of the films.

Table 4.5 Effective two photon absorption coefficients (β_{eff}) and saturation intensities (I_{sat}) calculated for the spin coated films prepared with triton by varying ZnO loading concentration

Film	β_{eff} ($\times 10^{-10}$) (m/W)	I_{sat} ($\times 10^{12}$) (W/m ²)
F1S3T	27.00	9.8
F2S3T	56.00	9.5
F3S3T	150.00	6.5
F4S3T	260.00	5.2
F5S3T	320.00	5.0
F6S3T	660.00	3.2
F7S3T	700.00	2.4
F8S3T	80.00	2.5
F9S3T	10.00	2.6

Figure 4.19 shows the NLO response of PMMA-triton film showing absence of nonlinearity, and confirms that the ZnO nanoparticles are responsible for the exhibited nonlinear absorption.

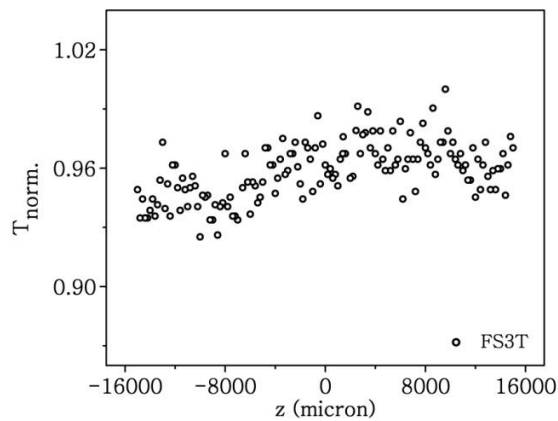


Figure 4.19 Open aperture Z-scan plot for PMMA-triton film

4.2.3. Fluence dependent studies

From the previous section it has been found that the films of dispersed ZnO nanotops with polymer showed RSA behaviour at lower concentrations of ZnO, at a fluence 3.3 J/cm^2 . Further, fluence dependent Z-scan of these films has been carried out to have a thorough knowledge of their nonlinear behaviour.

Films with 2 weight % ZnO, prepared with the help of oleic acid (F2S3O) and triton (F2S3T) are selected for the present study. The fluence is varied from 0.5 to 3.3 J/cm^2 . The Z-scan traces obtained are peculiar in such a way that an increase in transmission is seen at moderate laser fluences, while the transmission drastically decreases at higher fluences. Films with oleic acid and triton dispersed ZnO, exhibited the same behaviour as shown in Figure 4.20.

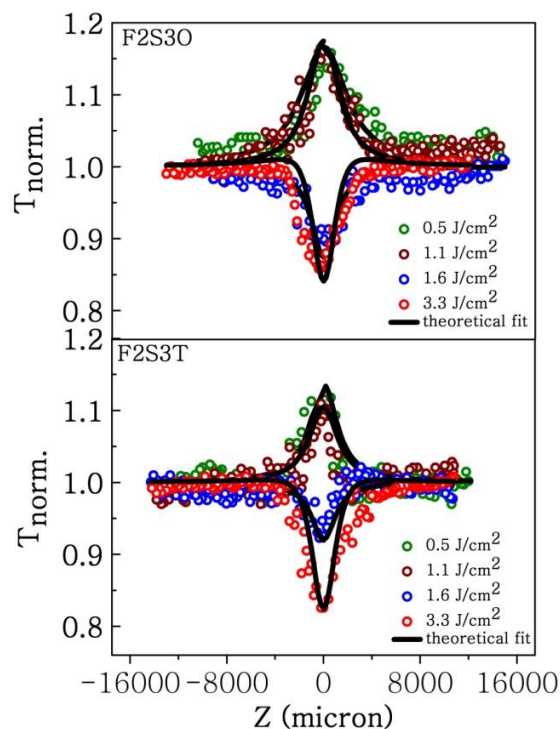


Figure 4.20 Open aperture Z-scan plot for F2S3O and F2S3T at various fluences

The switching of absorptive nonlinearity from absorption saturation to reverse saturation can be explained as follows. When the film is far away from the focus, the pump intensity is too low to induce nonlinearity and the transmittance is equal to unity. When the film is moved near to the focus, intensity of light on the sample is increased and the ground state gets depleted causing absorption saturation, so that the transmittance increases. This is because, the NLA coefficient is linearly related to the population difference between ground state and excited state of the nanoparticles. On the other hand, as the film reaches the focus, still higher intensities are seen by the film and RSA dominates causing strong optical limiting and hence transmittance decreases. As the fluence is further increased a valley started appearing and the depth of the valley is gradually increased. At sufficiently high fluence (3.3 J/cm^2), nonlinear absorption overrides the ground state bleaching completely and shows deep valley indicating only RSA. Table 4.6 summarizes the NLA coefficient and saturation intensity calculated for F2S3T and F2S3O for varying incident fluences.

Table 4.6 Effective two photon absorption coefficients (β_{eff}) and saturation intensities (I_{sat}) calculated for F2S3T and F2S3O by varying the input fluence

Fluence (J/cm^2)	F2S3T		F2S3O	
	$\beta_{\text{eff}} \times 10^{-10}$ (m/W)	$I_{\text{sat}} \times 10^{12}$ (W/m^2)	$\beta_{\text{eff}} \times 10^{-10}$ (m/W)	$I_{\text{sat}} \times 10^{12}$ (W/m^2)
0.5	0.1	2.8	0.1	3.0
1.1	0.1	7.6	0.1	5.0
1.6	36.0	6.0	59.0	6.0
3.3	56.0	9.5	62.0	9.5

The films are irradiated upto a fluence of 3.3 J/cm^2 without any signs of laser induced damage. Thus films with tunable absorptive nonlinearity is fabricated which can be utilized either as laser safety device or for mode-locking and Q-switching. Since the films prepared using both the dispersing agents (F2S3O and F2S3T) exhibit a fluence dependent transition from absorption saturation to reverse saturation the

basic mechanism behind the exhibited optical nonlinearity is not a genuine TPA. This again supports the findings that instead of genuine TPA, chances of two step absorption and TPA induced FCA is more in the films.

4.3. Conclusion

Composites of PMMA-ZnO nanotops are prepared with varying loading concentration of ZnO nanotops in the monomer. Use of dispersing agents helped to increase the loading concentration of ZnO up to 9 weight % without much affecting the quality of the films. Spin coated films are found to excel in exhibiting nonlinear absorption compared to dip coated films. Considerable linear absorption and good visible emission are exhibited by the films fabricated in the presence of dispersing agent compared to the films prepared without the help of dispersing agent. The open aperture Z-scan results show that the films exhibit a switch over from reverse saturation to absorption saturation with the increase in loading concentration of ZnO.

The films fabricated using oleic acid as dispersing agent shows RSA upto a loading concentration of 5 weight % ZnO. The effective TPA coefficient of the film with 5 weight % is measured to be 1.20×10^{-7} m/W with saturation intensity 2.2×10^{12} W/m². However the films exhibited a switch over to saturation of absorption at a loading of 6 weight %. Whereas films fabricated with the help of triton maintained RSA behaviour up to a loading of 7 weight % of ZnO though the effective TPA coefficient is less (7×10^{-8} m/W). Two photon absorption, two-step absorption, and free carrier absorption are found to have distinct roles in the observed nonlinear absorption of the samples. The saturation of absorption observed in the highly loaded films can be attributed to Pauli blocking and the increased surface states created in the films during fabrication. Fluence dependent studies on the films are carried out in order to confirm the nature of nonlinear absorption. Thus the PMMA-ZnO nanotop composite films can be utilized as saturable and reverse saturable absorbers.

CHAPTER 5

FABRICATION OF PS-ZnO AND PS/PMMA-ZnO FILMS WITH EXCELLENT NONLINEAR ABSORPTION

This chapter briefs on fabrication of PS-ZnO and PS/PMMA-ZnO composite films with nonlinear absorption property. Films are fabricated using polystyrene and ZnO nanotops by varying ZnO loading concentration. These films exhibited reverse saturable absorption even at very low loading concentration of ZnO nanotops. The matrix is then modified to a combination of PS and PMMA and spin coated films are fabricated. Switching of absorptive nonlinearity from reverse saturation to absorption saturation with an increased value of effective NLA coefficient is exhibited by these films when loading concentration of ZnO is increased.

5.1. Introduction

Engineered materials like nanoparticles and their films play a major role in the development of technological applications. Novel polymer-inorganic composite films with tailored properties have been receiving a great interest in this regard. The application of these kinds of films is determined by the individual properties of their polymer and inorganic component. Optical transparency and uniformity in nanoparticle distribution are the key factors to be considered for the fabrication of films for optical/nonlinear optical applications. Since polymer nanocomposite films can ensure these factors, wise selection of polymer matrix can lead to good quality films.

There are several polymers which are transparent in the visible region of electromagnetic spectrum. Polyimide, polyacrylamide, polystyrene, polyvinyl chloride, polymethyl methacrylate, polyvinyl alcohol, polyvinyl pyrrolidone, etc. are

polymers having good transparency. Even though there are a lot of transparent polymers available, there have been very few reports on these polymers being used as matrix for preparing polymer nanocomposite films. Inclusion of SiO₂ nanoparticles is reported to enhance the thermal stability of pure polystyrene (Zhang et al., 2012). Whereas Nenna et al. has developed a light extraction system using PS-ZnO films that can be suitable in OLED lighting applications (Nenna et al., 2012). Tu et al. reports that they have approached solution casting technique to obtain flexible and self-supporting ZnO-polystyrene nanocomposite films which exhibit UV absorbing properties (Tu et al., 2010). Suspensions of polystyrene-zinc oxide composite in aqueous and electrolyte solution are reported to exhibit good dielectric behaviour (Han and Zhao, 2008). Jeeju et al. reports Zinc oxide/polystyrene nanocomposites prepared by simple mixing followed by film deposition using spin coating technique. For composites in which the ZnO nanoparticle size ranges from 6.5 - 35 nm, they obtained TPA coefficient in the range 82 - 281 cm/GW (Jeeju et al., 2014).

The surface properties of spin coated films of polystyrene and polymethyl methacrylate blend has been popularly studied. PS-PMMA is an immiscible blend which exhibit phase separation. Most of the studies in PS-PMMA films are based on their surface morphology and the role of parameters like solvent, thickness, substrate and surface energy of the polymers in the observed domain formation (Gutmann et al., 2000; Kressler et al., 1994; Schmidt et al., 1989; Tanaka et al., 1996; Ton-That et al., 2001). Walheim et al. have prepared PS-PMMA composites by dissolving PS and PMMA in three different common solvents and fabricated films using three types of substrates (Walheim et al., 1997). Solution casted films of PS/PMMA-ZnO nanocomposite are reported to exhibit UV absorption properties (Ge et al., 2010). Liu et al. have fabricated composite of SiO₂ with Polystyrene-block-Polymethyl methacrylate copolymer and reports that polymer enables the uniform distribution of the inorganic SiO₂ particles in the organic matrix (Liu et al., 2012). In 2013, report by Cano et al. proved that PS/PMMA mixture can be used as a template for the uniform dispersion of TiO₂ nanoparticles (Cano et al., 2013).

The present study discusses the fabrication of polystyrene-ZnO nanocomposite films and their nonlinear optical response. The matrix is modified to a mixture of polystyrene and polymethyl methacrylate so as to improve the quality of the films and thereby the optical nonlinearity.

5.2. PS-ZnO nanocomposite films

5.2.1. Fabrication

In situ bulk polymerization technique which is discussed in the previous chapters is used for the preparation of PS-ZnO nanotop composite films. Preweighed ZnO nanotops are dispersed in styrene by ultrasonication. The monomer-ZnO dispersion is then polymerized to get polymer nanocomposite. The loading concentration of ZnO nanotops in styrene is varied in steps from 0.1 % to 2 % by weight. Uniform films are fabricated on a glass substrate using spin coating technique for a spin speed of 1000 rpm and having the number of coatings as three. Keeping the number of coats as three, composite films are also fabricated by dip coating technique, with dipping speed of 5000 $\mu\text{m/s}$ and retrieval speed of 500 $\mu\text{m/s}$. Dip and spin coated films are named PFD3 and PFS3 respectively where x stands for the loading concentration of ZnO nanotops in the film.

5.2.2. Characterization

The room temperature absorption spectra of the polymer nanocomposite films fabricated for various loading concentrations of ZnO, using spin coating and dip coating techniques, is shown in Figure 5.1. The spectra show a slight shift in the absorption edge to the longer wavelength region compared to that of the ZnO colloid (360 nm). The absorption maximum is at 362 nm for the dip coated films where as the spin coated films absorb at 364 nm. It is clear from the spectra that spin coated films are better ultraviolet (UV) light absorbers than dip coated films. The reason for increased absorption for the spin coated films can be attributed to the increased number of nanoparticles present in the films.

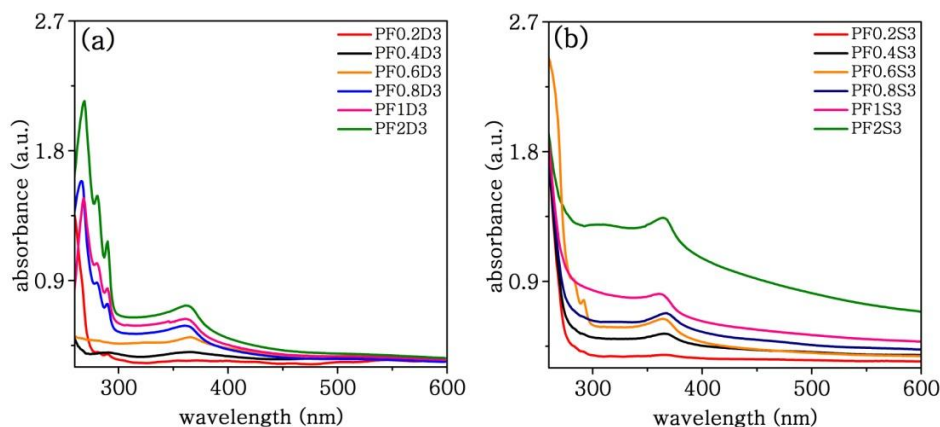


Figure 5.1 UV-vis absorption spectra of (a) dip coated and (b) spin coated films for various loading concentration of ZnO

Figure 5.2 shows the Tauc plot for the composite films with highest loading concentration of ZnO and fabricated by spin and dip coating techniques. The bandgap measured for the dip and spin coated films are 3.20 eV and 3.17 eV respectively. The bandgap calculated are in accordance with the UV-vis absorption spectra obtained for the films.

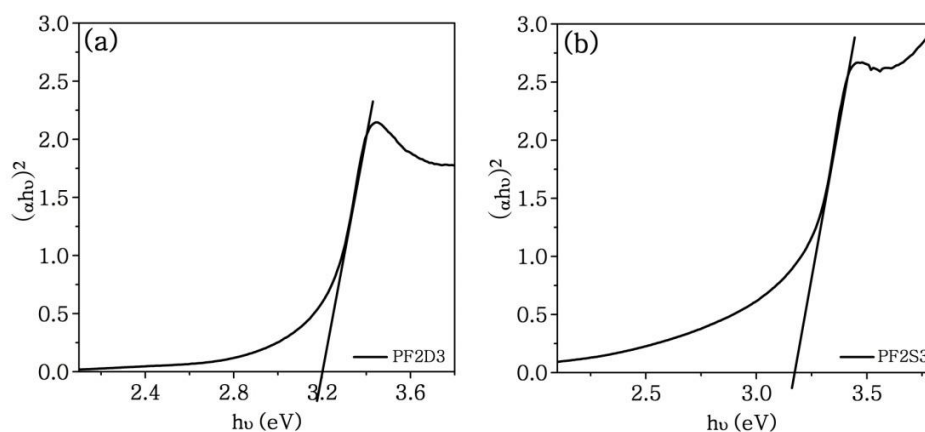


Figure 5.2 Tauc plot of (a) PF2D3 (b) PF2S3

The room temperature photoluminescence (PL) spectra of the composite films fabricated by both the techniques with ZnO loading concentration 2 weight % is shown in Figure 5.3. The emission in the UV region corresponds to the typical exciton emission or near band edge emission. This emission is attributed to the photo

generated electron recombination with holes in the valence band or in traps near the valence band. A broad emission can be seen in the blue, green and red region of the spectrum indicating the presence of surface defects. The films also emit in the red-NIR region as seen for the ZnO nanoparticle colloid. It is clear that the fabrication of the composite into film has not affected the inherent properties of nanoparticles. However the intensity of emission is less for the dip coated films compared to the spin coated one having the same loading concentration. This may be either due to the less number of particles present in the dip coated film or the fabrication technique modifying the defect states on the surface thereby quenching the visible emission.

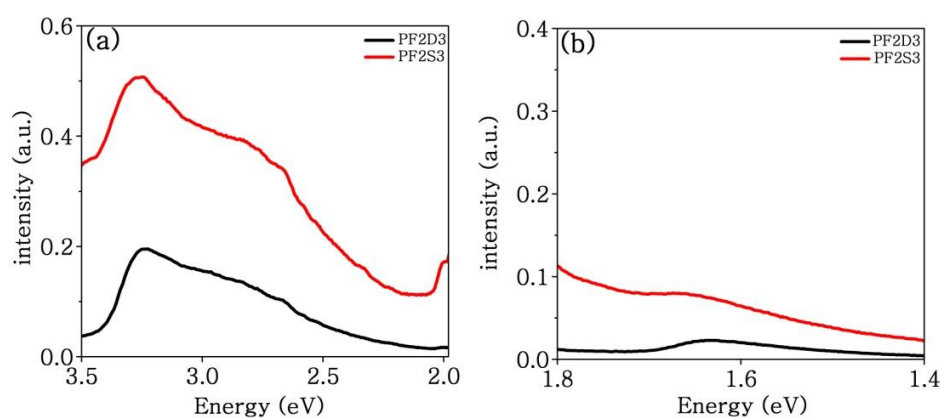


Figure 5.3 Photoluminescence spectra of (a) PF2D3
(b) PF2S3 for an excitation wavelength of 325 nm

Figure 5.4 shows the SEM images of dip coated and spin coated films fabricated with ZnO loading concentration of 0.5 weight %. The presence of more number of nanoparticles in the spin coated film is clearly seen from the SEM images. However the films are found to be having uniform surface.

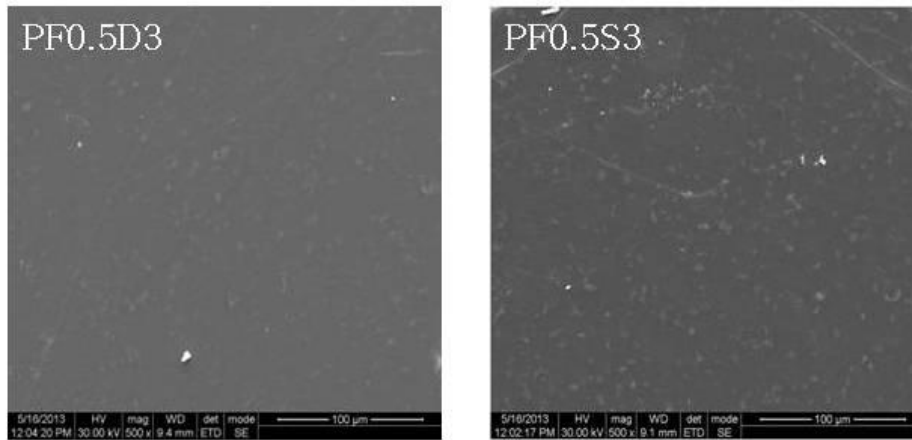


Figure 5.4 SEM image of (a) PF0.5D3 (b) PF0.5S3

The thickness of the films is measured using white light interferometer technique. The surface profile of the selected dip and spin coated films is shown in Figure 5.5. The images show a more uniform surface for spin coated films compared to the dip coated films.

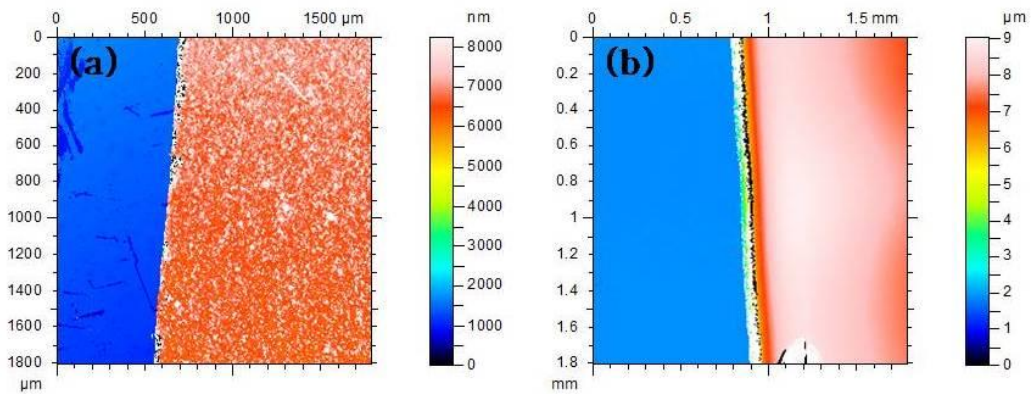


Figure 5.5 Surface profile of (a) dip coated and (b) spin coated films

Average thickness of the films is obtained from the step thickness profile (Figure 5.6.) and it is 7.3 μm for the dip coated films and 5.6 μm for the spin coated films.

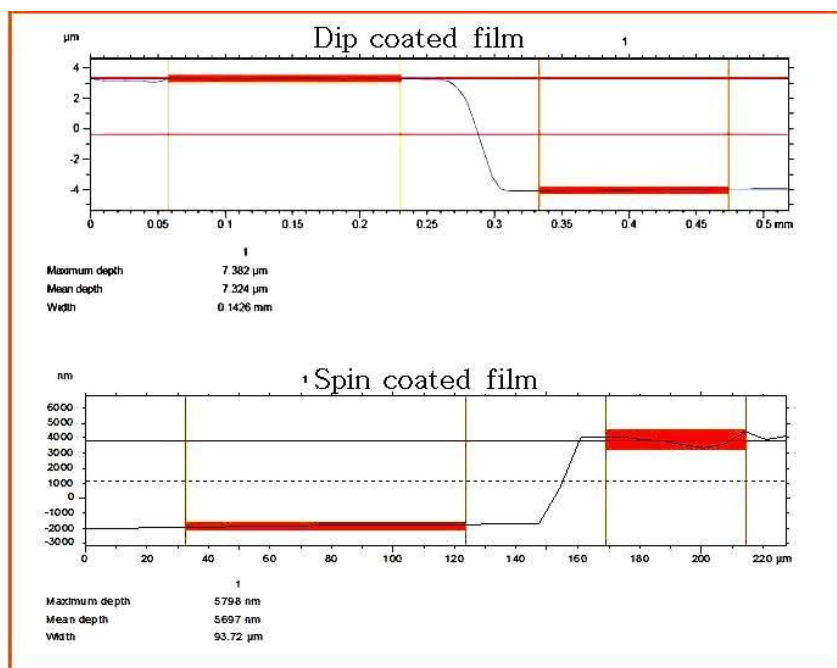


Figure 5.6 Step thickness profiles of selected films

5.2.3. Nonlinear absorption studies

Open aperture Z-scan technique is used to measure the nonlinearity of the fabricated films. All the films exhibited a normalized transmittance valley indicating their reverse saturation of absorption. The effective third order NLA coefficient (β_{eff}) is calculated by giving the experimental data a theoretical fit as per the equation 3.3 and the result is shown in Figure 5.7.

The effective two photon absorption coefficient measured at a fluence 16.5 J/cm^2 for the films with maximum loading concentration of ZnO in the monomer (2 weight %) fabricated by spin and dip coating are $180 \times 10^{-10} \text{ m/W}$ and $43 \times 10^{-10} \text{ m/W}$ respectively. The saturation intensity for the spin coated film is $4.9 \times 10^{12} \text{ W/m}^2$ with a linear transmittance 59 % and that of dip coated film is $7.9 \times 10^{12} \text{ W/m}^2$ with a linear transmittance 73 %. This shows that the films behave as better optical limiters compared to their colloid.

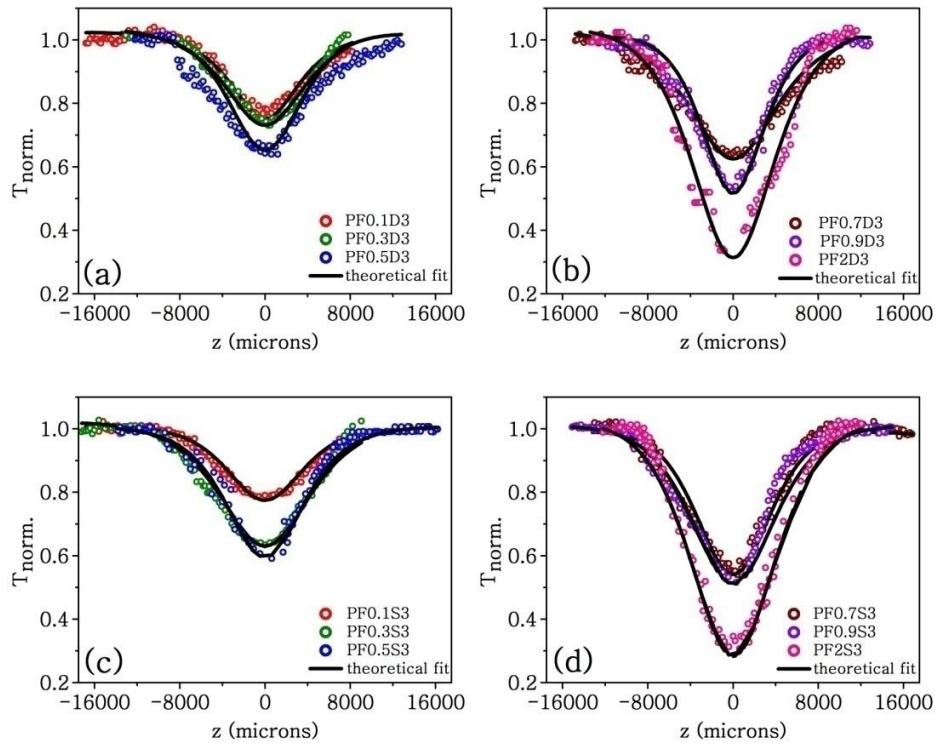


Figure 5.7 Open aperture Z-scan plots for (a) dip coated and (b) spin coated films with varying loading concentration of ZnO in the film

The effective NLA coefficient evaluated for various films plotted as a function of concentration, for spin and dip coated films is shown in Figure 5.8.

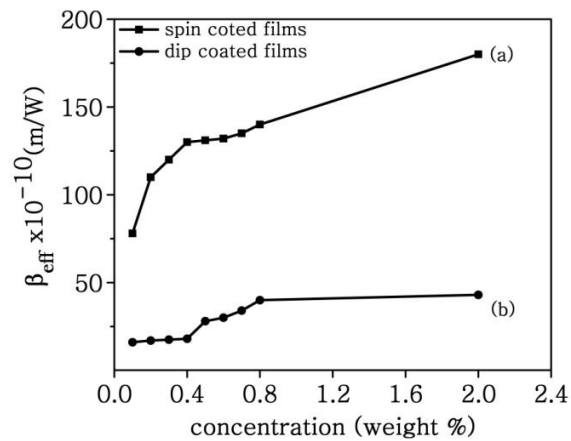


Figure 5.8 Variation of β_{eff} with loading concentration of ZnO in the monomer for a) spin coated and b) dip coated films.

The increase in the ZnO concentration in the monomer increases the effective NLA coefficient of the films. The enhanced value of NLA coefficient of the spin coated films compared to the dip coated films effectively show that the fabrication technique significantly affects the nature of the film formation, which in turn affects the nonlinearity.

The result of thermogravimetric analysis (TGA) of the composite films is shown in Figure 5.9.

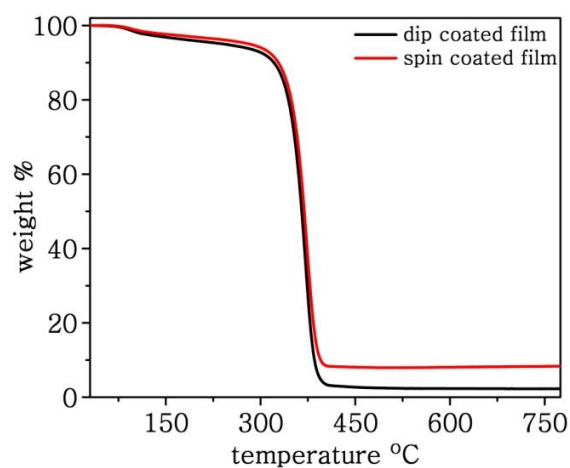


Figure 5.9 TGA plot of dip coated and spin coated films

The samples are heated from over a temperature range 30 °C to 800 °C. When the temperature reached 800 °C, polymer matrix got charred off and the residue is ZnO. The residue of the dip coated film (2.26 %) is found to be lower than that of spin coated film (8.34 %), confirming that the number of ZnO particles available for laser exposure will be less for dip coated film resulting in lower value of NLA coefficient, compared to spin coated film. When the Z-scan of pure polystyrene film is measured no trace of nonlinearity is observed. Therefore it is confirmed that the exhibited absorptive nonlinearity arises only from the incorporated ZnO nanotops (Haripadmam et al., 2014b).

5.3. PS/PMMA-ZnO nanocomposite films

5.3.1. Fabrication

As seen in chapter 4, use of a dispersing agent is found to be helpful for getting well dispersed nanoparticles in the films. So we have modified PS-ZnO composites by dispersing ZnO nanoparticles in triton and polymerizing with styrene. The composite is fabricated as films with the help of spin coating technique. Unfortunately the films cracked immediately after they have been fabricated. The cracking of the films may be due to the brittle nature of polystyrene and the incompatibility of polystyrene and triton. Composite films prepared using oleic acid dispersed ZnO also show the same tendency.

In order to solve this problem, a blend of PS and PMMA can be used, because PMMA is proven to be compatible with both the dispersing agents in chapter 4. Before introducing the nanoparticles to PS-PMMA blend, polymer films with different ratios (1:1, 1:5 and 1:10) of PS and PMMA are fabricated in order to optimize the transparency and miscibility of the polymers. Uniform films are fabricated proving that the addition of PMMA helps to improve the flexibility of polystyrene and make it suitable for film fabrication. The films fabricated differed in visible light transmittance as shown in Figure 5.10.

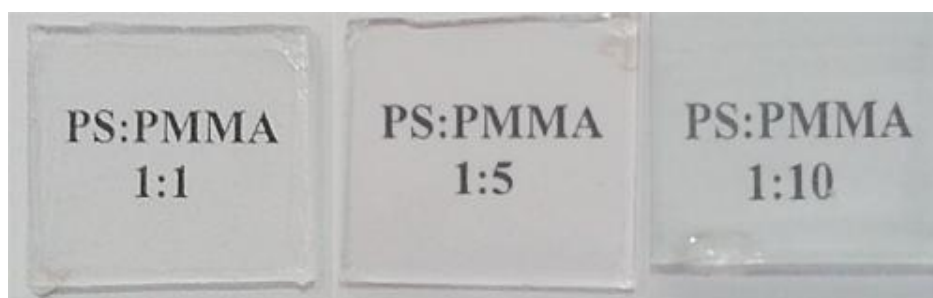


Figure 5.10 Photograph of PS/PMMA films

Among these, film with PS:PMMA as 1:1 is found to be having good transparency. As the amount of PMMA in the blend increases transparency is found

to decrease. When the amount of PS is increased in the blend, the resulting films showed a tendency to break easily and hence are not used for the later studies. Thus the ratio of PS:PMMA is maintained as 1:1 for further studies.

A mixture of PS-PMMA (1:1) and triton is prepared and fabricated film, to verify the compatibility of the dispersing agent with the modified matrix. It is observed that the optical transparency is maintained by the film and PS-PMMA matrix is compatible with the dispersing agent.

Polymer nanocomposites of ZnO are prepared with PS-PMMA and triton as the dispersing agent. *In situ* bulk polymerization technique which is discussed in the previous chapters is used here for the preparation of PS/PMMA-ZnO nanoparticle composite films. Preweighed ZnO nanoparticles are dispersed in triton and then sonicated with the mixture of styrene/MMA in 1:1 ratio. The monomer mixture containing ZnO is then polymerized to get the composite. The loading concentration of ZnO nanoparticles in the monomer mixture is varied in steps from 2 % to 8 % by weight. Uniform films are fabricated on a glass substrate using spin coating technique for a spin speed of 1000 rpm and having the number of coatings as three. The films are named PPF_xS3T where x stands for the loading concentration of ZnO nanoparticles in the film.

5.3.2. Characterization

Figure 5.11 shows the UV-vis absorption spectra of PS/PMMA-ZnO nanoparticle composite films fabricated using spin coating technique. The intensity of absorption increases with increase in loading concentration of ZnO in the films as expected and observed in chapter 4. The absorption edges (376 nm) have been shifted to longer wavelengths for the films, compared to the colloid.

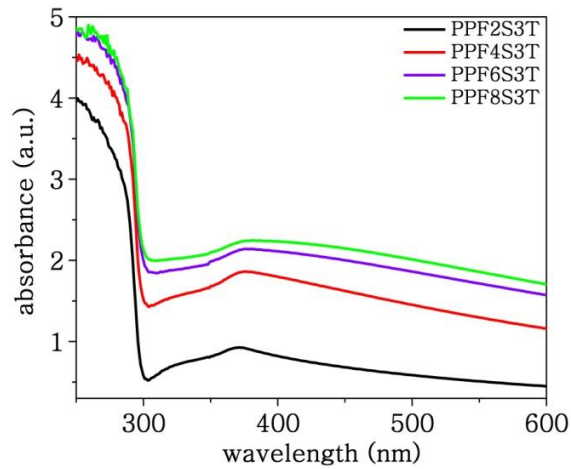


Figure 5.11 UV-vis absorption spectra of PS/PMMA-ZnO nanotop composite films with varying concentration of ZnO

Figure 5.12 shows the Tauc plot for selected films with lowest and highest ZnO loading concentration. The bandgap of the films found to decrease with increase in loading concentration as observed earlier. Bandgap values calculated from the plot are 1.79 eV for PPF8S3T and 2.61 eV for PPF2S3T.

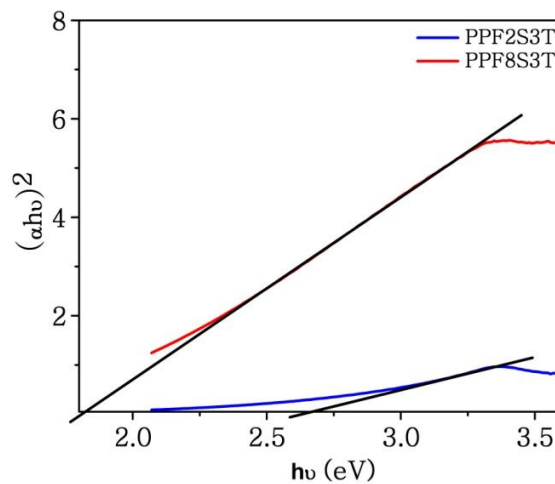


Figure 5.12 Tauc plot for selected PS/PMMA-ZnO nanotop composite films

The films exhibit characteristic band edge emission as shown in Figure 5.13. The films have broad visible emission in addition to the red-NIR emission. Band edge emission is more intense compared to red-NIR emission and the intensity of emission is increased with respect to increase in loading concentration. It has been observed

that as the loading concentration in the films increases the defects states also increases indicating the highly intense defect emissions in PPF8S3T.

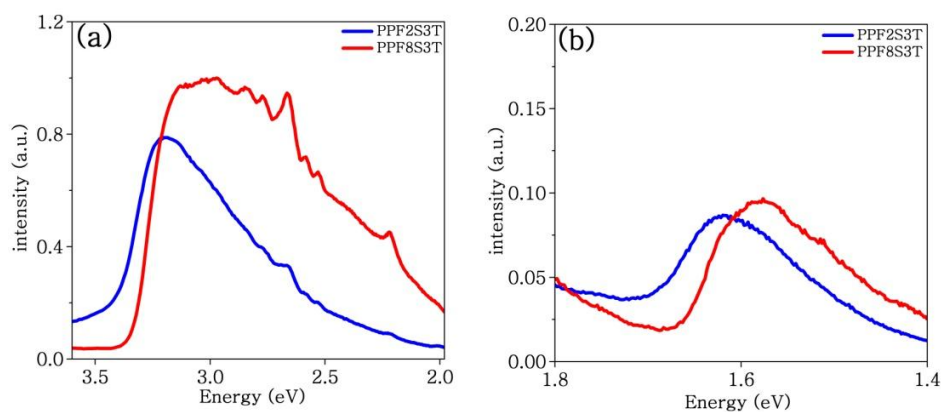


Figure 5.13 Photoluminescence spectra of selected PS/PMMA-ZnO nanotop composite films at excitation wavelength of 325 nm

Figure 5.14 shows the SEM image of PPF2S3T. The surface of the films is considerably uniform and the uniformity achieved is attributed to the presence of the dispersing agent, inter penetrating PS/PMMA blend and also to the fabrication technique.

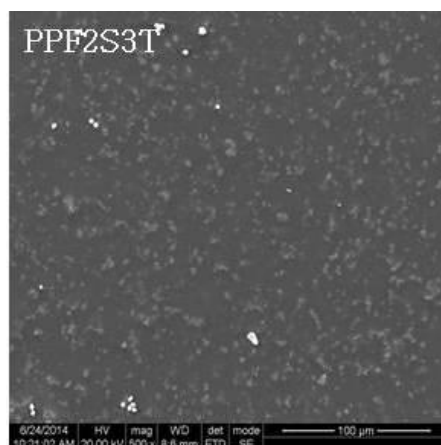


Figure 5.14 SEM image of PPF2S3T

The surface profile and 3D image of the surface of selected composite film taken by white light interferometric technique is shown in Figure 5.15. Both the images show a uniform surface with well dispersed ZnO nanotops.

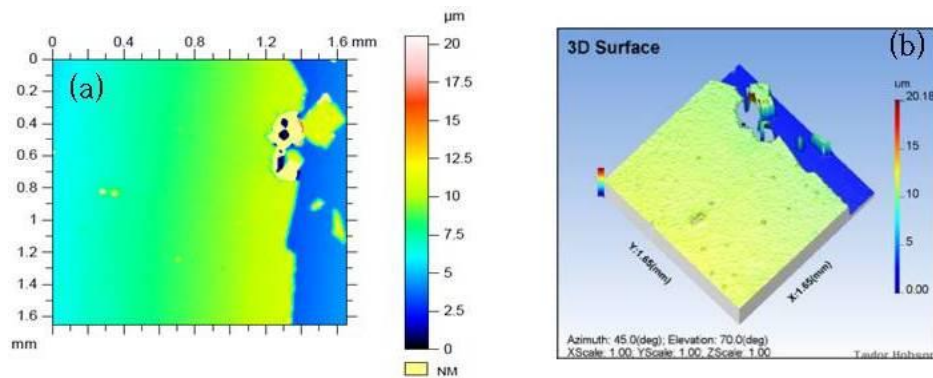


Figure 5.15 (a) Surface profile and (b) 3D surface image of selected film

Step thickness of the selected film is shown in Figure 5.16 and the average thickness for the films is measured to be 7.3 μm .

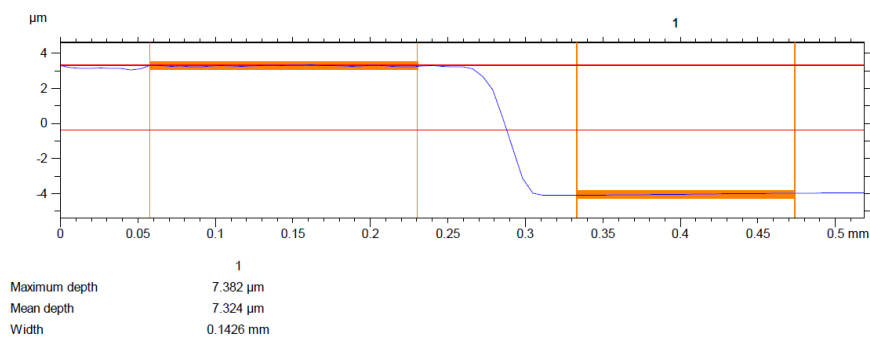


Figure 5.16 Step thickness profile of the selected film

5.3.3. Nonlinear absorption studies

Figure 5.17 shows the open aperture Z-scan results of the composite films at a fluence of 2.2 J/cm^2 . As observed in chapter 4, the films exhibited a switch over from reverse saturation to saturation of absorption with increase in loading concentration of ZnO. Films with 2, 4, and 6 weight % exhibited a decreased transmittance while film with 8 weight % exhibited an increase in transmittance with increase in incident intensity.

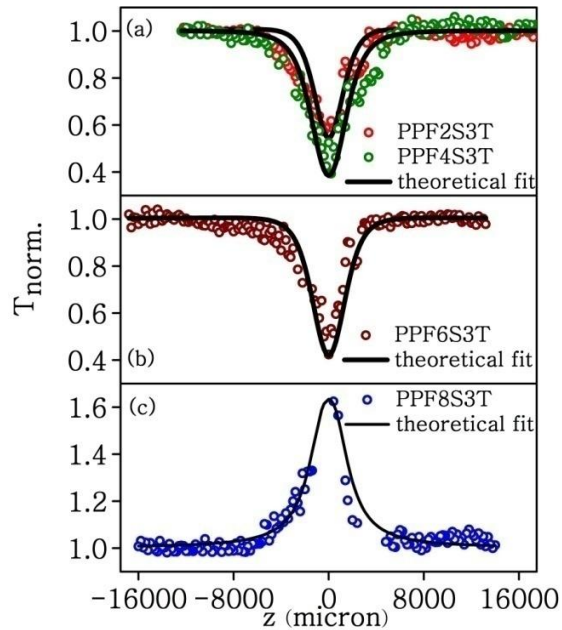


Figure 5.17 Open aperture Z-scan result of PS/PMMA-ZnO nanotop composite films

The experimental data is given theoretical fit and the effective nonlinear absorption coefficient and saturation intensity are calculated. All the calculated parameters for the dip coated and spin coated films are shown in Table 5.1.

Table 5.1 Effective two photon absorption coefficients (β_{eff}) and saturation intensities (I_{sat}) calculated for the spin coated films prepared with triton by varying ZnO loading concentration

Film	$\beta_{\text{eff}} (\times 10^{-10}) (\text{m/W})$	$I_{\text{sat}} (\times 10^{12}) (\text{W/m}^2)$
PPF2S3T	240	3.00
PPF4S3T	720	3.00
PPF6S3T	790	3.00
PPF8S3T	40	5.00

Comparing the values obtained for effective two photon absorption coefficient ($149.9 \times 10^{-10} \text{ m/W}$ for 10 weight % ZnO) by the results of Jeeju et al. (Jeeju et al., 2014) with our result, we have obtained a large enhancement in β_{eff} with a value $790 \times 10^{-10} \text{ m/W}$ (five times greater than the reported value) for the film with loading

of 6 weight % ZnO. Thus the films are found to be excellent optical limiters and can be used as transparent coatings for protection from the hazards of highly intense laser.

The optical limiting threshold is defined as the input fluence at which the transmittance falls to half the linear transmittance value. Limiting threshold gives a quantitative idea of the optical limiting performance of the sample. Figure 5.18 shows the input fluence Vs normalized transmittance plot for the film PPF6S3T which has the best absorption coefficient among the PS/PMMA-ZnO composite films. Optical limiting threshold for this film is measured to be 4.84 J/m^2 .

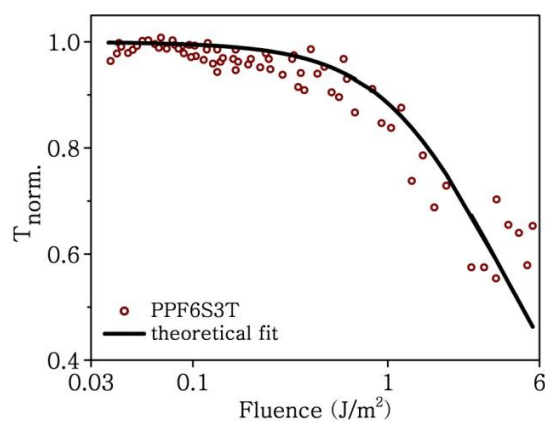


Figure 5.18 Input fluence Vs normalized transmittance plot of PPF6S3T

Fluence dependent studies have been carried out on the films to have an idea of the mechanism behind the exhibited nonlinearity. The incident fluence has been varied from 2.2 to 5.5 J/cm^2 and the corresponding open aperture Z-scan results are shown in Figure 5.19 for the film PPF2S3T.

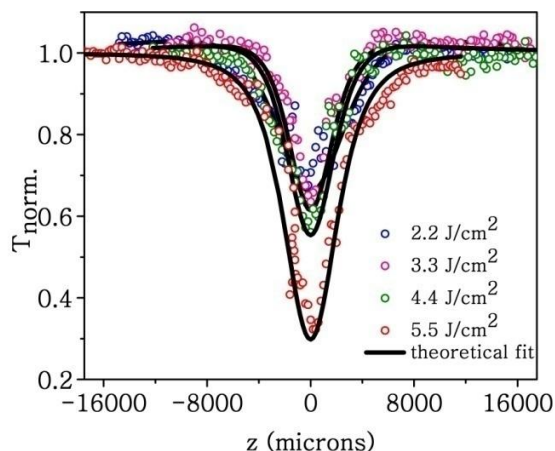


Figure 5.19 Fluence dependent response of nonlinear absorption of PPF2S3T

The output transmittance of the film decreases with increase in incident fluence indicating that the films are reverse saturable absorbers. The nonlinear absorption coefficient is found to be fluence dependent and hence the reason behind the exhibited saturable absorption is not a pure two photon absorption. There is a chance of excited state absorption also. The effective two photon absorption coefficients have been calculated for the film and is given in Table 5.2.

Table 5.2 Effective two photon absorption coefficients (β_{eff}) and saturation intensities (I_{sat}) calculated for PPF2S3T by varying the input fluence

Fluence (J/cm^2)	β_{eff} ($\times 10^{-10}$) (m/W)	I_{sat} ($\times 10^{12}$) (W/m^2)
2.2	240	3
3.3	250	4
4.4	400	4
5.5	410	4

The absorptive nonlinearity exhibited by the films can be explained in a similar way as given in chapter 4. In the present investigation, when the matrix is modified to PS/PMMA, in addition to the influence of the dispersing agent, the interpenetrating network of PS and PMMA also helps to get a well dispersed medium of ZnO nanotops. This is very clear from the surface profile of the spin coated film as

shown in Figure 5.15. The interpenetrating network of PS and PMMA with the help of triton separates the nanoparticles more effectively. However the more effective interaction between the polymer and the nanoparticles increases the electric charge interaction between them once the film is exposed to laser pulses. The dielectric confinement thus increases leading to an enhancement in the electric field inside the nanoparticles. Thus the polymer blend helps the nanotops to exhibit stronger nonlinear response.

Based on the linear absorption spectra of the films (Figure 5.11) we can attribute the enhancement in the observed nonlinear absorptive nature of the films to the increased absorption at the two-photon wavelength of 266 nm, indicating the existence of excited states suitable for two-step as well as genuine two-photon absorption processes (Khatei et al., 2012; Mary et al., 2011). However the observed NLA should have less contribution from genuine TPA and more contribution from a two-step absorption process (He et al., 2008; Rumi and Perry, 2010), since the absorption coefficient is fluence dependent. Since the laser pulsewidth used for the present study (7 ns) is greater than the free carrier lifetime of ZnO nanoparticles (Zhang et al., 1997), there is a chance for strong FCA by the photogenerated carriers. The variation of NLA coefficient with intensity also confirms this fact (Kurian et al., 2007). Thus in general; TPA, two-step absorption, and FCA have distinct roles in the observed nonlinear absorption of our samples.

As shown in figure 5.17, film with maximum loading of the nanotops exhibits saturation of absorption. The saturation of absorption observed in highly loaded film can be attributed to Pauli blocking. Also as shown in Figure 5.13, the highly loaded films exhibit more intense defect emission indicating the presence of more density of surface states. The bandgap values calculated for PPF8S3T is less compared to PPF2S3T. This also indicates the increased number of defects for the films. As the density of defects increases the rate of two photon absorption also increases as per equation 3.3. Thus there arises a situation in which most of the two photon excited

carriers get trapped in these defects, reducing the population of ground state and enhancing the chance of saturation of absorption (Haripadmam et al., 2014a).

5.4. Conclusion

Polystyrene-ZnO nanocomposite films with varying loading concentration of ZnO are fabricated using dip and spin coating techniques. All the films exhibited good UV absorption property. The films are characterized microscopically and found to have uniform surface and aggregation of nanotops is considerably reduced. The spin coated films are found to have comparatively high β_{eff} because, the amount of nanotops present in the spin coated films is more compared to the dip coated films. This has been proved using the TGA of the films. The spin coated films are found to be better candidates for optical limiting applications, having higher value of NLA coefficient compared to the dip coated films.

A blend of PS/PMMA is taken as matrix and composites are prepared with ZnO nanotops using triton as dispersing agent. These composites are prepared with varying loading concentration of ZnO nanotops and films are fabricated by spin coating technique. A switch over from reverse saturation to absorption saturation is observed for the films with increase in loading concentration of ZnO nanotops. By using very low loading concentration of nanotops, films with high β_{eff} and low saturation intensity can be fabricated. These films find applications in laser protection coatings. Increasing the loading concentration of ZnO in the composite enables to fabricate films with SA nature, applicable for Q-switching and mode locking purposes.

CHAPTER 6

SYNTHESIS AND FABRICATION OF POLYMER- ZnO/MWNT COMPOSITE FILMS WITH ENHANCED NONLINEAR ABSORPTION

This chapter describes the fabrication of polymer-ZnO/MWNT composite films for nonlinear optical applications. Hybrids of ZnO and MWNTs are synthesized by modifying the synthesis route for ZnO nanoparticles in two different ways. The synthesized samples exhibit RSA nature. Polymer nanocomposite films of the hybrid samples with two different matrices are fabricated using spin coating technique. The open aperture Z-scan results show that the films exhibited enhanced nonlinear absorption nature. The exhibited absorptive nonlinearity is of fifth order and the corresponding three photon absorption coefficients for the films are calculated. The mechanism behind the exhibited fifth order nonlinearity is understood and explained.

6.1. Introduction

Large scale synthesis of multiwalled carbon nanotubes (MWNTs) by Ebbesen and Ajayan and their subsequent report has stimulated large interest in studying and synthesising MWNTs for various applications (Ebbesen and Ajayan, 1992). Multiwalled carbon nanotubes attract great attention owing to their unique mechanical, electrical, thermal and optical properties (Bandaru, 2007; Dresselhaus et al., 2004; Dresselhaus, 1995; Lim et al., 2006b; Yakobson and Avouris, 2001). This novel material is used as mechanical reinforcement (Jose et al., 2007; Man et al., 2009), probe tips (Dai et al., 1996), catalysts, (Mu et al., 2004), field emission devices (Koohsorkhi et al., 2006), biosensors (Tang et al., 2006b) and energy storage devices (Frackowiak and Béguinet, 2002).

The dispersion and processing of nanotubes are challenging due to their inherent nature to get bundled due to strong van der Waals interaction energy of tube–tube contact (Girifalco et al., 2000). The bundling and entanglement of nanotubes hamper their properties also. This is the main reason why optical, especially nonlinear optical properties of CNTs are less exploited till date.

Functionalisation is an effective way to prevent aggregation of nanotubes and increase their stability. An oxidative treatment of carbon nanotubes (CNTs) is often preferred because, on treatment with oxidative acids, the ends and surfaces of nanotubes get covered with oxygen-containing groups such as carboxyl groups, ether groups, etc. (Kuznetsova et al., 2000). Different types of functionalisation techniques are available for CNTs to improve their properties (Andrews and Weisenberger, 2004; Sahoo et al., 2010). Among these, nitric acid functionalisation is mostly used to introduce carboxyl groups to CNTs (Kuznetsova et al., 2001; Marshall et al., 2006; Rosca et al., 2005; Tsai et al., 2013).

The nonlinear optical property of MWNT suspensions is first reported in 1998 by the research groups at the National University of Singapore followed by Chen et al. (Chen et al., 1999; Sun et al., 1998). Later these reports are followed by many research groups (Jena et al., 2007; Riggs et al., 2000; Wang et al., 2004). Wang et al. have reported a review on the recent developments of the carbon nanotube and its composites for nonlinear optical applications (Wang et al., 2009). Nonlinear optical properties of polymer-coated and polymer-grafted MWNTs are studied by Jin et al. (Jin et al., 2000). O’Flaherty and his group have prepared two kinds of polymer-MWNT composites with varying mass fraction of MWNTs and the samples exhibit optical limiting property. They found that the optical limiting nature of their samples increased with increase in mass fraction (O’Flaherty et al., 2003a; O’Flaherty et al., 2003b). Whereas Tang and Xu reports that a composite of MWNTs and PPA act as an optical limiter and their saturation intensity can be tuned by varying the nanotube content (Tang and Xu, 1999). Martinez et al. reports that carbon nanotubes doped

polymethyl methacrylate composites are suitable for passive mode locking (Martinez et al., 2008).

Hybrid of MWNTs with ZnO is a less exploited class of CNT-inorganic composite materials for nonlinear optical applications. The advantage of preparing a hybrid is that the synergistic effects of both the components enable the hybrid to possess properties of both, and make them suitable for a range of potential applications. There are a few reports on the synthesis and property evaluation of MWNT/ZnO hybrids (Chrissanthopoulos et al., 2007; Lazareck et al., 2006a; Lazareck et al., 2006b; Liu et al., 2006b). Ko et al. reports the use of MWNT seed layers to prepare ZnO nanorod arrays (Ko et al., 2012). According to them, the presence of MWNT seed layer helps to synthesise ZnO with good crystallinity and enhances their emission and surface wettability. In a similar report by Kim and Sigmund zinc oxide is produced on the outermost shells of MWNTs in the forms of ultrathin films, quantum dots, and nanowires/nanorods (Kim and Sigmund, 2002). Patra et al. have done a comparative study of electron field emission property of MWNTs and zinc coated MWNTs (Patra et al., 2013). Zhang et al. reports that CNT/ZnO has increased electroluminescence compared to ZnO (Zhang et al., 2008). Whereas Gültekin et al. reports the synthesis of a hybrid by mixing MWNTs to synthesised ZnO in the presence of water followed by heat treatment (Gültekin et al., 2013). CNT/ZnO hybrids have shown excellent performances as electrodes for super capacitors (Aravinda et al., 2013; Zhang et al., 2009), sensors (Vyas et al., 2012), photodiodes (Shao et al., 2013) and as nanoresonators (Wang and Adhikari, 2011). There are a couple of studies on MWNT/ZnO hybrid as nonlinear optical material. Zhu et al. have reported the preparation of a hybrid by coating ZnO on MWNTs which exhibited saturation of absorption (Zhu et al., 2006).

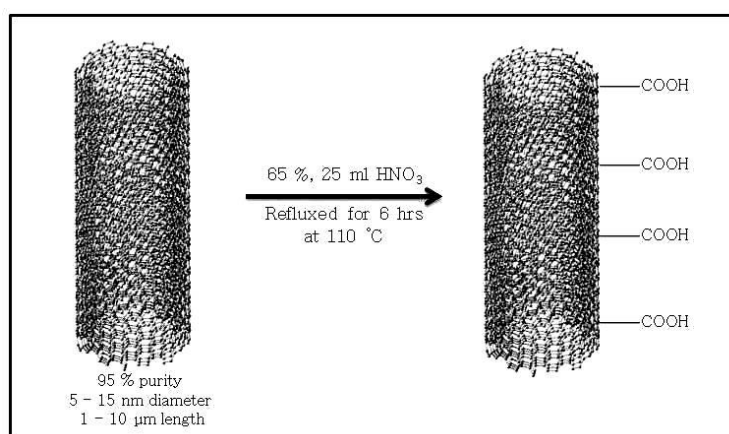
In the present study we synthesize and characterize functionalized MWNTs and ZnO/MWNT. The functionalised MWNTs and the synthesised hybrid are characterised well to study their properties. The nature of nonlinear absorption of the

samples is also revealed. Other than mixing nanoparticles and polymer chains in solution, the method of *in situ* polymerisation is reported to be advantageous (Spitalsky et al., 2010) because of the homogeneity of the resulting composites. This method allows the preparation of composites with high nanoparticle weight fraction. So in the present study we prepare polymer-nanotube and polymer-hybrid composite by *in situ* bulk polymerisation technique. Composite films of polymer-MWNT and polymer-hybrid are fabricated using spin coating technique and characterised adopting spectroscopic and microscopic methods. The response of these films against high intensity laser is also verified.

6.2. Functionalized MWNTs

6.2.1. Functionalisation

Pristine MWNTs (pMWNTs) with 95 % purity, having 5 - 15 nm diameter and 1-10 μm length, purchased from Bucky USA is used for the present study. Carboxyl groups (-COOH) are introduced to MWNTs by acid functionalisation, for better dispersion in solvents and better interaction with ZnO nanotops for the preparation of hybrid. Functionalisation is carried out as shown in Scheme 6.1.



Scheme 6.1 Scheme of the functionalization reaction of MWNT

Prewieghed pristine MWNTs are dispersed in 25 ml nitric acid (65 %) by ultrasonication for 30 minutes. Then it is refluxed in round bottom flask equipped

with a condenser, under magnetic stirring for 6 hrs at 110 °C in oil bath. The dispersion is diluted using deionised water and vacuum-filtered using millipore polycarbonate membrane. The filtrate is washed with deionised water several times until the pH of the solution reaches 7. It is then dried in vacuum at 60 °C for 12 hrs. The functionalized MWNT powder obtained is named as fMWNT. To study the effect of functionalisation on the nonlinear optical properties of MWNTs, pMWNTs are functionalised by using the same reagents but reducing the time of functionalisation to 3 hrs and is named as f3MWNTs.

6.2.2. Characterization

Figure 6.2 shows the UV-vis absorption spectra of pMWNTs, f3MWNTs and fMWNTs dispersed in methanol. The absorption of pMWNTs is observed to be broad whereas for functionalised MWNTs, a maximum is observed at 265 nm which can be attributed to the π - π^* transition. It has been reported that this absorption corresponds to the collective excitation of the π electron system polarized along the nanotube axis (Jena et al., 2007).

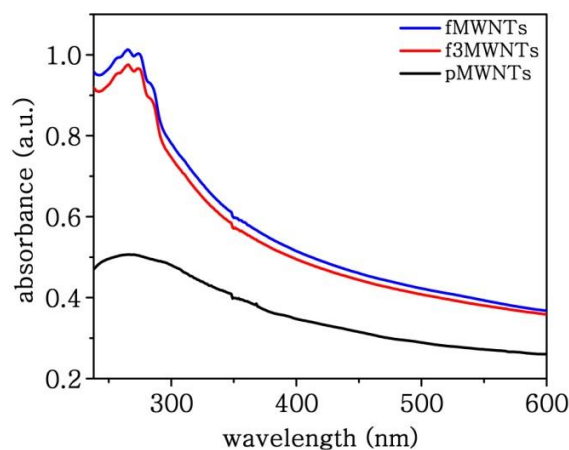


Figure 6.2 UV-vis absorption spectra of pristine and functionalised MWNTs.

The absorption decreased from UV to visible as reported earlier (Anand et al., 2011; Nguyen et al., 2011). Individual MWNTs show greater UV absorption intensity in the wavelength region between 200 - 1200 nm than the aggregation or bundles of

MWNTs (Chang et al., 2006; Yu et al., 2007). The intensity of absorption of CNTs increases with improved dispersion. Since fMWNTs exhibit absorption maximum at 265 nm, it can be confirmed that the functionalised MWNTs are not aggregated in the solvent. This is due to the presence of carboxyl groups, which are directly attached to the walls of the nanotubes and helps to increase their dispersion. The UV absorption intensity of fMWNTs is greater compared to f3MWNTs which again confirms the fact that proper functionalisation enhances the dispersion of MWNTs and thereby increases the UV absorption intensity.

The photoluminescence spectra of fMWNTs and f3MWNTs taken by exciting at 265 nm are shown in Figure 6.3. The spectra exhibit an emission peak at 3.75 eV (331 nm) and another broad emission between 2.2 eV and 1.7 eV (564 nm to 730 nm).

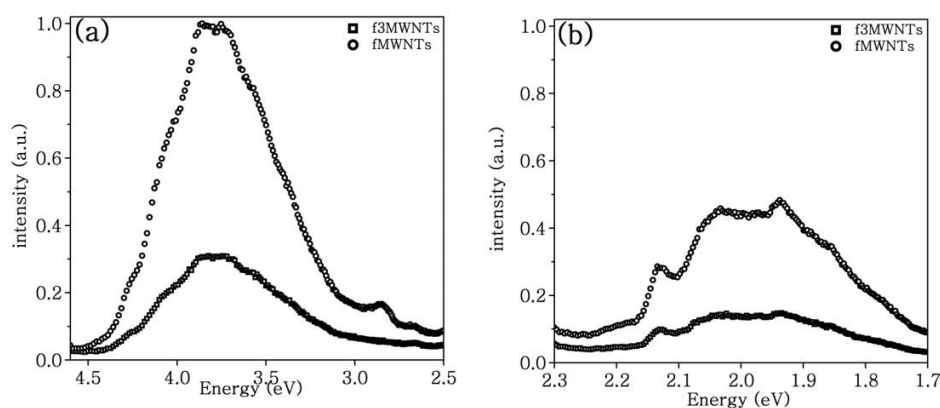


Figure 6.3 Photoluminescence spectra of functionalised MWNTs.

Pristine nanotubes do not exhibit any emission in the visible region of wavelength where as functionalised nanotubes, both fMWNTs and f3MWNTs, have emission in the visible region. The origin of emission for nanotubes is still a subject of debate. However the changes introduced to the electronic bands of the nanotubes during functionalisation and thereby trapping of the excitation energy by the induced defects can be one reason. The observed emission is also reported as an intrinsic property of the nanotubes. The intensity of fMWNTs is higher than f3MWNTs and the observed emission can be attributed to the changes occurring in the electronic band

of the nanotubes due to functionalisation. This indicates that functionalisation helps to introduce more surface defects to the nanotubes thereby enhancing their emission properties (Riggs et al., 2000; Sun et al., 2001; Sun et al., 2002).

Thermal stability of the fMWNT and f3MWNTs is compared with pMWNTs using TGA as shown in Figure 6.4. A weight loss of around 550 °C due to graphite structure degradation is observed in pMWNTs. Acid treated fMWNTs and f3MWNTs have a weight loss in the temperature range 150 - 350 °C. This weight loss can be attributed to the decomposition of carboxylic acid group introduced during acid treatment. Another major weight loss observed around 550 °C, can be attributed to graphite structures degradation (Datsyuk et al., 2008) in the sample. The residue of f3MWNTs and fMWNTs are found to be 83 % and 82 % respectively.

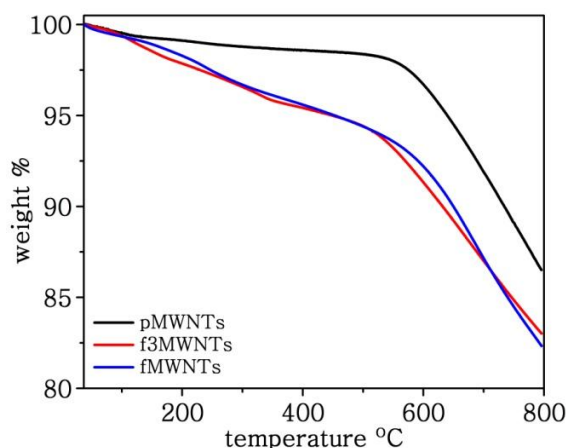


Figure 6.4 TGA plot of MWNTs.

6.2.3. Nonlinear absorption studies

The open aperture Z-scan results of MWNTs dispersed in acetone at a fluence 3.3 J/cm^2 is shown in Figure 6.5. The linear transmittance is kept as 65% and the sample is taken in a 1 mm cuvette. pMWNTs, fMWNTs and f3MWNTs are found to exhibit normalized transmittance valley indicating reverse saturable absorption nature. An increase in the dip of the valley in open aperture Z-scan trace indicates an increase in the NLA coefficient. As evident from Figure 6.4, fMWNTs exhibit better

nonlinear absorption property compared to pMWNTs and f3MWNTs. This very well explains that the observed nonlinearity is enhanced because of the presence of large number of defect states introduced to the nanotubes by functionalisation.

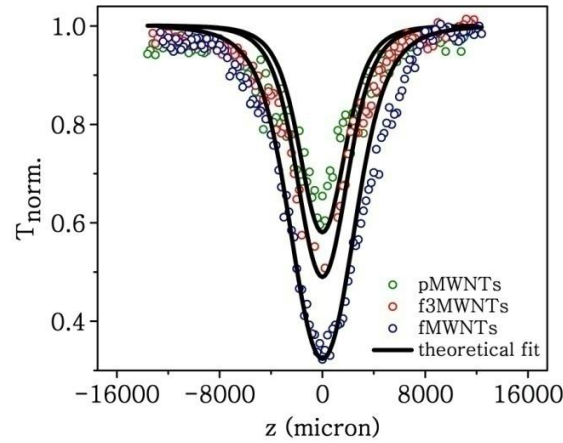


Figure 6.5 Open aperture Z-scan result of MWNTs.

The experimental data is given a theoretical fit to extract the nonlinear optical parameters associated with the process. The data is found to fit a fifth order nonlinear process according to the equation for transmittance (2.16). The effective fifth order nonlinear absorption coefficient (γ_{eff}) and saturation intensity are calculated for the dispersions.

For pMWNT, the effective three photon absorption coefficient is calculated to be $0.48 \times 10^{-22} \text{ m}^3/\text{W}^2$ with saturation intensity $9 \times 10^{12} \text{ W}/\text{m}^2$. It is observed that there is a linear increase in the value of γ_{eff} for fMWNTs and f3MWNTs. γ_{eff} is found to increase from $0.66 \times 10^{-22} \text{ m}^3/\text{W}^2$ to $2 \times 10^{-22} \text{ m}^3/\text{W}^2$ whereas the saturation intensity for both the samples reduced to $7 \times 10^{12} \text{ W}/\text{m}^2$. The calculated values clearly depicts that functionalisation has effectively increased the surface states, enhanced the dispersion and thereby increased the nonlinear absorption of MWNTs through an effective fifth order nonlinear absorption.

6.3. Polymer-fMWNTs composite films

6.3.1. Fabrication

Functionalised MWNTs which shows an increased nonlinear absorption is fabricated into films by preparing polymer nanocomposites. Composites of fMWNTs are prepared with PMMA and with 1:1 blend of PS and PMMA keeping the loading concentration of fMWNTs as 0.5 weight % in both cases. The nanotubes are first dispersed in triton and then in the monomer (7 ml). The dispersion is then polymerised using BPO as initiator. After cooling for 5 minutes, the composites are coated on a glass substrate using spin coating technique with a spin speed of 1000 rpm. The number of coats is kept as three. The films are named as FCS3T and PPCS3T where the matrix used is PMMA and PS/PMMA respectively.

6.3.2. Characterization

Figure 6.6 shows the UV-vis absorption spectra of the films FCS3T and PPCS3T. The films absorb in UV region as observed for fMWNT dispersions indicating that the nanotubes are well dispersed in the composite films.

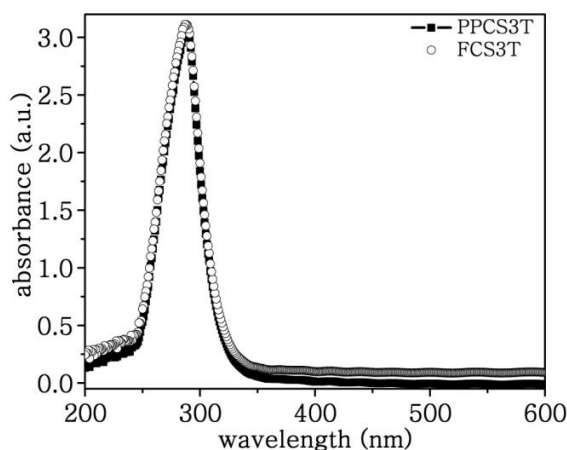


Figure 6.6 UV-vis absorption spectra of FCS3T and PPCS3

The films exhibit an absorption maxima at 277 nm corresponding to the π - π^* transition. The absorption maximum has red shifted from 265 nm to 277 nm in the composite films. The observed red shift can be attributed to the interaction of the

PMMA chains on the surface of nanotubes which result in uncoiling the PMMA chain (Kuila et al., 2007).

Figure 6.7 shows the SEM image of FCS3T which shows that the film is formed with a uniform surface, indicating that the nanotubes are not aggregated. The observed uniformity can be attributed to the functionalisation of nanotubes followed by their dispersion in the matrix.

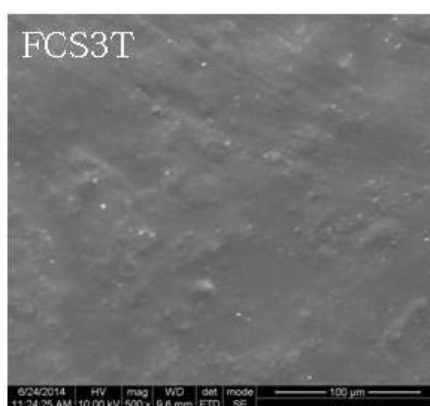


Figure 6.7 SEM image of FCS3T

Thickness of the films is measured using white light interferometric technique. Figure 6.8a and 6.8b shows the surface profile and the 3D image of the selected film. The thickness is measured to be 16 μm from the step thickness profile as shown in Figure 6.9.

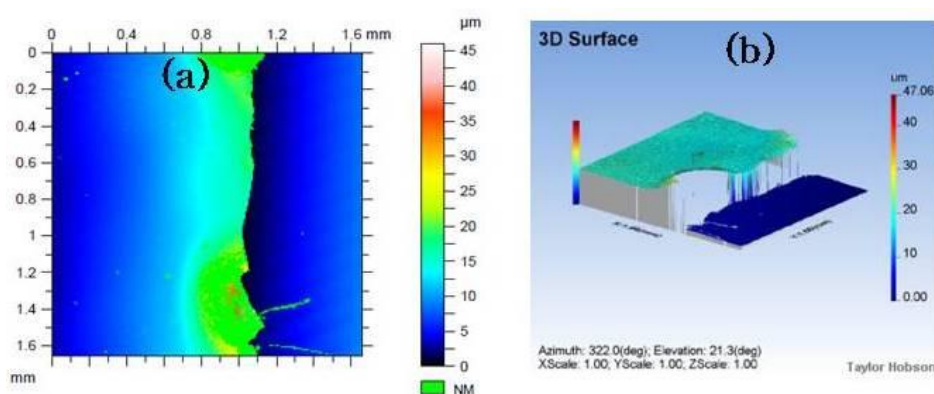


Figure 6.8 (a) Surface profile and (b) 3D surface image of selected film

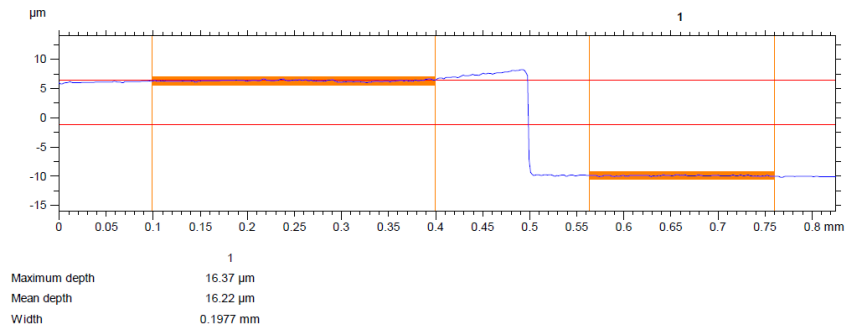


Figure 6.9 Step thickness profile of the selected film

6.3.3. Nonlinear absorption studies

The nonlinear absorption of the films is investigated using open aperture Z-scan technique at a fluence of 2.2 J/cm^2 . Both the films of fMWNTs exhibit reverse saturation of absorption as shown in Figure 6.10(a).

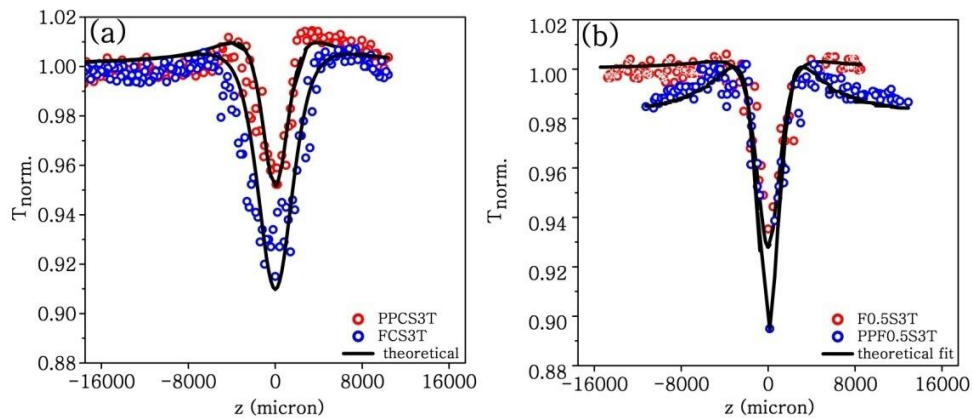


Figure 6.10 Nonlinear optical response of (a) polymer-fMWNT and (b) polymer-ZnO nanotop composite films

The experimental data fit to a three photon absorption process and the parameters associated with fifth order optical nonlinearity are calculated. The value of γ_{eff} is calculated to be $2.6 \times 10^{-22} \text{ m}^3/\text{W}^2$ for PPCS3T with saturation intensity $56 \times 10^{12} \text{ W/m}^2$. Whereas for the film FCS3T, γ_{eff} is calculated to be $2.8 \times 10^{-22} \text{ m}^3/\text{W}^2$ with saturation intensity $3.8 \times 10^{12} \text{ W/m}^2$. A slight increase in the value of effective three photon absorption coefficient and a very large decrease in

saturation intensity are observed for the film FCS3T, indicating PMMA is a suitable matrix for preparing polymer-MWNT composite film.

Figure 6.10(b) shows the nonlinear absorption behaviour of PMMA-ZnO nanotop (F0.5S3T) and PS/PMMA-ZnO nanotop (PPF0.5S3T) composite films with ZnO loading concentration 0.5 weight %. As observed in previous chapters, these films exhibit RSA by third order optical nonlinearity. The effective two photon absorption coefficient and saturation intensity of F0.5S3T is calculated to be 15×10^{-10} m/W and 9.8×10^{12} W/m² respectively. For PPF0.5S3T the corresponding values are 75×10^{-10} m/W and 3×10^{12} W/m² respectively.

6.4. ZnO-fMWNT hybrids

6.4.1. ZnO/acetic acid dispersed fMWNT

6.4.1.1. Synthesis

Hybrid nanostructures of the ZnO nanotops with fMWNTs is synthesised by modifying the synthesis procedure adopted for ZnO nanotops. The ratio of ZnO formed and fMWNTs added, are optimised to get hybrid without excess aggregation of MWNTs. In the initial stage, 0.219 gm zinc acetate is dissolved in 1 % 10 ml acetic acid. Aqueous solution of 0.05 % 10 ml PVP is added to it as capping agent. 2 mg fMWNT is dispersed in acetic acid (1 %, 10 ml) separately by ultrasonication for 3 hrs. The acetic acid dispersion of fMWNTs is mixed with the precursor and ultrasonicated for 30 min. After 24 hrs the precursor is precipitated using 6 milli mol NaOH and stirring is continued for 12 hrs. The precipitate is filtered, washed and dried at 100 °C for 12 hrs in vacuum oven. The dried sample is then powdered using mortar and pestle. The amount of fMWNT in the synthesis reaction is varied as 2, 4 and 6 mg and the hybrids formed are named H2, H4 and H6 respectively.

6.4.1.2. Characterization

Figure 6.11 shows the UV-vis absorption spectra of hybrids synthesised by varying the loading concentration of fMWNTs in the precursor.

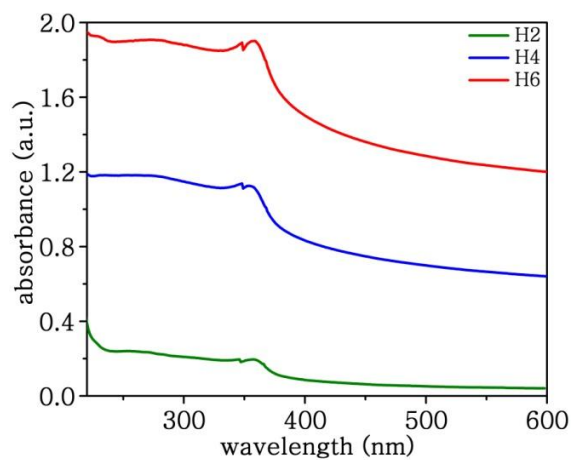


Figure 6.11 UV-vis absorption spectra of the hybrids

It is clear from the spectra that intensity of absorption increases with increase in concentration of nanotubes. The spectra show broad absorption upto 300 nm corresponding to fMWNTs and absorption peak at 356 nm corresponding to ZnO nanotops. As the loading of nanotubes increase, an absorption peak at 272 nm starts emerging.

6.4.1.3. Nonlinear absorption studies

Figure 6.12 shows the nonlinear optical response of the hybrids dispersed in water measured using open aperture Z-scan technique.

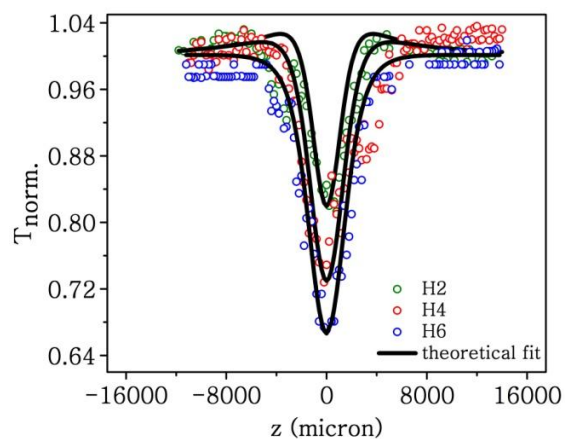


Figure 6.12 Nonlinear optical response of the hybrids

The linear transmittance is kept at 65 % and the sample is scanned at a fluence 3.3 J/cm². The scan shows that the hybrid dispersions exhibit RSA. The experimental data fit well to a three photon process and the corresponding nonlinear parameters are calculated as shown in Table 6.1. It is clear from the table that the effective value of γ is increasing with increase in the loading of fMWNTs. The combined nonlinear effect of ZnO nanotops and fMWNTs makes the hybrid sample more nonlinear active compared to ZnO nanotops. Thus it can be concluded that the presence of fMWNTs enhances the absorptive nonlinearity of the hybrid.

Table 6.1 Effective three photon absorption coefficients (γ_{eff}) and saturation intensities (I_{sat}) calculated for the hybrid dispersions

Sample	γ_{eff} ($\times 10^{-22}$) (m^3/W^2)	I_{sat} ($\times 10^{12}$) (W/m^2)
H2	0.120	7
H4	0.130	7
H6	0.200	10

6.4.2. Polymer-hybrid composite films

6.4.2.1. Fabrication

Nanocomposites of hybrid with PMMA are prepared by taking 0.5 weight % of each hybrid. The hybrid is first dispersed in triton followed by MMA. Using BPO, the dispersions are polymerised and coated on a glass substrate using spin coating technique with a spin speed of 1000 rpm. The number of coats is kept as three. The films are named FHxS3T where 'x' stands for the loading of fMWNTs in the hybrid.

6.4.2.2. Characterization

Figure 6.13 shows the UV-vis absorption spectra of the hybrid nanocomposite films. The films exhibit absorption maximum at 287 nm corresponding to fMWNTs and the absorption decays towards the higher wavelengths. Film FH6S3T shows an increased absorption both in UV and visible region.

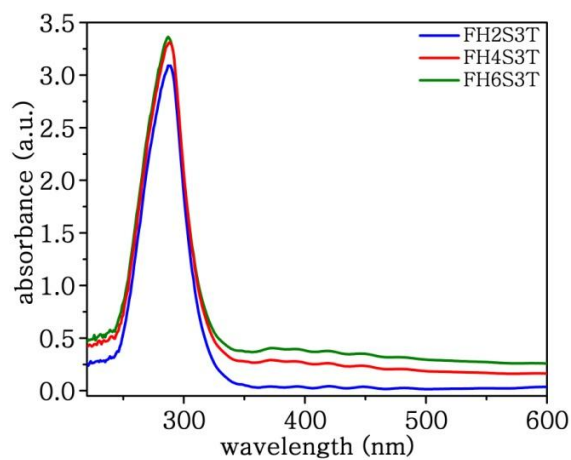


Figure 6.13 UV-vis absorption spectra of hybrid composite films

6.4.2.3. Nonlinear absorption studies

Figure 6.14 shows the nonlinear absorption of the hybrid composite films measured using open aperture Z-scan technique. All the films exhibit a decrease in transmittance with increase in intensity of incident laser. It is to be noted that the RSA nature of the composite films increases from FH2S3T to FH6S3T.

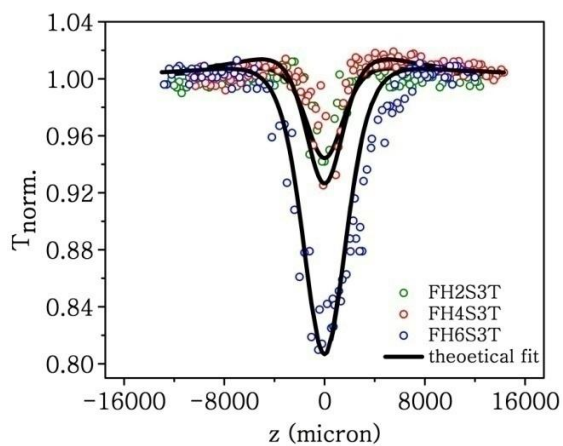


Figure 6.14 Nonlinear optical response of hybrid composite films

6.4.3. ZnO/PVP dispersed MWNT

6.4.3.1. Synthesis

The synthesis procedure of hybrid explained in the previous section is modified to get another set of hybrid samples with improved dispersion and enhanced

nonlinear absorption. The maximum loading of fMWNTs in the synthesis of the hybrid without any aggregation is found to be 6 mg in the previous section. So here the amount of fMWNTs is fixed at 6 mg for the hybrid synthesis. 6 mg fMWNTs are dispersed in aqueous solution of 0.05 % 10 ml PVP and is added to the zinc acetate precursor. After 24 hrs the precursor is precipitated using 6 milli mol NaOH. The precipitate is filtered after 12 hrs of continuous stirring and washed and dried at 100 °C for 12 hrs in vaccum oven. The dried ZnO/MWNT is then powdered and named ‘H’ for convenience.

6.4.3.2. Nonlinear absorption studies

Figure 6.15 shows the nonlinear absorption spectra of the hybrid dispersed in water measured using open aperture Z-scan technique at an input fluence, 3.3 J/cm^2 . The linear transmittance of the dispersion is kept as 65 % and the sample is taken in 1 mm cuvette.

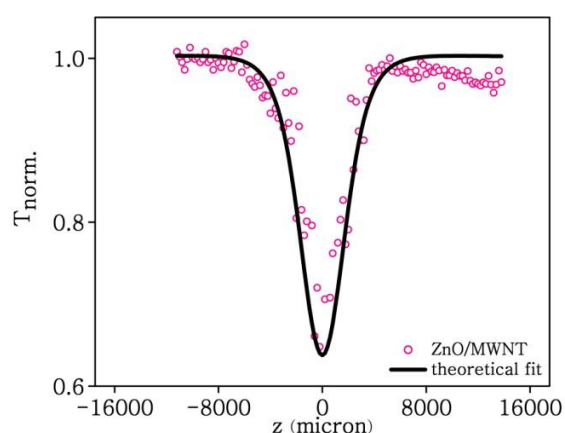


Figure 6.15 Open aperture Z-scan of hybrid dispersed in water at a fluence 3.3 J/cm^2

The colloid exhibits RSA nature with a fifth order nonlinearity. The effective three photon absorption coefficient and saturation intensity calculated are $0.6 \times 10^{-22} \text{ m}^3/\text{W}^2$ and $3 \times 10^{12} \text{ W/m}^2$ respectively. It is clear that the nonlinear absorption coefficient is three times higher for the hybrid prepared by dispersing fMWNTs in PVP compared to the hybrid prepared by acetic acid dispersed fMWNTs.

In order to study the reason for the higher value of γ for this hybrid, detailed characterisations of ZnO/MWNTs are done.

6.4.3.3. Characterization

Figure 6.16 shows the FTIR spectra of fMWNTs and the hybrid. In fMWNTs and the hybrid, the broad band at wavenumber 3422 cm^{-1} correspond to the stretching vibration of O-H. The band at 1721 cm^{-1} in fMWNTs is associated with the C=O stretching of the carboxylic acid (-COOH) group which is shifted to 1733 cm^{-1} for the hybrid due to the presence of ZnO nanotops. Corresponding to the C=C stretching of nanotubes there is a band at wavenumber 1578 cm^{-1} for the fMWNTs where as it is shifted to 1583 cm^{-1} in the hybrid. The bands at 1193 cm^{-1} for fMWNTs and 1021 cm^{-1} for the hybrid corresponds to the C-O bonds present in the sample. The presence of ZnO nanotops can be confirmed in the hybrid from the band at 499 cm^{-1} corresponding to Zn-O stretching vibration.

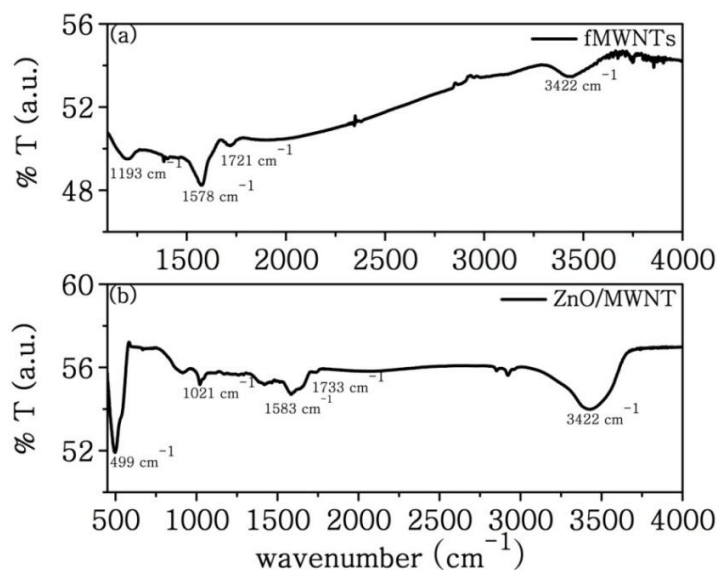


Figure 6.16 FTIR spectra of (a) fMWNTs (b) Hybrid

Figure 6.17 shows the UV-absorption spectrum of the hybrid dispersed in water. It is clear that the hybrid exhibits two absorption peaks corresponding to their

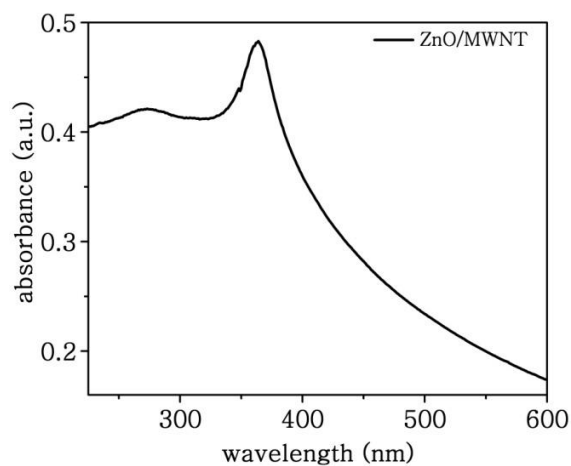


Figure 6.17 UV-vis absorption spectra of the hybrid

individual components. An absorption peak at 273 nm corresponds to fMWNTs whereas the peak at 364 nm corresponds to ZnO nanotops. This indicates that the hybrid is formed uniformly preserving the properties of their individual components.

The XRD pattern of the hybrid powder is shown in Figure 6.18. The pattern shows that highly crystallized nanostructure are obtained.

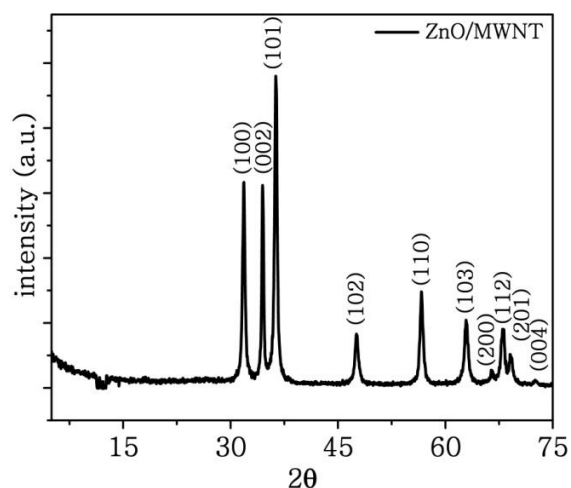


Figure 6.18 XRD pattern of the hybrid

Figure 6.19 shows the SEM image of the hybrid. It is very much clear that the nanotops and the nanotubes have formed a very good hybrid.

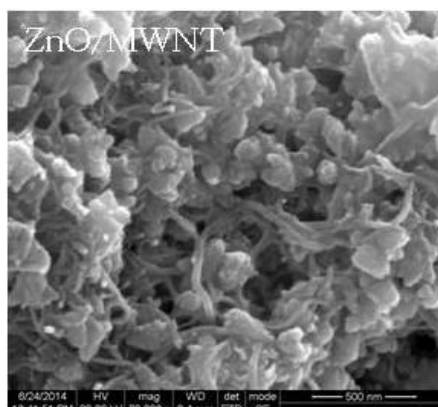


Figure 6.19 SEM image of the hybrid

Figure 6.20 represents the thermal analysis carried out for the hybrid and its components. ZnO nanotops exhibit a small weight loss (2.5 %) in the range 130 °C to 540 °C caused by the decomposition of the chemisorbed PVP on the surface of the ZnO nanoparticles. fMWNTs has a weight loss in the temperature range 150 - 350 °C due to decarboxylation. Another major weight loss is observed for the nanotubes around 550 °C, which can be attributed to graphite structures degradation. On introducing fMWNTs to ZnO, the hybrid formed appears to be almost stable in the temperature range of analysis.

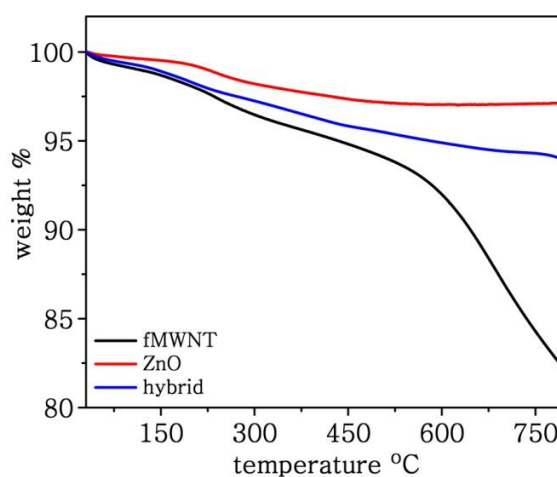


Figure 6.20 TGA plot of fMWNTs, ZnO and the hybrid

Raman spectra of the pristine and functionalised MWNTs along with the hybrid are shown in Figure 6.21. The spectra shows the characteristic bands D and G where D band corresponds to the defect states (vacancies and sp^3 carbons) and G band to the stretching vibrations of the carbon - carbon bonds (sp^2 carbons). As seen from the figure, the D band appears at 1346 cm^{-1} for the pristine MWNTs which shifts to 1349 cm^{-1} after functionalisation. The hybrid shows D band at 1352 cm^{-1} . Whereas the G band is at 1572 cm^{-1} for MWNTs before and after functionalisation and it shifts to 1581 cm^{-1} during the formation of the hybrid.

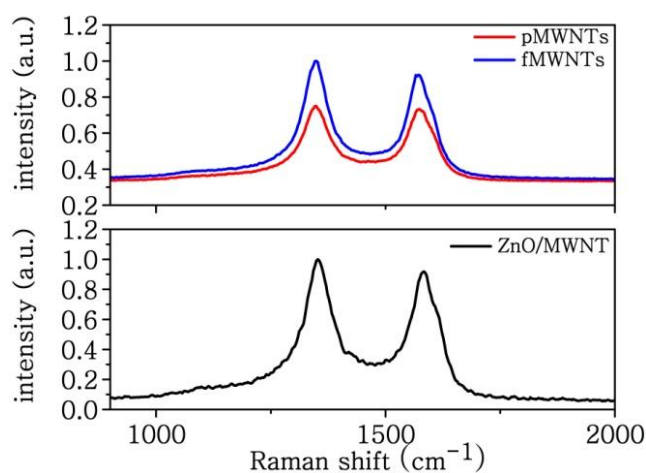


Figure 6.21 Raman spectra of pMWNTs, fMWNTs and the hybrid

The intensity of the G and D bands are a commonly accepted indicator of the sample crystallinity. The intensity ratio I_G/I_D is an important factor indicating the degree of disorder of the material. The ratio I_G/I_D is measured to be 0.97, 0.92 and 0.91 for pMWNTs, fMWNTs and the hybrid respectively. The decrease in the ratio for fMWNTs and hybrid indicates the presence of defect states in the sample.

Figure 6.22 shows the photoluminescent spectrum of the hybrid powder dispersed in methanol. The excitation wavelength is 325 nm. The emission of the hybrids resembles that of ZnO nanotops having the characteristic UV emission followed by a broad visible defect related emission.

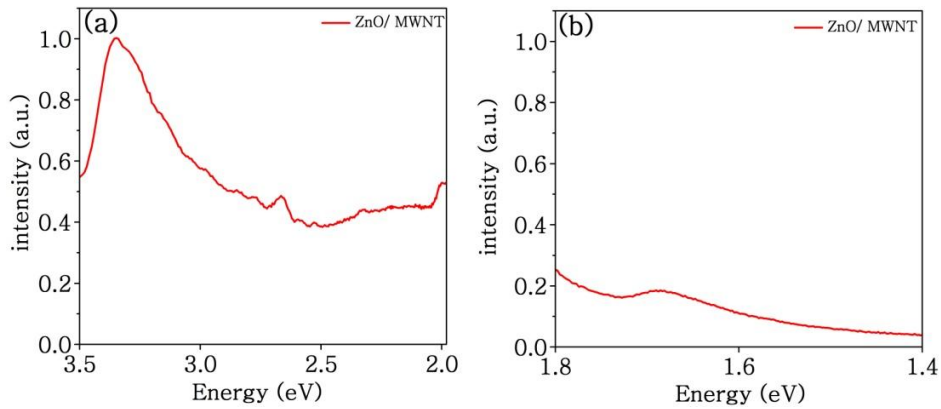


Figure 6.22 Photoluminescent spectrum of the hybrid at an excitation wavelength 325 nm

6.4.3.4. Fluence dependent transition from SA to RSA in hybrid colloid

Figure 6.23 shows the nonlinear absorption spectra of the hybrid dispersed in water measured using open aperture Z-scan technique for various input fluences starting from 0.5 J/cm^2 to 5.5 J/cm^2 .

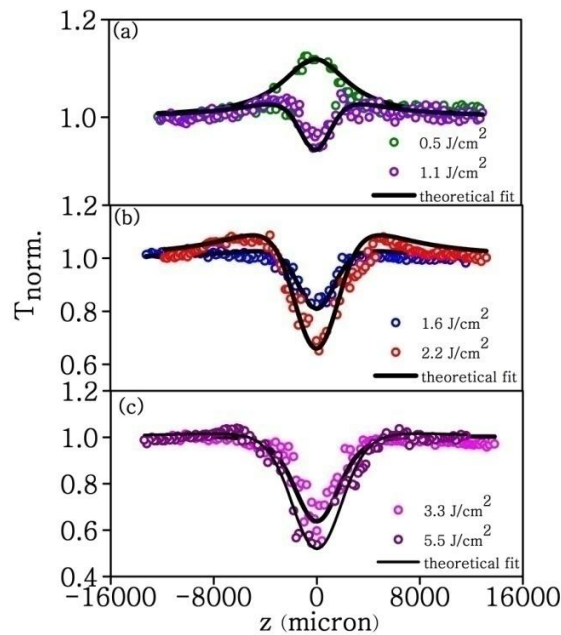


Figure 6.23 Open aperture Z-scan plot for the hybrid dispersion at various incident fluences

The scan showed a transition from SA to RSA with the increase in input fluence. At low fluence 0.5 J/cm^2 , the sample showed SA nature due to photoinduced

bleaching. The sample absorption is quenched at low fluences because in this regime, most of the carriers are filled. As the sample is exposed to higher fluences, it began exhibiting RSA nature. The dip of the scans increases with fluence. The experimental data fit well to a theoretical plot according to the fifth order nonlinear absorption. The fifth order nonlinear absorption coefficient here is an effective value since the absorption of the sample is fluence dependent. Thus the effective fifth order nonlinear absorption coefficient for the hybrid dispersions scanned at varying fluences is shown in Table 6.2.

Table 6.2 Effective three photon absorption coefficients (γ_{eff}) and saturation intensities (I_{sat}) calculated for the hybrid colloid by varying input fluence

Fluence (J/cm ²)	$\gamma_{\text{eff}} \times 10^{-22}$ (m ³ /W ²)	$I_{\text{sat}} \times 10^{12}$ (W/m ²)
0.5	0.06	6.2
1.1	0.38	6.0
1.6	0.40	5.8
2.2	0.50	5.8
3.3	0.6	3.0
5.5	1.4	3.0

6.4.4. Polymer-ZnO/MWNT composite films

6.4.4.1. Fabrication

Two sets of polymer-hybrid composite films are prepared using the synthesised hybrid, ZnO/MWNT. Nanocomposites of PMMA-hybrid and PS/PMMA-hybrid are prepared by varying the loading concentration of the hybrid. The composite preparation technique followed is *in situ* polymerisation, using BPO as the initiator. Spin coating technique is used to fabricate the films. Films are fabricated at a spin speed of 1000 rpm on a glass substrate, keeping the number of coats as three. With respect to the matrix used and the loading concentration of the hybrid, PMMA-hybrid composite films and PS/PMMA-hybrid composite films are

named as FHxS3T and PPHxS3T respectively where ‘H’ represents ZnO/MWNT and ‘x’ stands for its loading concentration.

6.4.4.2. Characterization

Figure 6.24 shows the UV-vis absorption spectra of the composite films fabricated with the hybrid in the two matrices. The absorption spectra of the films fabricated with PMMA as matrix shows a high intense absorption around 214 nm representing the MWNTs present in the hybrid. Whereas the films fabricated with PS/PMMA as matrix shows moderate broad absorption. These spectra depicts that PMMA is more suitable matrix for hybrid dispersions than the blend of PS and PMMA.

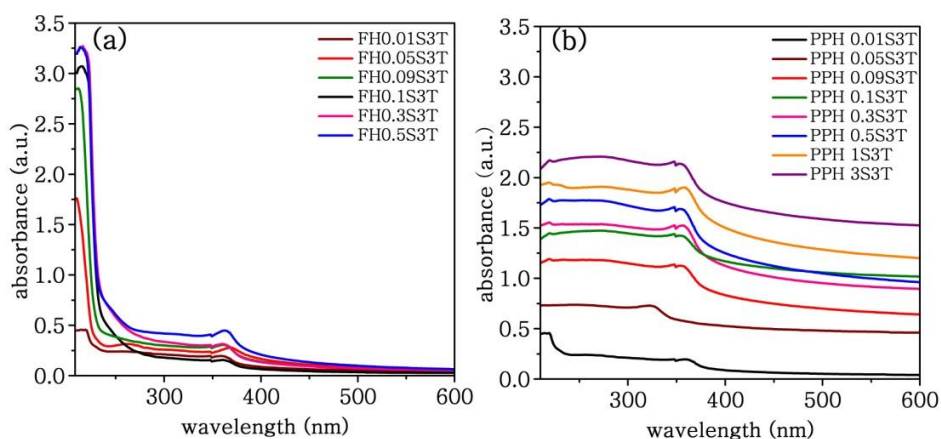


Figure 6.24 UV- vis absorption spectra of the composite films of the hybrid with (a) PMMA and (b) PS/PMMA for varying loading of the hybrid

The photoluminescence spectra taken for all the composite films by exciting at 325 nm, are shown in Figure 6.25. All the films have emission in UV region followed by a broad blue-green emission. The red-NIR emission is also observed, similar to the hybrid dispersions. Hence it can be concluded that the polymer do not repair the defect states much and enable the films to act as better visible light emitters.

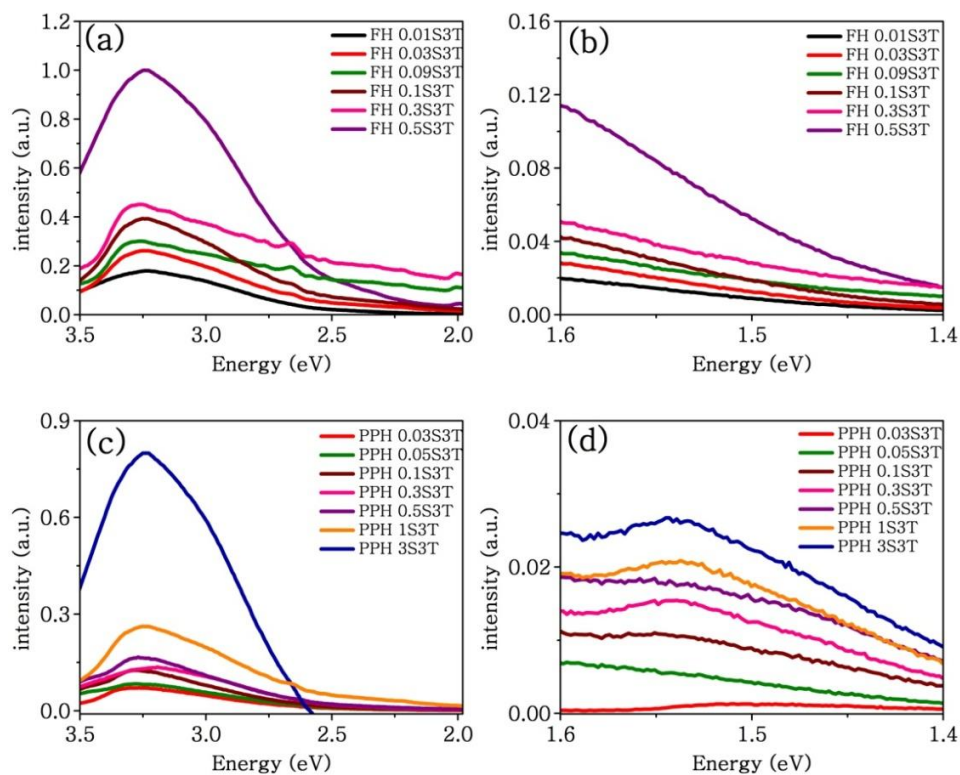


Figure 6.25 Photoluminescent spectra of the composite films of the hybrid with (a)&(b) PMMA and (c)&(d) PS/PMMA for varying loading of the hybrid

Figure 6.26 shows the SEM image of the composite films fabricated with PMMA-hybrid and PS/PMMA-hybrid for hybrid loading concentration 0.5 weight %.

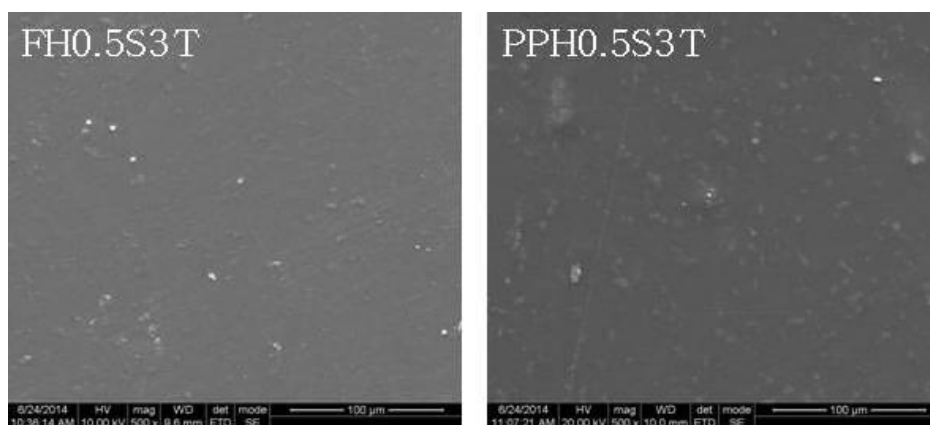


Figure 6.26 SEM image of the composite films (a) FH0.5S3T and (b) PPH0.5S3T

Both the films show a uniform surface profile indicating the well dispersed nanoparticles in the films.

The uniformity of the surface of the fabricated films are again confirmed from the surface profile of the selected films obtained from a white light interferometer. As shown in Figure 6.27 there are no aggregated nanoparticles on the surface of the films.

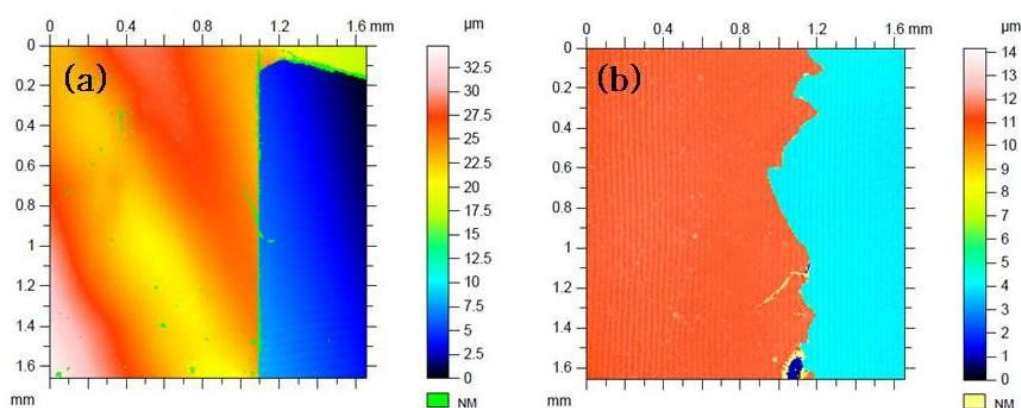


Figure 6.27 Surface profile of the selected composite films of hybrid with PMMA and (b) PS/PMMA

The thickness of the composite films are also measured using white light interferometer and the step thickness profile is shown in Figure 6.28. The thickness is measured to be 16.7 μm and 9.5 μm for PMMA-hybrid and PS/PMMA-hybrid films respectively.

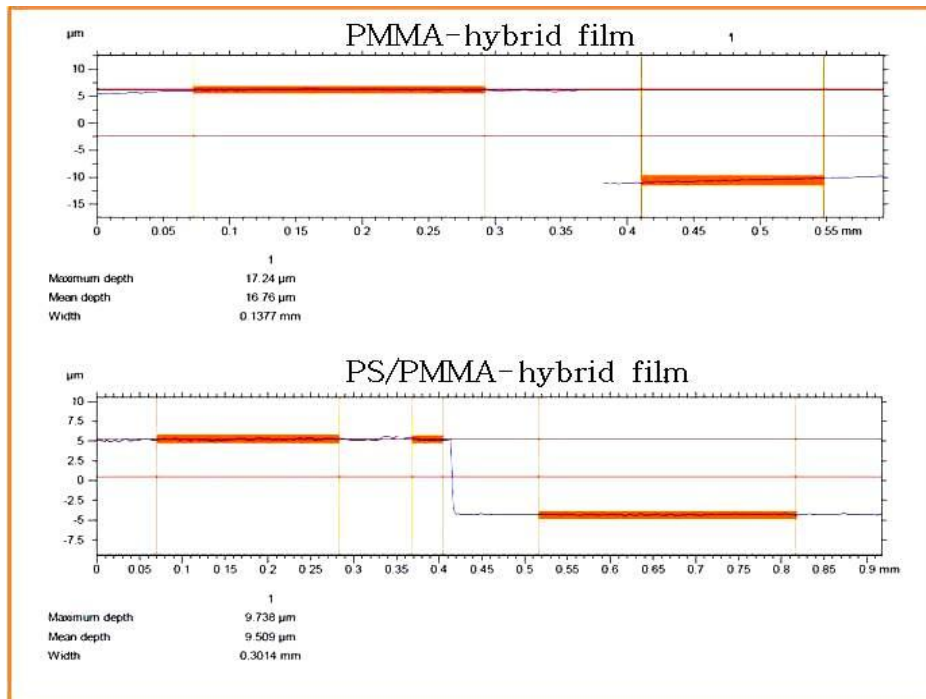


Figure 6.28 Step thickness profile of the selected composite films of hybrid with (a) PMMA and (b) PS/PMMA

6.4.4.3. Nonlinear absorption studies

Figure 6.29 shows the open aperture Z-scan result of PMMA-ZnO/MWNT composite films for various concentrations of the hybrid. The loading concentration used here is too low and is varied from 0.01 to 0.5 weight % of the monomer. The films exhibit RSA nature at a fluence of 2.2 J/cm^2 for the entire set of samples with varying loading concentration. The loading concentration could not be further increased as the linear transmittance reduced considerably and hence Z-scans are not performed for those samples.

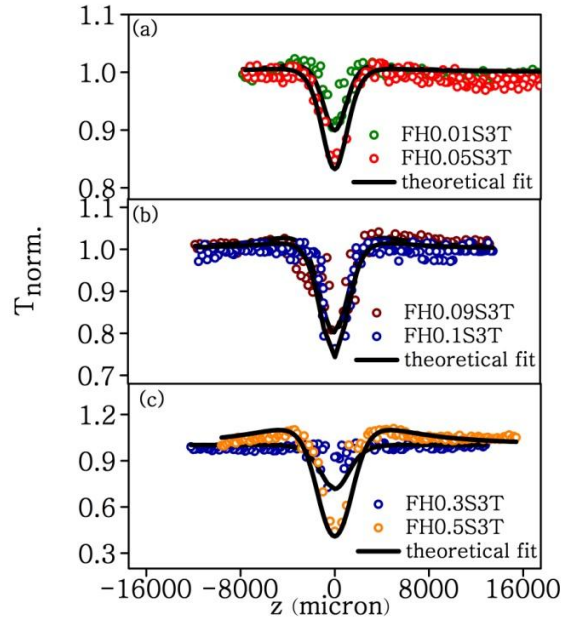


Figure 6.29 Nonlinear optical response of the composite films of hybrid with PMMA for varying loading of the hybrid

The experimental data is given a theoretical fit and the data fit to a three photon process. The three photon absorption coefficient calculated is an effective value (γ_{eff}) and are given in Table 6.3 along with the value of saturation intensity. The value of γ_{eff} is found to increase with increase in loading concentration, for the range of the study.

Table 6.3 Effective three photon absorption coefficients (γ_{eff}) and saturation intensities (I_{sat}) calculated for PMMA-hybrid composite films

Sample	LT (%)	$\gamma_{\text{eff}} \times 10^{-22} \text{ (m}^3/\text{W}^2\text{)}$	$I_{\text{sat}} \times 10^{12} \text{ (W/m}^2\text{)}$
FH0.01S3T	78	5.80	3.99
FH0.05S3T	76	8.20	9.00
FH0.09S3T	72	11.00	9.00
FH0.1S3T	70	15.60	9.00
FH0.3S3T	69	16.60	9.00
FH0.5S3T	56	108.00	1.50

FH0.5S3T is the film with maximum achievable loading concentration of ZnO and good linear transmittance. Figure 6.30 shows the nonlinear optical response of the film FH0.5S3T from 0.5 J/cm^2 to 5.5 J/cm^2 .

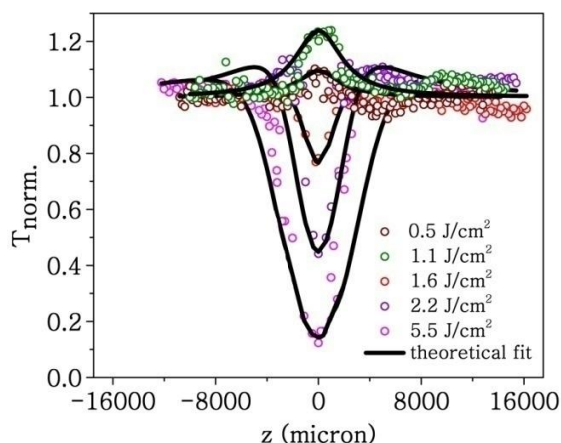


Figure 6.30 Fluence dependent nonlinear optical response of FH0.5S3T

The film exhibited saturation of absorption at lower fluences. As the fluence is increased, the absorption switched to reverse saturation. Upto 5.5 J/cm^2 the films exhibited RSA nature without any damage. Table 6.4 summarises the calculated values of three photon absorption coefficient and saturation intensity for the film FH0.5S3T at various fluences.

Table 6.4 Effective three photon absorption coefficients (γ_{eff}) and saturation intensities (I_{sat}) calculated for FH0.5S3T by varying the input fluence

Fluence (J/cm^2)	$\gamma_{\text{eff}} \times 10^{-22} (\text{m}^3/\text{W}^2)$	$I_{\text{sat}} \times 10^{12} (\text{W/m}^2)$
0.5	10.00	6.4
1.1	12.00	6.4
1.6	36.00	6.0
2.2	54.00	2.0
5.5	140.00	2.0

Figure 6.31 shows the nonlinear optical response of PS/PMMA-hybrid composite films at a fluence 2.2 J/cm^2 . The hybrid composite films exhibited RSA nature even if the matrix is changed.

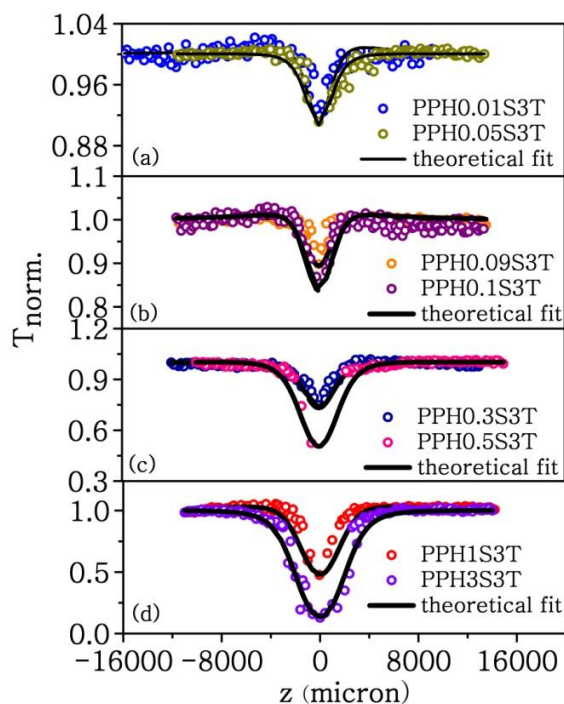


Figure 6.31 Nonlinear optical response of the composite films of hybrid with PS/PMMA for varying loading of the hybrid

The experimental data fit well with a three photon absorption process theory and the calculated values are shown in Table 6.5. The effective three photon absorption coefficient increases with increase in loading concentration of the hybrid in the matrix, as expected. PS/PMMA-hybrid films can accommodate more loading of the hybrid than PMMA-hybrid films. In this case the loading concentration could be increased to 3 weight % with fair linear transmittance and for those samples the higher effective three photon absorption coefficient are observed.

Table 6.5 Effective three photon absorption coefficients (γ_{eff}) and saturation intensities (I_{sat}) calculated for PS/PMMA-hybrid composite films

Sample	LT (%)	$\gamma_{\text{eff}} \times 10^{-22} (\text{m}^3/\text{W}^2)$	$I_{\text{sat}} \times 10^{12} (\text{W}/\text{m}^2)$
PPH0.01S3T	91	5.600	6.00
PPH0.05S3T	90	6.400	6.00
PPH0.09S3T	87	8.200	6.00
PPH0.1S3T	86	12.00	6.00
PPH0.3S3T	79	25.00	6.00
PPH0.5S3T	76	58.00	2.60
PPH1S3T	68	120.00	1.80
PPH3S3T	23	1800.00	0.36

Figure 6.32 shows the fluence dependent response of PPH0.5S3T. This film also exhibited a transition from saturation of absorption to reverse saturation with increase in incident fluence. PS/PMMA-hybrid films also could withstand upto $5.5 \text{ J}/\text{cm}^2$ without damage and exhibiting optical limiting. The absorption coefficient calculated are shown in Table 6.6.

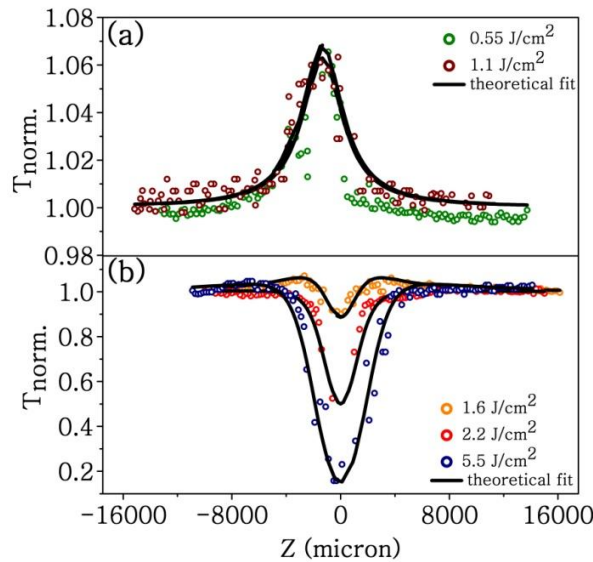


Figure 6.32 Fluence dependent nonlinear optical response of PPH0.5S3T

Table 6.6 Effective three photon absorption coefficients (γ_{eff}) and saturation intensities (I_{sat}) calculated for PPH0.5S3T by varying the input fluence

Fluence (J/cm^2)	$\gamma_{\text{eff}} \times 10^{-22}$ (m^3/W^2)	$I_{\text{sat}} \times 10^{12}$ (W/m^2)
0.55	0.08	5.00
1.10	1.60	5.00
1.65	24.00	2.60
2.20	58.00	2.60
5.51	68.00	2.40

Figures 6.30 and 6.32 shows that the polymer-hybrid films exhibit large fifth order nonlinearity. These studies reveal that the absorption coefficient is fluence dependent and hence the process behind the exhibited nonlinearity is not a genuine three photon absorption. The films show saturation of absorption at lower fluences which gradually switch over to reverse saturation and enhances with increased fluence. At lower intensities the film may undergo ground state bleaching and hence exhibit saturation of absorption. As the incident intensity is increased, excited state absorption (ESA) occurs, varying the absorption coefficient with intensity. At higher intensities the larger number of incident photons lead to an enhanced population of the real excited states, which contribute to the “effective” absorption coefficient. A close evaluation of the UV–Visible absorption spectrum (Figure 6.24) of the film reveals that the sample has good linear absorption in the excitation wavelength. Thus there is a chance for the exhibited nonlinearity to be evolved from three cascaded one photon absorption (1PA:1PA:1PA) processes. Here strong 1PA absorption populates the first excited state considerably and a sequential 1PA from this excited state results in a 2PA state. One more cascaded 1PA from the second excited state leads to an equivalent effective 3PA. This strong one-photon absorption and subsequent ESA will be much stronger because two-photon processes typically have a much smaller transition probability compared to one-photon processes. Thus the NLA in the films can be concluded to be arising from an “effective” three photon nonlinearity, which

originated from sequential excited state absorptions. Similar reports are available where such a process has been reported (Anand et al., 2011).

6.5. Conclusion

Modified MWNTs are prepared with acid treatment of the purchased MWNTs. The nanotubes are characterised and studied their properties by spectroscopic, microscopic and thermal analysis techniques. The dispersion of the nanotubes in acetone exhibited fifth order nonlinear absorption having RSA nature. Composite films of the MWNTs with PMMA and PS/PMMA are fabricated using spin coating technique. The films are characterised spectroscopically which exhibited good UV absorption and emission properties. The films also exhibited RSA nature which enables these films to be used as optical limiters.

Hybrids of the ZnO nanotops with MWNTs are prepared by two methods modifying the synthesis route for ZnO nanotops. The two types of hybrids prepared are well characterised using spectroscopic and microscopic techniques along with their thermal studies. The nonlinear optical response of the dispersion of the hybrid in water is also analysed using open aperture Z-scan technique. Composite films of the hybrid with polymer are fabricated using spin coating technique. These films exhibited a fifth order nonlinearity by cascaded absorption of three photons. The effective three photon absorption coefficient and the saturation intensity are calculated for the films. PS/PMMA-hybrid films with 3 weight % hybrid shows an effective three photon absorption coefficient $1800 \times 10^{-22} \text{ m}^3/\text{W}^2$ and saturation intensity, $0.36 \times 10^{12} \text{ W/m}^2$ at a fluence of 2.2 J/cm^2 . These films find applications in protective coatings from the hazards of high intensity lasers.

CHAPTER 7

CONCLUSIONS

There is a critical need of materials that exhibit considerable nonlinear absorption because of the wide spread application of nonlinear optical materials for device fabrication in industrial and scientific fields. The protection of photosensitive components of sensitive equipments like detectors and sensors can be fulfilled with the help of laser protection coatings using polymer nanocomposites exhibiting RSA behaviour. Saturable absorber, applicable for pulse shortening and Q-switching can also be fabricated using polymer nanocomposites. The present investigation is aimed at fabricating technological oriented materials like films of polymer nanocomposites with considerable linear and nonlinear absorption because films due to their geometry, inherently favour their integration into devices.

The key factors which are achieved in this thesis are listed below:

1. Synthesis of ZnO nanoparticles of top like structure having very good absorptive nonlinearity and complete characterization of these novel nanostructures.
2. Fabrication of PMMA-ZnO nanotop composite films by spin coating and dip coating techniques and complete optimization of the film fabrication parameters to get films exhibiting nonlinear absorption.
3. Fabrication of PMMA-ZnO nanotop composite films whose nature of nonlinear absorption is tunable with respect to the loading concentration of ZnO nanotops.
4. Fabrication of PS-ZnO and PS/PMMA-ZnO films with enhanced nonlinear absorption and decreased saturation intensity.
5. Synthesis of a hybrid material with ZnO nanotops and fMWNTs with fifth order absorptive nonlinearity.
6. Fabrication of polymer nanocomposite films of ZnO/MWNTs with improved absorptive nonlinearity compared to their individual components.

The first chapter is an introductory chapter and gives a general idea on the concept of nonlinear optics and its basics. The chapter details various processes associated with optical nonlinearity and the mechanism of NLO processes in various materials. A general idea on the different experimental methods to measure the parameters associated with each nonlinear optical process is explained. The wide areas of fields where nonlinear optical effects are utilised are reviewed along with the materials which exhibit nonlinear optical properties. A review on the linear and nonlinear optical properties of ZnO nanoparticles and MWNTs is performed in order to have a thorough knowledge of the material parameters associated with their nonlinear optical properties. The role of polymer nanocomposite films in the field of linear and nonlinear optics is also described. The scope and objective of the thesis is also detailed in the last section.

Experimental technique used for the present study is detailed in Chapter 2. The synthesis technique for ZnO nanoparticles and ZnO/MWNTs is described. The preparation of polymer nanocomposites and the fabrication technique for preparing films is also explained. The characterisation techniques used in the present investigation are explained with necessary theory. The last part of this chapter describes the process of nonlinear absorption in detail. A brief account of the theory and mechanism reported for exhibiting nonlinear absorption, like saturable and reverse saturable absorption, two photon absorption (TPA), multi photon absorption (MPA), excited state absorption (ESA), free carrier absorption (FCA), etc., are narrated with necessary theory. The techniques for measuring the parameters associated with nonlinear absorption is explained and a note on the open aperture Z-scan technique is given with the procedure used for curve fitting on the experimental data to calculate the nonlinear optical parameters.

In the third chapter, the first section explains, the detailed synthesis method of novel ZnO nanotops. The ZnO nanopowder is synthesised by solution precipitation technique with the help of two different capping agents. The nanoparticles are

characterised spectroscopically and microscopically and studied their properties thoroughly. PVP-capped nanoparticles which are named as ZnO nanotops are found to have better linear and nonlinear optical response. The effective nonlinear absorption coefficient and saturation intensity measured for the colloid are 2.1×10^{-11} m/W and 12.6×10^{12} W/m² respectively. PMMA-ZnO nanotop composites are prepared and fabricated into films using spin and dip coating technique. These films exhibited good nonlinear optical absorption. The spin coated films exhibits improved nonlinear absorption compared to their colloid and dip coated films of same ZnO loading concentration. The reason for the same is explained based on TGA analysis of the film sample. The RSA behaviour of the spin coated films of PMMA-ZnO composite is increased with increase in loading concentration. An effective two photon absorption resulting from two photon absorption and excited state absorption is found to be the mechanism behind the exhibited optical nonlinear absorption. The nonlinear absorption coefficient measured for the spin coated film with 2 weight % ZnO loading is 1.4×10^{-10} m/W with a saturation intensity 12.6×10^{12} W/m².

In order to have enhanced nonlinear absorption without agglomeration of the nanostructures incorporated in the films, the nanocomposite preparation is modified. The nanoparticles are dispersed with the help of dispersing agents. These films exhibits enhanced reverse saturable absorption compared to films prepared without the help of dispersing agents. Triton is found to be a better dispersing agent, providing good dispersion of nanoparticles, visible light transmittance and increased nonlinear absorption. The films exhibited a transition from RSA to SA with respect to increase in loading concentration of ZnO nanoparticles incorporated in the films. The mechanism behind the nonlinearity is analyzed. It is found that two step absorption, two photon absorption and free carrier absorption dominate in the films. The observed SA nature is explained on the basis of Pauli blocking. For a loading concentration of 5 weight % ZnO, the effective TPA coefficient is measured to be 1.20×10^{-7} m/W with saturation intensity 2.20×10^{12} W/m². Films fabricated with the

help of triton exhibited RSA behaviour up to a loading of 7 weight % of ZnO though the effective TPA coefficient is less (7×10^{-8} m/W). Hence polymer nanocomposite films useful as saturable and reverse saturable absorber are fabricated in this study.

The fifth chapter comprise of the fabrication of polymer nanocomposite films of PS-ZnO and PS/PMMA-ZnO. The matrix has been changed to PS followed by a modified PS/PMMA matrix and films are fabricated with ZnO nanotops. All the films exhibits improved linear absorption property. The spin coated films of PS/PMMA-ZnO are found to have uniform surface morphology and enhanced nonlinear absorption with an effective two photon absorption coefficient 7.90×10^{-8} m/W and saturation intensity much reduced to 3×10^{12} W/m².

Purchased MWNTs are treated with nitric acid and used for preparing hybrid with ZnO nanotops. The sixth chapter includes the synthesis of these hybrid, their film fabrication and nonlinear absorption studies. The modified nanotubes dispersed in acetone, exhibited a fifth order nonlinear absorption process with RSA behaviour. Composite films of the MWNTs with PMMA and PS/PMMA are fabricated using spin coating technique. The well characterised films exhibited good UV absorption and photoluminescence properties. The films posses RSA nature which has increased compared to their dispersion in water.

The sixth chapter also covers the synthesis of hybrids nanoparticles of ZnO nanotops with MWNTs, performed by two methods. The two types of hybrids prepared are characterised well. The nonlinear absorption of the dispersion of the hybrid in water is analysed using open aperture Z-scan technique. Composite films of the hybrid with PMMA and PS/PMMA are fabricated using spin coating technique. These films show a fifth order nonlinearity by cascaded absorption of three photons. The effective three photon absorption coefficient and the saturation intensity of each film is calculated. Even though the γ value of PS/PMMA-hybrid composite film with 0.5 weight % of hybrid is less when compared to PMMA-hybrid composite film, the

PS/PMMA matrix helps to increase the loading concentration and thereby helps to achieve films with high nonlinear absorption. The films are found to be applicable as optical limiting materials.

Future directions

In the present study polymer nanocomposite films are fabricated which exhibited considerable optical nonlinearity. This is the first step to device fabrication. It has been observed that tuning the inherent properties of the material highly influence their linear and nonlinear optical properties. Further studies can be done in fabricating polymer nanocomposite films of ZnO/MWNT with still lower saturation intensity. Also an effort to tune the nonlinearity of films to enable them sensitive for broader spectrum of incident wavelength is under consideration. Device fabrication using films which exhibit SA and RSA behaviour is also aimed at.

REFERENCES

1. Aber, J. E., Newstein, M. C. and Garetz, B. A. (2000). Femtosecond optical Kerr effect measurements in silicate glasses. *JOSA B*, 17(1): 120-127.
2. Ábrahám, N. and Dékány, I. (2010). Size-dependent photoluminescence properties of bare ZnO and polyethylene imine stabilized ZnO nanoparticles and their Langmuir–Blodgett films. *Colloids and Surfaces A: Physicochemical and Engineering Aspects*, 364(1–3): 26-33.
3. Ahmad, M., Ahmed, E., Hong, Z. L., Jiao, X. L., Abbas, T. and Khalid, N. R. (2013). Enhancement in visible light-responsive photocatalytic activity by embedding Cu-doped ZnO nanoparticles on multi-walled carbon nanotubes. *Applied Surface Science*, 285: 702-712.
4. Ai, X., Fei, H., Yang, Y., Han, L., Nie, R., Zhang, Y., Zhao, C., Xiao, L., Li, T., Zhao, J. and Yu, J. (1994). Polar enhancement of the nonlinear optical properties of Fe₂O₃ microcrystallites. *Journal of Luminescence*, 60–61(0): 364-367.
5. Ajayan, P. M. (1999). Nanotubes from carbon. *Chemical Reviews*, 99(7): 1787-1799.
6. Ali, Q. M. and Palanisamy, P. K. (2006). Z-scan determination of the third-order optical nonlinearity of organic dye nile blue chloride. *Modern Physics Letters B*, 20(11): 623-632.
7. Amin, G., Asif, M. H., Zainelabdin, A., Zaman, S., Nur, O. and Willander, M. (2011). Influence of pH, precursor concentration, growth time, and temperature on the morphology of ZnO nanostructures grown by the hydrothermal method. *Journal of Nanomaterials*, 2011: 1-9.
8. Anand, B., Ntim, S. A., Muthukumar, V. S., Sankara S. S. S., Philip, R. and Mitra, S. (2011). Improved optical limiting in dispersible carbon nanotubes and their metal oxide hybrids. *Carbon*, 49(14): 4767-4773.
9. Anand, B., Podila, R., Lingam, K., Krishnan, S. R., Sai, S. S. S., Philip, R. and Rao, A. M. (2013). Optical diode action from axially asymmetric nonlinearity in an all-carbon solid-state device. *Nano Letters*, 13(12): 5771-5776.
10. Andrews, R. and Weisenberger, M. (2004). Carbon nanotube polymer composites. *Current Opinion in Solid State and Materials Science*, 8(1): 31-37.

11. Antony, J., Chen, X. B., Morrison, J., Bergman, L., Qiang, Y., McCready, D. E. and Engelhard, M. H. (2005). ZnO nanoclusters: Synthesis and photoluminescence. *Applied Physics Letters*, 87(24): 241917.
12. Anžlovar, A., Orel, Z. C. and Žigon, M. (2008). Nanocomposites with nano-to-sub-micrometer size zinc oxide as an effective UV absorber. *Polimeri: časopis za plastiku i gumu*, 29(2): 84-87.
13. Aravinda, L. S., Nagaraja, K. K., Nagaraja, H. S., Bhat, K. U. and Bhat, B. R. (2013). ZnO/carbon nanotube nanocomposite for high energy density supercapacitors. *Electrochimica Acta*, 95: 119-124.
14. Atmeh, M. and Alcock-Earley, B. E. (2011). A conducting polymer/Ag nanoparticle composite as a nitrate sensor. *Journal of Applied Electrochemistry*, 41(11): 1341-1347.
15. Baldwin, G. C. (1969). *An introduction to nonlinear optics*. New York: Plenum Press.
16. Bandaru, P. R. (2007). Electrical properties and applications of carbon nanotube structures. *Journal of Nanoscience and Nanotechnology*, 7(4-5): 1-29.
17. Bao, Q., Zhang, H., Wang, Y., Ni, Z., Yan, Y., Shen, Z. X., Loh, K. P. and Tang, D. Y. (2009). Atomic-Layer Graphene as a Saturable Absorber for Ultrafast Pulsed Lasers. *Advanced Functional Materials*, 19(19): 3077-3083.
18. Beecroft, L. L. and Ober, C. K. (1997). Nanocomposite materials for optical applications. *Chemistry of Materials*, 9(6): 1302-1317.
19. Bloembergen, N., Burns, W. K. and Matsuoka, M. (1969). Reflected third harmonic generated by picosecond laser pulses. *Optics Communications*, 1(4): 195-198.
20. Botti, S., Ciardi, R., De Dominicis, L., Asilyan, L. S., Fantoni, R. and Marolo, T. (2003). DFWM measurements of third-order susceptibility of single-wall carbon nanotubes grown without catalyst. *Chemical Physics Letters*, 378(1): 117-121.
21. Boyd, R. W. (2003). *Nonlinear Optics*. San Diego, USA: Academic press.
22. Boyd, R. W., Shi, Z. and De Leon, I. (2014). The third-order nonlinear optical susceptibility of gold. *Optics Communications*, 326: 74-79.

23. Bragg, W. L. (1912). The Specular Reflection of X-rays. *Nature*, 90: 410.
24. Bredas, J. L., Adant, C., Tackx, P., Persoons, A. and Pierce, B. M. (1994). Third-order nonlinear optical response in organic materials: theoretical and experimental aspects. *Chemical Reviews*, 94(1): 243-278.
25. Brinker, C. J., Frye G.C., Hurd, A. J. and Ashley C. S. (1991). Fundamentals of sol-gel dip-coating. *Thin Solid Films*, 201: 97-108.
26. Buchalter, B., and Meredith, G. R. (1982). Third-order optical susceptibility of glasses determined by third harmonic generation. *Applied Optics*, 21(17), 3221-3224.
27. Burns, W. and Bloembergen, N. (1971). Third-harmonic generation in absorbing media of cubic or isotropic symmetry. *Physical Review B*, 4(10): 3437-3450.
28. Butcher, P. N. and Cotter, D. (1991). *The elements of nonlinear optics*. Cambridge University Press:UK.
29. Cano, L., Gutierrez, J. and Tercjak, A. (2012). Rutile TiO₂ Nanoparticles Dispersed in a Self-Assembled Polystyrene-block-polymethyl Methacrylate Diblock Copolymer Template. *The Journal of Physical Chemistry C*, 117(2): 1151-1156.
30. Chan, Y.-P., Lin, J.-H., Hsu, C.-C. and Hsieh, W.-F. (2008). Near-resonant high order nonlinear absorption of ZnO thin films. *Optics Express*, 16(24): 19900-19908.
31. Chang, W. H., Cheong, I. W., Shim, S. E. and Choe, S. (2006). The dispersion stability of multi-walled carbon nanotubes in the presence of poly (styrene/ α -methyl styrene/acrylic acid) random terpolymer. *Macromolecular Research*, 14(5): 545-551.
32. Chang, W.-C., Cheng, Y.-Y., Yu, W.-C., Yao, Y.-C., Lee, C.-H. and Ko, H.-H. (2012). Enhancing performance of ZnO dye-sensitized solar cells by incorporation of multiwalled carbon nanotubes. *Nanoscale Research Letters*, 7(1): 1-7.
33. Chattopadhyay, M., Kumbhakar, P., Tiwary, C. S., Mitra, A. K., Chatterjee, U. and Kobayashi, T. (2009). Three-photon-induced four-photon absorption and nonlinear refraction in ZnO quantum dots. *Optics Letters*, 34(23): 3644-3646.

34. Chaudhuri, T., Kothari, A., Tiwari, D. and Ray, A. (2013). Photoconducting nanocomposite films of PbS nanocrystals in insulating polystyrene. *Physica Status Solidi (a)*, 210(2): 356-360.
35. Chen, C. S., Liu, T. G., Lin, L. W., Xie, X. D., Chen, X. H., Liu, Q. C., Liang, B., Yu, W. W. and Qiu, C. Y. (2013). Multi-walled carbon nanotube-supported metal-doped ZnO nanoparticles and their photocatalytic property. *Journal of Nanoparticle Research*, 15(1): 1-9.
36. Chen, L., Xie, H. and Yu, W. (2011). Functionalization methods of carbon nanotubes and its applications. In Marulanda, J. M. (Eds.), *Carbon Nanotubes Applications on Electron Devices* (pp.213-232). Croatia: InTech.
37. Chen, P., Wu, X., Sun, X., Lin, J., Ji, W. and Tan, K. L. (1999). Electronic structure and optical limiting behavior of carbon nanotubes. *Physical Review Letters*, 82(12): 2548-2551.
38. Chen, Y., Lin, Y., Liu, Y., Doyle, J., He, N., Zhuang, X., Bai, J. and Blau, W. J. (2007). Carbon nanotube-based functional materials for optical limiting. *Journal of Nanoscience and Nanotechnology*, 7(4-5): 1268-1283.
39. Cheng, B. and Samulski, E. T. (2004). Hydrothermal synthesis of one-dimensional ZnO nanostructures with different aspect ratios. *Chemical Communications*, (8): 986-987.
40. Cho, S., Jung, S.-H. and Lee, K.-H. (2008). Morphology-controlled growth of ZnO nanostructures using microwave irradiation: from basic to complex structures. *The Journal of Physical Chemistry C*, 112(33): 12769-12776.
41. Chrissanthopoulos, A., Baskoutas, S., Bouropoulos, N., Dracopoulos, V., Tasis, D. and Yannopoulos, S. N. (2007). Novel ZnO nanostructures grown on carbon nanotubes by thermal evaporation. *Thin Solid Films*, 515(24): 8524-8528.
42. Coleman, V. A, and Jagadish, C. (2006). Basic properties and applications of ZnO. In C. Jagadish & S. Pearton (Eds.), *Zinc Oxide Bulk, Thin Films and Nanostructures: Processing, Properties and Applications* (pp.1-20). Elsevier:Netherlands.
43. Cullity, B. D. (2001). *Elements of X-ray Diffraction*. USA: Addison-Wesley.
44. Dai, H., Hafner, J. H., Rinzler, A. G., Colbert, D. T. and Smalley, R. E. (1996). Nanotubes as nanoprobe in scanning probe microscopy. *Nature*, 384(6605): 147-150.

45. Datsyuk, V., Kalyva, M., Papagelis, K., Parthenios, J., Tasis, D., Siokou, A., Kallitsis, I. and Galiotis, C. (2008). Chemical oxidation of multiwalled carbon nanotubes. *Carbon*, 46(6): 833-840.
46. De Graef, M. (2003). *Introduction to conventional transmission electron microscopy* Cambridge University Press:UK.
47. Dehghani, Z., Nazerdeylami, S., Saievar-Iranizad, E. and Majles A. M. H. (2011). Synthesis and investigation of nonlinear optical properties of semiconductor ZnS nanoparticles. *Journal of Physics and Chemistry of Solids*, 72(9): 1008-1010.
48. Deiss, J. L., Anizan, P., El Hadigui, S. and Wecker, C. (1996). Steric stability of TiO₂ nanoparticles in aqueous dispersions. *Colloids and Surfaces A: Physicochemical and Engineering Aspects*, 106(1): 59-62.
49. Deng, Y., Sun, Y., Wang, P., Zhang, D., Ming, H. and Zhang, Q. (2008). *In situ* synthesis and nonlinear optical properties of Ag nanocomposite polymer films. *Physica E: Low-dimensional Systems and Nanostructures*, 40(4): 911-914.
50. Dharmadhikari, A. K., Roy, B., Roy, S., Dharmadhikari, J. A., Mishra, A. and Kumar, G. R. (2004). Higher-order optical nonlinearities in 4'-dimethylamino-N-methyl-4-stilbazolium tosylate. *Optics Communications*, 235(1-3): 195-200.
51. Djurišić, A. B. and Leung, Y. H. (2006). Optical properties of ZnO nanostructures. *Small*, 2(8-9): 944-961.
52. Djurišić, A. B., Ng, A. M. C. and Chen, X. Y. (2010). ZnO nanostructures for optoelectronics: material properties and device applications. *Progress in Quantum Electronics*, 34(4): 191-259.
53. Dresselhaus, M. S. (1995). Carbon nanotubes. *Carbon*, 33(7): 871-872.
54. Dresselhaus, M. S., Dresselhaus, G. and Jorio, A. (2004). Unusual properties and structure of carbon nanotubes. *Annual Review of Materials Research*, 34: 247-278.
55. Du, T., Song, H. and Ilegbusi, O. J. (2007). Sol-gel derived ZnO/PVP nanocomposite thin film for superoxide radical sensor. *Materials Science and Engineering: C*, 27(3): 414-420.
56. Dumbrava, A., Prodan, G. and Moscalu, F. (2013). Investigations on the influence of surfactant in morphology and optical properties of zinc oxide

- nanopowders for dye-sensitized solar cells applications. *Materials Science in Semiconductor Processing*, 16(4): 1095-1104.
57. Ebbesen, T. W. and Ajayan, P. M. (1992). Large-scale synthesis of carbon nanotubes. *Nature*, 358(6383): 220-222.
 58. El-Hady, M. M. A., Farouk, A. and Sharaf, S. (2013). Flame retardancy and UV protection of cotton based fabrics using nano ZnO and polycarboxylic acids. *Carbohydrate Polymers*, 92(1): 400-406.
 59. Ellmer, K., Klein, A. and Rech, B. (2008). *Transparent conductive Zinc Oxide: Basics and Applications in Thin Film Solar Cells*. Springer:Heidelberg.
 60. Enculescu, I., Sima, M., Enculescu, M., Enache, M., Vasile, V. and Neumann, R. (2007). Influence of geometrical properties on light emission of ZnO nanowires. *Optical Materials*, 30(1): 72-75.
 61. Erhart, P., Albe, K. and Klein, A. (2006). First-principles study of intrinsic point defects in ZnO: Role of band structure, volume relaxation, and finite-size effects. *Physical Review B*, 73(20): 205203 (1-9).
 62. Fainman, Y., Ma, J. and Lee, S. H. (1993). *Non-linear optical materials and applications*. *Materials Science Reports*, 9(2): 53-139.
 63. Fakhroueian, Z., Harsini, F. M., Chalabian, F., Katouzian, F., Shafiekhani, A. and Esmaeilzadeh, P. (2013). Influence of modified ZnO quantum dots and nanostructures as new antibacterials. *Advances in Nanoparticles*, 2(03): 247-258.
 64. Fan, Z. and Lu, J. G. (2005). Zinc oxide nanostructures: synthesis and properties. *Journal of Nanoscience and Nanotechnology*, 5(10): 1561-1573.
 65. Farouk, A., Moussa, S., Ulbricht, M., Schollmeyer, E. and Textor, T. (2014). ZnO-modified hybrid polymers as an antibacterial finish for textiles. *Textile Research Journal*, 84(1): 40-51.
 66. Farouk, A., Textor, T., Schollmeyer, E., Tarbuk, A. and Grancacic, A. M. (2010). Sol-gel-derived inorganic-organic hybrid polymers filled with ZnO nanoparticles as an ultraviolet protection finish for textiles. *AUTEX Research Journal*, 10: 58-63.
 67. Frackowiak, E. and Béguin, F. (2002). Electrochemical storage of energy in carbon nanotubes and nanostructured carbons. *Carbon*, 40(10): 1775-1787.

68. Franken, P. A., Hill, A. E., Peters, C. W. and Weinreich, G. (1961). Generation of optical harmonics. *Physical Review Letters*, 7(4): 118-119.
69. Fuentes-Hernandez, C., Ramos-Ortiz, G., Tseng, S.-Y., Gaj, M. P. and Kippelen, B. (2009). Third-harmonic generation and its applications in optical image processing. *Journal of Materials Chemistry*, 19(40): 7394-7401.
70. Garmire, E. (2012). Overview of nonlinear optics. open source. In N. Kamanina (Eds.), *Nonlinear Optics* (pp.3-52). InTech:Croatia.
71. Ge, J., Zeng, X., Tao, X., Li, X., Shen, Z., Yun, J. and Chen, J. (2010). Preparation and characterization of PS-PMMA/ZnO nanocomposite films with novel properties of high transparency and UV-shielding capacity. *Journal of Applied Polymer science*, 118(3): 1507-1512.
72. Girifalco, L. A., Hodak, M. and Lee, R. S. (2000). Carbon nanotubes, buckyballs, ropes, and a universal graphitic potential. *Physical Review B*, 62(19): 131(04-10).
73. Gültekin, D., Alaf, M. and Akbulut, H. (2013). Synthesis and characterization of ZnO nanopowders and ZnO-CNT nanocomposites prepared by chemical precipitation route. *Acta Physica Polonica A*, 123 (2): 275.
74. Guo, L., Yang, S., Yang, C., Yu, P., Wang, J., Ge, W. and Wong, G. K. L. (2000). Highly monodisperse polymer-capped ZnO nanoparticles: preparation and optical properties. *Applied Physics Letters*, 76(20): 2901-2903.
75. Gutmann, J. S., Müller-Buschbaum, P., Schubert, D. W., Stribeck, N., Smilgies, D. and Stamm, M. (2000). Roughness correlations in ultra-thin polymer blend films. *Physica B: Condensed Matter*, 283(1-3): 40-44.
76. Hall, D. B., Underhill, P. and Torkelson, J. M. (1998). Spin coating of thin and ultrathin polymer films. *Polymer Engineering & Science*, 38(12): 2039-2045.
77. Han, L.-L., Cui, L., Wang, W.-H., Wang, J.-L. and Du, X.-W. (2012). On the origin of blue emission from ZnO quantum dots synthesized by a sol-gel route. *Semiconductor Science and Technology*, 27(6): 1-8.
78. Han, M. and Zhao, K. (2008). Dielectric Behavior of Suspensions of Polystyrene- Zinc Oxide Composite Microspheres. *The Journal of Physical Chemistry C*, 112(25): 9192-9202.

79. Haripadmam, P. C., John, H., Philip, R. and Gopinath, P. (2014a). Switching of absorptive nonlinearity from reverse saturation to saturation in polymer-ZnO nanotop composite films. *Applied Physics Letters*, 105: 221102 (1-5).
80. Haripadmam, P. C., Kavitha, M. K., John, H., Krishnan, B. and Gopinath, P. (2012). Optical limiting studies of ZnO nanotops and its polymer nanocomposite films. *Applied Physics Letters*, 101: 071103 (1-5).
81. Haripadmam, P.C., John, H., Philip, R. and Gopinath, P. (2014b). Enhanced optical limiting in polystyrene-ZnO nanotop composite films. *Optics Letters*, 39(3): 474-477.
82. He, G. S., Tan, L.-S., Zheng, Q. and Prasad, P. N. (2008). Multiphoton absorbing materials: molecular designs, characterizations, and applications. *Chemical Reviews*, 108(4): 1245-1330.
83. Heijman, S. G. J. and Stein, H. N. (1995). Electrostatic and sterical stabilization of TiO₂ dispersions. *Langmuir*, 11(2): 422-427.
84. Hong, R., Pan, T., Qian, J. and Li, H. (2006). Synthesis and surface modification of ZnO nanoparticles. *Chemical Engineering Journal*, 119(2): 71-81.
85. Horikoshi, S. and Serpone, N. (2014). *Microwaves in Nanoparticle Synthesis. Fundamentals and Applications*. Wiley:Germany.
86. Iijima, S. (1991). Helical microtubules of graphitic carbon. *Nature*, 354(6348): 56-58.
87. Irimpan, L., Ambika, D., Kumar, V., Nampoore, V. P. N. and Radhakrishnan, P. (2008b). Effect of annealing on the spectral and nonlinear optical characteristics of thin films of nano-ZnO. *Journal of Applied Physics*, 104(3): 033118(1-9).
88. Irimpan, L., Deepthy, A., Krishnan, B., Nampoore, V. P. N. and Radhakrishnan, P. (2008a). Nonlinear optical characteristics of self-assembled films of ZnO. *Applied Physics B*, 90(3-4): 547-556.
89. Ismail, B., Abaab, M. and Rezig, B. (2001). Structural and electrical properties of ZnO films prepared by screen printing technique. *Thin Solid Films*, 383(1): 92-94.
90. Janotti, A. and Van de Walle, C. G. (2007). Native point defects in ZnO. *Physical Review B*, 76(16): 165202(1-22).

91. Janotti, A., Varley, J., Lyons, J. and Van de Walle, C., (2012). Controlling the Conductivity in Oxide Semiconductors. In J. Wu, J. Cao, W. -Q. Han, A. Janotti and H. -C. Kim (Eds.), *Functional Metal Oxide Nanostructures*. (pp.23-35). DOI:10.1007/978-1-4419-9931-3_2.
92. Jeeju, P. P., Jayalekshmi, S. and Chandrasekharan, K. (2014). Nonlinear optical properties of ZnO/poly (vinyl alcohol) nanocomposite films. *Optoelectronic Materials and Thin Films* 163:163- 166.
93. Jeeju, P. P., Jayalekshmi, S., Chandrasekharan, K. and Sudheesh, P. (2012). Size dependent nonlinear optical properties of spin coated zinc oxide-polystyrene nanocomposite films. *Optics Communications*, 285(24): 5433-5439.
94. Jena, K. C., Bisht, P. B., Shaijumon, M. M. and Ramaprabhu, S. (2007). Study of optical nonlinearity of functionalized multi-wall carbon nanotubes by using degenerate four wave mixing and Z-scan techniques. *Optics Communications*, 273(1): 153-158.
95. Jiang, Z., Huang, Z., Yang, P., Chen, J., Xin, Y. and Xu, J. (2008). High PL-efficiency ZnO nanocrystallites/PPV composite nanofibers. *Composites Science and Technology*, 68(15): 3240-3244.
96. Jin, Z., Sun, X., Xu, G., Goh, S. H. and Ji, W. (2000). Nonlinear optical properties of some polymer/multi-walled carbon nanotube composites. *Chemical Physics Letters*, 318(6): 505-510.
97. Jose, M. V., Steinert, B. W., Thomas, V., Dean, D. R., Abdalla, M. A., Price, G. and Janowski, G. M. (2007). Morphology and mechanical properties of Nylon 6/MWNT nanofibers. *Polymer*, 48(4): 1096-1104.
98. Kajzar, F. and Messier, J. (1987). Original technique for third-harmonic-generation measurements in liquids. *Review of Scientific Instruments*, 58(11): 2081-2085.
99. Kanbara, H., Fujiwara, S., Tanaka, K., Nasu, H. and Hirao, K. (1997). Third-order nonlinear optical properties of chalcogenide glasses. *Applied Physics Letters*, 70(8): 925-927.
100. Kaneva, N. V. and Dushkin, C. D. (2011). Preparation of nanocrystalline thin films of ZnO by sol-gel dip coating. *Bulgarian Chemical Communications*, 43(2): 259-263.

101. Karthikeyan, B., Anija, M. and Philip, R. (2006). In situ synthesis and nonlinear optical properties of Au: Ag nanocomposite polymer films. *Applied Physics Letters*, 88(5): 053104(1-3).
102. Kavitha, M. K., John, H. and Gopinath, P. (2014). Polyvinyl pyrrolidone assisted low temperature synthesis of ZnO nanocones and its linear and nonlinear optical studies. *Materials Research Bulletin*, 49: 132-137.
103. Kelly, K. L., Coronado, E., Zhao, L. L. and Schatz, G. C. (2003). The optical properties of metal nanoparticles: the influence of size, shape, and dielectric environment. *The Journal of Physical Chemistry B*, 107(3): 668-677.
104. Khatei, J., Sandeep, C. S. S., Philip, R. and Rao, K. S. R. K. (2012). Near-resonant two-photon absorption in luminescent CdTe quantum dots. *Applied Physics Letters*, 100(8): 081901(1-3).
105. Khrenov, V., Klapper, M., Koch, M. and Müllen, K. (2005). Surface functionalized ZnO particles designed for the use in transparent nanocomposites. *Macromolecular Chemistry and Physics*, 206(1): 95-101.
106. Kim, H. and Sigmund, W. (2002). Zinc oxide nanowires on carbon nanotubes. *Applied Physics Letters*, 81(11): 2085-2087.
107. Knutsen, K. E., Galeckas, A., Zubiaga, A., Tuomisto, F., Farlow, G. C., Svensson, B. G. and Kuznetsov, A. Y. (2012). Zinc vacancy and oxygen interstitial in ZnO revealed by sequential annealing and electron irradiation. *Physical Review B*, 86(12): 121203(1-5).
108. Ko, Y. H., Kim, M. S. and Yu, J. S. (2012). Structural and optical properties of ZnO nanorods by electrochemical growth using multi-walled carbon nanotube-composed seed layers. *Nanoscale Research Letters*, 7(1): 1-6.
109. Kole, A. K., Kumbhakar, P. and Chatterjee, U. (2014). Observations on nonlinear optical properties of ZnS nanosheet, ZnS–ZnO composite nanosheet and porous ZnO nanostructures dispersed in aqueous medium. *Chemical Physics Letters*, 591: 93-98.
110. Kołodziejczak-Radzimska, A. and Jesionowski, T. (2014). Zinc Oxide—From Synthesis to Application: A Review. *Materials*, 7(4): 2833-2881.
111. Kong, D. G., Chang, Q., Ye, H. A., Gao, Y. C., Wang, Y. X., Zhang, X. R., Yang, K., Wu, W. Z. and Song, Y. L. (2009). The fifth-order nonlinearity of CS₂. *Journal of Physics B: Atomic, Molecular and Optical Physics*, 42(6): 065401 (1-4).

112. Koohsorkhi, J., Abdi, Y., Mohajerzadeh, S., Hosseinzadegan, H., Komijani, Y. and Soleimani, E. A. (2006). Fabrication of self-defined gated field emission devices on silicon substrates using PECVD-grown carbon nano-tubes. *Carbon*, 44(13): 2797-2803.
113. Kressler, J., Higashida, N., Shimomai, K., Inoue, T. and Ougizawa, T. (1994). Temperature Dependence of the Interaction Parameter between Polystyrene and Poly (methyl methacrylate). *Macromolecules*, 27(9): 2448-2453.
114. Krishnakumar, V., Shanmugam, G. and Nagalakshmi, R. (2012). Large third-order optical nonlinearity of Mg-doped PbS/PVA freestanding nanocomposite films. *Journal of Physics D: Applied Physics*, 45(16): 165102(1-7).
115. Kuila, B. K., Malik, S., Batabyal, S. K. and Nandi, A. K. (2007). In-situ synthesis of soluble poly (3-hexylthiophene)/multiwalled carbon nanotube composite: Morphology, structure, and conductivity. *Macromolecules*, 40(2): 278-287.
116. Kulyk, B., Sahraoui, B., Krupka, O., Kapustianyk, V., Rudyk, V., Berdowska, E., Tkaczyk, S. and Kityk, I. (2009). Linear and nonlinear optical properties of ZnO/PMMA nanocomposite films. *Journal of Applied Physics*, 106(9): 093102(1-6).
117. Kumar, V., Swart, H. C., Ntwaeaborwa, O. M., Kroon, R. E., Terblans, J. J., Shaat, S. K. K., Yousif, A. and Duvenhage, M. M. (2013). Origin of the red emission in zinc oxide nanophosphors. *Materials Letters*, 101: 57-60.
118. Kumari, V., Kumar, V., Malik, B. P., Mohan, D. and Mehra, R. M. (2011). Laser induced nonlinear optical properties of zinc oxide thin film prepared by sol-gel method. *Journal of Nano- and Electronic Physics*, 3(1): 601-609.
119. Kurian, P. A., Vijayan, C., Sandeep, C. S. S., Philip, R. and Sathiyamoorthy, K. (2007). Two-photon-assisted excited state absorption in nanocomposite films of PbS stabilized in a synthetic glue matrix. *Nanotechnology*, 18(7): 075708(1-7).
120. Kuzmany, H., Kukovecz, A., Simon, F., Holzweber, M., Kramberger, C. and Pichler, T. (2004). Functionalization of carbon nanotubes. *Synthetic Metals*, 141(1): 113-122.
121. Kuznetsova, A., Mawhinney, D. B., Naumenko, V., Yates Jr, J. T., Liu, J. and Smalley, R. E. (2000). Enhancement of adsorption inside of single-walled nanotubes: opening the entry ports. *Chemical Physics Letters*, 321(3): 292-296.

122. Kuznetsova, A., Popova, I., Yates, J. T., Bronikowski, M. J., Huffman, C. B., Liu, J., Smalley, R. E., Hwu, H. H. and Chen, J. G. (2001). Oxygen-containing functional groups on single-wall carbon nanotubes: NEXAFS and vibrational spectroscopic studies. *Journal of the American Chemical Society*, 123(43): 10699-10704.
123. Lafrentz, M., Brunne, D., Rodina, A. V., Pavlov, V. V., Pisarev, R. V., Yakovlev, D. R., Bakin, A. and Bayer, M. (2013). Second-harmonic generation spectroscopy of excitons in ZnO. *Physical Review B*, 88(23): 235207(1-20).
124. Lakowicz, J. R. and Geddes, C. D. (1991). *Topics in fluorescence spectroscopy*. USA:Springer.
125. Lazareck, A. D., Cloutier, S. G., Kuo, T.-F., Taft, B. J., Kelley, S. O. and Xu, J. M. (2006a). DNA-directed synthesis of zinc oxide nanowires on carbon nanotube tips. *Nanotechnology*, 17(10): 2661-2664.
126. Lazareck, A. D., Kuo, T.-F., Xu, J. M., Taft, B. J., Kelley, S. O. and Cloutier, S. G. (2006b). Optoelectrical characteristics of individual zinc oxide nanorods grown by DNA directed assembly on vertically aligned carbon nanotube tips. *Applied Physics Letters*, 89(10): 103109(1-3).
127. Lee, T. K., Bristow, A. D., Hübner, J. and van Driel, H. M. (2006). Linear and nonlinear optical properties of Au-polymer metallodielectric Bragg stacks. *Journal of Optical Society of America B*, 23(10): 2142-2147.
128. Lehraki, N., Aida, M. S., Abed, S., Attaf, N., Attaf, A. and Poulain, M. (2012). ZnO thin films deposition by spray pyrolysis: Influence of precursor solution properties. *Current Applied Physics*, 12(5): 1283-1287.
129. Leiter, F., Alves, H., Pfisterer, D., Romanov, N. G., Hofmann, D. M. and Meyer, B. K. (2003). Oxygen vacancies in ZnO. *Physica B: Condensed Matter*, 340: 201-204.
130. Li, D., Leung, Y. H., Djurišić, A. B., Liu, Z. T., Xie, M. H., Shi, S. L., Xu, S. J. and Chan, W. K. (2004). Different origins of visible luminescence in ZnO nanostructures fabricated by the chemical and evaporation methods. *Applied Physics Letters*, 85(9): 1601-1603.
131. Li, M., Xing, G., Xing, G., Wu, B., Wu, T., Zhang, X. and Sum, T. C. (2013). Origin of green emission and charge trapping dynamics in ZnO nanowires. *Physical Review B*, 87(11): 115309(1-8).

132. Li, S., Lin, M. M., Toprak, M. S., Kim, D. K. and Muhammed, M. (2010). Nanocomposites of polymer and inorganic nanoparticles for optical and magnetic applications. *Nano Reviews*, 1: 1-19.
133. Li, S., Toprak, M. S., Jo, Y. S., Dobson, J., Kim, D. K. and Muhammed, M. (2007). Bulk synthesis of transparent and homogeneous polymeric hybrid materials with ZnO quantum dots and PMMA. *Advanced Materials*, 19(24): 4347-4352.
134. Lim, J. -H., Kang, C. -K., Kim, K. -K., Park, I. -K., Hwang, D. -K., and Park, S. -J. (2006a). UV Electroluminescence Emission from ZnO Light-Emitting Diodes Grown by High-Temperature Radiofrequency Sputtering. *Advanced Materials*, 18: 2720-2724.
135. Lim, S. H., Elim, H. I., Gao, X. Y., Wee, A. T. S., Ji, W., Lee, J. Y. and Lin, J. (2006b). Electronic and optical properties of nitrogen-doped multiwalled carbon nanotubes. *Physical Review B*, 73(4): 045402(1-6).
136. Lima, J. F. d., Martins, R. F. and Serra, O. A. (2012). Transparent UV-absorbers thin films of zinc oxide: Ceria system synthesized via sol-gel process. *Optical Materials*, 35(1): 56-60.
137. Lin, J.-H., Chen, Y.-J., Lin, H.-Y. and Hsieh, W.-F. (2005). Two-photon resonance assisted huge nonlinear refraction and absorption in ZnO thin films. *Journal of Applied Physics*, 97(3): 033526(1-6).
138. Lin, Z., Wang, Z., Chen, C. and Lee, M.-H. (2003b). Mechanism of linear and nonlinear optical effects of KDP and urea crystals. *Journal of Chemical Physics*, 118(5): 2349-2356.
139. Lin, Z., Wang, Z., Chen, C., Chen, S. K. and Lee, M.-H. (2003a). Mechanism for linear and nonlinear optical effects in $\text{KBe}_2\text{BO}_3\text{F}_2$ (KBBF) crystal. *Chemical Physics Letters*, 367(5): 523-527.
140. Liu, C.-H., Chiu, L.-K., Yeh, J.-Y. and Tsiang, R. C.-C. (2012). Making organic-inorganic nanocomposites via selective dispersion of PS-tethered SiO_2 particles in polystyrene-block-polymethylmethacrylate copolymer. *Journal of Nanomaterials*, 2012: (1-7).
141. Liu, J., Li, X. and Dai, L. (2006b). Water-Assisted Growth of Aligned Carbon Nanotube-ZnO Heterojunction Arrays. *Advanced Materials*, 18(13): 1740-1744.

142. Liu, P. (2005). Modifications of carbon nanotubes with polymers. *European Polymer Journal*, 41(11): 2693-2703.
143. Liu, P. and Su, Z. (2006). Preparation and Characterization of PMMA/ZnO Nanocomposites via In-Situ Polymerization Method. *Journal of Macromolecular Science, Part B: Physics*, 45(1): 131-138.
144. Liu, X. C., Shi, E. W., Chen, Z. Z., Zhang, H. W., Xiao, B. and Song, L. X. (2006a). High-temperature ferromagnetism in (Co, Al)-codoped ZnO powders. *Applied Physics Letters*, 88(25): 252503(1-3).
145. Liu, X., Matsumura, K., Tomita, Y., Yasui, K., Kojima, K. and Chikama, K. (2010). Nonlinear optical responses of nanoparticle-polymer composites incorporating organic (hyperbranched polymer)-metallic nanoparticle complex. *Journal of Applied Physics*, 108(7): 073102(1-9).
146. Liu, X., Wu, X., Cao, H. and Chang, R. P. H. (2004). Growth mechanism and properties of ZnO nanorods synthesized by plasma-enhanced chemical vapor deposition. *Journal of Applied Physics*, 95(6): 3141-3147.
147. Lopes, P., Corbellini, M., Ferreira, B. L., Almeida, N., Fredel, M., Fernandes, M. H. and Correia, R. (2009). New PMMA-co-EHA glass-filled composites for biomedical applications: Mechanical properties and bioactivity. *Acta Biomaterialia*, 5(1): 356-362.
148. Luo, S. J., Yang, J. T., Du, W. F. and Laref, A. (2011). Mechanism of Linear and Nonlinear Optical Properties of the Urea Crystal Family. *The Journal of Physical Chemistry A*, 115(20): 5192-5200.
149. Ma, P.-C., Siddiqui, N. A., Marom, G. and Kim, J.-K. (2010). Dispersion and functionalization of carbon nanotubes for polymer-based nanocomposites: a review. *Composites Part A: Applied Science and Manufacturing*, 41(10): 1345-1367.
150. Macutkevicius, J., Seliuta, D., Valusis, G., Adomavicius, R., Krotkus, A., Kuzhir, P., Paddubskaya, A., Maksimenko, S., Kuznetsov, V. and Mazov, I., Simonova, I. (2012). Multi-walled carbon nanotubes/PMMA composites for THz applications. *Diamond and Related Materials*, 25: 13-18.
151. Maensiri, S., Laokul, P. and Promarak, V. (2006). Synthesis and optical properties of nanocrystalline ZnO powders by a simple method using zinc acetate dihydrate and poly (vinyl pyrrolidone). *Journal of Crystal Growth*, 289(1): 102-106.

152. Maier, S. A. and Atwater, H. A. (2005). Plasmonics: Localization and guiding of electromagnetic energy in metal/dielectric structures. *Journal of Applied Physics*, 98(1): 011101(1-10).
153. Makino, T. (2005). Optical properties of ZnO-based quantum structures. *Superlattices and Microstructures*, 38(4): 231-244.
154. Man, Y. H., Li, Z. C. and Zhang, Z. J. (2009). Interface-dependent mechanical properties in MWNT-filled polycarbonate. *Materials Transactions*, 50(6): 1355-1359.
155. Mang, A., Reimann, K. and Rübénacke, S. (1995). Band gaps, crystal-field splitting, spin-orbit coupling, and exciton binding energies in ZnO under hydrostatic pressure. *Solid State Communications*, 94(4): 251-254.
156. Marshall, M. W., Popa-Nita, S. and Shapter, J. G. (2006). Measurement of functionalised carbon nanotube carboxylic acid groups using a simple chemical process. *Carbon*, 44(7): 1137-1141.
157. Martinez, A., Uchida, S., Song, Y.-W., Ishigure, T. and Yamashita, S. (2008). Fabrication of Carbon nanotube poly-methyl-methacrylate composites for nonlinear photonic devices. *Optics Express*, 16(15): 11337-11343.
158. Mary, A. P. R., Sandeep, C. S. S., Narayanan, T. N., Philip, R., Moloney, P., Ajayan, P. M. and Anantharaman, M. R. (2011). Nonlinear and magneto-optical transmission studies on magnetic nanofluids of non-interacting metallic nickel nanoparticles. *Nanotechnology*, 22(37): 375702(1-7).
159. Mathews, S. J., Kumar, C. S., Giribabu, L. and Venugopal Rao, S. V.(2007). Large third-order optical nonlinearity and optical limiting in symmetric and unsymmetrical phthalocyanines studied using Z-scan. *Optics Communications*, 280(1): 206-212.
160. Miragliotta, J. A. (1995). Analytical and device-related applications of nonlinear optics. *Johns Hopkins APL Technical Digest*, 16(4): 349-357.
161. Moreno, R. and Ferrari, B., (2012). Nanoparticles dispersion and the effect of related parameters in the EPD kinetics. In J. H. Dickerson and A. R. Boccarrccini (Eds.), *Electrophoretic Deposition of Nanomaterials*, (pp.73-128). DOI:10.1007/978-1-4419-9730-2_2.
162. Mu, P., Haolin, T., Shichun, M. and Runzhang, Y. (2004). Synthesis of platinum/multi-wall carbon nanotube catalysts. *Journal of Materials Research*, 19(08): 2279-2284.

163. Mukherjee, D., Barghi, S. and Ray, A. K. (2013). Preparation and Characterization of the TiO₂ Immobilized Polymeric Photocatalyst for Degradation of Aspirin under UV and Solar Light. *Processes*, 2014(2): 12-23.
164. Munn, R. W. and Ironside, C. N. (1993). *Principles and applications of nonlinear optical materials*. Springer: UK
165. Murti, Y. and Vijayan, C. (2014). *Essentials of Nonlinear Optics*. DOI 10.1007/978-94-011-2158-3
166. Nalwa, H. S. (1999). *Handbook of Nanostructured Materials and Nanotechnology*. Academic Press: USA.
167. Naranjo, F., González-Herráez, M., Fernández, H., Solis, J. and Monroy, E. (2007). Third order nonlinear susceptibility of InN at near band-gap wavelengths. *Applied Physics Letters*, 90(9): 091903-091903-3.
168. Naseema, K., Sujith, K. V., Manjunatha, K. B., Kalluraya, B., Umesh, G. and Rao, V. (2010). Synthesis, characterization and studies on the nonlinear optical parameters of hydrazones. *Optics & Laser Technology*, 42(5): 741-748.
169. Nenna, G., Mauro, D. A. D. G., Massera, E., Bruno, A., Fasolino, T. and Minarini, C. (2012). Optical properties of polystyrene-ZnO nanocomposite scattering layer to improve light extraction in organic light-emitting diode. *Journal of Nanomaterials*, 2012: 1-5.
170. Newbury, D. E., Joy, D. C., Echlin, P., Fiori, C. E. and Goldstein, J. I. (1986). Advanced scanning electron microscopy and X-ray microanalysis. *New York.: Plenum Press. Review by WMS in J. Microsc*, 146: 109.
171. Nguyen, T. T., Nguyen, S. U., Phuong, D. T., Nguyen, D. C. and Mai, A. T. (2011). Dispersion of denatured carbon nanotubes by using a dimethylformamide solution. *Advances in Natural Sciences: Nanoscience and Nanotechnology*, 2(3): 035015(1-4).
172. Nie, W. (1993). Optical nonlinearity: phenomena, applications, and materials. *Advanced Materials*, 5(7-8): 520-545.
173. Nussbaumer, R. J., Caseri, W. R., Smith, P. and Tervoort, T. (2003). Polymer-TiO₂ Nanocomposites: A Route Towards Visually Transparent Broadband UV Filters and High Refractive Index Materials. *Macromolecular Materials and Engineering*, 288(1): 44-49.

174. O'Flaherty, S. M., Hold, S. V., Brennan, M. E., Cadek, M., Drury, A., Coleman, J. N. and Blau, W. J. (2003a). Nonlinear optical response of multiwalled carbon-nanotube dispersions. *Journal of Optical Society of America B*, 20(1): 49-58.
175. O'Flaherty, S. M., Murphy, R., Hold, S. V., Cadek, M., Coleman, J. N. and Blau, W. J. (2003b). Material investigation and optical limiting properties of carbon nanotube and nanoparticle dispersions. *The Journal of Physical Chemistry B*, 107(4): 958-964.
176. Ohtomo, A. and Tsukazaki, A. (2005). Pulsed laser deposition of thin films and superlattices based on ZnO. *Semiconductor Science and Technology*, 20(4): S1-S13.
177. Özgür, Ü., Alivov, Y. I., Liu, C. A., Teke, A., Reshchikov, M. A., Doğan, S., Avrutin, V., Cho, S.-J. and Morkoc, H. (2005). A comprehensive review of ZnO materials and devices. *Journal of Applied Physics*, 98(4): 041301(1-103).
178. Özgür, Ü., Hofstetter, D. and Morkoç, H. (2010). ZnO devices and applications: a review of current status and future prospects. *Proceedings of the IEEE*, 98(7): 1255-1268.
179. Palomba, M., Carotenuto, G., Cristino, L., Di Grazia, M. A., Nicolais, F. and De Nicola, S. (2012). Activity of antimicrobial silver polystyrene nanocomposites. *Journal of Nanomaterials*, 2012: 1-7.
180. Pan, A., Yu, R., Xie, S., Zhang, Z., Jin, C. and Zou, B. (2005). ZnO flowers made up of thin nanosheets and their optical properties. *Journal of Crystal Growth*, 282(1): 165-172.
181. Panchakarla, L. S. and Govindaraj, A. (2008). Covalent and non-covalent functionalization and solubilization of double-walled carbon nanotubes in nonpolar and aqueous media. *Journal of Chemical Sciences*, 120(6): 607-611.
182. Papadopoulos, M. G., Sadlej, A. J. and Leszczynski, J. (2006). *Non-linear Optical Properties of Matter*. Springer: USA.
183. Pasquarelli, R. M., Ginley, D. S. and O'Hayre, R. (2011). Solution processing of transparent conductors: from flask to film. *Chemical Society Reviews*, 40(11): 5406-5441.
184. Patra, R., Ghosh, S., Sharma, H. and Vankar, V. D. (2013). High stability field emission from zinc oxide coated multiwalled carbon nanotube films. *Advanced Materials Letters*, 4(11): 849-855.

185. Peić, A., Dimopoulos, T., Resel, R., Abermann, S., Postl, M., List, E. J. W. and Brückl, H. (2012). Effect of AZO substrates on self-seeded electrochemical growth of vertically aligned ZnO nanorod arrays and their optical properties. *Journal of Nanomaterials*, 2012: 1-14.
186. Peng, Z., Dai, G., Chen, P., Zhang, Q., Wan, Q. and Zou, B. (2010). Synthesis, characterization and optical properties of star-like ZnO nanostructures. *Materials Letters*, 64(8): 898-900.
187. Philip, R., Anija, M., Yelleswarapu, C. S. and Rao, D. V. G. L. N. (2007). Passive all-optical diode using asymmetric nonlinear absorption. *Applied Physics Letters*, 91(14): 141118(1-4).
188. Plank, N. O. V., Welland, M. E., MacManus-Driscoll, J. L. and Schmidt-Mende, L. (2008). The backing layer dependence of open circuit voltage in ZnO/polymer composite solar cells. *Thin Solid Films*, 516(20): 7218-7222.
189. Pradeep, C., Mathew, S., Nithyaja, B., Radhakrishnan, P. and Nampoory, V. P. N. (2013). Studies of nonlinear optical properties of Pico Green dye using Z-scan technique. *Applied Physics A*, 115(1): 291-295.
190. Pradeep, T. (2012). *A Textbook of Nanoscience and Nanotechnology*. Tata McGraw-Hill Education: New Delhi.
191. Pramodini, S. and Poornesh, P. (2014a). Effect of conjugation length on nonlinear optical parameters of anthraquinone dyes investigated using He-Ne laser operating in CW mode. *Optics & Laser Technology*, 62: 12-19.
192. Pramodini, S., Sudhakar, Y. N., SelvaKumar, M. and Poornesh, P. (2014b). Studies on third-order optical nonlinearity and power limiting of conducting polymers using the z-scan technique for nonlinear optical applications. *Laser Physics*, 24(2014): 045408(1-7).
193. Pyshkin, S. L. and Ballato., J. M. (Eds.) (2013). *Optoelectronics-Advanced Materilas and devices*. DOI:10.5772/51181.
194. Rahman, M. M. (Eds.) (2011). *Nanotechnology and Nanomaterials*. DOI: 10.5772/27238
195. Raman, C. V. and Krishnan, K. S. (1928). A new class of spectra due to secondary radiation. *Indian journal of Physics*, 2: 379-396.
196. Rao, S. V., Anusha, P. T., Prashant, T. S., Swain, D. and Tewari, S. P. (2011). Ultrafast Nonlinear Optical and Optical Limiting Properties of Phthalocyanine

- Thin Films Studied Using Z-Scan. *Materials Sciences and Applications*, 2(05): 299-306.
197. Reddy, K. P. J. (1991). Applications of reverse saturable absorbers in laser science. *Current Science*, 61(8): 520-526.
 198. Ribeiro, T., Baleizão, C. and Farinha, J. P. S. (2014). Functional Films from Silica/Polymer Nanoparticles. *Materials*, 7(5): 3881-3900.
 199. Riggs, J. E., Walker, D. B., Carroll, D. L. and Sun, Y.-P. (2000). Optical Limiting Properties of Suspended and Solubilized Carbon Nanotubes. *The Journal of Physical Chemistry B*, 104(30): 7071-7076.
 200. Rosca, I. D., Watari, F., Uo, M. and Akasaka, T. (2005). Oxidation of multiwalled carbon nanotubes by nitric acid. *Carbon*, 43(15): 3124-3131.
 201. Roy, A. S., Gupta, S., Sindhu, S., Parveen, A. and Ramamurthy, P. C. (2013). Dielectric properties of novel PVA/ZnO hybrid nanocomposite films. *Composites: Part B*. 47:314-319.
 202. Roy, R., Roy, R. A. and Roy, D. M. (1986). Alternative perspectives on “quasi-crystallinity”: non-uniformity and nanocomposites. *Materials Letters*, 4(8, 9): 323-328.
 203. Rumi, M. and Perry, J. W. (2010). Two-photon absorption: an overview of measurements and principles. *Advances in Optics and Photonics*, 2(4): 451-518.
 204. Sahoo, N. G., Rana, S., Cho, J. W., Li, L. and Chan, S. H. (2010). Polymer nanocomposites based on functionalized carbon nanotubes. *Progress in Polymer Science*, 35(7): 837-867.
 205. Sahu, N., Parija, B. and Panigrahi, S. (2009). Fundamental understanding and modeling of spin coating process: A review. *Indian Journal of Physics*, 83(4): 493-502.
 206. Saito, N., Haneda, H., Sekiguchi, T., Ohashi, N., Sakaguchi, I. and Koumoto, K. (2002). Low-temperature fabrication of light-emitting zinc oxide micropatterns using self-assembled monolayers. *Advanced Materials*, 14(6): 418-421.
 207. Sakka, Y., Tang, F., Fudouzi, H. and Uchikoshi, T. (2005). Fabrication of porous ceramics with controlled pore size by colloidal processing. *Science and Technology of Advanced Materials*, 6(8): 915-920.

208. Sambasivarao, V. S., Thermal Stability and Ionic Conductivity of High-Temperature Proton Conducting Ionic Liquid-Polymer Composite Electrolyte Membranes for Fuel Cell Applications. In L. Li. Et al., *Polymer Composites for Energy Harvesting, Conversion, and Storage*, American Chemical Society: Washington DC.
209. Sato, R., Ohnuma, M., Oyoshi, K. and Takeda, Y. (2014). Experimental investigation of nonlinear optical properties of Ag nanoparticles: Effects of size quantization. *Physical Review B*, 90(12): 125417(1-6).
210. Scarselli, M., Castrucci, P. and De Crescenzi, M. (2012). Electronic and optoelectronic nano-devices based on carbon nanotubes. *Journal of Physics: Condensed Matter*, 24(31): 313202.
211. Schmidt, J. J., Gardella Jr, J. A. and Salvati Jr, L. (1989). Surface studies of polymer blends. 2. An ESCA and IR study of poly (methyl methacrylate)/poly (vinyl chloride) homopolymer blends. *Macromolecules*, 22(12): 4489-4495.
212. Schmidt-Mende, L. and MacManus-Driscoll, J. L. (2007). ZnO–nanostructures, defects, and devices. *Materials Today*, 10(5): 40-48.
213. Seitz, F. and Turnbull, D. (Eds.) (1959). *Solid State Physics*. <http://www.sciencedirect.com/science/bookseries/00811947/8>
214. Sekiguchi, T., Miyashita, S., Obara, K., Shishido, T. and Sakagami, N. (2000). Hydrothermal growth of ZnO single crystals and their optical characterization. *Journal of Crystal Growth*, 214: 72-76.
215. Sendhil, K., Vijayan, C. and Kothiyal, M. P. (2005). Nonlinear optical properties of a porphyrin derivative incorporated in Nafion polymer. *Optical Materials*, 27(10): 1606-1609.
216. Sentein, C., Guizard, B., Giraud, S., Yé, C. and Ténégal, F. (2009). Dispersion and stability of TiO₂ nanoparticles synthesized by laser pyrolysis in aqueous suspensions, In *Journal of Physics: Conference Series*, 170: 1-9.
217. Shao, D., Yu, M., Lian, J. and Sawyer, S. (2013). Heterojunction photodiode fabricated from multiwalled carbon nanotube/ZnO nanowire/p-silicon composite structure. *Applied Physics Letters*, 102(2): (1-3).
218. Sheik-Bahae, M., Said, A. A. and Van Stryland, E. W. (1989). High-sensitivity, single-beam n₂ measurements. *Optics Letters*, 14(17): 955-957.

219. Sheik-Bahae, M., Said, A. A., Wei, T.-H., Hagan, D. J. and Van Stryland, E. W. (1990). Sensitive measurement of optical nonlinearities using a single beam. *Quantum Electronics, IEEE Journal of Quantum Electronics*, 26(4): 760-769.
220. Shen, H., Cheng, B. L., Lu, G. W., Guan, D. Y., Chen, Z. H. and Yang, G. Z. (2006). Picosecond nonlinear optical responses of Au/PVP composite films. *Journal of Physics D: Applied Physics*, 39(1): 233-236.
221. Shen, Y.-R. (1984). *The principles of nonlinear optics*. Wiley-Interscience: New York.
222. Shong, C. W., Haur, C. S. and Wee, A. T. S. (2010). *Science at the nanoscale: an introductory textbook*. Pan Stanford Publishing: Singapore.
223. Siddabattuni, S. and Schuman, T. P. (2014). Polymer-Ceramic Nanocomposite Dielectrics for Advanced Energy Storage. In L. Li. Et al., *Polymer Composites for Energy Harvesting, Conversion, and Storage*, American Chemical Society: Washington DC.
224. Singh, P., Kumar, A., Kaushal, A., Kaur, D., Pandey, A. and Goyal, R. N. (2008). *In situ* high temperature XRD studies of ZnO nanopowder prepared via cost effective ultrasonic mist chemical vapour deposition. *Bulletin of Materials Science*, 31(3): 573-577.
225. Skandani, A. A., Masghouni, N., Case, S. W., Leo, D. J. and Al-Haik, M. (2012). Enhanced vibration damping of carbon fibers-ZnO nanorods hybrid composites. *Applied Physics Letters*, 101(7): 073111(1-4).
226. Slepko, A. D., Hegmann, F. A., Zhao, Y., Tykwinski, R. R. and Kamada, K. (2002). Ultrafast optical Kerr effect measurements of third-order nonlinearities in cross-conjugated iso-polydiacetylene oligomers. *The Journal of Chemical Physics*, 116(9): 3834-3840.
227. Smith, E. and Dent, G. (2005). *Modern Raman spectroscopy: a practical approach*. John Wiley & Sons: England.
228. Son, D. I., You, C. H., Kim, W. T., Jung, J. H. and Kim, T. W. (2009). Electrical bistabilities and memory mechanisms of organic bistable devices based on colloidal ZnO quantum dot-polymethylmethacrylate polymer nanocomposites. *Applied Physics Letters*, 94(13): 132103(1-3).
229. Spitalsky, Z., Tasis, D., Papagelis, K. and Galiotis, C. (2010). Carbon nanotube-polymer composites: chemistry, processing, mechanical and electrical properties. *Progress in Polymer Science*, 35(3): 357-401.

230. Sreeja, R., John, J., Aneesh, P. M. and Jayaraj, M. K. (2010). Linear and nonlinear optical properties of luminescent ZnO nanoparticles embedded in PMMA matrix. *Optics Communications*, 283(14): 2908-2913.
231. Sridevi, D. and Rajendran, K. V. (2009). Synthesis and optical characteristics of ZnO nanocrystals. *Bulletin of Materials Science*, 32(2): 165-168.
232. Srikant, V. and Clarke, D. R. (1998). On the optical band gap of zinc oxide. *Journal of Applied Physics*, 83(10): 5447-5451.
233. Srivastava, S., Haridas, M. and Basu, J. K. (2008). Optical properties of polymer nanocomposites. *Bulletin of Materials Science*, 31(3): 213-217.
234. Studenikin, S. A., Golego, N. and Cocivera, M. (1998). Fabrication of green and orange photoluminescent, undoped ZnO films using spray pyrolysis. *Journal of Applied Physics*, 84(4): 2287-2294.
235. Sun, D. and Sue, H.-J. (2009). Tunable ultraviolet emission of ZnO quantum dots in transparent poly (methyl methacrylate). *Applied Physics Letters*, 94(25): 253106(1-3).
236. Sun, R., Lu, Y.-T., Yan, B.-L., Lu, J.-M., Wu, X.-Z., Song, Y.-L. and Ge, J.-F. (2014). Third-order nonlinear optical properties of the poly (methyl methacrylate)-phenothiazinium dye hybrid thin films. *Thin Solid Films*, 551: 153-157.
237. Sun, X., Yu, R. Q., Xu, G. Q., Hor, T. S. A. and Ji, W. (1998). Broadband optical limiting with multiwalled carbon nanotubes. *Applied Physics Letters*, 73(25): 3632-3634.
238. Sun, Y.-P., Huang, W., Lin, Y., Fu, K., Kitaygorodskiy, A., Riddle, L. A., Yu, Y. J. and Carroll, D. L. (2001). Soluble Dendron-Functionalized Carbon Nanotubes: Preparation, Characterization, and Properties. *Chemistry of Materials*, 13(9): 2864-2869.
239. Sun, Y.-P., Zhou, B., Henbest, K., Fu, K., Huang, W., Lin, Y., Taylor, S. and Carroll, D. L. (2002). Luminescence anisotropy of functionalized carbon nanotubes in solution. *Chemical Physics Letters*, 351(5): 349-353.
240. Sutherland, R. L. (2003). *Handbook of nonlinear optics* (Second edition). Marcel Dekker CRC press:NY.

241. Takagahara, T. (1993). Effects of dielectric confinement and electron-hole exchange interaction on excitonic states in semiconductor quantum dots. *Physical Review B*, 47(8): 4569-4584.
242. Tanaka, K., Takahara, A. and Kajiyama, T. (1996). Film thickness dependence of the surface structure of immiscible polystyrene/poly (methyl methacrylate) blends. *Macromolecules*, 29(9): 3232-3239.
243. Tang, B. Z. and Xu, H. (1999). Preparation, alignment, and optical properties of soluble poly (phenylacetylene)-wrapped carbon nanotubes. *Macromolecules*, 32(8): 2569-2576.
244. Tang, E., Cheng, G., Pang, X., Ma, X. and Xing, F. (2006a). Synthesis of nano-ZnO/poly (methyl methacrylate) composite microsphere through emulsion polymerization and its UV-shielding property. *Colloid and Polymer Science*, 284(4): 422-428.
245. Tang, E., Liu, H., Sun, L., Zheng, E. and Cheng, G. (2007). Fabrication of zinc oxide/poly (styrene) grafted nanocomposite latex and its dispersion. *European Polymer Journal*, 43(10): 4210-4218.
246. Tang, X., Bansaruntip, S., Nakayama, N., Yenilmez, E., Chang, Y. And Wang, Q. (2006b). Carbon Nanotube DNA Sensor and Sensing Mechanism. *Nano Letters*. 6(8):1632-1636.
247. Tans, S. J., Devoret, M. H., Dai, H., Thess, A., Smalley, R. E., Georliga, L. J. and Dekker, C. (1997). Individual single-wall carbon nanotubes as quantum wires. *Nature* 386 (6624), 474-477.(1997):
248. Tao, P., Li, Y., Rungta, A., Viswanath, A., Gao, J., Benicewicz, B. C., Siegel, R. W. and Schadler, L. S. (2011). TiO₂ nanocomposites with high refractive index and transparency. *Journal of Materials Chemistry*, 21(46): 18623-18629.
249. Tauc, J. (1966). The optical properties of solids, In *The Optical Properties of Solids*.15(2):627-637.
250. Thalhammer, M. and Penzkofer, A. (1983). Measurement of third-order nonlinear susceptibilities by non-phase matched third-harmonic generation. *Applied Physics B*, 32(3): 137-143.
251. Thankappan, A., S, D., Thomas, S. and Nampoore, V. P. N. (2013b). Optical characterization of ZnO nanoplates embedded in polymeric matrices for optical limiting applications. *Optics & Laser Technology*, 52(0): 37-42.

252. Thirugnanam, T. (2013). Effect of polymers (PEG and PVP) on sol-gel synthesis of microsized zinc oxide. *Journal of Nanomaterials*, 2013: 1-7.
253. Tong, Y., Liu, Y., Shao, C. L. and Mu, R. X. (2006). Structural and optical properties of ZnO nanotower bundles. *Applied Physics Letters*, 88(12): 123111.
254. Ton-That, C., Shard, A. G., Teare, D. O. H. and Bradley, R. H. (2001). XPS and AFM surface studies of solvent-cast PS/PMMA blends. *Polymer*, 42(3): 1121-1129.
255. Treacy, M. M. J., Ebbesen, T. W. and Gibson, J. M. (1996). Exceptionally high Young's modulus observed for individual carbon nanotubes. *Nature*, 381: 678-680.
256. Tsai, P.-A., Kuo, H.-Y., Chiu, W.-M. and Wu, J.-H. (2013). Purification and functionalization of single-walled carbon nanotubes through different treatment procedures. *Journal of Nanomaterials*, 2013: 1-9.
257. Tu, Y., Zhou, L., Jin, Y. Z., Gao, C., Ye, Z. Z., Yang, Y. F. and Wang, Q. L. (2010). Transparent and flexible thin films of ZnO-polystyrene nanocomposite for UV-shielding applications. *Journal of Materials Chemistry*, 20(8): 1594-1599.
258. Tuhl, A., Manaa, H., Makhseed, S., Al-Awadi, N., Mathew, J., Ibrahim, H. M., Nyokong, T. and Behbehani, H. (2012). Reverse saturation absorption spectra and optical limiting properties of chlorinated tetrasubstituted phthalocyanines containing different metals. *Optical Materials*, 34(11): 1869-1877.
259. Tutt, L. W. and Boggess, T. F. (1993). A review of optical limiting mechanisms and devices using organics, fullerenes, semiconductors and other materials. *Progress in Quantum Electronics*, 17(4): 299-338.
260. Tynell, T. and Karppinen, M. (2014). Atomic layer deposition of ZnO: a review. *Semiconductor Science and Technology*, 29(4): 043001(1-15).
261. Van Dijken, A., Meulenkaamp, E., Vanmaekelbergh, D. and Meijerink, A. (2000). The luminescence of nanocrystalline ZnO particles: the mechanism of the ultraviolet and visible emission. *Journal of Luminescence*, 87: 454-456.
262. Van Stryland, E. W., Woodall, M., Vanherzeele, H. and Soileau, M. (1985). Energy band-gap dependence of two-photon absorption. *Optics Letters*, 10(10): 490-492.

263. Vivien, L., Anglaret, E., Riehl, D., Bacou, F., Journet, C., Goze, C., Andrieux, M., Brunet, M., Lafonta, F. and Bernier, P. Hache, F. (1999). Single-wall carbon nanotubes for optical limiting. *Chemical Physics Letters*, 307(5): 317-319.
264. Vivien, L., Lancon, P., Riehl, D., Hache, F. and Anglaret, E. (2002). Carbon nanotubes for optical limiting. *Carbon*, 40(10): 1789-1797.
265. Vivien, L., Riehl, D., Lancon, P., Hache, F. and Anglaret, E. (2001). Pulse duration and wavelength effects on the optical limiting behavior of carbon nanotube suspensions. *Optics Letters*, 26(4): 223-225.
266. Vutha, A. C., Tiwari, S. and Thareja, R. (2006). Random laser action in ZnO doped polymer. *Journal of Applied Physics*, 99(12): 123509(1-4).
267. Vyas, R., Sharma, S., Gupta, P., Prasad, A. K., Tyagi, A. K., Sachdev, K. and Sharma, S. K. (2012). CNT-ZnO nanocomposite thin films: O₂ and NO₂ sensing. *Advanced Materials Research*, 585: 235-239.
268. Walheim, S., Böltau, M., Mlynek, J., Krausch, G. and Steiner, U. (1997). Structure formation via polymer demixing in spin-cast films. *Macromolecules*, 30(17): 4995-5003.
269. Wang, C.-Y. and Adhikari, S. (2011). ZnO-CNT composite nanotubes as nanoresonators. *Physics Letters A*, 375(22): 2171-2175.
270. Wang, J., Chen, Y. and Blau, W. J. (2009). Carbon nanotubes and nanotube composites for nonlinear optical devices. *Journal of Materials Chemistry*, 19(40): 7425-7443.
271. Wang, S. X., Zhang, L. D., Su, H., Zhang, Z. P., Li, G. H., Meng, G. W., Zhang, J., Wang, Y. W., Fan, J. C. and Gao, T. (2001). Two-photon absorption and optical limiting in poly (styrene maleic anhydride) TiO₂ nanocomposites. *Physics Letters A*, 281(1): 59-63.
272. Wang, Y., Xie, X. and Goodson, T. (2005). Enhanced third-order nonlinear optical properties in dendrimer-metal nanocomposites. *Nano Letters*, 5(12): 2379-2384.
273. Wang, Z. L. (2004). Zinc oxide nanostructures: growth, properties and applications. *Journal of Physics: Condensed Matter*, 16(25): R829-R858.
274. Wang, Z., Liu, C., Xiang, H., Li, Z., Gong, Q., Qin, Y., Guo, Z. and Zhu, D. (2004). Ultrafast third-order nonlinear optical response of two soluble multi-

- wall carbon nanotubes. *Journal of Physics D: Applied Physics*, 37(7): 1079-1082.
275. Wei, X. Q., Man, B. Y., Liu, M., Xue, C. S., Zhuang, Z. H. and Yang, C. (2007). Blue luminescent centers and microstructural evaluation by XPS and Raman in ZnO thin films annealed in vacuum, N₂ and O₂. *Physica B: Condensed Matter*, 388(1): 145-152.
 276. Willander, M., Nur, O., Zaman, S., Zainelabdin, A., Bano, N. and Hussain, I. (2011). Zinc oxide nanorods/polymer hybrid heterojunctions for white light emitting diodes. *Journal of Physics D: Applied Physics*, 44(22): 224017.
 277. Willander, M., Zhao, Q., Hu, Q.-H., Klason, P., Kuzmin, V., Al-Hilli, S. M., Nur, O. and Lozovik, Y. E. (2008). Fundamentals and properties of zinc oxide nanostructures: Optical and sensing applications. *Superlattices and Microstructures*, 43(4): 352-361.
 278. Wu, L. Y. L., Leng, B. and Bisht, A. (2014). Metal–polymer nano-composite films with ordered vertically aligned metal cylinders for sub-wavelength imaging. *Applied Physics A*: 1-8.
 279. Wu, X., Wang, R., Zou, B., Wu, P., Wang, L., Xu, J. and Huang, W. (1997). The effects of different interfacial environments on the optical nonlinearity of nanometer-sized CdO organosol. *Applied Physics Letters*, 71(15): 2097-2099.
 280. Xing, G., Ji, W., Zheng, Y. and Ying, J. Y. (2008). Two-and three-photon absorption of semiconductor quantum dots in the vicinity of half of lowest exciton energy. *Applied Physics Letters*, 93(24): 241114(1-3).
 281. Xiong, H.-M. (2010). Photoluminescent ZnO nanoparticles modified by polymers. *Journal of Materials Chemistry*, 20(21): 4251-4262.
 282. Xu, C. X., Sun, X. W., Chen, B. J., Shum, P., Li, S. and Hu, X. (2004). Nanostructural zinc oxide and its electrical and optical properties. *Journal of Applied Physics*, 95(2): 661-666.
 283. Yakobson, B. I. and Avouris, P. (2001). Mechanical properties of carbon nanotubes. In Dresselhaus, M. S., Dresselhaus, G. and Avouris, P.(Eds). *Carbon nanotubes*(pp 287-327), Berlin Heidelberg: Springer.
 284. Yang, C. L., Wang, J. N., Ge, W. K., Guo, L., Yang, S. H. and Shen, D. Z. (2001). Enhanced ultraviolet emission and optical properties in polyvinyl pyrrolidone surface modified ZnO quantum dots. *Journal of Applied Physics*, 90(9): 4489-4493.

285. Yang, L., Wang, G., Tang, C., Wang, H. and Zhang, L. (2005). Synthesis and photoluminescence of corn-like ZnO nanostructures under solvothermal-assisted heat treatment. *Chemical Physics Letters*, 409(4): 337-341.
286. Yang, P., Yan, H., Mao, S., Russo, R., Johnson, J., Saykally, R., Morris, N., Pham, J., He, R. and Choi, H.-J. (2002). Controlled growth of ZnO nanowires and their optical properties. *Advanced Functional Materials*, 12(5): 323-331.
287. Yelin, D. and Silberberg, Y. (1999). Laser scanning third-harmonic-generation microscopy in biology. *Optics Express*, 5(8): 169-175.
288. You, G., Zhou, P., Zhang, C., Dong, Z., Chen, L. and Qian, S. (2006). Ultrafast nonlinear optical response of silver/bismuth oxide nanocomposite films with different silver concentrations. *Journal of Luminescence*, 119: 370-377.
289. Yu, J., Grossiord, N., Koning, C. E. and Loos, J. (2007). Controlling the dispersion of multi-wall carbon nanotubes in aqueous surfactant solution. *Carbon*, 45(3): 618-623.
290. Yuwono, A. H., Xue, J., Wang, J., Elim, H. I., Ji, W., Li, Y. and White, T. J. (2003). Transparent nanohybrids of nanocrystalline TiO₂ in PMMA with unique nonlinear optical behavior. *Journal of Materials Chemistry*, 13(6): 1475-1479.
291. Zan, L., Tian, L., Liu, Z. and Peng, Z. (2004). A new polystyrene-TiO₂ nanocomposite film and its photocatalytic degradation. *Applied Catalysis A: General*, 264(2): 237-242.
292. Zhang, R., Fan, L., Fang, Y. and Yang, S. (2008). Electrochemical route to the preparation of highly dispersed composites of ZnO/carbon nanotubes with significantly enhanced electrochemiluminescence from ZnO. *Journal of Materials Chemistry*, 18(41): 4964-4970.
293. Zhang, S. B., Wei, S.-H. and Zunger, A. (2001). Intrinsic n-type versus p-type doping asymmetry and the defect physics of ZnO. *Physical Review B*, 63(7): 075205(1-7).
294. Zhang, W. H., Fan, X. D., Tian, W. and Fan, W. W. (2012). Polystyrene/nano-SiO₂ composite microspheres fabricated by Pickering emulsion polymerization: preparation, mechanisms and thermal properties. *Express Polymers Letters*, 6(7): 532-542.
295. Zhang, X. J., Ji, W. and Tang, S. H. (1997). Determination of optical nonlinearities and carrier lifetime in ZnO. *Journal of Optical Society of America B*, 14(8): 1951-1955.

296. Zhang, Y., Sun, X., Pan, L., Li, H., Sun, Z., Sun, C. and Tay, B. K. (2009). Carbon nanotube–ZnO nanocomposite electrodes for supercapacitors. *Solid State Ionics*, 180(32): 1525-1528.
297. Zhang, Y., Zhuang, S., Xu, X. and Hu, J. (2013). Transparent and UV-shielding ZnO- PMMA nanocomposite films. *Optical Materials*, 36(2): 169-172.
298. Zhang, Z., He, W. Q., Gu, C. M., Shen, W. Z., Ogawa, H. and Guo, Q. X. (2007). Determination of the third-and fifth-order nonlinear refractive indices in InN thin films. *Applied Physics Letters*, 91(22): 221902(1-3).
299. Zhaoyuan, N. and Huoquan, L. (2005). Effects of annealing on luminescence of ZnO films deposited on Si substrates by RF magnetron sputtering. *Plasma Science and Technology*, 7(1): 2665-2668.
300. Zhu, Y., Elim, H. I., Foo, Y. L., Yu, T., Liu, Y., Ji, W., Lee, J. Y., Shen, Z., Wee, A. T.-S. and Thong, J. T.-L. Sow, C. H. (2006). Multiwalled carbon nanotubes beaded with ZnO nanoparticles for ultrafast nonlinear optical switching. *Advanced Materials*, 18(5): 587-592.
301. Zitter, R. N. (1969). Saturated optical absorption through band filling in semiconductors. *Applied Physics Letters*, 14(2): 73-74.
302. Znaidi, L. (2010). Sol–gel-deposited ZnO thin films: a review. *Materials Science and Engineering: B*, 174(1): 18-30.
303. Zubiaga, A., Garcia, J. A., Plazaola, F., Tuomisto, F., Saarinen, K., Pérez, J. Z. and Muñoz-Sanjósé, V. (2006). Correlation between Zn vacancies and photoluminescence emission in ZnO films. *Journal of Applied Physics*, 99(5): 053516(1-6).

LIST OF PUBLICATIONS BASED ON THE THESIS

PUBLISHED

1. Haripadmam, P. C., Kavitha, M. K., John, H., Krishnan, B. and Gopinath, P. (2012). Optical limiting studies of ZnO nanotops and its polymer nanocomposite films. *Applied Physics Letters*, 101: 071103 (1-5).
2. Kavitha, M. K., Haripadmam, P. C., Gopinath, P., Krishnan, B., John, H. (2013). Effect of morphology and solvent on two-photon absorption of nano zinc oxide. *Materials Research Bulletin*, 48(5):1967–1971.
3. Haripadmam, P.C., John, H., Philip, R. and Gopinath, P. (2014). Enhanced optical limiting in polystyrene–ZnO nanotop composite films. *Optics Letters*, 39(3): 474-477.
4. Haripadmam, P. C., John, H., Philip, R. and Gopinath, P. (2014). Switching of absorptive nonlinearity from reverse saturation to saturation in polymer-ZnO nanotop composite films. *Applied Physics Letters*, 105: 221102 (1-5).
5. Fifth order nonlinear optical absorption in ZnO/MWNT and polymer-ZnO/MWNT composite films. (Under review in RSC Advances)

Presentations in conferences/seminars

Oral presentations

1. Haripadmam, P. C., Honey, J. and Pramod, G. Spherical Nano Metal Oxide: A promising material for Optical Limiting. *IIST Research Scholars' Day, IIST, Thiruvananthapuram, 16-17 December (2011). BEST PAPER AWARD*

2. Haripadmam, P. C., Honey, J. and Pramod, G. Studies on the Two Photon Absorption Coefficient of ZnO Nanotop - Polystyrene Composite Films. *IIST Research Scholars' Day, IIST, Thiruvananthapuram, 17-19 December (2012)*.
3. Haripadmam, P. C., Honey, J. and Pramod, G. Effect of fabrication technique on optical limiting property of Polystyrene-ZnO nanotop composite films. *31st Young Physicists' Colloquium, Saha Institute of Nuclear Physics, Kolkata, 22-23 August (2013)*.
4. Haripadmam, P. C., Honey, J. and Pramod, G. Improvement in Optical Limiting Properties of PMMA-ZnO nanocomposites films prepared using oleic acid as a dispersing agent. *IIST Research scholars' Day, IIST, Thiruvananthapuram, 16-17 December (2013)*. **BEST PAPER AWARD**
5. Haripadmam, P. C., Honey, J. and Pramod, G. Fifth order nonlinear optical absorption in PMMA-ZnO/MWNT composite film. *International conference on Photonics and Solar water splitting, Ernakulam, 12-13 March (2015)*. **BEST PAPER AWARD**

Poster Presentations

1. Haripadmam, P.C., Kavitha, M. K., Honey, J. and Pramod, G. Fiber optic chemical sensor using polyaniline-modified cladding. *XXXV OSI Symposium, International Conference on contemporary trends in optics and optoelectronics, IIST, Valiyamala, 17-19 January, (2011)*.
2. Haripadmam, P. C., Honey, J. and Pramod, G. Improvement in Optical Limiting Properties of PMMA-ZnO nanocomposites films prepared using triton as a dispersing agent. *DAE-BRNS National Laser Symposium (NLS-22), MIT, Manipal University, Manipal, 8-11 January, (2014)*.

3. Haripadmam, P.C., Kavitha, M. K., Honey, J. and Pramod, G. Effect of loading concentration of ZnO in enhancing the two photon absorption coefficient of polystyrene-ZnO nanotop composite films. *37th National Symposium of Optical Society of India, Pondicherry University, Pondicherry, 23-25 January (2013).*

BEST POSTER AWARD

4. Haripadmam, P. C., Honey, J. and Pramod, G. Comparative study of the influence of fabrication technique on the two photon absorption coefficient of polystyrene-ZnO nanotop composite films. *25th Kerala Science Congress, Technopark, Thiruvananthapuram, 29th January-1st February (2013).*
5. Haripadmam, P. C., Honey, J. and Pramod, G. Saturable and reverse saturable absorption exhibited by polymer-ZnO nanotop composite films. *20th National Conference on Atomic and Molecular Physics, IIST, Thiruvananthapuram, 09-12 December (2014).*